5 The Crystal Chemistry of the Phosphate Minerals

Danielle M.C. Huminicki and Frank C. Hawthorne

Department of Geological Sciences
University of Manitoba
Winnipeg, Manitoba, Canada R3T 2N2

INTRODUCTION

Phosphorus was discovered in 1669 by Hennig Brand. The word *phosphorus* originates from the two Greek words *phôs*, meaning light, and *phoros*, meaning bearer, due to the phosphorescent nature of white phosphorus. Phosphorus is the tenth most abundant element on Earth and tends to be concentrated in igneous rocks. It is an incompatible element in common rock-forming minerals, and hence is susceptible to concentration via fractionation in geochemical processes. It reaches its highest abundance in sedimentary rocks: the major constituents of phosphorite are the minerals of the apatite group. Phosphorus is the second most abundant inorganic element in our bodies (after Ca); it makes up about 1% of our body weight, occurring primarily in bones and teeth. Phosphorus (atomic number 15) is a non-metal in group VA of the periodic table, and has the ground-state electronic configuration $1s^2\ 2s^2\ 2p^6\ 3s^2\ 3p_x^1\ 3p_y^1\ 3p_z^1$ or [Ne]$3s^2 3p^3$. There are three orbitals occupied with only one electron each in the third energy level (the *M* shell). Phosphorus participates in essentially covalent bonds; electron gain to form P^{3-} from P requires considerable energy (on the order of 1450 kJ mol^{-1}). Loss of electrons is also difficult due to the high ionization potentials of P (the sum of the first three ionization potentials is 60.4 eV).

CHEMICAL BONDING

Here we use bond-valence theory (Brown 1981) and its developments (Hawthorne 1985a, 1994, 1997) to consider structure topology and hierarchical classification of crystal structures, and we point out that bond-valence theory can be considered as a simple form of molecular-orbital theory (Burdett and Hawthorne 1993; Hawthorne 1994, 1997).

STEREOCHEMISTRY OF ($P\phi_4$) POLYHEDRA IN MINERALS

The variation of P-ϕ (ϕ: O^{2-}, OH^-) distances and ϕ-P-ϕ angles is of great interest for several reasons:

(1) mean bond-length and empirical cation and anion radii play an important role in systematizing chemical and physical properties of crystals;

(2) variations in individual bond-lengths give insight into the stereochemical behavior of structures, particularly with regard to the factors affecting structure stability;

(3) there is a range of stereochemical variation beyond which a specific oxyanion or cation-coordination polyhedron is not stable; it is obviously useful to know this range, both for assessing the stability of hypothetical structures (calculated by DLS [Distance Least-Squares] refinement, Dempsey and Strens 1976; Baur 1977) and for assessing the accuracy of experimentally determined structures.

Here, we examine the variation in P-ϕ distances in minerals and review previous work on polyhedral distortions in ($P\phi_4$) tetrahedra. Data for 408 ($P\phi_4$) tetrahedra were taken from 244 refined crystal structures with $R \leq 6.5\%$ and standard deviations of $\leq$0.005 Å on P-ϕ bond-lengths; structural references are given in Appendix A.

1529-6466/02/0048-0005$10.00 DOI: 10.2138/rmg.2002.48.5

Variation in <P-ϕ> distances

The variation in <P-ϕ_4> distances (< > denotes a mean value; in this case, of P in tetrahedral coordination) is shown in Figure 1. The grand <P-ϕ> distance (i.e., the mean value of the <P-ϕ> distances) is 1.537 Å, in agreement with the value of 1.537 Å given by Baur (1974). The minimum and maximum <P-ϕ> distances are 1.459 and 1.602 Å, respectively (the larger values in Fig. 1 are considered unreliable), and the range of variation is 0.143 Å. Shannon (1976) lists the radius of $^{[4]}$P as 0.17 Å; assuming a mean anion-coordination number of 3.25 and taking the appropriate O/OH ratio, the sum of the constituent radii is 0.17 + 1.360 = 1.53 Å, in accord with the grand <P-ϕ> distance of 1.537 Å. Brown and Shannon (1973) showed that variation in <M-O> distance correlates with bond-length distortion Δ (= Σ[l(o) – *l*(m)] / *l*(m); *l*(o) = observed bond-length, *l*(m) = mean bond-length) when the bond-valence curve of the constituent species shows a strong curvature, and when the range of distortion is large. There is no significant correlation between <P-ϕ> and Δ; this is in accord with the bond-valence curve for P-O given by Brown (1981).

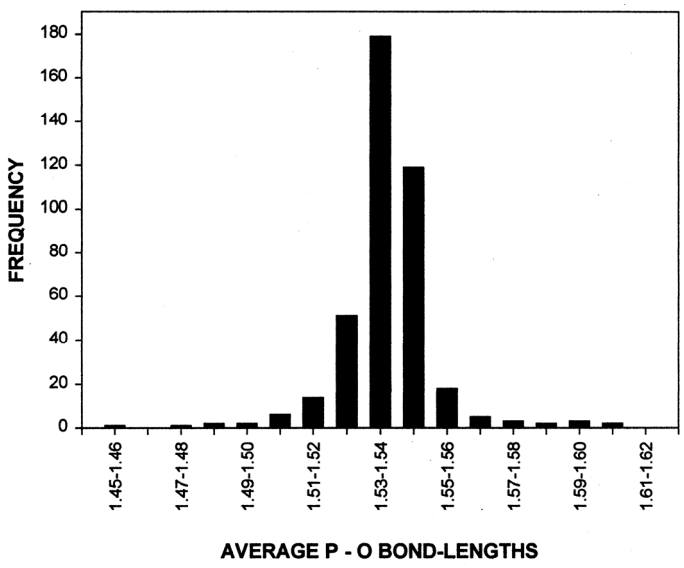

Figure 1. Variation in average P-O distance in minerals containing (Pϕ_4) tetrahedra.

Variation in P-ϕ distances

The variation in individual P-ϕ distances is shown in Figure 2; the grand mean P-ϕ distance is 1.537 Å, in close agreement with the value of 1.537 Å found by Baur (1974). The minimum and maximum observed P-ϕ distances are 1.439 and 1.625 Å, respectively, and the range of variation is 0.186 Å; the distribution is a skewed Gaussian. According to the bond-valence curve for P (the universal curve for second-row elements) from Brown (1981), the range of variation in P-ϕ bond-valence is 1.05-1.67 vu (valence units).

General polyhedral distortion in P-bearing minerals

Baur (1974) considered geometrical distortion in (PO_4) tetrahedra in great detail. In particular, he examined the variation in <P-ϕ> distance as a function of the mean coordination number of the simple anions of the phosphate group, and as a function of the dispersion of P-O distances, O-P-O angles and O-O angles from their respective mean values (described as distortion parameters). Baur (1970) found a correlation between <P-O> (corrected for dependence on the dispersion of the individual P-O distances from their mean value in the [PO_4] group) and the mean coordination numbers (including hydrogen bonds) of the constituent simple anions: <P-O> = 1.514(2) + 0.0059(7) CN, r = 0.49; the

amount of variation explained is 24% in a sample size of 211. The correlation is shown in Figure 3, together with the regression line and the ideal relation calculated from the anion radii of Shannon (1976).

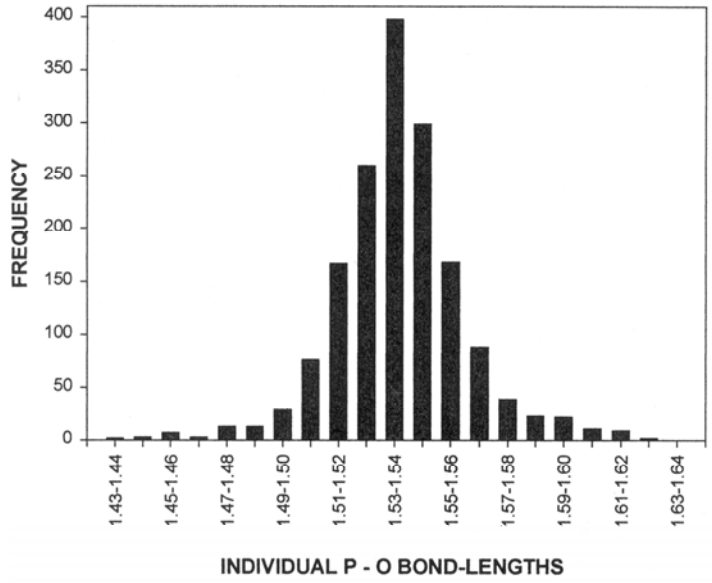

Figure 2. Variation in individual P-O distance in minerals containing ($P\phi_4$) tetrahedra.

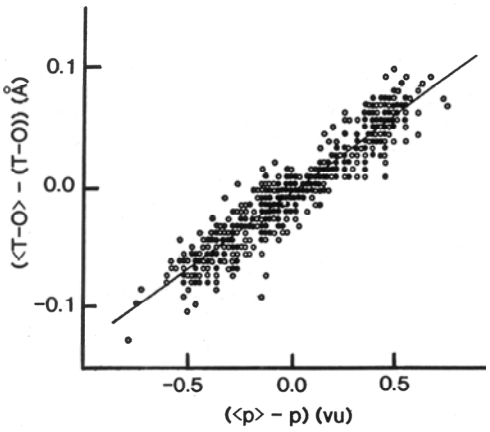

Figure 3. Variation in <T-O>-(T-O) for (PO_4) groups as a function of <p>-p, the deviation of the anion from exact agreement with Pauling's second rule; after Baur (1974).

Baur (1974) and Griffen and Ribbe (1979) have considered polyhedral distortions in general. Baur (1974) identified three types of distortion: (1) bond-length distortion; (2) bond-angle distortion; (3) polyhedron edge-length distortion, whereas Griffen and Ribbe (1979) considered two of these three distortion parameters, omitting bond-angle distortion. Baur (1974) showed that the variation in P-O distances (expressed as deviation from the <P-O> distance) correlates well with the deviation from ideal agreement with Pauling's second rule (Pauling 1929, 1960) (Fig. 4). This correlation is in accord with the general concepts of bond-valence theory (Brown and Shannon 1973; Brown 1981). Baur (1974) also showed that the dispersion (distortion) of P-O distances is much higher than the dispersion in corresponding O-O distances, and stated that the (PO_4) group can be "viewed, to a first approximation, as a rigid regular arrangement of O atoms, with the P atom displaced from their centroid".

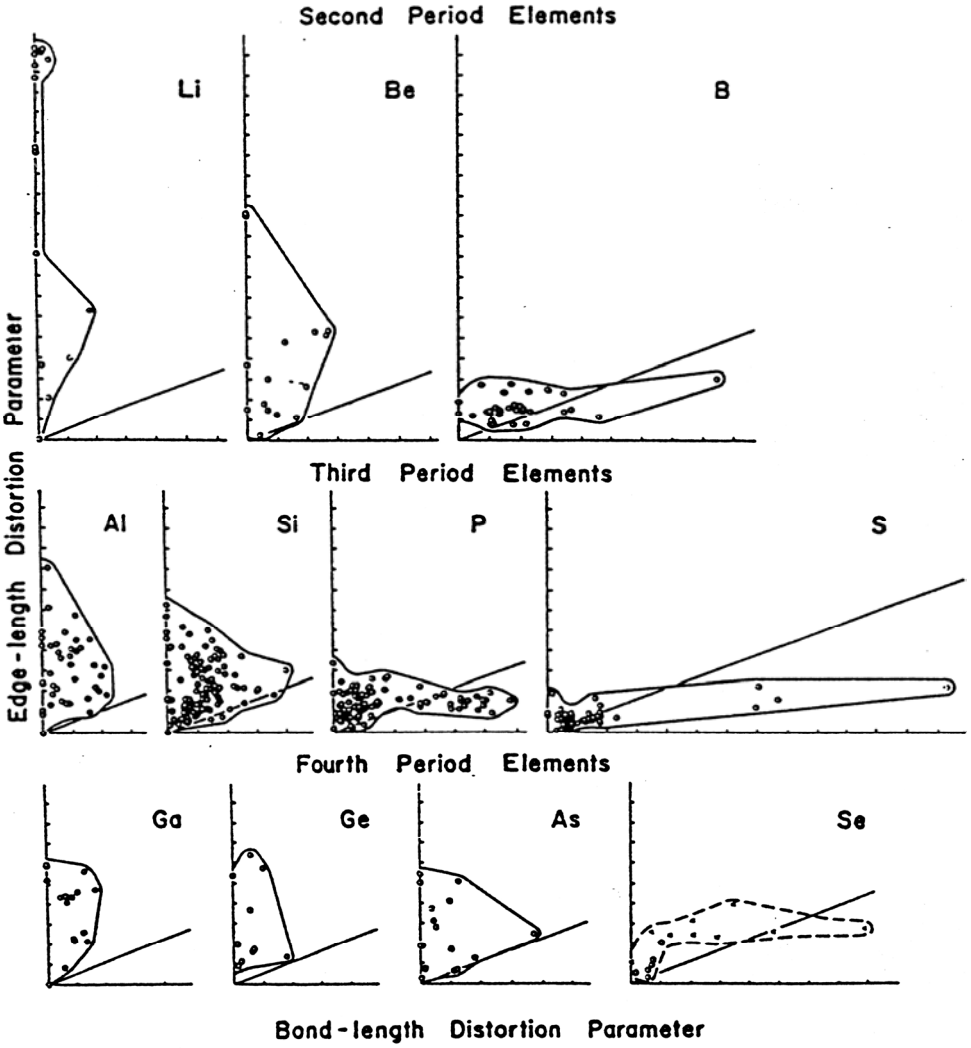

Figure 4. Variation in BLDP (Bond-Length Distortion Parameter) and ELDP (Edge-Length Distortion Parameter) for second-, third- and fourth-period non-transition elements in tetrahedral coordination by oxygen. Used by permission of E. Schweizerbart'sche Verlagsbuchhandlung, from Griffen and Ribbe (1979), *Neues Jarhrbuch für Mineralogie Abhandlungen*, Vol. 137, Fig. 2, p. 59.

Griffen and Ribbe (1979) considered two ways in which polyhedra may distort (i.e., depart from their holosymmetric geometry): (1) the central cation may displace from its central position [bond-length distortion]; (2) the anions may displace from their ideal positions [edge-length distortion]; these authors designate these as BLDP (Bond-Length Distortion Parameter) and ELDP (Edge-Length Distortion Parameter), respectively. Figure 4 shows the variation in both these parameters for the second-, third- and fourth-period (non-transition) elements in tetrahedral coordination. Some very general features of interest (Griffen and Ribbe 1979) are apparent from Figure 4:

(1) A BLDP value of zero only occurs for an ELDP value of zero; presuming that ELDP is a measure also of the O-T-O angle variation, this is in accord with the idea that variation in orbital hybridization (associated with variation in O-T-O angles) must accompany variation in bond-length.

(2) Large values of BLDP are associated with small values of ELDP, and vice versa. The variation in mean ELDP correlates very highly with the grand mean tetrahedral-edge length for each period (Fig. 5).

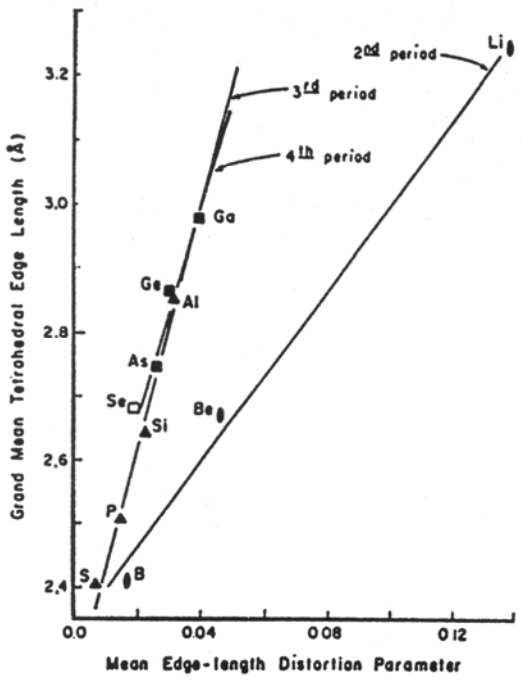

Figure 5. Variation in grand mean tetrahedral edge-length with mean ELDP for the second-, third- and fourth-period elements of the periodic table. Used by permission of E. Schweizerbart'sche Verlagsbuchhandlung, from Griffen and Ribbe (1979), *Neues Jarhrbuch für Mineralogie Abhandlungen*, Vol. 137, Fig. 6a, p. 65.

Griffen and Ribbe (1979) suggested that the smaller the tetrahedrally-coordinated cation, the more the tetrahedron of anions resists edge-length distortion because the anions are in contact, whereas the intrinsic size of the interstice is larger than the cation which can easily vary its cation-oxygen distances by 'rattling' within the tetrahedron. This general conclusion is in accord with the conclusion of Baur (1974) for the (PO_4) group.

HIERARCHICAL ORGANIZATION OF CRYSTAL STRUCTURES

The most fundamental characteristic of a mineral is its crystal structure, a complete description of which involves the identities, amounts and arrangement of atoms that constitute the mineral. The physical, chemical and paragenetic characteristics of a mineral arise as natural consequences of its crystal structure and the interaction of that structure with the environment in which it occurs. A structural hierarchy is an arrangement of crystal structures that reflects the systematic change in the character of their bond topologies. As the bond topology is a representation of the energetic characteristics of a structure (Hawthorne 1994, 1997), an adequate structural hierarchy of minerals should provide an epistemological basis for the interpretation of the role of minerals in Earth processes. This is not yet the case for any major class of minerals, but significant advances have been made. Bragg (1930) classified the major rock-forming silicate minerals according to the type of polymerization of ($Si,Al)O_4$ tetrahedra, and this scheme was extended by Zoltai (1960) and Liebau (1985); it is notable that this scheme parallels Bowen's reaction series (Bowen 1928) for silicate minerals in igneous rocks. Much insight can be derived from such structural hierarchies, particularly with regard to controls on bond topology (Hawthorne 1983a, 1994), mineral chemistry (Schindler and

Hawthorne 2001a,b; Schindler et al. 2002) and mineral paragenesis (Moore 1965b, 1973a; Hawthorne 1984, 1998; Hawthorne et al. 1987; Schindler and Hawthorne 2001c).

Hawthorne (1983a) proposed that structures be ordered or classified according to the polymerization of those cation coordination polyhedra with higher bond-valences. Higher bond-valence polyhedra polymerize to form *homo-* or *heteropolyhedral clusters* that constitute the *fundamental building block (FBB)* of the structure. The *FBB* is repeated, often polymerized, by translational symmetry operators to form the *structural unit*, a complex (usually anionic) polyhedral array (not necessarily connected) the excess charge of which is balanced by the presence of *interstitial* species (usually large, low-valence cations) (Hawthorne 1985a). The possible modes of cluster polymerization are obviously (1) unconnected polyhedra; (2) finite clusters; (3) infinite chains; (4) infinite sheets; (5) infinite frameworks.

POLYMERIZATION OF ($P\phi_4$) AND OTHER ($T\phi_4$) TETRAHEDRA

Bond valence is a measure of the strength of a chemical bond, and, in a coordination polyhedron, can be approximated by the formal valence divided by the coordination number (the Pauling bond-strength). Thus, in a (PO_4) group, the mean bond-valence is 5/4 = 1.25 vu. The valence-sum rule (Brown 1981) states that the sum of the bond valences incident at an atom is equal to the magnitude of the formal valence of that atom. Thus any oxygen atom linked to the central P cation receives ~1.25 vu from that cation, and hence must receive ~0.75 vu from other coordinating cations. Hence an oxygen atom is unlikely to link to two P atoms as it would receive, on average, $2 \times 1.25 = 2.50$ vu and the linking oxygen atom would violate the valence-sum rule. For this reason (PO_4) groups are unlikely to polymerize in crystal structures. This conclusion is not completely followed, as there are three (very rare) minerals in which (PO_4) groups polymerize [canaphite: $Na_2Ca[P_2O_7]$ $(H_2O)_4$, wooldridgeite: $Na_2CaCu^{2+}{}_2[P_2O_7]_2(H_2O)_{10}$ and kanonerovite: $Ma_3Mn^{2+}[P_3O_{10}](H_2O)_{12}]$, and polyphosphates are common among synthetic compounds (Corbridge 1985). It was commonly thought that polyphosphates would be unstable in the presence of any H-bearing species as H would attack the bridging anion, resulting in depolymerization. However, the common existence of hydrated polyphosphates (Corbridge 1985) vitiates this argument. The only attempt to consider this problem in any detail is due to Byrappa (1983) who presented very limited experimental data and concluded that polyphosphates cannot form under hydrothermal conditions with $P(H_2O) > 6$ atm. This conclusion accounts for the absence of condensed phosphates in many phosphate parageneses (e.g., granitic pegmatites). However, many phosphate minerals crystallize under surficial conditions and yet only three minerals with polymerized phosphate groups are currently known. Our lack of understanding concerning this issue is obviously an important gap in our knowledge of phosphate crystal chemistry. Suffice it to say here that polymerized (PO_4) groups are sufficiently rare in minerals that phosphates cannot be classified in an analogous way to silicates (i.e., by the polymerization characteristics of the principal oxyanion).

The simple anions of a (PO_4) group each require ~0.75 vu to satisfy their bond-valence requirements. What type of linkage with other tetrahedral oxyanions is possible with this constraint? Obviously, any tetrahedral oxyanion with a mean bond-valence of $\leq$0.75 vu, which includes (AlO_4), (BO_4), (BeO_4) and (LiO_4) groups. Moreover, P-O bonds in specific structural arrangements may have bond valences somewhat less that 1.25 vu, raising the possibility that (PO_4) groups might polymerize with (SiO_4) groups. Phosphates show all of these particular polymerizations, in accord with the valence-sum rule.

POLYMERIZATION OF ($P\phi_4$) TETRAHEDRA AND OTHER ($M\phi_N$) POLYHEDRA

In oxysalt minerals, the coordination number of oxygen is most commonly [3] or [4]. This being the case, the *average* bond-valence incident at the oxygen atom bonded to one P cation is ~0.75/3 = 0.25 vu and ~0.75/2 = 0.38 vu for the other cation-oxygen bonds. The more common non-tetrahedrally coordinated cations available in geochemical systems are [6]-coordinated divalent (e.g., Mg, Fe^{2+}, Mn^{2+}) and trivalent (e.g., Al, Fe^{3+}) cations, and [7]- and higher coordinated monovalent (e.g., Na, K) and divalent (e.g., Ca, Sr) cations. The average bond-valences involved in linkage to these cations are $^{[6]}M^{2+} \approx 0.33$, $^{[6]}M^{3+} \approx 0.50$, $^{[7]}M^{1+} \approx 0.14$, $^{[7]}M^{2+} \approx 0.29$ vu. Hence, (PO_4) groups link easily to all of these cations, particularly in hydroxy-hydrated phosphates where hydrogen bonds (0.1-0.3 vu) commonly supply additional bond-valence to the (simple) anions of the structure.

A STRUCTURAL HIERARCHY FOR PHOSPHATE MINERALS

This promiscuous polymerization suggests that we should classify the phosphates according to the types of polymerization of their principal coordination polyhedra, as suggested by Hawthorne (1983a, 1998) and discussed briefly above. The most common polymerizations in phosphate minerals are between tetrahedra and tetrahedra, between tetrahedra and octahedra, and between tetrahedra and large-cation polyhedra (i.e., [7]-coordinated and above). Hence we will divide the phosphates into the following three principal groups, involving

(1) polymerization of tetrahedra;

(2) polymerization of tetrahedra and octahedra;

(3) polymerization of tetrahedra and > [6]-coordinated polyhedra.

Large-cation polyhedra occur in group (1) and group (2) phosphates, as cations such as Al and Ca often occur together in minerals. In principle, octahedra should not occur (by definition) in group (3) phosphates; however, in some cases, the structural affinity of the mineral indicates it to be a large-cation phosphate mineral (e.g., whitlockite, $Ca_{18}Mg_2(PO_4)_{12}(PO_3\{OH\})_2$).

In accord with the above discussion, phosphate minerals are classified into three distinct groups. The first group, involving polymerization of ($T\phi_4$) tetrahedra (T = P plus Be, Zn, B, Al and Si), is fairly small, in accord with the observation that mixed oxyanion minerals are uncommon. The second group, involving polymerization of (PO_4) tetrahedra and ($M\phi_6$) octahedra, is very large. Within this group, the structures are arranged as suggested by Hawthorne (1983a), similar to the classification of the sulfate minerals given by Hawthorne et al. (2000), according to the mode of polymerization of the tetrahedra and octahedra: (1) unconnected polyhedra; (2) finite clusters of polyhedra; (3) infinite chains of polyhedra; (4) infinite sheets of polyhedra; (5) infinite frameworks of polyhedra. Within each class, structures are arranged in terms of increasing connectivity of the constituent polyhedra of the structural unit. Detailed chemical and crystallographic information, together with references, are given in Appendix A. In the following figures, (PO_4) groups are dashed-line-shaded, and cell dimensions with an arrow on one end only are (slightly) tilted to the plane of the figure.

STRUCTURES WITH POLYMERIZED ($T\phi_4$) GROUPS

As noted above, (PO_4) tetrahedra can polymerize with other (PO_4) groups, plus tetrahedrally coordinated Be, Zn, B, Al and Si. However, in minerals, only the following polymerizations are known: (PO_4)-(PO_4), (PO_4)-($Be\phi_4$), (PO_4)-(ZnO_4) and (PO_4)-(AlO_4).

Although there seems no obvious reason why (PO_4) should not polymerize with ($B\phi_4$) or ($Si\phi_4$) groups, this has not been observed, although there are several minerals containing both (PO_4) and ($B\phi_4$) or ($Si\phi_4$) groups in which the different polyhedra do not polymerize.

Table 1. Phosphate minerals* based on ($T\phi_4$) clusters.

Mineral	***Cluster***	***Space group***	*Figure*
Canaphite	$[P_2O_7]$	*Pc*	6a,b
Wooldridgeite	$[P_2O_7]$	*Fdd*2	6c,d,e
Kanonerovite	$[P_3O_{10}]$	$P2_1/n$	7a
"Pyrocoproite"**	P_2O_7	–	–
"Pyrophosphate"**	P_2O_7	–	–
"Arnhemite"**	P_2O_7	–	–
Gainesite *	$[Be(PO_4)_4]$	$I4_1/amd$	7b
McCrillisite	$[Be(PO_4)_4]$	$I4_1/amd$	7b
Selwynite	$[Be(PO_4)_4]$	$I4_1/amd$	7b

* For isostructural minerals, the name of the group is indicated by a * in this and all following tables;
** These names are used in the literature, but have not been approved by CNMMN of IMA.

Finite clusters of tetrahedra

The minerals in this class (Table 1) are dominated by polymerized (PO_4) groups; only in gainesite do (PO_4) tetrahedra polymerize with another type of ($T\phi_4$) group.

In **canaphite**, $Na_2Ca(H_2O)_4[P_2O_7]$, (PO_4) tetrahedra link to form $[P_2O_7]$ groups in the eclipsed configuration. When viewed down [100], the structure consists of layers of ($Na\phi_6$) and ($Ca\phi_6$) octahedra intercalated with intermittent layers of $[P_2O_7]$ groups (Fig. 6a). The layers of octahedra are not completely continuous (Fig. 6b); staggered α-PbO_2-like chains of ($Na\phi_6$) octahedra extend along *a* and are linked in the *b*-direction by ($Ca\phi_6$) octahedra to form a sheet of octahedra punctuated by dimers of vacant octahedra. Additional linkage is provided by an extensive network of hydrogen bonds involving the (H_2O) groups of the ($CaO_5\{H_2O\}$) and ($NaO_3\{H_2O\}_3$) octahedra.

In **wooldridgeite**, $Na_2Ca(H_2O)_6[Cu^{2+}{}_2(P_2O_7)_2(H_2O)_2](H_2O)_2]$, $[P_2O_7]$ groups occur in the eclipsed configuration. A key part of the wooldridgeite structure is the $[Cu^{2+}(P_2O_7)(H_2O)]$ chain (Fig. 6c) in which ($Cu\phi_6$) octahedra link by sharing one set of *trans* ligands (H_2O) to form a 7-Å chain (Moore 1970), decorated by $[P_2O_7]$ groups, that extends along [101] (and [10$\bar{1}$]). Each chain is flanked by a chain of corner-sharing ($Na\phi_6$) octahedra in which the Na- ϕ-Na linkage is through *cis* vertices and each ($Na\phi_6$) octahedron shares an edge with a ($Cu\phi_6$) octahedron, and these chains are linked in the [10$\bar{1}$] direction into a sheet by ($Ca\phi_6$) octahedra (Fig. 6d). These sheets stack along the [010] direction (Fig. 6e), with each sheet rotated 90° with respect to the adjacent sheets.

In **kanonerovite**, $Na_3Mn^{2+}[P_3O_{10}](H_2O)_{12}$, three ($PO_4$) tetrahedra link into a $[P_3O_{10}]$ fragment. All three (PO_4) tetrahedra of this trimeric group share one vertex with the same ($Mn^{2+}\phi_6$) octahedron (Fig. 7a) to form an $[Mn^{2+}(H_2O)_3P_3O_{10}]$ cluster. ($Na\phi_6$) octahedra

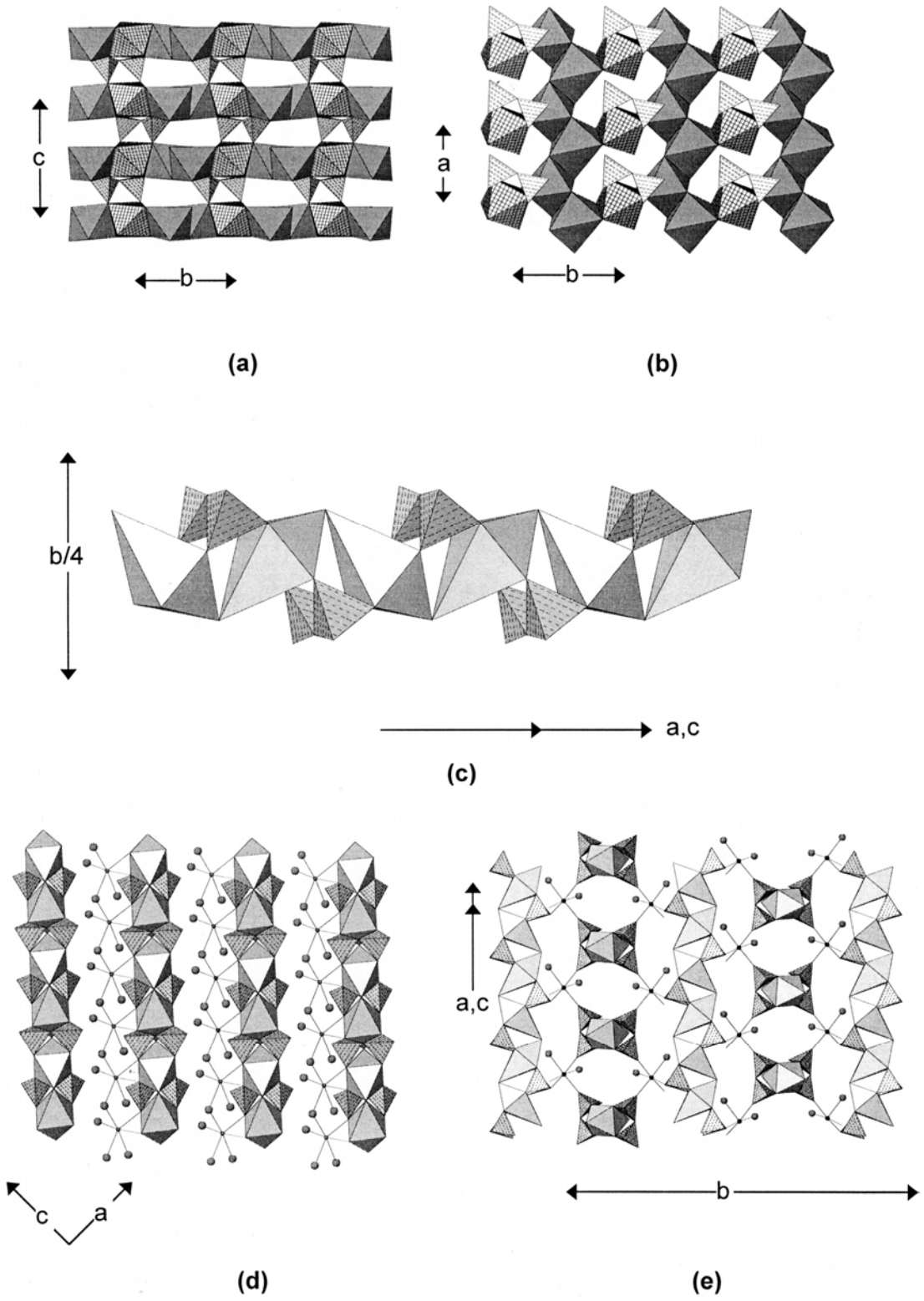

Figure 6. The crystal structures of canaphite and wooldridgeite: (a) canaphite projected onto (100); (b) canaphite projected onto (001); (Caϕ_6) octahedra are 4^4-net-shaded, (Naϕ_6) octahedra are shadow-shaded; (c) a perspective view of the $[Cu^{2+}(P_2O_7)(H_2O)]$ chain in wooldridgeite; (d) wooldridgeite projected onto (010); (e) wooldridgeite, showing two orthogonal sets of $[Cu^{2+}(P_2O_7)(H_2O)]$ chains; ($Cu^{2+}\phi_6$) octahedra are shadow-shaded, Na atoms are shown as small dark circles, (H_2O) groups are shown as large shaded circles.

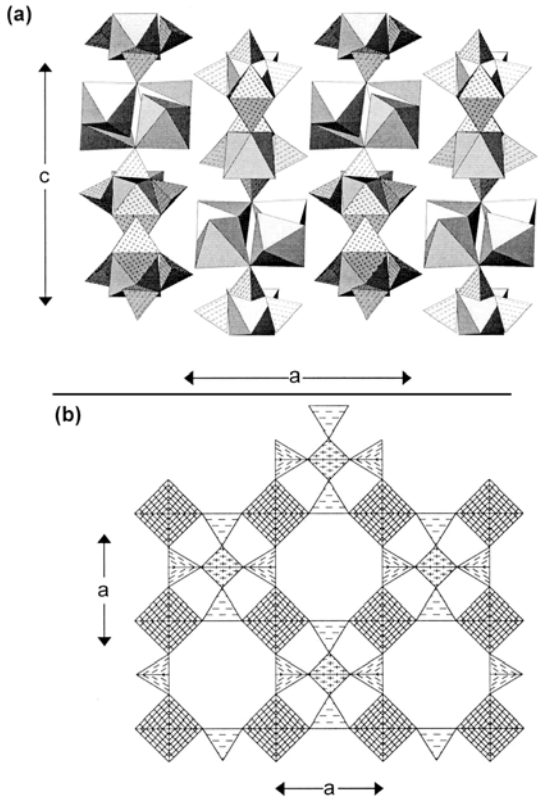

Figure 7. The crystal structures of kanonerovite and gainesite: (a) kanonerovite projected onto (010) showing the $[P_3O_{10}]$ trimers linked to $(Mn^{2+}\phi_6)$ octahedra (dot-shaded); the resulting clusters are linked by $(Na\phi_6)$ octahedra (shadow-shaded) and by hydrogen bonding involving (H_2O) groups (not shown); (b) the $[BeP_4O_{16}]$ pentamer that is the finite tetrahedron cluster in gainesite linked by (ZrO_6) octahedra (4^4-net-shaded).

link by sharing vertices to form clusters that link $[Mn^{2+}(H_2O)_3P_3O_{10}]$ clusters adjacent in the *c*-direction. All other linkage is via hydrogen bonds emanating from the (H_2O) groups of the $[Mn^{2+}(H_2O)_3P_3O_{10}]$ cluster and involving interstitial (H_2O) groups.

In **gainesite**, $Na_2Zr_2[Be(PO_4)_4]$, and the isostructural minerals **mccrillisite**, $Cs_2Zr_2[Be(PO_4)_4]$, and **selwynite**, $Na_2Zr[Be(PO_4)_4]$, a (BeO_4) tetrahedron links to four (PO_4) tetrahedra to form the pentameric cluster $[BeP_4O_{16}]$ that is topologically identical to the $[Si_5O_{16}]$ cluster in zunyite, $Al_{13}O_4[Si_5O_{16}](OH)_{18}Cl$. These clusters are linked in a continuous framework through (ZrO_6) octahedra (Fig. 7b). The Be and P sites in the gainesite structure are only half-occupied, and in the tetrahedral-octahedral framework, tetrahedral clusters alternate with cavities occupied by interstitial Na atoms.

Infinite chains of tetrahedra

The minerals in this class can be divided into two broad groups based on the (bond valence) linkage involved in the infinite chains. Minerals of this class are listed in Table 2.

Moraesite, $[Be_2(PO_4)(OH)](H_2O)_4$, contains chains (ribbons) of (PO_4) and (BeO_4) tetrahedra. The (PO_4) tetrahedra are four-connected and the (BeO_4) tetrahedra are three-connected, and the resulting $[Be_2(PO_4)(OH)]$ ribbons extend along the *c*-direction (Fig. 8a). These ribbons form a face-centered array (Fig. 8b) and are linked by hydrogen bonds involving interstitial (H_2O) groups.

Table 2. Phosphate minerals based on ($T\phi_4$) chains.

Mineral	*Chain*	*Space Group*	*Figure*
Moraesite	$[Be_2(PO_4)(OH)]$	$C2/C$	8a,b
Väyrynenite	$[Be(PO_4)(OH)]$	$P2_1/A$	8c,d
Fransoletite	$[Be_2(PO_4)_2(PO_3\{OH\})_2]$	$P2_1/A$	9a,b
Parafransoletite	$[Be_2(PO_4)_2(PO_3\{OH\})_2]$	$P\bar{1}$	–
Roscherite	$[Be_4(PO_4)_6(OH)_6]$	$C2/C$	9c,d
Zanazziite	$[Be_4(PO_4)_6(OH)_6]$	$C2/C$	9c,d
Spencerite	$[Zn(PO_4)(OH)(H_2O)]$	$P2_1/C$	9e,f

Väyrynenite, $Mn^{2+}[Be(PO_4)(OH)]$, contains chains of (PO_4) and (BeO_4) tetrahedra extending in the *a*-direction (Fig. 8c). (BeO_4) tetrahedra link by corner-sharing to form a pyroxenoid-like [TO_3] chain that is decorated on both sides by (PO_4) tetrahedra to form a ribbon in which the (BeO_4) tetrahedra are four-connected and the (PO_4) tetrahedra are two-connected. These ribbon-like chains are linked by edge-sharing pyroxene-like chains of ($Mn^{2+}O_6$) octahedra that also extend parallel to the *a*-axis. The resulting structural arrangement consists of modulated sheets of tetrahedra and octahedra (Fig. 8d).

The dimorphs, **fransoletite** and **parafransoletite**, have the composition $Ca_3[Be_2(PO_4)_2(PO_3\{OH\})_2](H_2O)_4$. The principal motif in each structure is a complex chain consisting of four-membered rings of alternating (PO_4) and (BeO_4) tetrahedra that link through common (BeO_4) tetrahedra; these chains extend in the *a*-direction (Fig. 9a). Viewed end-on (Fig. 9b), the chains form a square array and are linked by [6]- and [7]-coordinated Ca atoms that form sheets parallel to {001}; further interchain linkage occurs through H-bonding involving (H_2O) groups. The fransoletite and parafransoletite structures differ only in the relative placement of the octahedrally coordinated Ca atom and the disposition of adjacent chains along their length (Kampf 1992).

Roscherite and **zanazziite** are composed of very convoluted chains of $Be\phi_4$ and (PO_4) tetrahedra extending in the [101] direction (Fig. 9c; note that in this view, the two chains appear to join at a mirror plane parallel to their length; however, the plane in question is a glide plane and the two chains are displaced in the *c*-direction). The chain consists of four-membered rings of alternating $Be\phi_4$ and (PO_4) tetrahedra linked through (PO_4) tetrahedra that are not members of these rings (Fig. 9c). These chains are linked by ($\underline{Al}$,□)O_6 and (Mg,Fe^{2+})O_6 octahedra that form edge-sharing chains parallel to [110] and [1$\bar{1}$0]; the octahedral chains link to each other in the [001] direction by sharing *trans* vertices (Fig. 9d). The resultant octahedral-tetrahedral framework is strengthened by [7]-coordinated Ca occupying the interstices.

The structure and composition of these minerals is not completely understood. Roscherite (Slavík 1914) is the Mn^{2+}-dominant species and zanazziite (Leavens et al. 1990) is the Mg-dominant species. Lindberg (1958) also reported an Fe^{2+}-dominant species from the Sapucaia pegmatite, Minas Gerais, that is currently unnamed. The situation is complicated by the fact that the original crystal-structure determination of roscherite (Fanfani et al. 1975) was done on a crystal of what was later determined to be *zanazziite* with the ideal end-member formula $Ca_2Mg_4(Al_{0.67}G_{0.33})_2[Be_4(PO_4)_6(OH)_6](H_2O)_4$. Fanfani et al. (1977) report a triclinic structure for roscherite that is Mn^{2+}

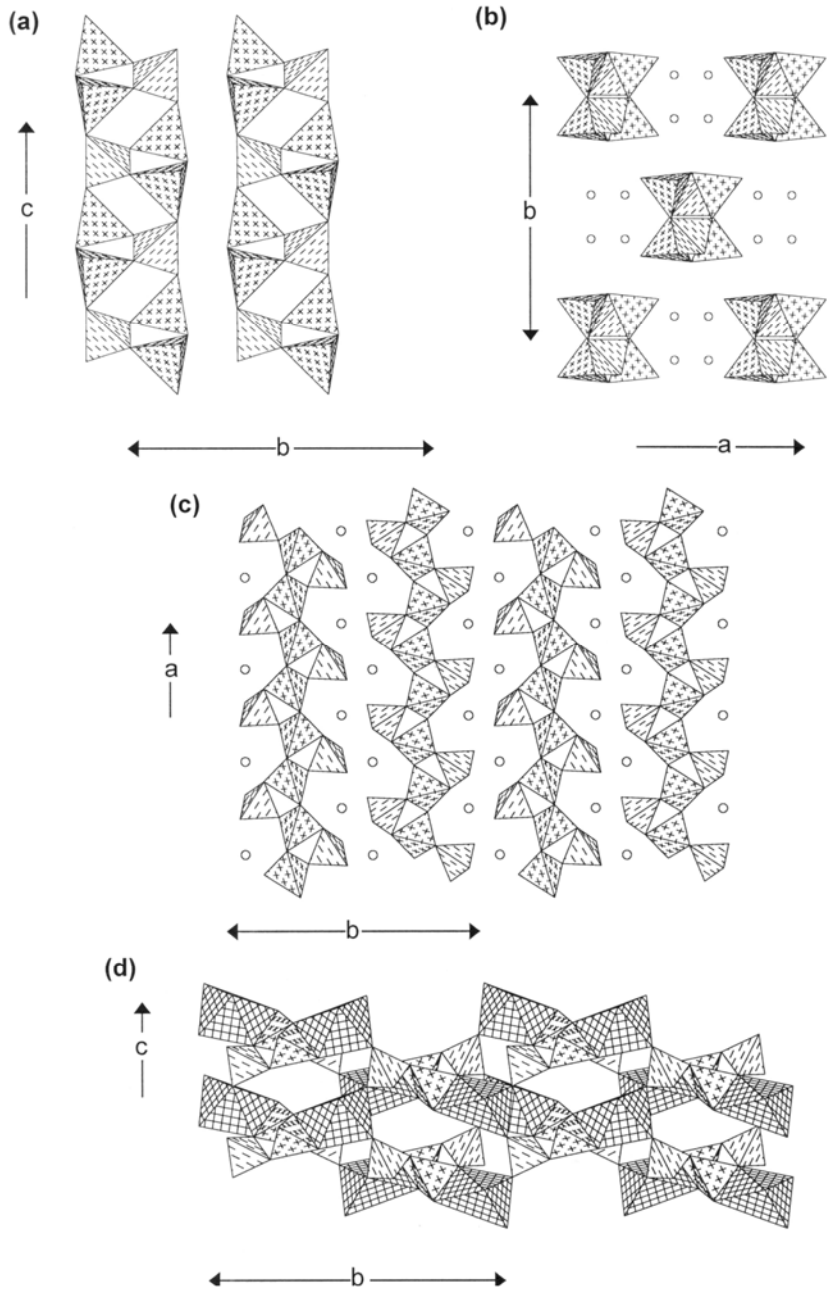

Figure 8. The crystal structures of moraesite and väyrynenite: (a) moraesite projected down the *a*-axis; (b) moraesite projected down the *c*-axis; (BeO_4) tetrahedra are cross-shaded, (H_2O) groups are shown as circles; (c) väyrynenite projected down the *c*-axis; Al atoms are shown as circles; (d) väyrynenite projected down the *a*-axis.

dominant, i.e., *roscherite* with the ideal end-member formula $Ca_2Mn^{2+}{}_4(Fe^{3+}{}_{0.67}G_{0.33})(G)[Be_4(PO_4)_6(OH)_4(H_2O)_2](H_2O)_4$. Note that the trivalent-cation content ($Al_{1.33}$ vs. $Fe^{3+}{}_{0.67}$) and type are different in the two species, and electroneutrality is maintained by replacement of OH by H_2O via the exchange Fe^{3+} + □ (vacancy) + 3 $H_2O \rightarrow Al^{3+}{}_2$ + 3 OH. Whether the monoclinic → triclinic transition is caused by the $Mn^{2+} \rightarrow$ Mg replacement or by the reaction noted above is not yet known.

Spencerite, $Zn_2[Zn(OH)(H_2O)(PO_4)]_2(H_2O)$, contains simple linear chains of alternating ($Zn\phi_4$) [$\phi_4 = O_2(OH)(H_2O)$] and (PO_4) tetrahedra extending along the *c*

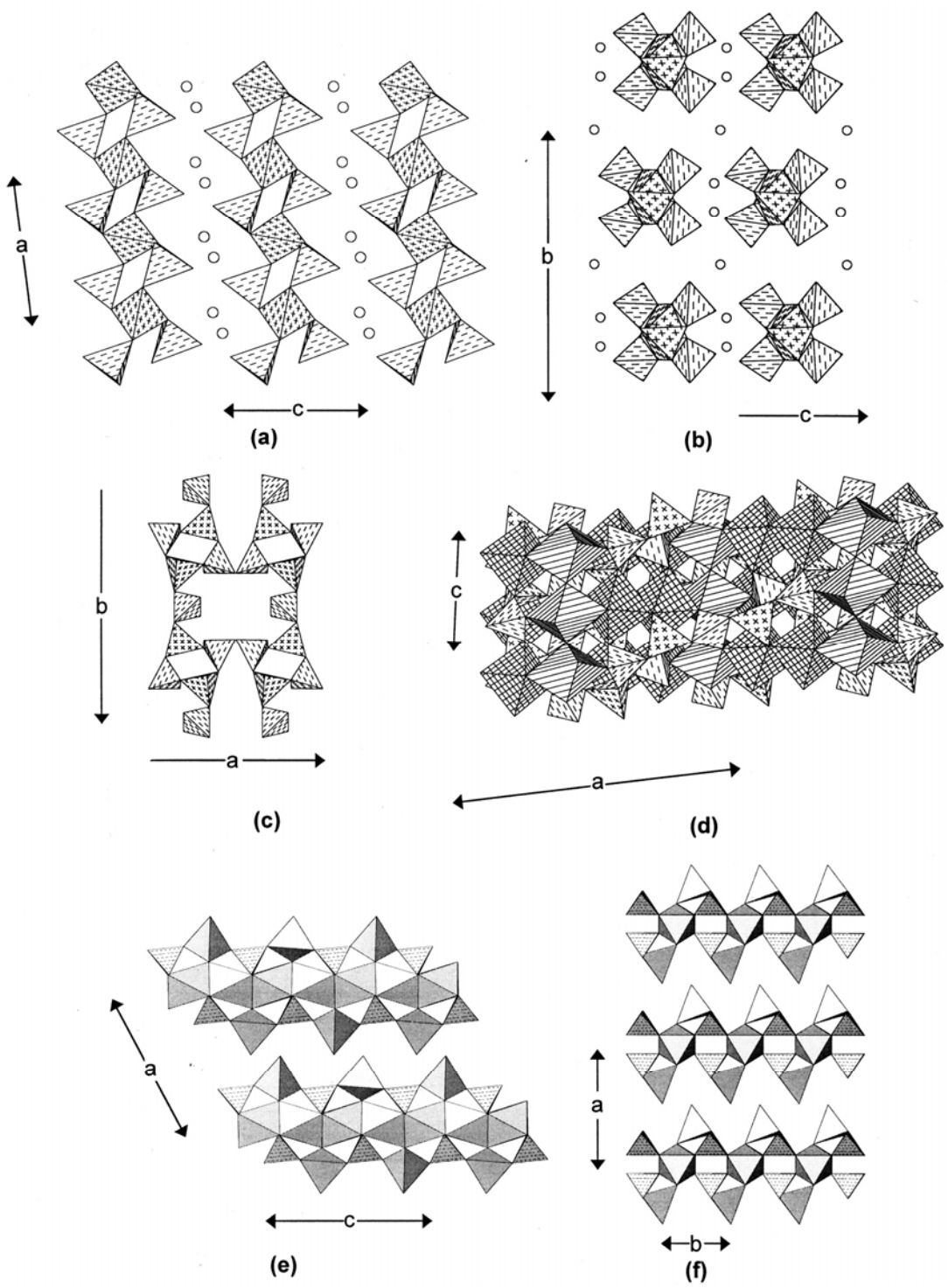

Figure 9. The crystal structures of fransoletite, roscherite and spencerite: (a) fransoletite projected onto (010); Mn^{2+} atoms are shown as circles; (b) fransoletite projected down the *a*-axis; a view in which the chains are seen end-on; (c) the structural unit in roscherite projected down the *c*-axis; note that the (PO_4) tetrahedra in the center of the figure do *not* share a common anion, but are separated in the *c*-direction; (d) roscherite projected onto (010); note that the trivalent octahedra (4^4-net-shaded) are only two-thirds occupied (by Al) and that Ca atoms are omitted for clarity; (e) spencerite projected onto (010); (f) spencerite projected onto (001); chains of (PO_4) and (ZnO_4) are seen 'end-on'.

Table 3. Phosphate minerals based on ($T\phi_4$) sheets.

Mineral	*Sheet*	*Space group*	*Figure*
Herderite	$[Be(PO_4)(OH)]$	$P2_1/a$	10a,b
Hydroxylherderite	$[Be(PO_4)(OH)]$	$P2_1/a$	10a,b
Uralolite	$[Be_4P_3O_{12}(OH)_3]$	$P2_1/n$	10c,d
Ehrleite	$[BeZn(PO_4)_2(PO_3\{OH\})]$	$P\bar{1}$	10e,f
Hopeite	$[Zn(PO_4)]$	$Pnma$	11a,b
Parahopeite	$[Zn(PO_4)]$	$P\bar{1}$	11c,d
Phosphophyllite	$[Zn(PO_4)]$	$P2_1/c$	12a,b
Veszelyite	$[Zn(PO_4)(OH)]$	$P2_1/a$	12c,d
Kipushite	$[Cu^{2+}{}_5Zn(PO_4)_2(OH)_6(H_2O)]$	$P2_1/c$	12e,f
Scholzite	$[Zn(PO_4)]$	$Pbc2_1$	13a,b
Parascholzite	$[Zn(PO_4)]$	$I2/c$	13c,d

direction (Fig. 9e) and cross-linked into heteropolyhedral sheets by ($Zn\phi_6$) octahedra. These sheets are also shown in Figure 9f, where it can be seen that the ($Zn\phi_6$) octahedra share all their vertices with ($Zn\phi_4$) and (PO_4) tetrahedra. The heteropolyhedral sheets link solely via hydrogen bonding that involves one (H_2O) group (not shown in Figs. 9e or 9f) held in the structure solely by hydrogen bonding.

Infinite sheets of tetrahedra

The minerals in this class (Table 3) can be divided into two groups: (PO_4)-(BeO_4) linkages, and (PO_4)-(ZnO_4) linkages.

Hydroxylherderite, $Ca[Be(PO_4)(OH)]$ and **herderite**, $Ca[Be(PO_4)F]$, are isostructural, although the structures were reported in different orientations, $P2_1/c$ and $P2_1/a$, respectively. The sheet unit consists of (PO_4) and ($Be\phi_4$) tetrahedra at the vertices of a two-dimensional net (Fig. 10a). Four-membered rings of alternating (PO_4) and ($Be\phi_4$) tetrahedra link directly by sharing vertices between (PO_4) and ($Be\phi_4$) tetrahedra; thus the sheet can be considered to be constructed from chains of four-membered rings that extend in the [110] and [1$\bar{1}$0] directions (Fig. 10a). These sheets stack in the *c*-direction (Fig. 10b) and are linked by layers of [8]-coordinated Ca atoms. Note that the structure reported by Lager and Gibbs (1974) seems to have been done on hydroxylherderite rather than herderite.

Uralolite, $Ca_2[Be_4P_3O_{12}(OH)_3](H_2O)_5$, contains ($PO_4$) and ($BeO_4$) tetrahedra linked into a sheet (Fig. 10c). Eight-membered rings of tetrahedra (P-Be-P-Be-P-Be-P-Be) link through common (PO_4) groups to form chains that extend along [101]. These chains link in the (010) plane via sharing of tetrahedral vertices, forming three-membered (Be-Be-Be and Be-Be-P) and four-membered (Be-Be-Be-P) rings. Interstitial [7]-coordinated Ca atoms lie within the eight-membered rings (in projection). The layers stack along the *b*-direction (Fig. 10d) and are linked by Ca atoms (circles) and H-bonding; in this view, the three- and four-membered rings are easily seen.

Ehrleite, $Ca_2[BeZn(PO_4)_2(PO_3\{OH\})](H_2O)_4$, has a very complicated sheet of tetrahedra, both from topological and chemical viewpoints. There is one distinct (BeO_4) tetrahedron that links to four ($P\phi_4$) groups (Fig. 10e); similarly, there is one (ZnO_4) tetrahedron and this links to four ($P\phi_4$) groups. The ($P\phi_4$) groups link only to three or two other tetrahedra. Four-membered rings of alternating (PO_4) and (BeO_4) tetrahedra link

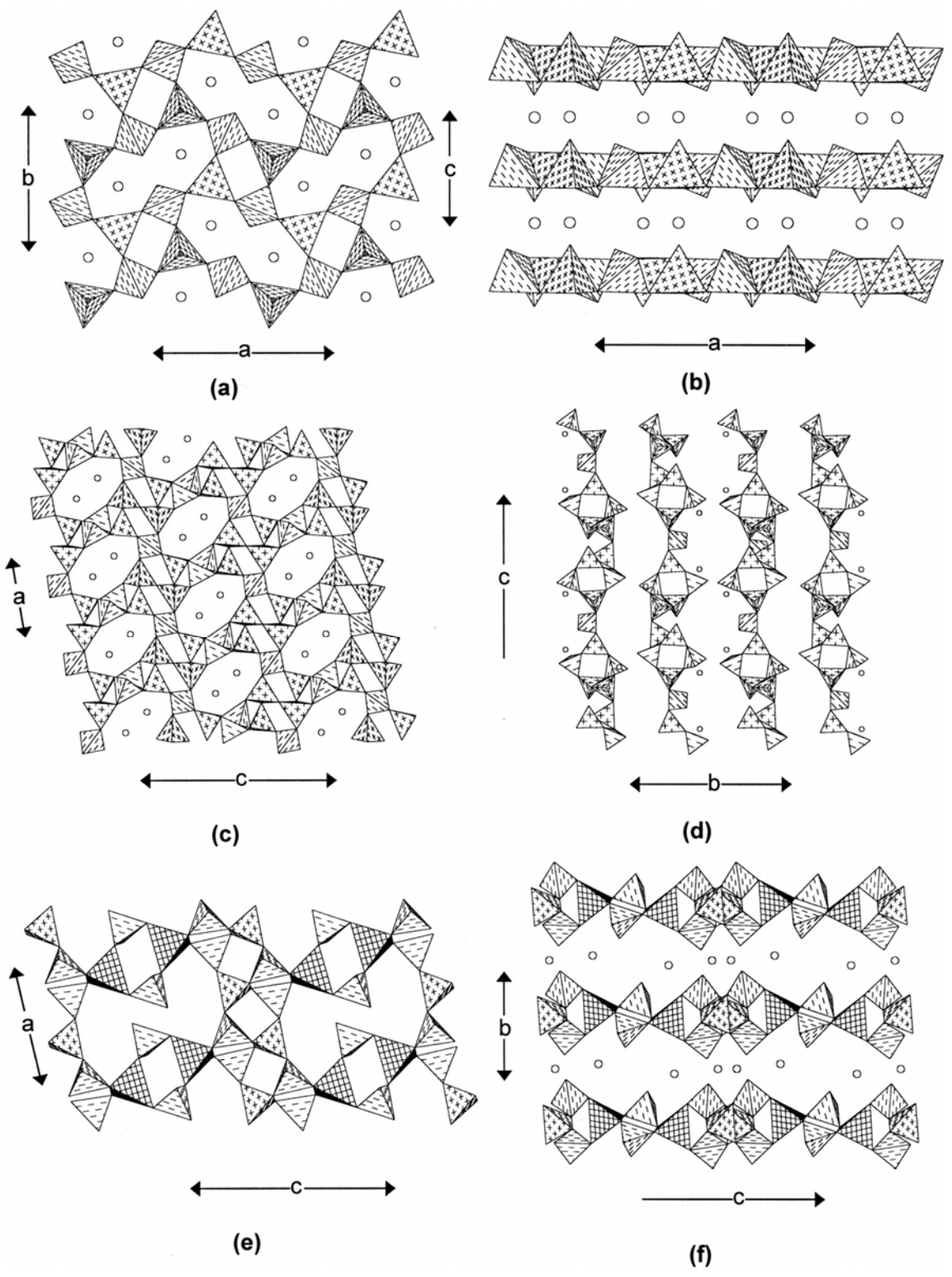

Figure 10. The crystal structures of herderite, uralolite and ehrleite: (a) herderite projected onto (001); (b) herderite projected onto (010); (c) uralolite projected onto (010); (d) uralolite projected down the *a*-axis; (e) the structural unit in ehrleite projected onto (010); (ZnO_4) tetrahedra are 4^4-net-shaded; (f) ehrleite projected down the *a*-axis. Ca atoms are shown as circles.

through common (BeO_4) tetrahedra to form chains in the *a*-direction (Fig. 10e). These chains are linked in the *c*-direction by four-membered rings of alternating (PO_4) and (ZnO_4) tetrahedra to form additional four-membered rings (Zn-P-Be-P). The result is an open sheet, parallel to (010), with buckled twelve-membered rings (Fig. 10e) into which project the H atoms of the acid-phosphate groups. These sheets stack along the *b*-direction (Fig. 10f) and are linked together by [7]-coordinated and [8]-coordinated interstitial Ca atoms.

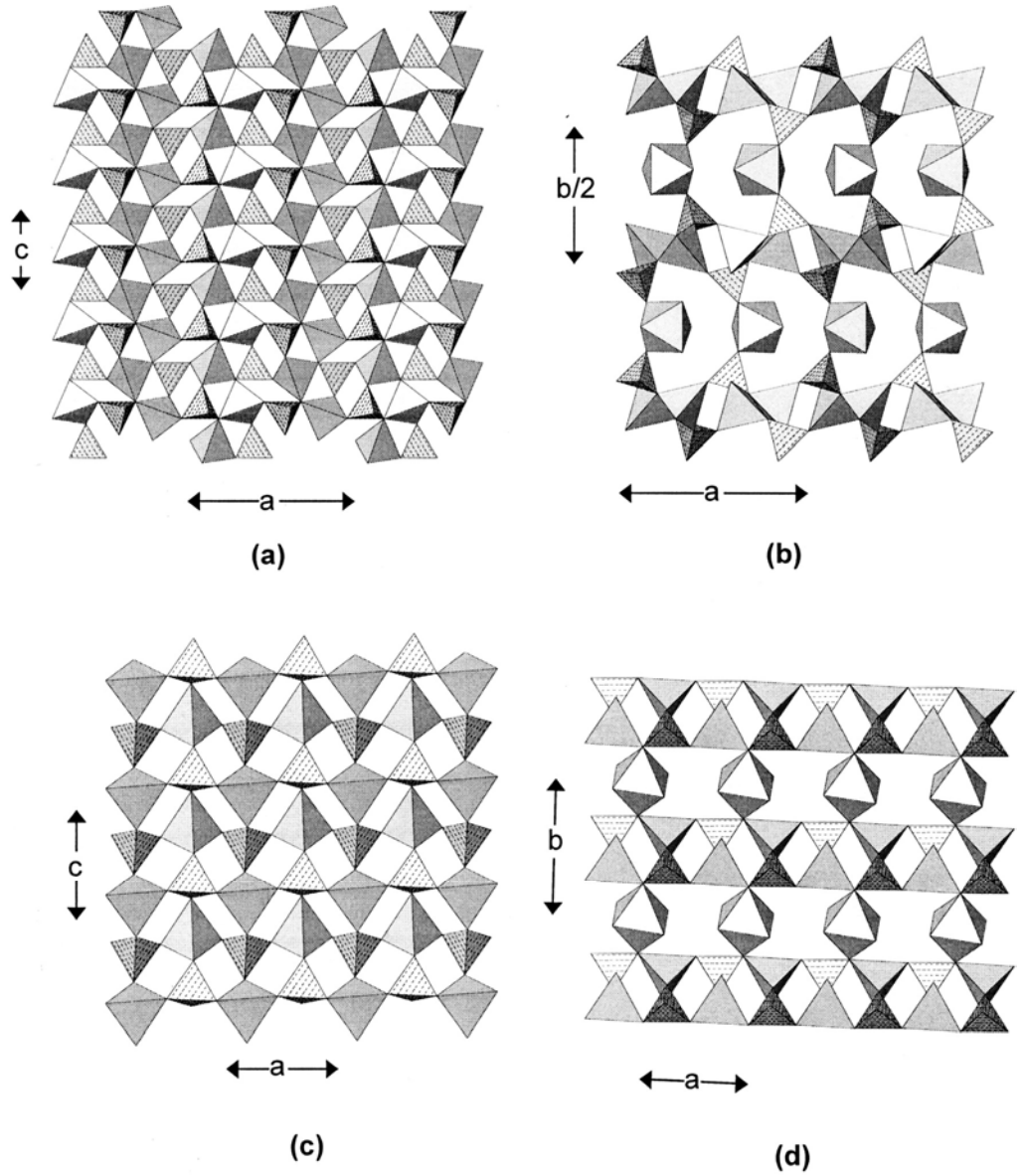

Figure 11. The crystal structures of hopeite and parahopeite: (a) hopeite projected onto (010); (b) hopeite projected onto (001); hydrogen bonds are omitted for clarity; (c) parahopeite projected onto (010); (d) parahopeite projected onto (001). ($Zn\phi_4$) tetrahedra and ($Zn\phi_6$) octahedra are shadow-shaded.

In **hopeite**, $Zn(H_2O)_4[Zn(PO_4)]_2$, kinked chains of ($Zn\phi_4$) tetrahedra extend in the *c*-direction, and adjacent chains are linked by (PO_4) tetrahedra to form a sheet parallel to (101) (Fig. 11a). The (ZnO_4) tetrahedra are four-connected, but the (PO_4) tetrahedra are only three-connected; this difference in connectivity is very important as it promotes structural linkage perpendicular to the sheet. A continuous sheet with this connectivity

requires unusual coordination numbers for some of the simple anions of the sheet: for the (PO_4) group, the anion coordination numbers within the sheet are [1], [2] × 2 and [3], and for the (ZnO_4) group, the anion coordination numbers within the sheet are [2] × 2 and [3] × 2. Hence the sheet is quite corrugated, as can be seen in Figure 11b: the (ZnO_4) tetrahedra form a central layer and the (PO_4) tetrahedra form two outer (or sandwiching) layers. The sheets are linked in the *b*-direction by ($ZnO_2\{H_2O\}_4$) octahedra (Fig. 11b), the [1]-coordinated anion of the phosphate group forming a ligand of the linking $^{[6]}$Zn cation. In **parahopeite**, $Zn(H_2O)_4[Zn(PO_4)]_2$, (PO_4) and (ZnO_4) tetrahedra lie at the vertices of a 4^4 net to form a sheet in which (PO_4) tetrahedra link only to (ZnO_4) tetrahedra, and vice versa. Thus all tetrahedra are four-connected, and all vertices (simple anions) are two-connected within the resultant sheet (Fig. 11c). These sheets are parallel to (101) and are linked in the *b*-direction by ($ZnO_2\{H_2O\}_4$) octahedra in which the *trans* O-atoms belong to adjacent sheets (Fig. 11d).

In **phosphophyllite**, $Fe^{2+}(H_2O)_4[Zn(PO_4)]_2$, ($PO_4$) and ($Zn\phi_4$) tetrahedra form a sheet (Fig. 12a**)** that is topologically identical to the [$Zn(PO_4)$] sheet in hopeite (Fig. 11a). These sheets are linked by ($Fe^{2+}O_2\{H_2O\}_4$) octahedra, similar to the linkage by ($ZnO_2\{H_2O\}_4$) octahedra in hopeite. However, in phosphophyllite, the O-atoms of the ($Fe^{2+}O_2\{H_2O\}_4$) octahedron are in a *trans* configuration (Fig. 12b), whereas in hopeite, the O-atoms of the ($ZnO_2\{H_2O\}_4$) octahedron are in a *cis* configuration (Fig. 11b).

In **veszeylite**, $Cu^{2+}{}_2(OH)_2(H_2O)_2[Zn(PO_4)(OH)]$, ($PO_4$) and ($Zn\phi_4$) tetrahedra occur at the vertices of a 4.8^2 net (Fig. 12c) in which each type of tetrahedron points both up and down relative to the plane of the sheet. Both (PO_4) and ($Zn\phi_4$) tetrahedra are three-connected within the sheet, and (PO_4) tetrahedra and ($Zn\phi_4$) tetrahedra always alternate in any path through the 4.8^2 net. In the four-membered ring, the tetrahedra point *uudd*, and in the eight-membered ring, the tetrahedra point *uuuudddd*. The ($Cu^{2+}\phi_6$) octahedra form an interrupted [$M\phi_2$] sheet (Hawthorne and Schindler 2000; Hawthorne and Sokolova 2002) in which the vacant octahedra are ordered as dimers. The sheets of tetrahedra and octahedra stack in the *c*-direction (Fig. 12d) with hydrogen bonds (not shown) providing additional linkage between octahedra and tetrahedra.

Kipushite, $[Cu^{2+}{}_5Zn(PO_4)_2(OH)_6(H_2O)]$, contains ($PO_4$) and ($ZnO_4$) tetrahedra that are arranged at the vertices of a 4.8^2 net (as occurs in veszelyite) and link by corner-sharing (Fig. 12e, c.f. Fig. 12c). ($Cu^{2+}\phi_6$) octahedra share edges to form a sheet with ordered vacancies. It is actually a sheet of the form $[M_6\phi_{12}] \equiv [M\phi_2]_6$ with $M_6 = Cu^{2+}{}_5\,\square$, where $\square$ is a vacant octahedron; these 'vacant octahedra' share a face with a (PO_4) tetrahedron on one side of the sheet of octahedra. Two of these sheets then link by sharing the apical vertices of their (PO_4) tetrahedra with octahedron vertices of the adjacent sheet to form a thick slab (Fig. 12f). These slabs stack in the *a*-direction and are linked by the (PO_4)-(ZnO_4) sheet through sharing of vertices between tetrahedra and octahedra.

In **scholzite**, $Ca(H_2O)_2[Zn(PO_4)]_2$, (ZnO_4) tetrahedra share pairs of vertices to form simple linear chains parallel in the *c*-direction. Adjacent (ZnO_4) tetrahedra are further linked by sharing vertices with a (PO_4) tetrahedron, and the (PO_4) tetrahedra are in a staggered arrangement along the length of the chain. Chains adjacent in the *b*-direction link through (PO_4) tetrahedra to form a sheet parallel to (100) (Fig. 13a). In this sheet, the (ZnO_4) tetrahedra are four-connected and the (PO_4) tetrahedra are three-connected. The bridging anions of the chain of (ZnO_4) tetrahedra are three-connected; all other anions of the sheet are two-connected except for the one-connected anion of the (PO_4) tetrahedron. The resulting sheet (Fig. 13a) forms quite a thick slab that is linked by two crystallographically distinct octahedrally coordinated Ca atoms (Fig. 13b). In

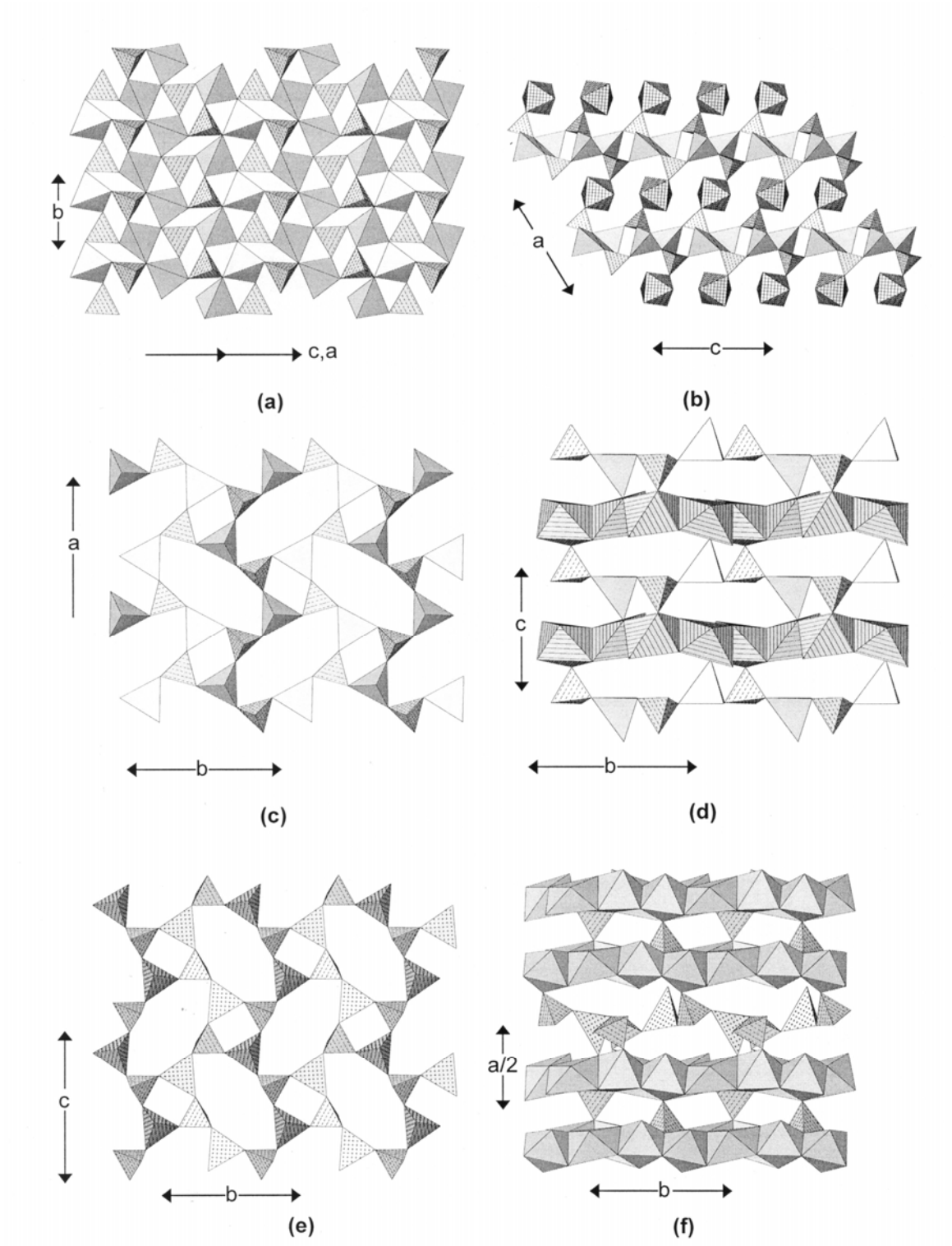

Figure 12. The crystal structures of phosphophyllite, veszelyite and kipushite: (a) phosphophyllite showing (PO_4) and ($Zn\phi_4$) tetrahedra at the vertices of a 4.8^2 net; (b) phosphophyllite projected onto (010); ($Zn\phi_4$) tetrahedra are shadow-shaded, ($Zn\phi_6$) octahedra are 4^4-net-shaded; (c) veszelyite projected onto (001); tetrahedra are arranged at the vertices of a 4.8^2 net; (d) veszelyite projected onto (100); ($Cu^{2+}\phi_6$) octahedra are line-shaded; (e) the sheet of corner-linked (PO_4) and (ZnO_4) tetrahedra in kipushite projected onto (100); (f) the structure of kipushite projected onto (001); ($Zn\phi_4$) tetrahedra are shadow-shaded.

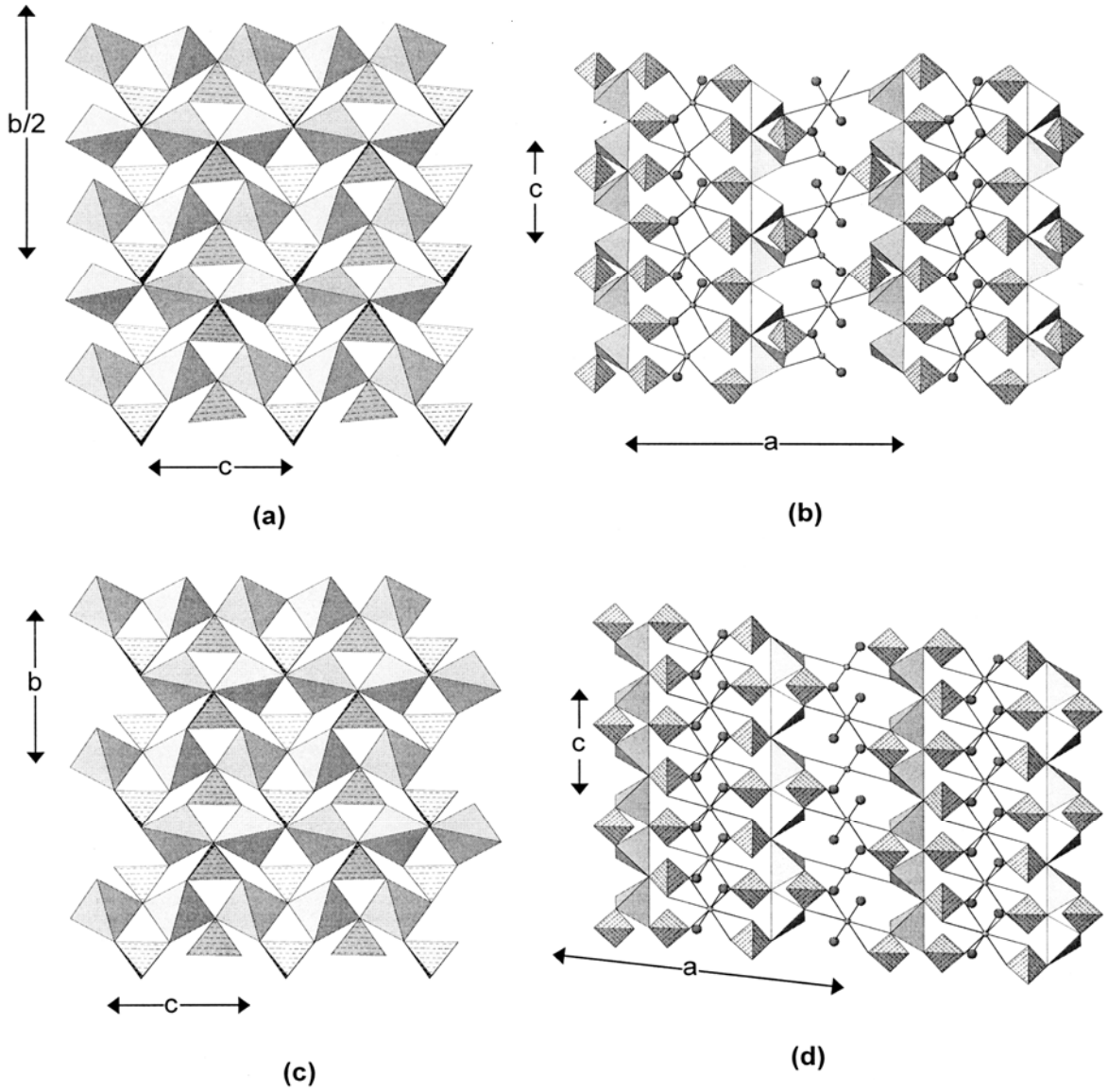

Figure 13. The crystal structures of scholzite and parascholzite: (a) scholzite projected onto (100); (b) scholzite projected onto (010); (c) parascholzite projected onto (100); (d) parascholzite projected onto (010). ($Zn\phi_4$) tetrahedra are shadow-shaded, Ca atoms are shown by small shaded circles, (H_2O) groups are shown by large shaded circles.

parascholzite, $Ca(H_2O)_2[Zn(PO_4)]_2$, the sheet of (PO_4) and (ZnO_4) tetrahedra (Fig. 13c) is topologically identical to the analogous sheet in scholzite (Fig. 13a). Scholzite and parascholzite are dimorphs, and the difference between these two structures involves linkage of the sheets in the *a*-direction (Figs. 13b,d). The details of the coordination of the interstitial Ca atoms differ in the two structures, leading to a different arrangement of adjacent sheets that produces an orthorhombic arrangement in scholzite and a monoclinic arrangement in parascholzite.

Infinite frameworks of tetrahedra

The minerals of this class (Table 4) are also dominated by PO_4-BeO_4 linkages. Only berlinite is different, as it is the only structure with polymerized (PO_4) and AlO_4 groups.

Table 4. Phosphate minerals based on ($T\phi_4$) frameworks.

Mineral	*Framework*	*Space group*	*Figure*
Berlinite	$[AlPO_4]$	$P3_12$	–
Beryllonite	$[BePO_4]$	$P2_1/n$	14a,b
Hurlbutite	$[Be_2(PO_4)_2]$	$P2_1/a$	14c,d
Babefphite	$[Be(PO_4)F]$	$F1$	14e,f
Tiptopite	$[Be_6(PO_4)_6]$	$P6_3$	15a,b
Weinebeneite	$[Be_3(PO_4)_2(OH)_2]$	Cc	15c,d
Pahasapaite	$[Be_{24}P_{24}O_{96}]$	$I23$	15e

Berlinite, $[AlPO_4]$, is a framework structure, topologically identical to the structure of α-quartz. Both structures have the same space group, *P*321, but the *c* dimension in berlinite is twice that of α-quartz in order to incorporate two distinct types of tetrahedra, AlO_4 and PO_4.

Beryllonite, $Na[Be(PO_4)]$, consists of a well-ordered framework of alternating four-connected (PO_4) and (BeO_4) tetrahedra arranged at the vertices of a 6^3 net, with (PO_4) and (BeO_4) tetrahedra pointing in opposing directions along the *b*-axis (Fig. 14a). This arrangement is topologically identical to the tridymite framework. These sheets stack along the *b*-direction and share tetrahedron corners to form four-membered and eight-membered rings (Fig. 14b). The resultant framework has large channels containing [6]- and [9]-coordinated interstitial Na.

Hurlbutite, $Ca[Be_2(PO_4)_2]$, consists of an ordered array of (PO_4) and (BeO_4) tetrahedra in which all tetrahedra are four-connected and there is alternation of (PO_4) and (BeO_4) tetrahedra in the structure. Viewed down [001] (Fig. 14c), the tetrahedra are arranged at the vertices of a 4.8^2 net with [7]-coordinated Ca occupying the interstices; these sheets link along the [001] direction by vertex-sharing (Fig. 14d).

Babefphite, $Ba[Be(PO_4)F]$, is a rather unusual mineral; it is an ordered framework of (PO_4) and (BeO_3F) tetrahedra. Projected down the *c*-direction, tetrahedra are arranged at the vertices of a 6^3 net (Fig. 14e) with the tetrahedra pointing (*uuuddd*). Projected down the *a*-direction, again the tetrahedra occur at the vertices of a 6^3 net (Fig. 14f) but the tetrahedra point (*uuuuuu*). Both the (PO_4) and the ($Be\phi_4$) tetrahedra are three-connected, and the F anions are the non-*T*-bridging species in the ($Be\phi_4$) tetrahedra. The interstices of the framework are occupied by [9]-coordinated Ba.

Tiptopite, $K_2(Li_{2.9}Na_{1.7}Ca_{0.7}G_{0.7})[Be_6(PO_4)_6](OH)_2(H_2O)_4$, is isotypic with the minerals of the cancrinite group: $Ca_2Na_6[Al_6(SiO_4)_6(CO_3)_2](H_2O)_2$ for the silicate species. The (PO_4) and (BeO_4) tetrahedra are arranged at the vertices of a two-dimensional net (Fig. 15a) such that all tetrahedra are three-connected when viewed down [001]. Prominent twelve-membered rings are arranged at the vertices of a 3^6 net such that they two-connect four-membered rings and three-connect through six-membered rings. These sheets link in the *c*-direction such that all tetrahedra are four-connected and, projected down the *b*-direction, form a two-dimensional net of four- and six-membered rings (Fig. 15b). The latter can be considered as a 6^3 net in which every third row of hexagons have a linear defect corresponding to an *a*-glide operation along *c*, i.e., double chains of hexagons extending in the *c*-direction and interleaved by single ladders of edge-sharing squares. Details of the rather complex relations between the interstitial species are discussed by Peacor et al. (1987).

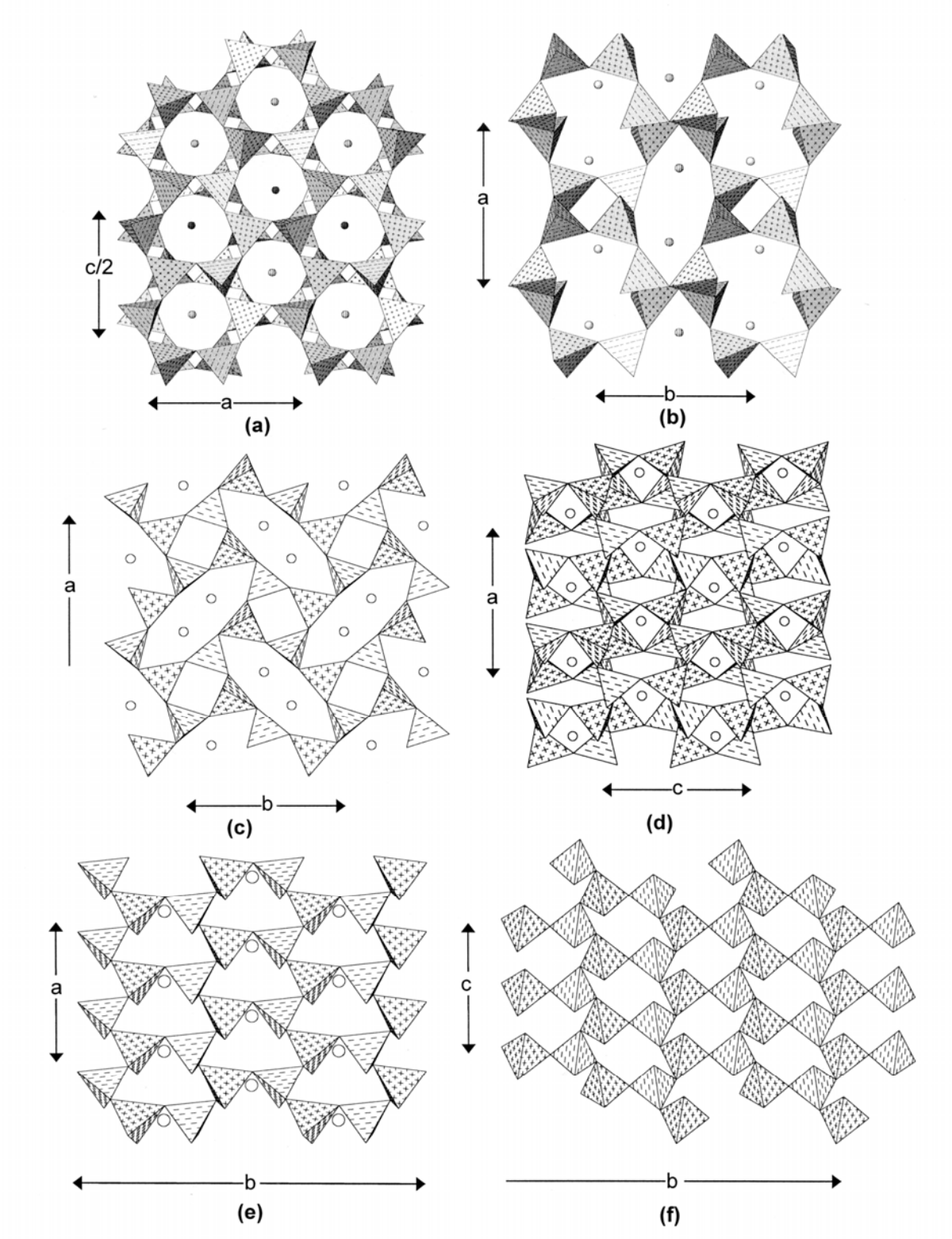

Figure 14. The crystal structures of beryllonite, hurlbutite and babefphite: (a) beryllonite projected onto (010); (b) beryllonite projected onto (001); (c) hurlbutite projected onto (001); (d) hurlbutite projected down the *c*-axis; (e) babefphite projected onto (001); tetrahedra occur at the vertices of a 6^3 net; (f) babefphite projected down the *a*-axis; tetrahedra occur at the vertices of a 6^3 net. Interstitial cations are shown as circles.

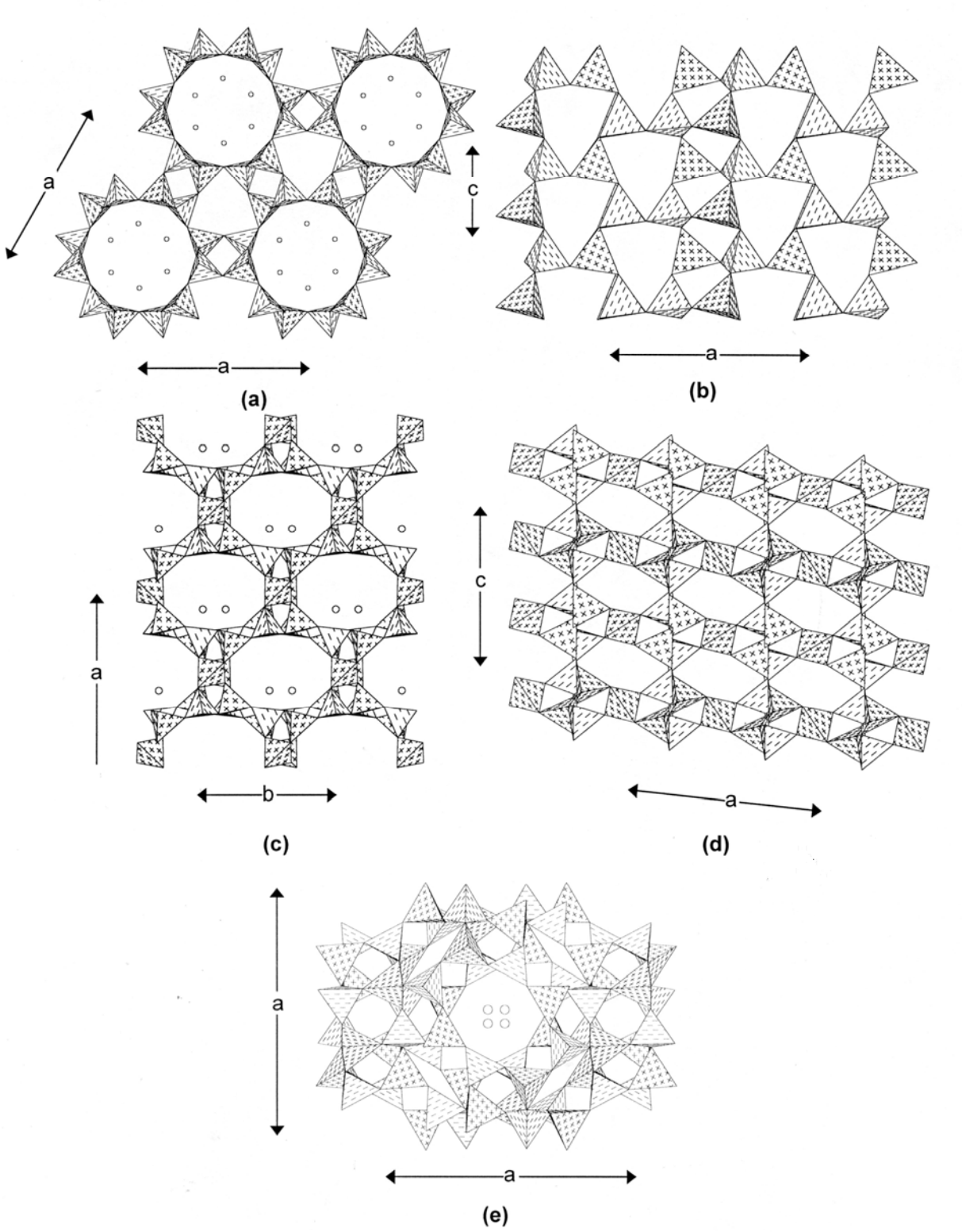

Figure 15. The crystal structures of tiptopite, weinebeneite, and pahasapaite: (a) tiptopite projected onto (001); (b) tiptopite projected onto (010); (c) weinebeneite projected down the c-axis; (d) weinebeneite projected onto (010); in both (c) and (d), 4.8^2 nets of tetrahedra link in the *a*-direction through an additional (BeO_4) group, (H_2O) groups are omitted for clarity; (e) pahasapaite projected onto (001); Li and (H_2O) are omitted for clarity. Interstitial cations are shown as circles.

Weinebeneite, $Ca[Be_3(PO_4)_2(OH)_2](H_2O)_4$, contains an ordered framework of (PO_4) and (BeO_4) tetrahedra; the (PO_4) tetrahedra connect only to (BeO_4) tetrahedra, but the (BeO_4) tetrahedra connect to both (PO_4) and (BeO_4) tetrahedra, the Be-Be linkages occurring through the (OH) groups of the framework. Viewed down [100], the structure consists of alternating (PO_4) and (BeO_4) tetrahedra at the vertices of a 4.8^2 net (view not shown). Projected onto (001) (Fig. 15c) and viewed down [010] (Fig. 15d), the 4.8^2 sheets stack in the [100] direction and link together through additional (non-sheet) (BeO_4) tetrahedra. Interstitial [7]-coordinated Ca is situated to one side of the large channels thus formed, with channel (H_2O) also bonded to the Ca.

Pahasapaite, $Ca_8Li_8[Be_{24}P_{24}O_{96}](H_2O)_{38}$, has an ordered array of (PO_4) and (BeO_4) tetrahedra arranged in a zeolite-rho framework, topologically similar to the minerals of the faujasite group and related to the synthetic aluminophosphate zeolite-like frameworks. Viewed along any crystallographic axis, the structure consists of prominent eight-membered rings of alternating (PO_4) and (BeO_4) tetrahedra (Fig. 15e) in an I-centered (F-centered in projection) array. The eight-membered rings are connected along the axial directions by linear triplets of four-membered rings, and to nearest-neighbor eight-membered rings through six-membered rings. All tetrahedra are four-connected; (PO_4) tetrahedra link only to (BeO_4) tetrahedra, and vice versa. The structure has large cages (Rouse et al. 1989) and prominent intersecting channels (Fig. 15e) that contain interstitial Li, [7]-coordinated Ca and strongly disordered (H_2O) groups.

STRUCTURES WITH ($T\phi_4$) AND ($M\phi_6$) GROUPS

As noted above, we classify the structures within each sub-group in terms of the connectivity of the constituent polyhedra of the structural unit. We use the nomenclature of Hawthorne (1983a) to denote the linkage: - denotes corner-sharing (e.g., *M*-*M*), = denotes edge-sharing (e.g., *M*=*M*), and ≡ denotes (triangular) face-sharing (e.g., $M \equiv M$).

Structures with unconnected (PO_4) groups

Phosphate minerals of this class are listed in Table 5. In these minerals, the (PO_4) groups and ($M\phi_6$) octahedra are linked together by hydrogen bonding.

In **struvite**, $[Mg(H_2O)_6][PO_4]$, the (PO_4) tetrahedra and $(Mg\{H_2O\}_6)$ octahedra are linked solely by hydrogen bonding from the (H_2O) groups bonded to Mg directly to the anions of the (PO_4) groups, or by hydrogen bonding from the interstitial (NH_4) group |

Table 5. Phosphate minerals based on isolated tetrahedra and octahedra and finite clusters of tetrahedra and octahedra.

Mineral	*Structural unit*	*Space group*	*Figure*
	Isolated polyhedra		
Strüvite	$[Mg(H_2O)_6][PO_4]$	$Pmn2_1$	16a
Phosphorrösslerite	$[Mg(H_2O)_6][PO_3(OH)]$	$C2/c$	16b
	Clusters		
Anapaite	$[Fe^{2+}(PO_4)_2(H_2O)_4]$	$P\bar{1}$	17a,b
Schertelite	$[Mg(PO_3\{OH\}_2(H_2O)_4]$	$Pbca$	17c,d
Morinite	$[Al_2(PO_4)_2F_4(OH)(H_2O)_2]$	$P2_1/m$	17e,f

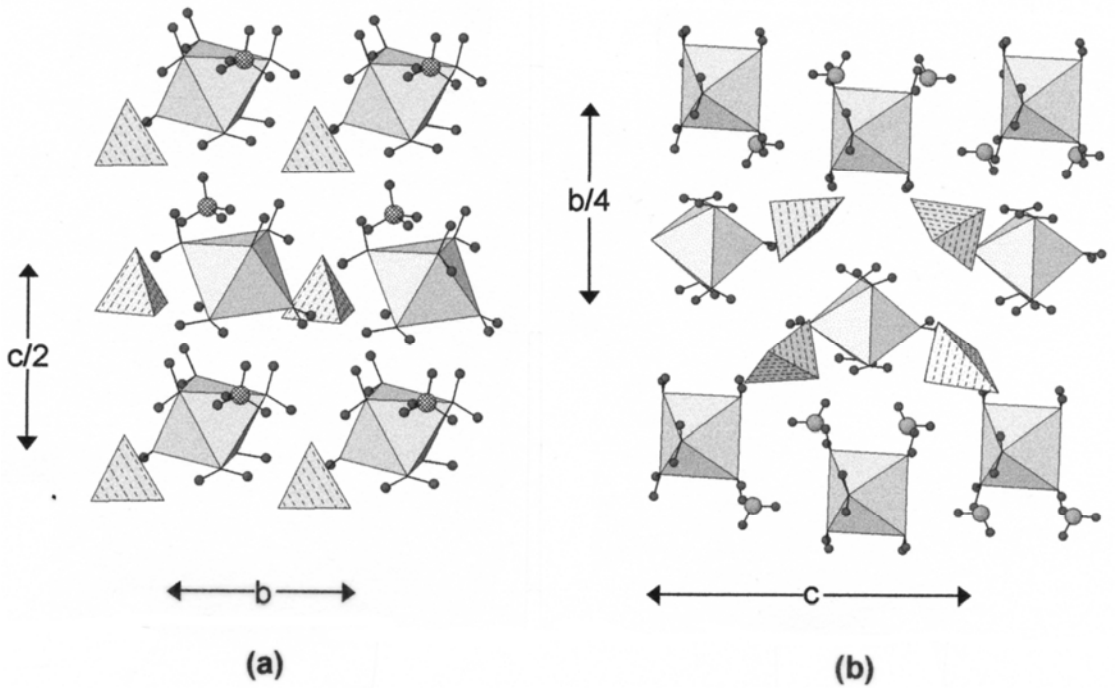

Figure 16. The crystal structures of struvite and phosphorrösslerite: (a) struvite projected onto (100); (b) phosphorrösslerite projected onto (100). ($Mg\{H_2O\}_6$) octahedra are shadow-shaded, hydrogen atoms are shown by small shaded circles, N [as part of the (NH_4) group] is shown as cross-hatched circles, O-atoms of interstitial (H_2O) groups are shown as large shaded circles.

(Fig. 16a). In **phosphorrösslerite**, $[Mg(H_2O)_6][PO_3(OH)](H_2O)$, the phosphate group is an acid phosphate, one of the phosphate anions being an (OH) group. The ($Mg\{H_2O\}_6$) octahedron hydrogen bonds to the ($P\phi_4$) group, but there is also an interstitial (H_2O) group that is held in the structure solely by hydrogen bonding (Fig. 16b), acting both as a hydrogen-bond donor and as a hydrogen-bond acceptor.

Structures with finite clusters of tetrahedra and octahedra

Phosphate minerals of this class are listed in Table 5.

M-T linkage. In **anapaite**, $Ca_2[Fe^{2+}(PO_4)_2(H_2O)_4]$, two ($PO_4$) groups link to *trans* vertices of an ($Fe^{2+}\phi_6$) octahedron to form an $[M(TO_4)_2\phi_4]$ cluster, where $M = Fe^{2+}$, T = P, and ϕ = (H_2O) (Fig. 17a). These clusters are arranged in open layers parallel to (001) (Fig. 17b), and these layers are linked by Ca atoms and by hydrogen bonding. The atomic arrangement in **schertelite**, $(NH_4)_2[Mg\{PO_3(OH)\}_2(H_2O)_4]$, is similar to that in anapaite (and also the sulfate minerals bloedite, $Na_2[Mg(SO_4)_2(H_2O)_4]$, and leonite, $K_2[Mn^{2+}(SO_4)_2(H_2O)_4]$, Hawthorne 1985b). The $[Mg(PO_3\{OH\})_2(H_2O)_4]$ clusters are arranged in a centered rectangular array (Fig. 17c), with the projection of the long axis of the cluster parallel to the *a*-direction. The clusters are arranged in layers parallel to (010) (Fig. 17d), and the clusters are linked by hydrogen bonding involving (H_2O) groups of the cluster and interstitial (NH_4) groups.

M-M, M-T linkage. In **morinite**, $NaCa_2[Al_2(PO_4)_2F_4(OH)(H_2O)_2]$, two ($Al\phi_6$) octahedra link through one vertex to form a dimer, and (two pairs of) vertices from each octahedron, *cis* to their common vertex, are linked by (PO_4) groups to form a cluster of the general form $[M_2(TO_4)_2\phi_7]$. These clusters are arranged in a centered array when viewed down [001] (Fig. 17e). Adjacent clusters are linked by $^{[8]}$Ca (Fig. 17f), $^{[5]}$Na in triangular-bipyramidal coordination, and by hydrogen bonds. As shown by Hawthorne

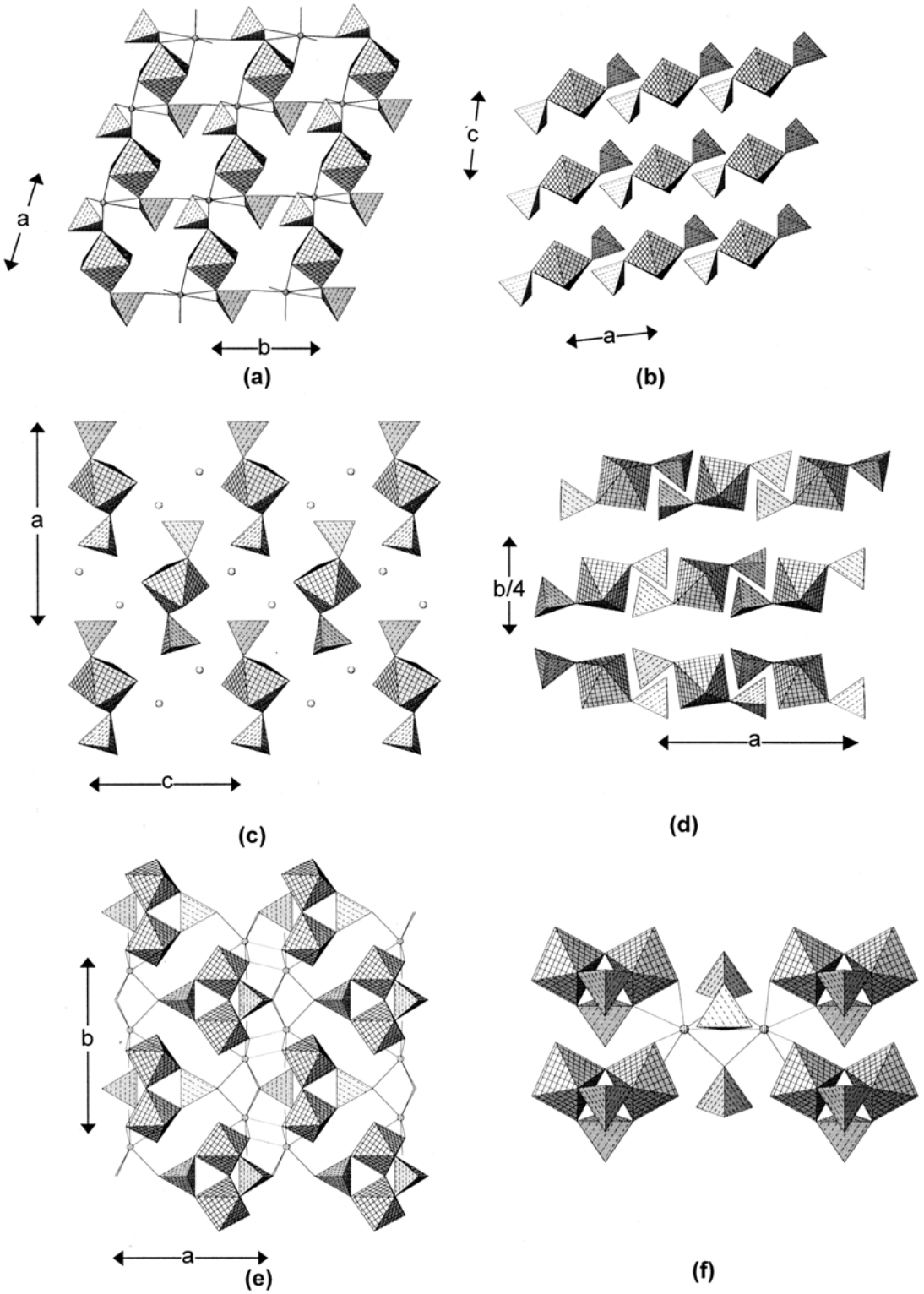

Figure 17. The crystal structures of anapaite, schertelite and morinite: (a) anapaite projected onto (001); (b) anapaite projected onto (010); (c) schertelite projected onto (010); N shown as circles; (d) schertelite projected onto (001); (e) morinite projected onto (001); Ca atoms are shown as circles, Na atoms and hydrogen bonds are not shown; (f) morinite, showing the linkage of adjacent clusters by interstitial Ca atoms.

Table 6. Phosphate minerals based on infinite chains of tetrahedra and octahedra.

Mineral	*Structural unit*	*Space group*	*Figure*
Bøggildite	$[Al_2(PO_4)F_9]$	$P2_1/c$	19a,b
Cassidyite	$[Ni(PO_4)_2(H_2O)_2]$	$P\bar{1}$	19c
Collinsite*	$[Mg(PO_4)_2(H_2O)_2]$	$P\bar{1}$	19c
Fairfieldite*	$[Mn^{2+}(PO_4)_2(H_2O)_2]$	$P\bar{1}$	19d
Messelite	$[Fe^{2+}(PO_4)_2(H_2O)_2]$	$P\bar{1}$	19d
Childrenite*	$[Al(PO_4)(OH)_2(H_2O)]$	*Bbam*	20a,b
Eosphorite	$[Al(PO_4)(OH)_2(H_2O)]$	*Bbam*	20a,b
Jahnsite*	$[Fe^{3+}(PO_4)_2(OH)]_2$	$P2/a$	20c,d
Rittmanite	$[Al(PO_4)_2(OH)]_2$	$P2/a$	20c,d
Whiteite	$[Al(PO_4)_2(OH)]_2$	$P2/a$	20c,d
Whiteite-(CaMnMg)	$[Al(PO_4)_2(OH)]_2$	$P2/a$	20c,d
Lun'okite	$[Al(PO_4)_2(OH)]_2$	*Pbca*	21a,b
Overite*	$[Al(PO_4)_2(OH)]_2$	*Pbca*	21a,b
Segelerite	$[Fe^{3+}(PO_4)_2(OH)]_2$	*Pbca*	21a,b
Wilhelmvierlingite	$[Fe^{3+}(PO_4)_2(OH)]_2$	*Pbca*	21a,b
Tancoite	$[Al(PO_4)_2(OH)]$	*Pbcb*	21c,d
Sinkankasite	$[Al(PO_3\{OH\})_2(OH)]$	$P\bar{1}$	21e,f
Bearthite	$[Al(PO_4)_2(OH)]$	$P2_1/m$	22a,b
Brackebuschite *	$[Mn^{3+}(VO_4)_2(OH)]$	$P2_1/m$	22a,b
Goedkenite	$[Al(PO_4)_2(OH)]$	$P2_1/m$	22a,b
Tsumebite	$[Cu^{2+}(PO_4)(SO_4)(OH)]$	$P2_1/m$	22a,b
Vauquelinite	$[Cu^{2+}(PO_4)(CrO_4)(OH)]$	$P2_1/n$	22c,d

(1979a), this $[M_2(TO_4)_2\phi_7]$ cluster is the basis of a short hierarchy of phosphate minerals of higher connectivity: minyulite, olmsteadite, hureaulite, phosphoferrite, kryzhanovskite, melonjosephite and whitmoreite.

Structures with infinite chains of (PO_4) tetrahedra and ($M\phi_6$) octahedra

The minerals of this class are listed in Table 6. The topologically distinct chains and their corresponding graphs are shown in Figure 18.

M-T linkage. **Bøggildite**, $Na_2Sr_2[Al_2(PO_4)F_9]$, is a rare phosphate-aluminofluoride mineral. The structural unit consists of a chain of alternating (PO_4) tetrahedra and (AlO_2F_4) octahedra that is decorated by flanking ($AlOF_5$) octahedra attached to the (PO_4) groups (Figs. 18a, 19a). The (PO_4) groups are three-connected and alternately point up and down along the length of the chain. The chain extends along the *b*-direction (Fig. 19b) and are linked by [8]- and [9]-coordinated Sr, and [7]- and [9]-coordinated Na. Bøggildite is the only phosphate-aluminofluoride mineral currently known.

The minerals of the **collinsite**, $Ca_2[Mg(PO_4)(H_2O)_2]$, and **fairfieldite**,

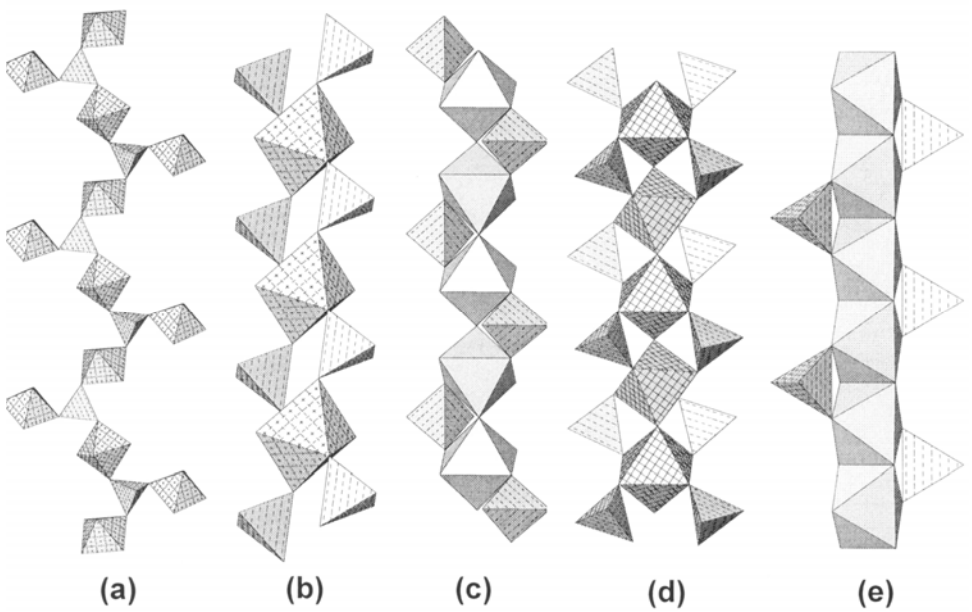

Figure 18. Topologically distinct chains of (PO_4) tetrahedra and ($M\phi_6$) octahedra, and their corresponding graphs: (a) the [$M(TO_4)\ \phi_9$] chain in bøggildite; (b) the [$M(TO_4)_2\phi_2$] chain in the minerals of the collinsite and fairfieldite groups; (c) the [$M(TO_4)\ \phi_3$] chain in the minerals of the childrenite group; (d) the [$M(TO_4)_2\phi$] chain in the minerals of the jahnsite group; (e) the [$M(TO_4)_2\phi$] chain in bearthite (and the minerals of the brackebuschite group).

$Ca_2[Mn^{2+}(PO_4)_2(H_2O)_2]$, groups are both based on a general [$M(TO_4)_2\phi_2$] chain that also occurs in the (non-phosphate) minerals of the kröhnkite, $Na_2[Cu^{2+}(SO_4)(H_2O)_2]$, group. This chain is formed of alternating ($M^{2+}O_4\{H_2O\}_2$) octahedra and pairs of (PO_4) tetrahedra (Figs. 19c,d), with the (H_2O) groups in a *trans* arrangement about the divalent cation (Fig. 18b). The repeat distance along the length of the chain is ~5.45 Å, and this is reflected in the *c*-dimensions of these minerals. The minerals of the collinsite and fairfieldite groups are often incorrectly grouped together as the fairfieldite group because they all have triclinic symmetry. However, the interaxial angles in the two groups are significantly different (see Appendix). Adjacent chains in both structures are linked by [7]-coordinated Ca atoms and by hydrogen bonding. The two structures differ in the details of their hydrogen bonding (Figs. 19c,d).

M-M, M-T linkage. **Childrenite**, $Mn^{2+}(H_2O)[Al(PO_4)(OH)_2]$, consists of [$Al\phi_5$] chains in which ($Al\phi_6$) octahedra link through pairs of *trans* vertices. The chains are decorated by (PO_4) groups that link adjacent octahedra and are arranged in a staggered fashion along the length of the chain (Fig. 18c) to give the general form [$M(TO_4)\phi_3$]. The chains extend in the *c*-direction in childrenite (Fig. 20a) and are cross-linked by [6]-coordinated Mn^{2+}, the coordination octahedra of which form an edge-sharing chain in the *c*-direction. Viewed down [001], the chains are arranged at the vertices of a primitive orthorhombic net, and four adjacent chains are linked through one ($Mn^{2+}\phi_6$) octahedra (Fig. 20b).

Jahnsite, $CaMn^{2+}Mg_2[Fe^{3+}(PO_4)_2(OH)](H_2O)_8$, consists of [$Fe^{3+}\phi_5$] chains of *trans*-corner-sharing octahedra that are decorated by bridging (PO_4) groups to give the general form [$M^{3+}(TO_4)_2\phi$] (Fig. 18d). These chains extend in the *b*-direction and have a repeat distance of ~7.1Å, leading Moore (1970) to designate these, and related, chains as the

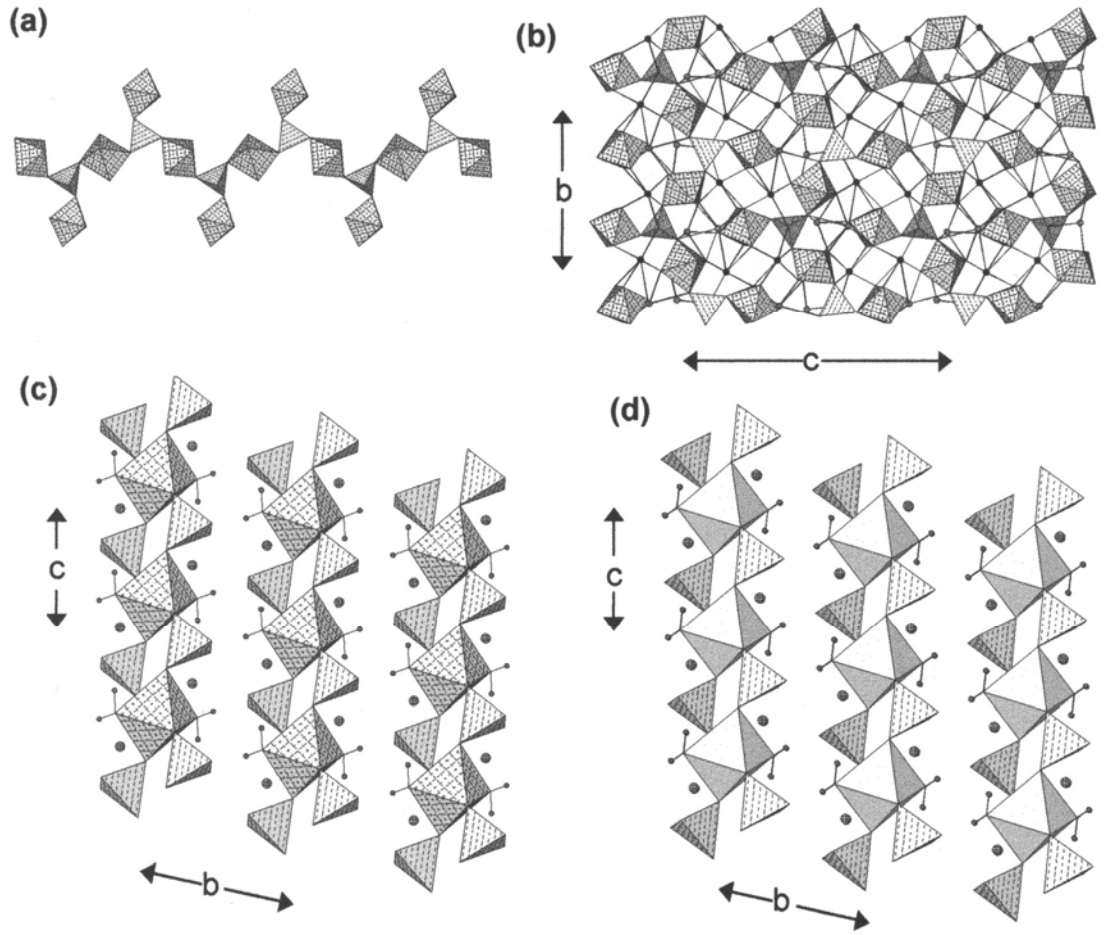

Figure 19. The crystal structures of bøggildite, collinsite and fairfieldite: (a) the $[Al_2(PO_4)F_9]$ chain in bøggildite; (b) bøggildite projected onto (100); Ca atoms are shown as dark circles, Na atoms are shown as shaded circles; (c) collinsite projected onto (100); (d) fairfieldite projected onto (100); Ca atoms are shown as shaded circles, H atoms are shown as small dark circles.

7-Å chains. These chains are linked in the *a*-direction by [6]-coordinated Ca (Fig. 20c) that form chains of edge-sharing polyhedra in the *b*-direction, forming slabs (Fig. 20d) parallel to (100) that are linked by octahedrally coordinated divalent-metal cations and by hydrogen bonding. In addition to the minerals of this group listed in Table 6, Matsubara (2000) reports the Fe^{2+} equivalent of jahnsite, ideally $CaFe^{2+}Fe^{2+}{}_2[Fe^{3+}(PO_4)_2(OH)]_2(H_2O)_8$, but this has not been approved as a valid species by the IMA.

Overite, $Ca_2Mg_2[Al(PO_4)_2(OH)]_2(H_2O)_8$, and **tancoite**, $Na_2LiH[Al(PO_4)_2(OH)]$, are both based on the $[Al(PO_4)_2(OH)]$ chain that is shown in Figure 18d, and in both structures, this chain defines the *c*-dimension, 7.11 Å in overite and 7.03 × 2 = 14.06 Å in tancoite. ($Al\phi_6$) octahedra link through one set of *trans* vertices, corresponding to the (OH) groups, to form an $[Al\phi_5]$ chain. Adjacent octahedra are linked by pairs of (PO_4) tetrahedra that point alternately up and down the *b*-direction in overite (Fig. 21a) and the *a*-direction in tancoite (Fig. 21c). In overite, the chains are linked in the *a*-direction by [8]-coordinated Ca to form slabs parallel to (010), the Ca linking to both tetrahedra and octahedra. These slabs are linked in the *b*-direction by ($MgO_2\{H_2O\}_4$) octahedra (Fig. 21b), and the resulting structure is strengthened by hydrogen bonds from the (H_2O) groups, all of which are bonded to the interstitial Mg cations. In tancoite, the chains are linked in the *b*-direction by [8]-coordinated Na and [5]-coordinated Li, forming slabs

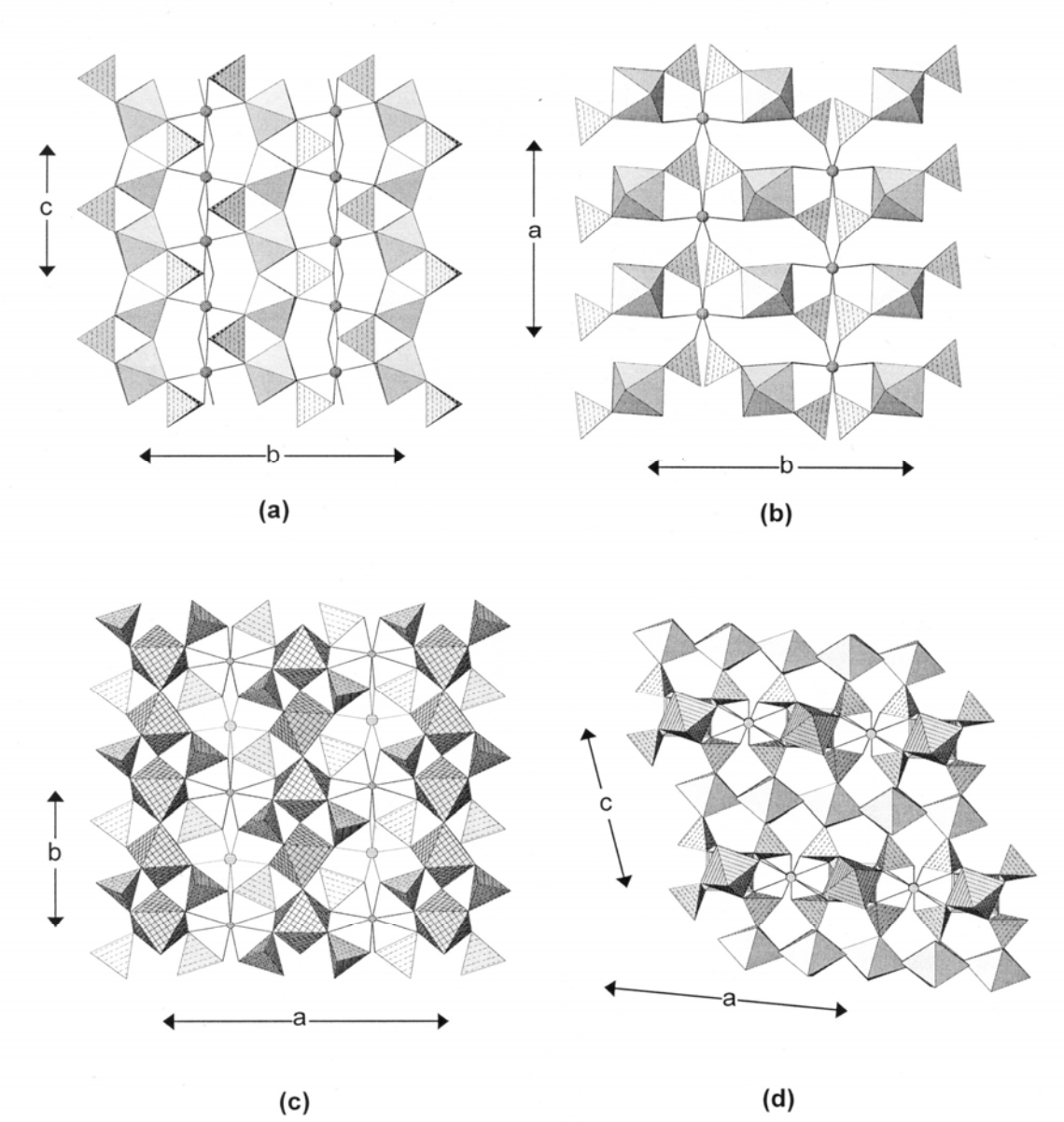

Figure 20. The crystal structures of childrenite and jahnsite: (a) childrenite projected onto (100); (b) childrenite projected onto (001); (Alϕ_6) octahedra are shadow-shaded, Mn^{2+} cations are shown as circles; (c) jahnsite projected onto (001); (d) jahnsite projected onto (010); ($Fe^{3+}\phi_6$) octahedra are 4^4-net-shaded, Ca atoms are shown as circles, ($Mn^{2+}\phi_6$) and (Mgϕ_6) octahedra are shadow-shaded.

parallel to (100) (Fig. 21c). These slabs are linked in the *a*-direction by [8]-coordinated Na (Fig. 21d). In addition, there is a symmetrical hydrogen-bond between two anions of adjacent (PO_4) groups.

Sinkankasite, $Mn^{2+}(H_2O)_4[Al(PO_3\{OH\})_2(OH)](H_2O)_2$, is also based on the [$M(T\phi_4)_2\phi$] chain of Figure 18d, extending in the *c*-direction to give a repeat of ~7 Å. However, it is topochemically different from the analogous chain in overite and tancoite because one of the tetrahedron vertices is occupied by (OH), forming an acid-phosphate group. The chains are linked in the *b*-direction (Fig. 21e) by ($Mn^{2+}O_2\{H_2O\}_4$) octahedra to form a thick slab parallel to (100). These slabs stack in the *a*-direction (Fig. 21f) and

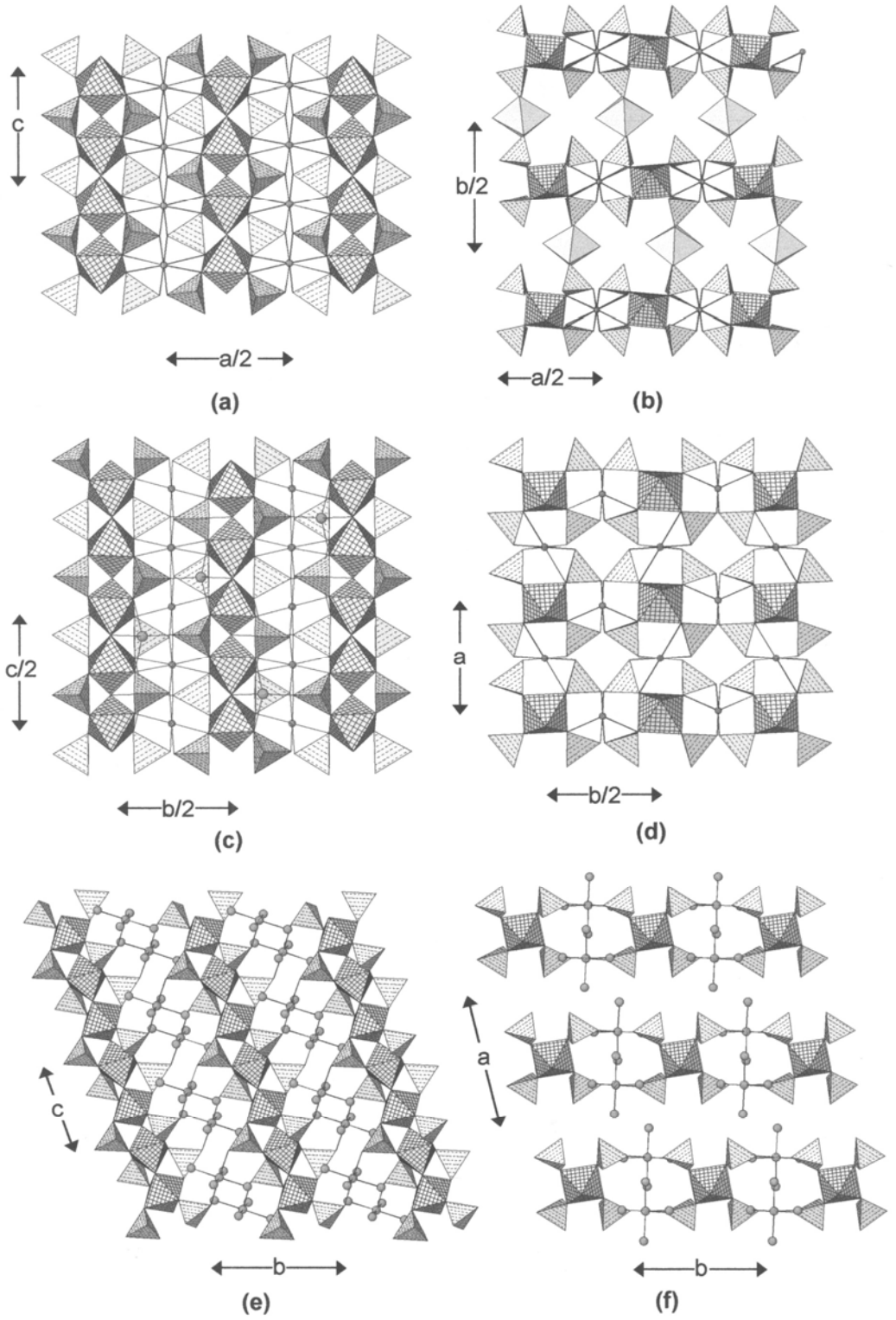

Figure 21. The crystal structures of overite, tancoite and sinkankasite: (a) overite projected onto (010); (b) overite projected onto (001); Ca atoms are shown as small shaded circles; (c) tancoite projected onto (100); (d) tancoite projected onto (001); Na atoms are shown as small shaded circles, Li atoms are shown as large shaded circles; (e) sinkankasite projected onto (100); (f) sinkankasite projected onto (001); hydrogen atoms and bonds are omitted for clarity, ($Al\phi_6$) octahedra are 4^4-net-shaded.

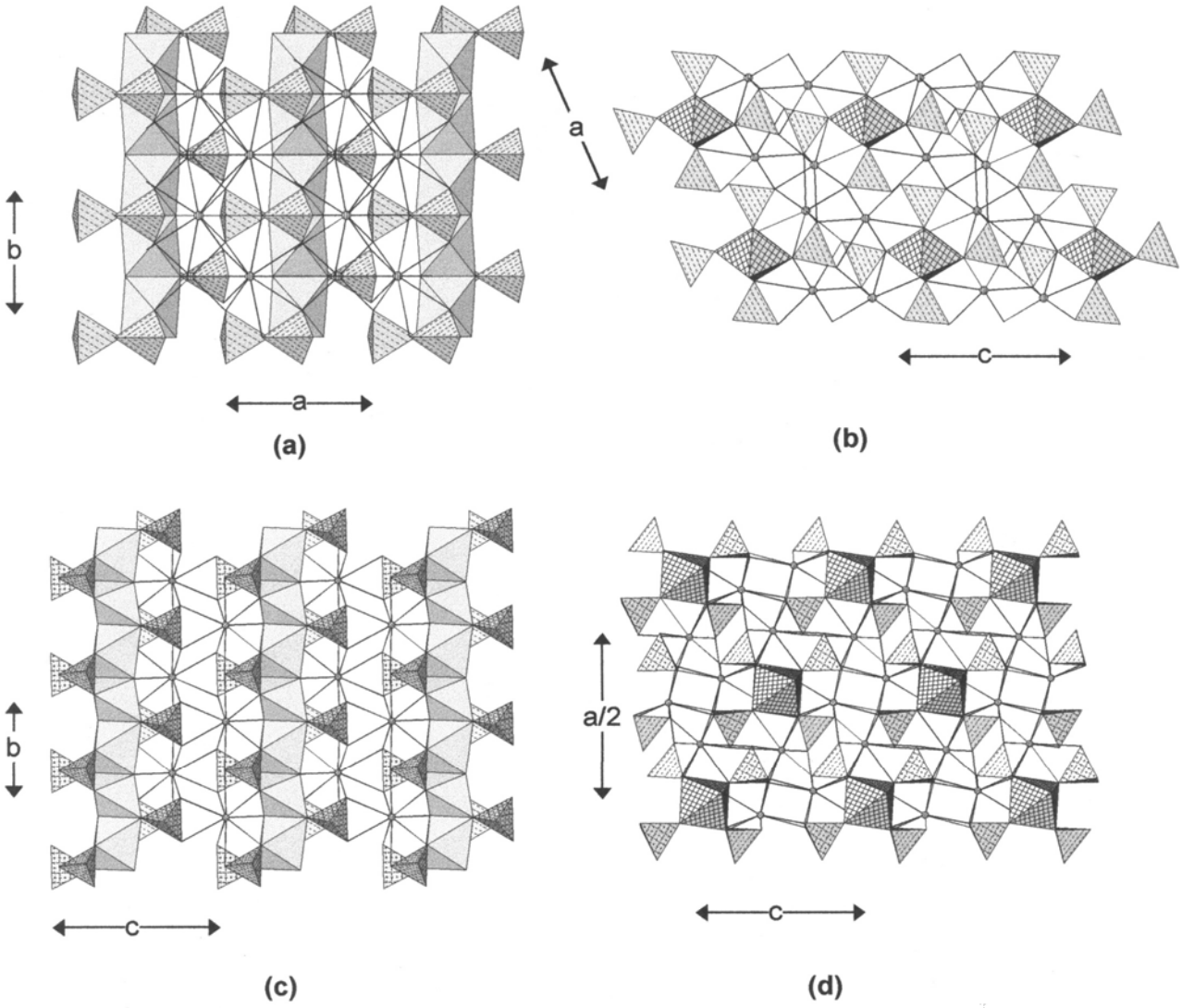

(b) bearthite projected onto (010); ($Al\phi_6$) octahedra are shadow-shaded in (a) and 4^4-net-shaded in (b), interstitial Ca is shown as shaded circles; (c) vauquelinite projected onto (100); (d) vauquelinite projected onto (010); (CrO_4) tetrahedra are square-pattern-shaded, ($Cu^{2+}\phi_6$) octahedra are shadow-shaded in (c) and 4^4-net-shaded in (d), Pb^{2+} is shown as shaded circles.

are linked solely by hydrogen bonds involving the H atom of the acid-phosphate group, the (H_2O) groups of the interstitial ($Mn^{2+}O_2\{H_2O\}_4$) octahedron, and interstitial (H_2O) groups not bonded directly to any cations.

M=M, M-T linkage. **Bearthite**, $Ca_2[Al(PO_4)_2(OH)]$, contains ($Al\phi_6$) octahedra which share one set of *trans* edges with adjacent octahedra to form an [$Al\phi_4$] chain. Adjacent octahedra are linked (bridged) by (PO_4) tetrahedra in a staggered arrangement on either side of the chain to form a decorated chain of the general form [$M(TO_4)_2\phi$] (Fig. 18e). These chains are linked in the *a*-direction by [10]-coordinated Ca (Fig. 22a). Viewed along [010] (Fig. 22b), the chains resemble four-membered pinwheels; linkage in the *c*-direction is also provided by interstitial Ca cations. A topologically identical chain, [$M(TO_4)_2\phi$], occurs in **vauquelinite**, $Pb^{2+}{}_2[Cu^{2+}(PO_4)(CrO_4)(OH)]$; however, there are two symmetrically (and chemically) distinct tetrahedra in vauquelinite, (PO_4) and (CrO_4) (Fig. 22c). In vauquelinite, ($Cu^{2+}\phi_6$) octahedra form the [$M\phi_4$]-type chain, (PO_4)

tetrahedra bridge vertices of adjacent octahedra in the chain, and (CrO_4) tetrahedra link to one vertex of the edge shared between adjacent octahedra (Fig. 22c). The resulting [$Cu^{2+}(PO_4)(CrO_4)(OH)$] chains extend in the *b*-direction, and are linked in the *a*-direction and *c*-direction by [9]-coordinated Pb^{2+}. When viewed end-on (Fig. 22d), the chains resemble four-membered pinwheels.

Structures with infinite sheets of (PO_4) tetrahedra and ($M\phi_6$) octahedra

The minerals of this class are listed in Table 7.

Table 7. Phosphate minerals based on infinite sheets of tetrahedra and octahedra.

Mineral	*Structural Unit*	*Space Group*	*Figure*
Johnwalkite	$[Nb(PO_4)_2O_2]$	$Pb2_1m$	23a.b
Olmsteadite*	$[Nb(PO_4)_2O_2]$	$Pb2_1m$	23a,b
Brianite	$[Mg(PO_4)_2]$	$P2_1/c$	23c,d
Merwinite*	$[Mg(SiO_4)_2]$	$P2_1/c$	23c,d
Newberyite	$[Mg(PO_3OH)(H_2O)_3]$	$Pbca$	24a,b
Hannayite	$[Mg_3(PO_3\{OH\})_4]$	$P\bar{1}$	24c,d
Minyulite	$[Al_2(PO_4)_2F(H_2O)_4]$	$Pba2$	25a,b
Benauite	$[Fe^{3+}_3(PO_4)(PO_3\{OH\})(OH)_6]$	$R\bar{3}m$	25c,d
Crandallite	$[Al_3(PO_4)(PO_3\{OH\})(OH)_6]$	$R\bar{3}m$	25c,d
Eylettersite	$[Al_3(PO_4)(PO_3\{OH\})(OH)_6]$	$R\bar{3}m$	25c,d
Florencite-(Ce)	$[Al_3(PO_4)(PO_3\{OH\})(OH)_6]$	$R\bar{3}m$	25c,d
Florencite-(La)	$[Al_3(PO_4)(PO_3\{OH\})(OH)_6]$	$R\bar{3}m$	25c,d
Florencite-(Nd)	$[Al_3(PO_4)(PO_3\{OH\})(OH)_6]$	$R\bar{3}m$	25c,d
Gorceixite	$[Al_3(PO_4)(PO_3\{OH\})(OH)_6]$	$R\bar{3}m$	25c,d
Plumbogummite	$[Al_3(PO_4)(PO_3\{OH\})(OH)_6]$	$R\bar{3}m$	25c,d
Waylandite	$[Al_3(PO_4)(PO_3\{OH\})(OH)_6]$	$R\bar{3}m$	25c,d
Zairite	$[Fe^{3+}_3(PO_4)_2(OH)_6]$	$R\bar{3}m$	25c,d
Gordonite	$[Al_2(PO_4)_2(OH)_2(H_2O)_2]$	$P\bar{1}$	26a,b
Laueite*	$[Fe^{3+}_2(PO_4)_2(OH)_2(H_2O)_2]$	$P\bar{1}$	26a,b
Mangangordonite	$[Al_2(PO_4)_2(OH)_2(H_2O)_2]$	$P\bar{1}$	26a,b
Paravauxite	$[Al_2(PO_4)_2(OH)_2(H_2O)_2]$	$P\bar{1}$	26a,b
Sigloite	$[Al_2(PO_4)_2(OH)_2(H_2O)_2]$	$P\bar{1}$	26a,b
Ushkovite	$[Fe^{3+}_2(PO_4)_2(OH)_2(H_2O)_2]$	$P\bar{1}$	26a,b
Curetonite	$[Al(PO_4)(OH)]$	$P2_1/n$	26c,d
Kastningite	$[Al_2(PO_4)_2(OH)_2(H_2O)_2]$	$P\bar{1}$	27a,b
Stewartite*	$[Fe^{3+}_2(PO_4)_2(OH)_2(H_2O)_2]$	$P\bar{1}$	27a,b
Pseudolaueite	$[Fe^{3+}(PO_4)(OH)(H_2O)]_2$	$P2_1/a$	27c,d
Strunzite*	$[Fe^{3+}(PO_4)(OH)(H_2O)]_2$	$P\bar{1}$	28a,b
Ferrostrunzite	$[Fe^{3+}(PO_4)(OH)(H_2O)]_2$	$P\bar{1}$	28a,b
Metavauxite	$[Al(PO_4)(OH)(H_2O)]_2$	$P2_1/c$	28c,d
Montgomeryiteeeee	$[MgAl_4(PO_4)_6(OH)_4(H_2O)]$	$C2/c$	29a,b
Mitryaevaite	$[Al_5(PO_4)_2(PO_3\{OH\})_2F_2(OH)_2(H_2O)_8]$	$P\bar{1}$	29c,d
Bonshtedite	$[Fe^{2+}(PO_4)(CO_3)]$	$P2_1/m$	29e,f
Bradleyite*	$[Mg(PO_4)(CO_3)]$	$P2_1/m$	29e,f
Sidorenkoite	$[Mn^{2+}(PO_4)(CO_3)]$	$P2_1/m$	29e,f
Bermanite*	$[Mn^{3+}(PO_4)(OH)]_2$	$P2_1$	30a,b

Ercitite	$[Mn^{3+}(PO_4)(OH)]_2$	$P2_1/n$	30a,b
Schoonerite	$[Mn^{2+}Fe^{2+}{}_2ZnFe^{3+}(PO_4)_3(OH)_2(H_2O)_7]$	$Pmab$	30c,d
Nissonite	$[Cu^{2+}Mg(PO_4)(OH)(H_2O)_2]$	$C2/c$	31a,b,c
Foggite	$[Al(PO_4)(OH)_2]$	$A2_122$	32a,b,c
Earlshannonite	$[Fe^{3+}(PO_4)(OH)]_2$	$P2_1/c$	32d,e
Whitmoreite*	$[Fe^{3+}(PO_4)(OH)]_2$	$P2_1/c$	32d,e
Mitridatite*	$[Fe^{3+}{}_3(PO_4)_3O_2]$	Aa	33a
Robertsite	$[Mn^{3+}{}_3(PO_4)_3O_2]$	Aa	33a
Arupite	$[Ni_3(PO_4)_2(H_2O)_8]$	$C2/m$	34a,b
Vivianite *	$[Fe^{2+}{}_3(PO_4)_2(H_2O)_8]$	$C2/m$	34a,b
Bobierrite	$[Mg_3(PO_4)_2(H_2O)_8]$	$C2/c$	34c,d

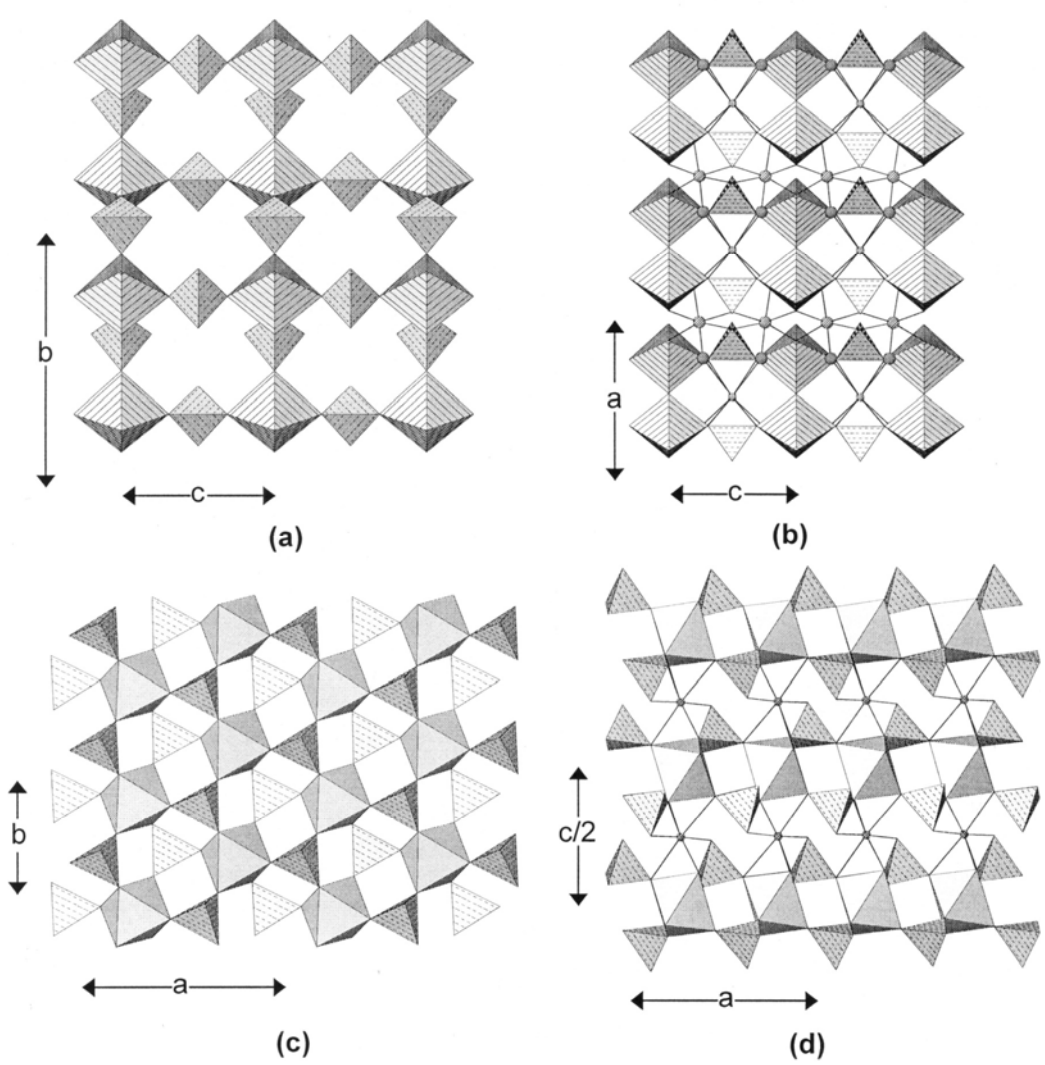

Figure 23. The crystal structures of olmsteadite and brianite: (a) olmsteadite projected onto (100); (b) olmsteadite projected onto (010); (NbO_6) octahedra are line-shaded, Fe^{2+} atoms are shown as line-shaded circles, (H_2O) groups are shown as dot-shaded circles; (c) brianite projected onto (001); (d) brianite projected onto (010); (MgO_6) octahedra are shadow-shaded, interstitial cations are shown as circles.

M-T linkage. The minerals of the **olmsteadite**, $K_2Fe^{2+}{}_4(H_2O)_4[Nb_2(PO_4)_4O_4]$, group consist of ($PO_4$) tetrahedra and ($NbO_6$) octahedra at the vertices of a 4^4 plane net, linked by sharing corners to form a sheet parallel to (100) (Fig. 23a, above). In the *c*-direction, the (PO_4) groups link to *trans* vertices of the (NbO_6) octahedra, but in the *b*-direction, the (PO_4) groups link to *cis* vertices of the (NbO_6) octahedra, and these *cis* vertices alternate above and below the plane of the sheet in the *b*-direction. The sheets link in pairs by sharing octahedron corners to form slabs that incorporate the interstitial [8]-coordinated K (Fig. 23b). These slabs are linked in the *a*-direction by rutile-like [$M\phi_4$] chains of ($Fe^{2+}\phi_6$) octahedra that extend in the *c*-direction.

Brianite, $Na_2Ca[Mg(PO_4)_2]$ is a member of the merwinite group (Table 7) and consists of (PO_4) tetrahedra and (MgO_6) octahedra at the vertices of a $(4^3)_2\ 4^6$ plane net. The (PO_4) groups link to both the upper and lower corners of the octahedra (Fig. 23c) to

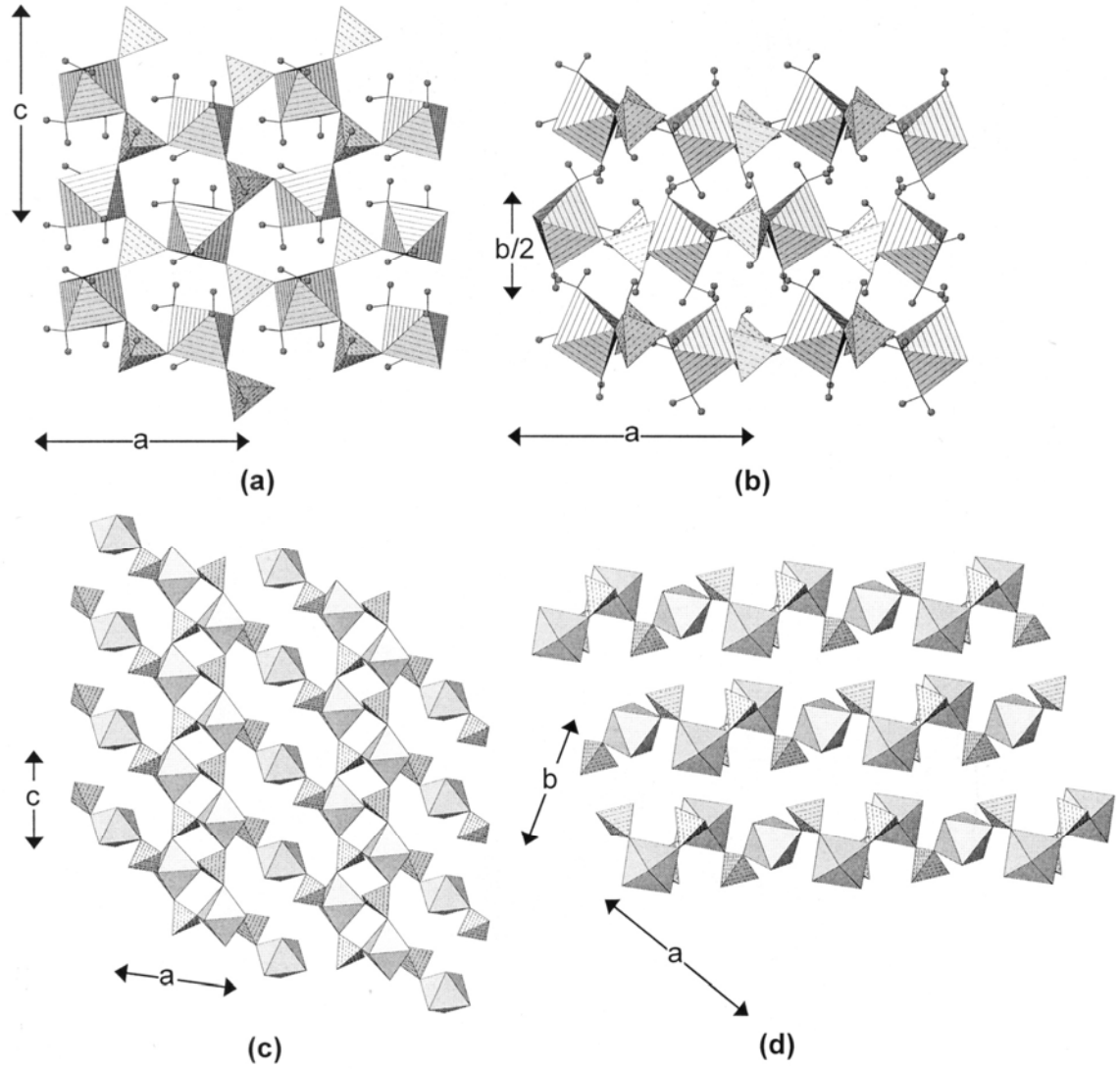

Figure 24. The crystal structures of newberyite and hannayite: (a) newberyite projected onto (010); (b) newberyite projected onto (001); ($Mg\phi_6$) octahedra are line-shaded, H atoms are shown as small shaded circles; (c) hannayite projected onto (010); (d) hannayite projected onto (001); ($Mg\phi_6$) octahedra are shadow-shaded.

form pinwheels (Moore 1973b) and the resulting sheet has a layer of octahedra sandwiched between two layers of tetrahedra (Fig. 23d). These sheets are linked in the *c*-direction by interstitial Na and Ca.

Newberyite, $[Mg(PO_3\{OH\})(H_2O)_3]$, consists of $(P\phi_4)$ tetrahedra and $(Mg\phi_6)$ octahedra at the vertices of a 6^3 plane net; the two different types of polyhedra alternate on any path through the net (Fig. 24a), and the (PO_4) tetrahedra point both up and down relative to the plane of the sheet. Both tetrahedra and octahedra are three-connected, and all one-connected vertices in the net are 'tied-off' by H atoms. Thus the $(P\phi_4)$ group is actually an acid-phosphate group, $(PO_3\{OH\})$, and the three one-coordinated anions of the $(Mg\phi_6)$ octahedron are (H_2O) groups. Hawthorne (1992) used newberyite as an example of the role of H atoms in controlling the dimensional character of a structural unit. The sheets in newberyite stack in the *b*-direction (Fig. 24b) and are linked solely by hydrogen bonds. Newberyite is an unusual structure in that it undergoes a low-temperature crystal-to-amorphous transition (Sales et al. 1993). When heated above 150°C (but below 600°C), newberyite becomes amorphous. With continued heating above 150°C, the amorphous phase develops chains of polymerized (PO_4) tetrahedra (up to 13 tetrahedra long), until at 600°C, crystalline $Mg_2P_2O_7$ forms. Heating under (unspecified) pressure results in a phase of the form $Mg_3(PO_3\{OH\})[P_2O_7](H_2O)_{4.5}$, the only known crystalline phosphate containing two different phosphate anions (Sales et al. 1993).

Hannayite, $(NH_4)_2[Mg_3(PO_3\{OH\})_4(H_2O)_8]$, consists of a very exotic sheet of alternating $(PO_3\{OH\})$ tetrahedra and $(Mg\phi_6)$ octahedra in a very open array. Alternating tetrahedra and octahedra fuse to form an $[M(TO_4)\phi_4]$ chain. Pairs of these chains meld by sharing corners between tetrahedra and octahedra to form ribbons of the type $[M(TO_4)\phi_3]$ that extend in the *c*-direction. These ribbons are linked in the *a*-direction by *trans* $[Mg(PO_4)_2\phi_4]$ clusters to form an open sheet parallel to (010) (Fig. 24c). These sheets stack in the *b*-direction (Fig. 24d) and are linked by hydrogen bonds directly from sheet to sheet, and by hydrogen bonds involving the interstitial (NH_4) groups.

M-M, M-T linkage. **Minyulite**, $K[Al_2(PO_4)_2F(H_2O)_4]$, contains a sheet that is made up of $[Al_2(PO_4)_2F(H_2O)_4O_2]$ clusters that are topologically identical to the $[Al_2(PO_4)_2F_4(OH)(H_2O)_2]$ clusters in morinite (Fig. 17e). These clusters occur at the vertices of a 4^4 net (Fig. 25a) and link by sharing vertices between tetrahedra and octahedra. This arrangement leads to large interstices within the sheet, and these are occupied by [10]-coordinated K atoms **(**Fig. 25a); the sheet is parallel to (001). When viewed in the *b*-direction, it can be seen (Fig. 25b) that each sheet consists of a layer of tetrahedra and a layer of octahedra. The interstitial K atoms actually lie completely *within* each sheet and hence do not participate in intersheet linkage. All (H_2O) groups of the structural unit occur on the underside of each sheet (Fig. 25b) and adjacent sheets are linked solely by hydrogen bonds.

The minerals of the **crandallite**, $Ca[Al_3(PO_4)(PO_3\{OH\})(OH)_6]$, group are based on an open sheet of corner-sharing $(Al\phi_6)$ octahedra that is decorated with (PO_4) and $(PO_3\{OH\})$ groups. This sheet can be envisaged as parallel $[M\phi_5]$ chains of octahedra that extend in the *a*- (plus symmetrically equivalent) direction (Fig. 25c) and are linked into a sheet by sharing corners with linking octahedra; thus all octahedra are four-connected within this sheet. There are prominent three-membered and six-membered rings of octahedra within this sheet, and the $(P\phi_4)$ tetrahedra share three vertices with octahedra of the three-membered rings (Fig. 25c). There is only one crystallographically distinct $(P\phi_4)$ group in the structure of crandallite, and hence the normal and acid phosphate group must be disordered. The resultant $[M^{3+}_3(T\phi_4)\phi_6]$ sheets (Fig. 25c) stack in the *c*-direction (Fig. 25d) and are linked by hydrogen bonds between the $(OH)_6$ anions

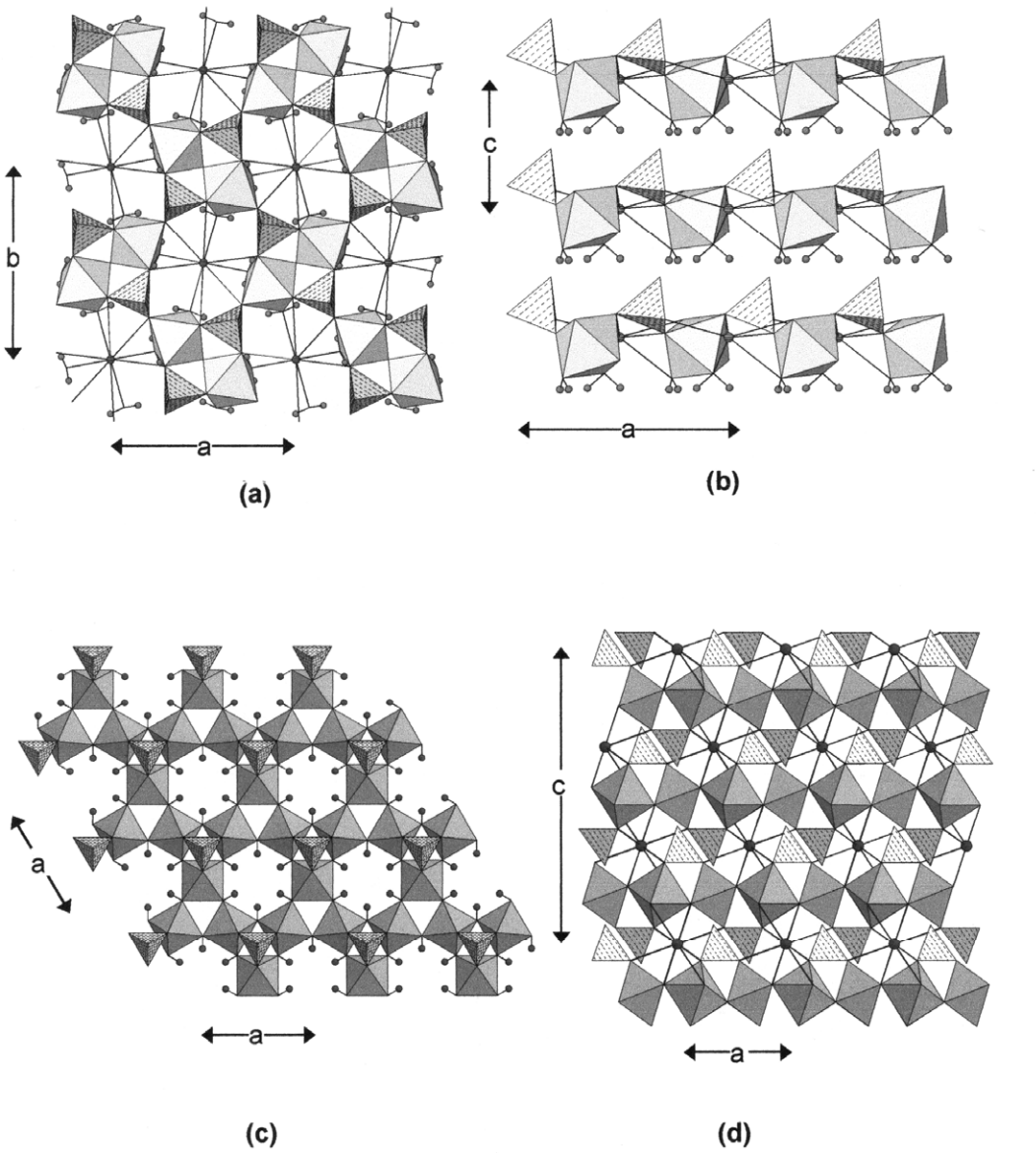

Figure 25. The crystal structures of minyulite and crandallite: (a) minyulite projected onto (001); (b) minyulite projected onto (010); (c) crandallite projected onto (001); (d) crandallite projected onto (001). (Alϕ_6) octahedra are shadow-shaded, H atoms are shown as small shaded circles, K atoms are shown as large shaded circles, Ca atoms are shown as dark circles.

of the octahedra and the 'free' vertex of the (Pϕ_4) group in the adjacent sheet, and by [10]-coordinated Ca. **Viséite** is a poorly crystalline mineral that McConnell (1952, 1990) has proposed as an aluminophosphate isotype of analcime. However, Kim and Kirkpatrick (1996) showed that viséite is a mixture of several phases; the dominant phase has a structure similar to that of crandallite, plus admixed phases that include an unidentified aluminophosphate, opal and a zeolitic framework aluminosilicate.

A prominent feature in **laueite**, $Mn^{2+}(H_2O)_4[Fe^{3+}{}_2(PO_4)_2(OH)_2(H_2O)_2](H_2O)_2$, and the minerals of the laueite group (Table 7) is the 7-Å chain shown in Figure 18c. ($Fe^{3+}\phi_6$) octahedra link by sharing *trans* vertices to form an [$M\phi_5$] chain that is decorated by flanking (PO_4) groups, and the resulting chains extend in the *c*-direction, giving a *c*-repeat of ~7.1 Å (see Appendix). These chains meld in the *a*-direction by sharing one quarter of the flanking (PO_4) vertices with octahedra of adjacent chains to form an $[Fe^{3+}{}_2(PO_4)_2(OH)_2(H_2O)_2]$ sheet (Fig. 26a); note that the sheet is written with two

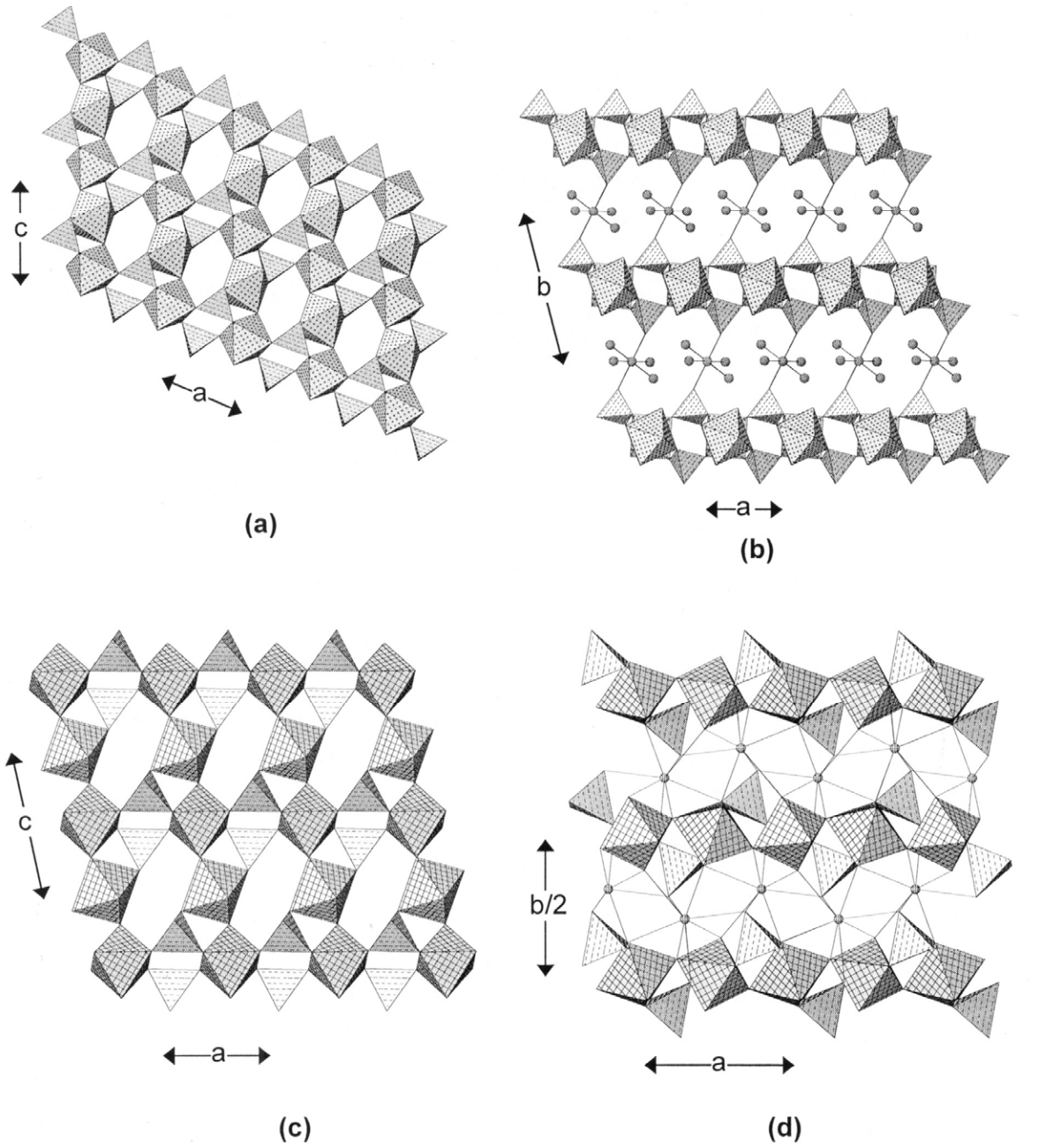

Figure 26. The crystal structures of laueite and curetonite: (a) laueite projected onto (010); (b) laueite projected onto (001); (H_2O) groups not bonded to any cations are not shown; (c) curetonite projected onto (010); (d) curetonite projected onto (001). (Feϕ_6) and (Alϕ_6) octahedra are dot-shaded and 4^4-net-shaded, respectively; Mn^{2+} and Ba are shown as shaded circles, selected (H_2O) groups are shown as grey circles.

octahedrally coordinated cations, rather than as $[M(TO_4)\phi_2]_2$ because the two octahedra are topologically distinct. In the resulting sheet, the (PO_4) tetrahedra are three-connected. Note that there are two distinct octahedra in these sheets, one of which is six-connected within the sheet, and the other of which is only four-connected and has (H_2O) at two vertices. Another prominent feature of this sheet is the $[M(TO_4)_2\phi_2]$ chain (Fig. 18b) that extends from SE to NW in Figure 26a. Thus we could also think of the laueite sheet as composed of $[Fe^{3+}(PO_4)_2O_2]$ chains that are linked by ($Fe^{3+}O_6$) octahedra. This occur-

rence of two different types of chain in a more highly connected structural unit is a common feature in minerals, and reflects Nature's parsimony in designing structural arrangements in crystals. These sheets stack in the *b*-direction and are linked by ($Mn^{2+}O_2\{H_2O\}_4$) octahedra (Fig. 26b), and by hydrogen bonds involving the interstitial (H_2O) groups bonded to Mn^{2+} *and* interstitial (H_2O) groups held in the structure solely by hydrogen bonds.

Curetonite, $Ba_2[Al_2(PO_4)_2(OH)_2F_2]$, contains an $[Al_2(PO_4)_2(OH)_2F_2]$ sheet (Fig. 26c) topologically identical to the analogous sheet in laueite (Figs. 26a). Note that the formula of curetonite has previously been written as half the formula unit given above, but that formulation ignored the fact that there are two topologically distinct ($Al\phi_6$) octahedra in the structural unit. There is another interesting wrinkle in the chemistry of curetonite, replacement of Al by Ti and (OH) by O^{2-}, which can give local areas of titanite-like arrangement within the sheet. The sheets stack in the *b*-direction (Fig. 26d) and are linked by interstitial [10]-coordinated Ba.

Stewartite, $Mn^{2+}(H_2O)_4[Fe^{3+}{}_2(PO_4)_2(OH)_2(H_2O)_2](H_2O)_2$, and **pseudolaueite**, $Mn^{2+}(H_2O)_4[Fe^{3+}{}_2(PO_4)_2(OH)_2(H_2O)_2](H_2O)_2$, are polymorphs of laueite. Both contain $[Fe^{3+}{}_2(PO_4)_2(OH)_2(H_2O)O^{P}{}_2]$ chains (cf. Fig. 18c), but the way in which these chains cross-link to form a sheet is different from the analogous linkage in laueite. In stewartite, there are three symmetrically distinct ($Fe\phi_6$) octahedra in the 7-Å chain, with coordinations ($\{OH\}_2O_2\{H_2O\}_2$), ($\{OH\}_2O_2\{H_2O\}_2$) and ($\{OH\}_2O_4$) with multiplicities of 1, 1 and 2, respectively. In laueite, there are two symmetrically distinct ($Fe\phi_6$) octahedra in the 7-Å chain, with coordinations ($\{OH\}_2O_2\{H_2O\}_2$) and ($\{OH\}_2O_4$) with multiplicities of 2 and 2, respectively. However, the cross-linkage of chains is different from in laueite, as is apparent from the presence of $[Fe^{3+}(PO_4)_2\phi_2]$ chains in laueite (Fig. 26a) and only fragments of this chain in stewartite (Fig. 27a). These sheets stack in the *c*-direction, linked by ($Mn^{2+}O_2\{H_2O\}_4$) octahedra (Fig. 27b) and hydrogen bonds involving (H_2O) bonded to interstitial cations and (H_2O) held in the structure solely by hydrogen bonding. In pseudolaueite, the $[Fe^{2+}{}_2(PO_4)_2(OH)_2(H_2O)O^{P}{}_2]$ chains condense to form a sheet (Fig. 27c) topologically distinct from those in laueite and stewartite; Moore (1975b) discusses in detail the isomeric variation in these (and related) sheets. These sheets stack along the *c*-direction (Fig. 27d) and are linked by ($Mn^{2+}O_2\{H_2O\}_4$) octahedra and by hydrogen bonds.

The sheets in **strunzite**, $Mn^{2+}(H_2O)_4[Fe^{3+}(PO_4)_2(OH)(H_2O)]_2$, and **metavauxite**, $Fe^{2+}(H_2O)_6[Al(PO_4)(OH)(H_2O)]_2$, are built from topologically identical $[M(TO_4)\phi_3]$ chains. In strunzite, the 7-Å chains extend in the *c*-direction and cross-link to form an $[Fe^{3+}(PO_4)(OH)(H_2O)]$ sheet (Fig. 28a) that is a graphical isomer of the $[Fe^{3+}{}_2(PO_4)_2(OH)_2(H_2O)_2]$ sheet in stewartite (Fig. 27a). These sheets stack in the *a*-direction (Fig. 28b) and are linked by ($Mn^{2+}O_2\{H_2O\}_4$) octahedra and hydrogen bonds. In metavauxite, the 7-Å chains also extend in the *c*-direction, and cross-link to form an $[Al(PO_4)(OH)(H_2O)]$ sheet (Fig. 28c). These sheets stack in the *a*-direction (Fig. 28d) and are linked by hydrogen bonds emanating from the interstitial ($Fe^{2+}\{H_2O\}_6$) groups.

Montgomeryite, $Ca_4Mg(H_2O)_{12}[Al_2(PO_4)_3(OH)_2]_2$, contains 7-Å chains of the form $[M(T\phi_4)\phi_2]$ (Fig. 18c) in which alternate octahedra are decorated by two tetrahedra that attach to *trans* vertices (Fig. 29a) to give a chain of the form $[M_2(TO_4)_4\phi_4]$ that extends in the [101] direction. These chains meld in the [10$\bar{1}$] direction by sharing flanking (PO_4) groups to form an $[Al_2(PO_4)_3(OH)_2]$ sheet that is parallel to (010) (Fig. 29a). These sheets stack in the [010] direction (Fig. 29b). The decorating tetrahedra of the 7-Å chains project above and below the plane of the sheet, and one Ca cation occurs in the interstices created by these tetrahedra, being coordinated by four O-atoms of the sheet and four interstitial (H_2O) groups. The second Ca cation links to four anions of the sheet and

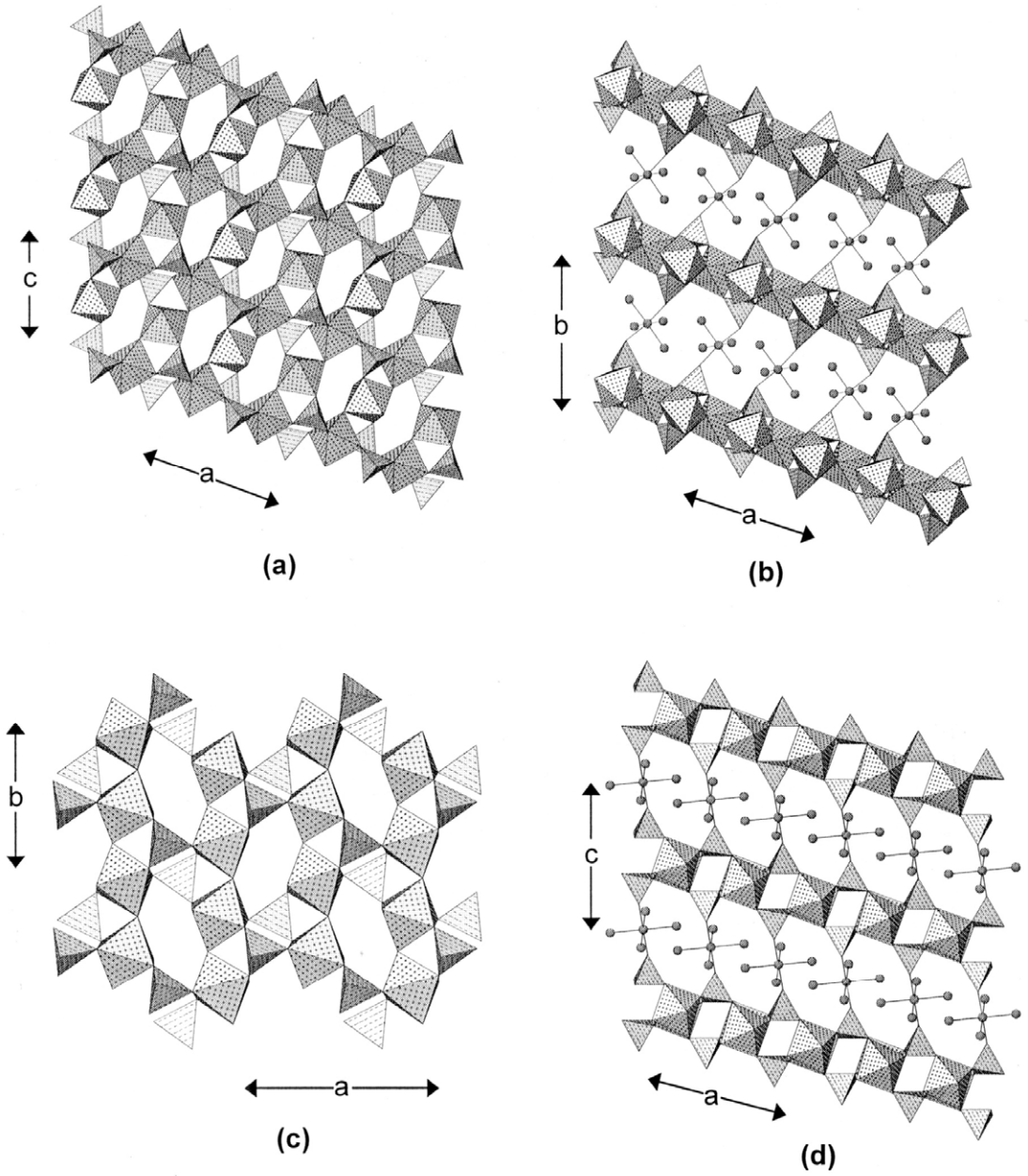

Figure 27. The crystal structures of stewartite and pseudolaueite: (a) stewartite projected onto (010); (b) stewartite projected onto (001); (c) pseudolaueite projected onto (001); (d) pseudolaueite projected onto (010). ($Fe^{3+}\phi_6$) octahedra are dot-shaded, Mn^{2+} and (H_2O) are shown as shaded circles.

shares four interstitial (H_2O) groups with an adjacent Ca that, in turn, links to the adjacent sheet. Further intersheet linkage is provided by octahedrally coordinated interstitial Mg that bonds to four interstitial (H_2O) groups.

Mitryaevaite, $[Al_5(PO_4)_2(PO_3\{OH\})_2F_2(OH)_2(H_2O)_8](H_2O)_{6.5}$, has quite a complex sheet that, nevertheless, can be related to other sheets in this group. An important motif in this sheet is an $[M_5(TO_4)_4\phi_{17}]$ fragment (Fig. 29c) of the $[M(TO_4)\phi]$ chain (Fig. 18c) that extends along ~[120]. These fragments meld in the ~[110] direction through tetrahedron-

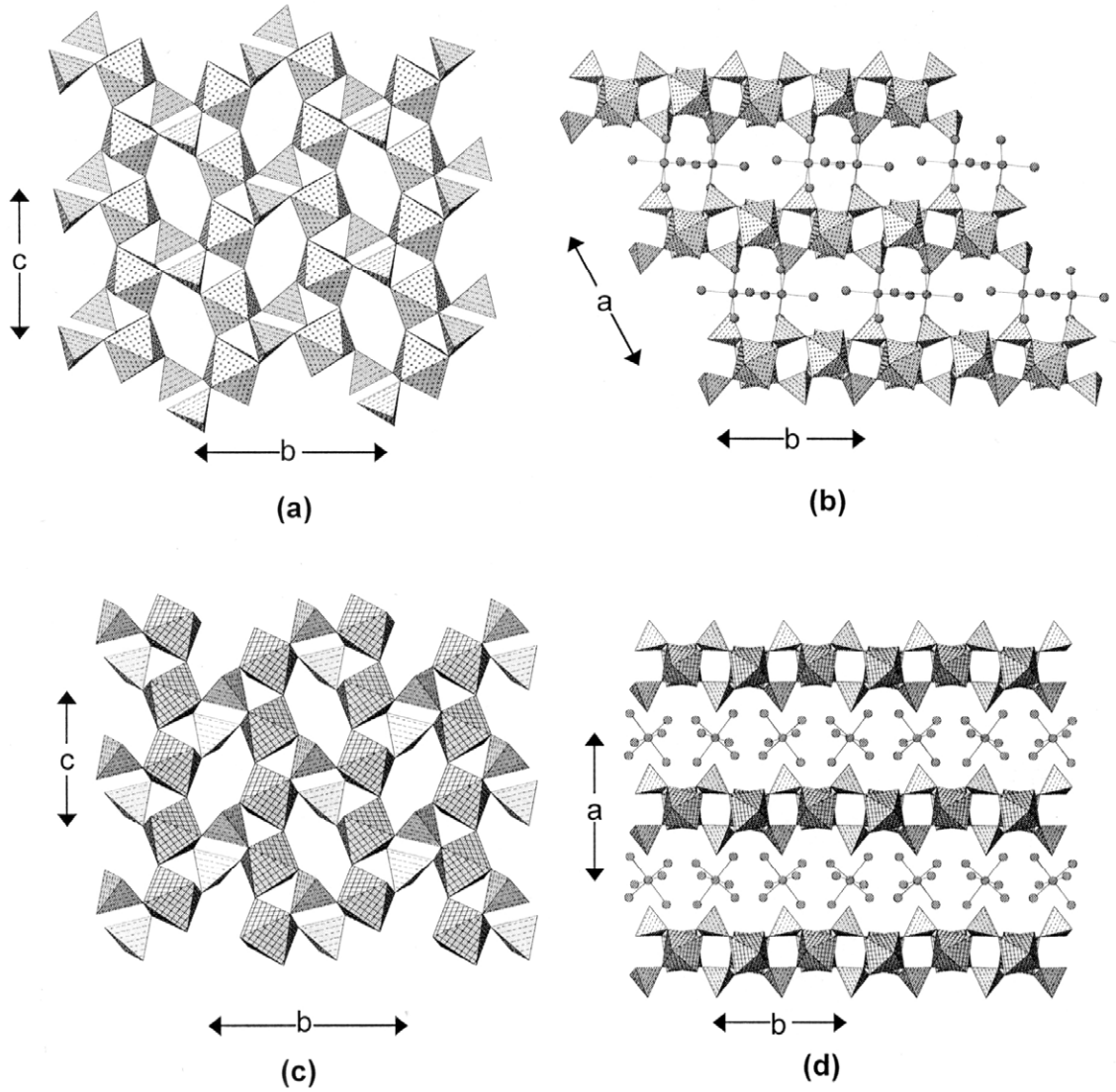

Figure 28. The crystal structures of strunzite and metavauxite: (a) strunzite projected onto (100); (b) strunzite projected onto (001); ($Fe^{3+}\phi_6$) octahedra are dot-shaded; (c) metavauxite projected onto (100); (d) metavauxite projected onto (001); ($Al\phi_6$) octahedra are 4^4-net-shaded, interstitial Mn^{2+} and (H_2O) groups are shown as shaded circles.

octahedron linkages to form a sheet (Fig. 29c) parallel to (110). The chain fragments are inclined to the plane of the sheet, giving it a very corrugated appearance in cross-section (Fig. 29d). These sheets stack in the *c*-direction and are linked by hydrogen bonds via inclined sheets of interstitial (H_2O) groups that do not bond to any cation.

~~~~~~

Figure 29 (next page). The crystal structures of montgomeryite, mitryaevaite and sidorenkoite: (a) montgomeryite projected onto (010); (b) montgomeryite projected onto (001); (c) mitryaevaite projected onto (001), showing the [$Al_5(P\phi_4)_4\phi_{12}$] sheet that is made up of [$M_5(TO_4)_4\phi_{17}$] fragments (one is shown in black) of the 7-Å [$M(TO_4)\ \phi$] chain; (d) mitryaevaite projected onto (100); ($Al\phi_6$) octahedra are 4^4-net-shaded, Mg are shown as small shaded circles, (H_2O) groups are shown as large shaded circles in (b) and small unshaded circles in (d); (e) sidorenkoite projected onto (100); (f) sidorenkoite projected onto (010); ($Mn^{2+}\phi_6$) octahedra are shadow-shaded, (CO_3) groups are lined triangles.
~~~~~~

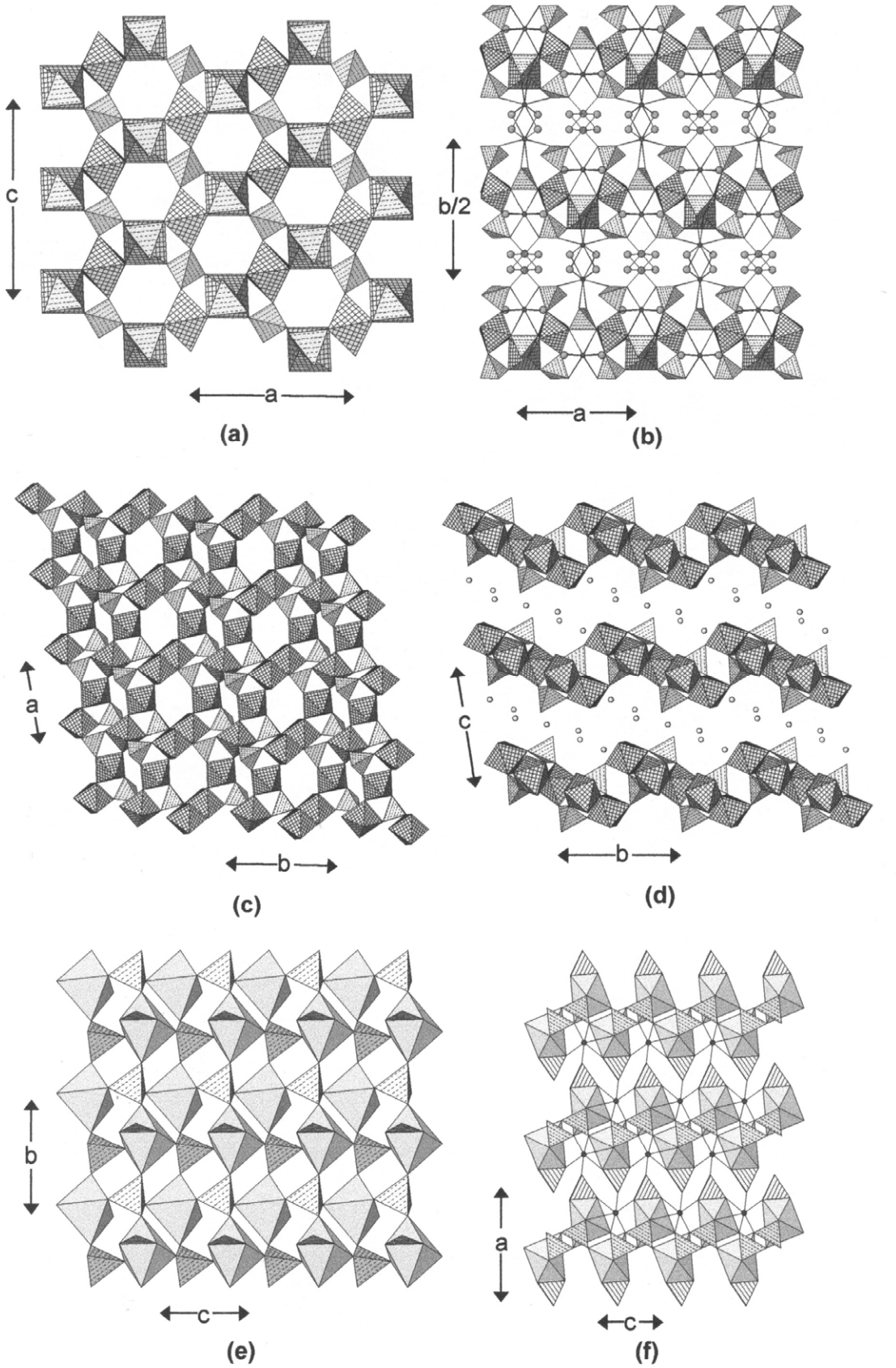
c
a
(a)
b/2
a
(b)
a
b
(c)
c
b
(d)
b
c
(e)
a
c
(f)

Sidorenkoite, $Na_3[Mn^{2+}(PO_4)(CO_3)]$, and the other minerals of the **bradleyite** group consist of (PO_4) groups and ($M^{2+}O_6$) octahedra at the vertices of a 4^4 plane net and link by sharing corners to form a sheet parallel to (100) (Fig. 29e). This leaves two octahedron vertices that do not link to (PO_4) groups; these link to (CO_3) groups that decorate the sheet above and below the plane of the sheet (Fig. 29f). These sheets are linked in the *a*-direction by [6]- and [7]-coordinated interstitial Na cations.

M=M, M-T linkage. **Bermanite**, $Mn^{2+}(H_2O)_4[Mn^{3+}(PO_4)(OH)]_2$, and **ercitite**, $Na_2(H_2O)_4[Mn^{3+}(PO_4)(OH)]_2$, are not formally isostructural as they have different space-group symmetries, but they contain topologically and chemically identical structural units. ($M\phi_6$) octahedra share pairs of *trans* edges to form an [$M\phi_4$] chain decorated with flanking tetrahedra that link vertices of adjacent octahedra (Fig. 18e). These chains extend parallel to [101] and link together by sharing octahedral vertices to form an [$M(TO_4)\phi$] sheet that is parallel to (010) in bermanite and ercitite (Fig. 30a). These sheets stack in the *b*-direction and are linked by ($Mn^{2+}O_2\{H_2O\}_4$) octahedra and by hydrogen bonds (Fig. 30b). The interstitial linkage is somewhat different in ercitite. One Mn^{2+} atom plus one vacancy (space group $P2_1$) is replaced by two Na atoms (space group $P2_1/m$), the Mn^{2+} and □ being ordered in bermanite and giving rise to the non-centrosymmetric space group.

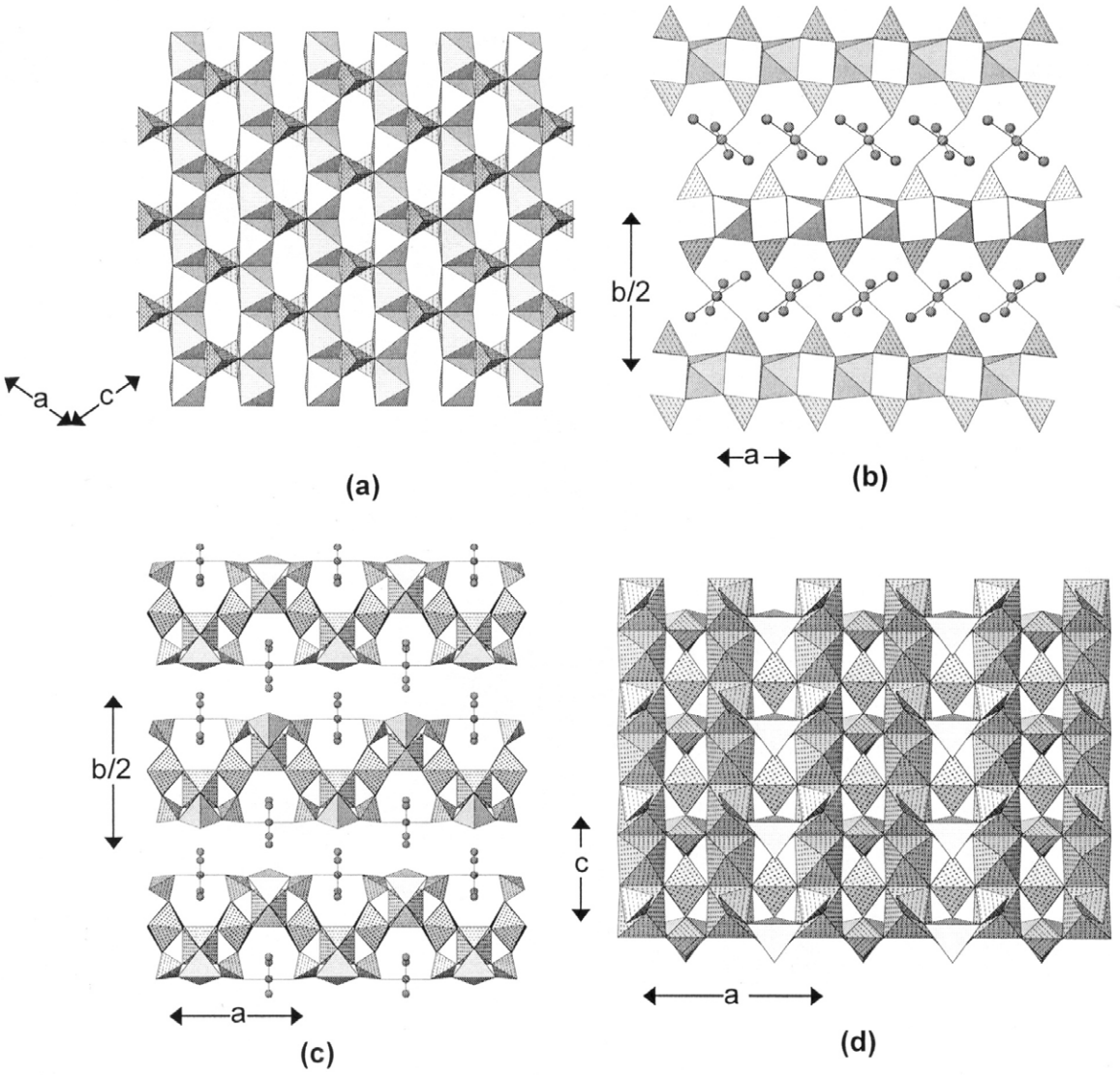

M=M, M-M, M-T linkage. **Schoonerite**, $[Mn^{2+}Fe^{2+}{}_2ZnFe^{3+}(PO_4)_3(OH)_2(H_2O)_7](H_2O)_2$, is a very complicated structure, and its assignment to a specific structural class is somewhat ambiguous. Figures 30c,d show the polyhedra and their connectivity. Inspection of Figure 30c indicates the sheet-like nature of the structure. However, the sheet includes both divalent *and* trivalent cations, and is further complicated by the fact that Zn is [5]-coordinated. There are two prominent motifs within the sheet, an $[Fe^{2+}\phi_4]$ chain of edge-sharing octahedra extending in the *c*-direction, and an $[Fe^{3+\,[5]}Zn(PO_4)_2\phi_6]$ cluster. These link in the *a*-direction to form a continuous sheet (Fig. 30d) that is further strengthened by $(Mn^{2+}O_2\{H_2O\}_4)$ octahedra occupying dimples in the sheet. These sheets stack in the *b*-direction and are linked by hydrogen bonds. Assigning the divalent cations as interstitial species results in a finite-cluster structure, not in accord with the dense distribution of polyhedra in the sheet arrangement of Figure 30d. However, we must recognize a somewhat arbitrary aspect of the assignment here. Another aspect that suggests a sheet structure is the 7-Å chain that extends in the *a*-direction; this chain involves both Fe^{3+} and Fe^{2+}.

Nissonite, $[Cu^{2+}Mg(PO_4)(OH)(H_2O)_2]_2(H_2O)$, consists of a thick slab of polyhedra linked solely by hydrogen bonds. $(Mg\phi_6)$ octahedra and (PO_4) tetrahedra lie at the vertices of a 6^3 plane net (Fig. 31a); this layer, $[Mb(PO_4)(OH)(H_2O)_2]$, is topologically identical with the $[Mg(PO_3\{OH\})(H_2O)_3]$ sheet in newberyite (Fig. 24a). However, the tetrahedra in newberyite point alternately up and down relative to the plane of the sheet, whereas the tetrahedra in nissonite all point in the same direction; hence these sheets are topologically identical but graphically distinct, and are geometrical isomers (Hawthorne 1983a, 1985a). Edge-sharing $[Cu^{2+}{}_2O_8(OH)_2]$ dimers link by sharing corners to form the sheet shown in Figure 31b. The $[Mg(PO_4)(OH)(H_2O)_2]$ sheets sandwich the $[Cu^{2+}{}_2O_8(OH)_2]$ sheet to form a thick slab parallel to (100). These slabs link through hydrogen bonds both directly and involving interstitial (H_2O) groups not bonded to any cation (Fig. 31c).

Foggite, $Ca[Al(PO_4)(OH)_2](H_2O)$, contains $[Al\phi_4]$ α-PbO_2-like chains of edge-sharing $(Al\phi_6)$ octahedra that extend in the *c*-direction and are cross-linked into a sheet by (PO_4) tetrahedra (Fig. 32a). These sheets are parallel to (010), and are linked by [8]- and [10]-coordinated interstitial Ca (Fig. 32b) and by hydrogen bonds involving interstitial (H_2O) groups. The structure of foggite is strongly related to the pyroxene structure, specifically calcium tschermakite. Figure 32c depicts the structure of foggite projected onto (100), showing the *M*(1)-like chains and their associated tetrahedra. Moore et al. (1975b) expressed the relation as follows:

Foggite	$[CaAl_2P_2O_8(OH)_4]$-$Ca(H_2O)_2$
Px	$[CaAl_2{}^{[6]}T_2O_{12}]$-$Ca^{[4]}T_2$

Whitmoreite, $Fe^{2+}(H_2O)_4[Fe^{3+}(PO_4)(OH)]_2$, consists of a fairly densely packed sheet of (PO_4) tetrahedra and $(Fe^{3+}\phi_6)$ octahedra parallel to (100) (Fig. 32d). Pairs of $Fe^{3+}\phi_6$ octahedra condense to form edge-sharing $[Fe^{3+}{}_2\phi_{10}]$ dimers that occupy the vertices of a 4^4 plane net and link by sharing corners. This results in an interrupted sheet of octahedra, the interstices of which are occupied by (PO_4) tetrahedra (Fig. 32d). These sheets stack in the *a*-direction, and are linked by interstitial $(Fe^{2+}O_2\{H_2O\}_4)$ octahedra and by hydrogen bonds (Fig. 32e).

~~~~~~~~~~~~~~~~~~~~~~~~~~~~~~~~~~~~

Figure 30 (opposite page). The crystal structures of bermanite and schoonerite: (a) bermanite projected onto (010); (b) bermanite projected onto (001); (c) schoonerite projected onto (001); note that Zn is [5]-coordinated; (d) schoonerite projected onto (010). $(Mn^{3+}\phi_6)$ octahedra and $(Zn\phi_4)$ tetrahedra are shadow-shaded, $(\{Mn^{2+},Fe^{2+},Fe^{3+}\}\phi_6)$ octahedra are dot-shaded, Mn^{2+} and (H_2O) groups are shown as shaded circles.
~~~~~~~~~~~~~~~~~~~~~~~~~~~~~~~~~~~~

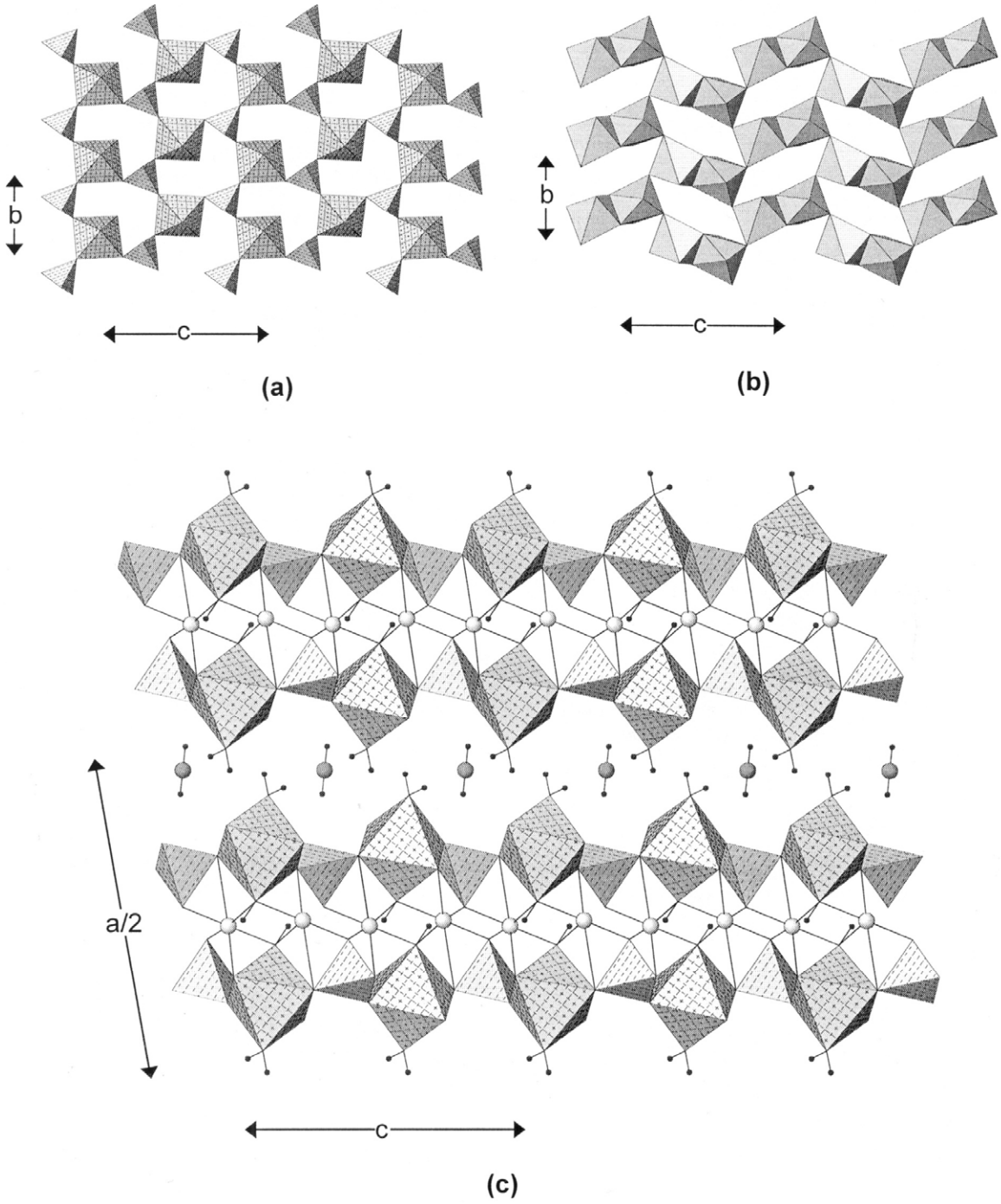

Figure 31. The crystal structure of nissonite: (a) the $[Mg(PO_4)(OH)(H_2O)_2]$ layer parallel to (100); (b) the $[Cu^{2+}{}_2O_8(OH)_2]$ layer parallel to (100); (c) a view of the $[Cu^{2+}Mg(PO_4)(OH)(H_2O)_2]$ sheet in the *b*-direction, showing the $[Cu^{2+}{}_2O_8(OH)_2]$ layer sandwiched by two $[Mg(PO_4)(OH)(H_2O)_2]$ layers. ($Mg\phi_6$) octahedra are square-pattern-shaded, ($Cu^{2+}\phi_6$) octahedra are shadow-shaded, Cu^{2+} cations are shown as light circles, H atoms are shown as small black circles, O atoms of interstitial (H_2O) groups are shown as shaded circles.

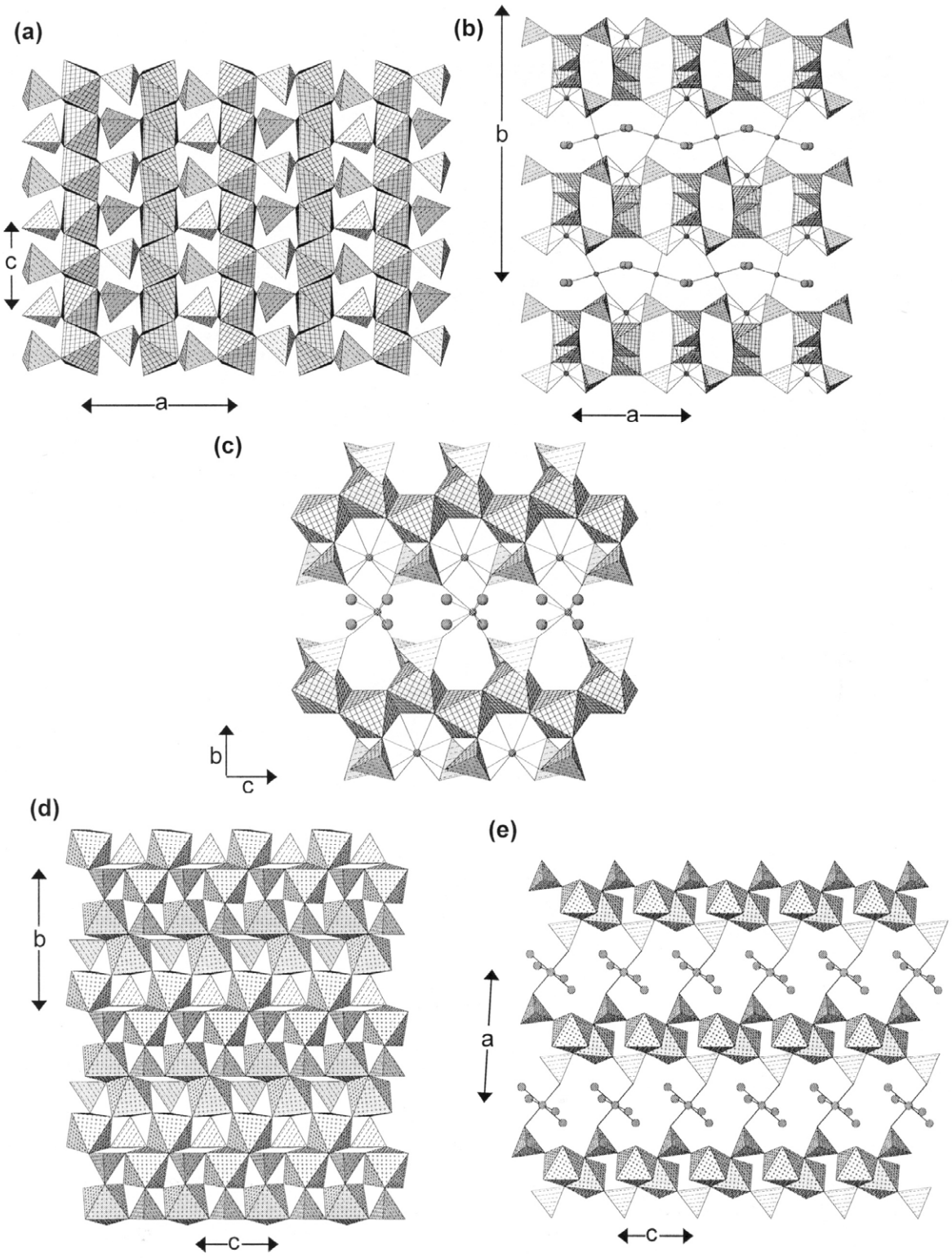

Figure 32. The crystal structures of foggite and whitmoreite: (a) foggite projected onto (010); (b) foggite projected onto (001); (c) foggite projected onto (100), showing its similarity to the monoclinic pyroxene (calcium tschermaks) structure; (d) whitmoreite projected onto (100); (e) whitmoreite projected onto (010). ($Al\phi_6$) octahedra are 4^4-net-shaded, ($Fe^{3+}\phi_6$) octahedra are dot-shaded, Ca atoms are shown as small shaded circles, (H_2O) groups are shown as large shaded circles, Fe^{2+} atoms are shown as small shaded circles in (e).

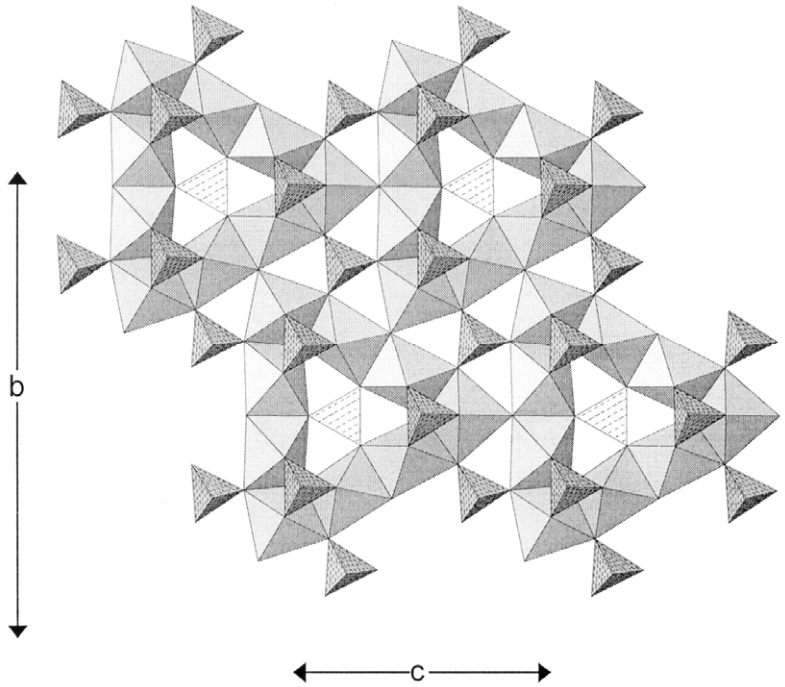

Figure 33. The crystal structure of mitridatite projected onto (100); ($Fe^{3+}\phi_6$) octahedra are shadow-shaded.

Mitridatite, $Ca_6(H_2O)_6[Fe^{3+}{}_9O_6(PO_4)_9](H_2O)_3$, has a sheet structural unit of exotic complexity. ($Fe^{3+}\phi_6$) octahedra share edges to form nonameric triangular rings that are braced by a central (PO_4) group that shares corners with six octahedra (Fig. 33). These clusters link by their corners linking to the mid-points of the edges of adjacent clusters. The resulting interstices are occupied by (PO_4) tetrahedra that point in the opposite direction to the tetrahedra occupying the centres of the clusters. These sheets are linked by [7]-coordinated interstitial Ca and by hydrogen bonds involving interstitial (H_2O) bonded to Ca and interstitial (H_2O) groups not bonded to any cation.

Vivianite, $[Fe^{2+}{}_3(PO_4)_2(H_2O)_8]$, contains two crystallographically distinct Fe^{3+} cations that are octahedrally coordinated by ($O_2\{H_2O\}_4$) and ($O_4\{H_2O\}_2$), respectively. Pairs of ($Fe^{2+}O_4\{H_2O\}_2$) octahedra share edges to form a dimer that is decorated by two (PO_4) groups that each link to corners of each octahedron, forming an $[Fe^{2+}{}_2(PO_4)_2\phi_6]$ cluster. These clusters are linked in the *c*-direction by ($Fe^{2+}O_2\{H_2O\}_4$) octahedra (Fig. 34a). These chains link in the *a*-direction (Fig. 34b) by corner-sharing between tetrahedra and octahedra to form sheets parallel to (010). The sheets are linked solely by hydrogen bonds in the *b*-direction (Fig. 34a). **Bobierrite**, $[Mg_3(PO_4)(H_2O)_8]$, has a structure very similar to that of vivianite. The sheets of octahedra and tetrahedra are topologically identical (Figs. 34c,d), but the attitude of adjacent sheets in the *b*-direction is sufficiently different such that the hydrogen-bond linkage between the sheets differs from that in vivianite. In vivianite, the hydrogen-bond linkages are at an angle to the plane of the sheet (Fig. 34a), whereas in bobierrite, the hydrogen-bond linkages are orthogonal to the plane of the sheet (Fig. 34c). These difference in the attitude of adjacent sheets is reflected in the symmetries of the two structures: *C*2/*m* (vivianite) versus *C*2/*c* (bobierrite).

Structures with infinite frameworks of (PO_4) tetrahedra and ($M\phi_6$) octahedra

The minerals of this class are listed in Table 8; graphs are not shown for framework structures because representing such a structure in two dimensions is not satisfactory and the representation can be confusing.

Table 8. Phosphate minerals based on infinite frameworks of tetrahedra and octahedra.

Mineral	*Structural unit*	*Space group*	*Figure*
Kolbeckite	$[Sc(PO_4)(H_2O)_2]$	$P2_1/n$	35a,b
Metavariscite*	$[Al(PO_4)(H_2O)_2]$	$P2_1/n$	35a,b
Phosphosiderite	$[Fe^{3+}(PO_4)(H_2O)_2]$	$P2_1/n$	35a,b
Strengite	$[Fe^{3+}(PO_4)(H_2O)_2]$	$Pbca$	35c,d
Variscite*	$[Al(PO_4)(H_2O)_2]$	$Pbca$	35c,d
Kosnarite	$[Zr_2(PO_4)_3]$	$R\bar{3}c$	35e,f
Isokite	$[Mg(PO_4)F]$	$C2/c$	36a,b
Lacroixite	$[Al(PO_4)F]$	$C2/c$	36a,b
Panasqueraite	$[Mg(PO_4)(OH)]$	$C2/c$	36a,b
Titanite *	$[Ti(SiO_4)O]$	$C2/c$	36a,b
Amblygonite *	$[Al(PO_4)F]$	$C\bar{1}$	36c,d
Montebrasite	$[Al(PO_4)(OH)]$	$C\bar{1}$	36c,d
Natromontebrasite	$[Al(PO_4)(OH)]$	–	36c,d
Tavorite	$[Fe^{3+}(PO_4)(OH)]$	–	36c,d
Cyrilovite	$[Fe^{3+}{}_3(PO_4)_2(OH)_4]$	$P4_12_12$	37a,b
Wardite*	$[Al_3(PO_4)_2(OH)_4]$	$P4_12_12$	37a,b
Fluellite	$[Al_2(PO_4)F_2(OH)]$	$Fddd$	37c,d
Wavellite	$[Al_3(PO_4)_2(OH)_3(H_2O)_2]$	$Pcmn$	37e,f
Augelite	$[Al_2(PO_4)(OH)_3]$	$C2/m$	38a,b
Jagowerite *	$[Al(PO_4)(OH)]_2$	$P\bar{1}$	38c,d
Marićite	$[Fe^{2+}(PO_4)]$	$Pmnb$	38e,f
Kovdorskite	$[Mg_2(PO_4)(OH)(H_2O)_3]$	$P2_1/a$	39a,b
Libethenite	$[Cu^{2+}{}_2(PO_4)(OH)]$	$Pnnm$	39c,d
Adamite*	$[Cu^{2+}{}_2(AsO_4)(OH)]$	$Pnnm$	39c,d
Tarbuttite	$[Zn_2(PO_4)(OH)]$	$P\bar{1}$	39e,f
Paradamite*	$[Zn_2(AsO_4)(OH)]$	$P\bar{1}$	39e,f
Mixite*	$[Cu^{2+}{}_6(AsO_4)_3(OH)_6]$	$P6_3/m$	40a,b
Petersite-(Y)	$[Cu^{2+}{}_6(PO_4)_3(OH)_6]$	$P6_3/m$	40a,b
Brazilianite	$[Al_3(PO_4)_2(OH)_4]$	$P2_1/n$	40c,d
Pseudomalachite	$[Cu^{2+}{}_5(PO_4)_2(OH)_2(H_2O)]$	$P2_1/c$	41a,b
Reichenbachite	$[Cu^{2+}{}_5(PO_4)_2(OH)_4(H_2O)]$	$P2_1/a$	41c,d
Ludjibaite	$[Cu^{2+}{}_5(PO_4)_2(OH)_4(H_2O)]$	$P\bar{1}$	41e,f
Magniotriplite	$[Mg_2(PO_4)F]$	$I2/a$	42a,b
Triplite *	$[Mn^{2+}{}_2(PO_4)F]$	$I2/c$ (?)	42a,b
Zweiselite	$[Fe^{2+}{}_2(PO_4)F]$	$I2/a$ (?)	42a,b
Triploidite *	$[Mn^{2+}{}_2(PO_4)(OH)]$	$P2_1/a$	42c,d
Wagnerite	$[Mg_2(PO_4)F]$	$P2_1/a$	42c,d
Wolfeite	$[Fe^{2+}{}_2(PO_4)(OH)]$	$P2_1/a$	42c,d
Alluaudite *	$[Fe^{2+}(Mn,Fe^{2+},Fe^{3+},Mg)_2(PO_4)_3]$	$I2/a$	43a,b
Hagendorfite	$[Mn^{2+}(Fe^{2+},Mg,Fe^{3+})_2(PO_4)_3]$	$I2/a$	43a,b
Maghagendorfite	$[Mn^{2+}(Mg,Fe^{2+},Fe^{3+})_2(PO_4)_3]$	–	43a,b
Quingheite			43a,b
Varulite	$[Mn^{2+}(Mn,Fe^{2+},Fe^{3+})_2(PO_4)_3]$	–	43a,b
Rosemaryite	$[Mn^{2+}Fe^{3+}Al(PO_4)_3]$	$C2/c$ (?)	43c,d
Wyllieite *	$[Mn^{2+}Fe^{2+}Al(PO_4)_3]$	$P2_1/n$	43c,d
Bobfergusonite	$[Mn^{2+}Fe^{3+}Al(PO_4)_6]$	$P2_1/n$	43e,f
Ludlamite	$[Fe^{2+}{}_3(PO_4)_2(H_2O)_4]$	$P2_1/a$	45a,b
Melonjosephite	$[(Fe^{2+},Fe^{3+})(PO_4)(OH)]$	$Pnam$	45c,d

Bertossaite *	$[Al(PO_4)(OH)]_4$	*I*aa*	45e,f
Palermoite	$[Al(PO_4)(OH)]_4$	*Imcb*	45e,f
Arrojadite*	$[Fe^{2+}{}_{14}Al(PO_4)_{12}(OH)_2]$	*C*2/*c*	–
Dickinsonite	$[Mn^{2+}{}_{14}Al(PO_4)_{12}(OH)_2]$	*C*2/*c*	–
Farringtonite	$[Mg_3(PO_4)_2]$	$P2_1/n$	46a,b
Beusite	$[Mn^{2+}{}_3(PO_4)_2]$	$P2_1/c$	46c,d
Graftonite*	$[Fe^{2+}{}_3(PO_4)_2]$	$P2_1/c$	46c,d
Bederite	$[Mn^{2+}{}_2\,Fe^{3+}{}_2\,Mn^{3+}{}_2(PO_4)_6]$	*Pcab*	47a,b,c
Wicksite	$[Fe^{2+}{}_4\,MgFe^{3+}(PO_4)_6]$	*Pcab*	47a,b,c
Aheylite	$[Al_6(PO_4)_4(OH)_8]$	$P\bar{1}$	47d,e
Chalcosiderite	$[Fe^{3+}{}_6(PO_4)_4(OH)_8]$	$P\bar{1}$	47d,e
Coeruleolactite	$[Al_6(PO_4)_4(OH)_8]$	$P\bar{1}$	47d,e
Faustite	$[Al_6(PO_4)_4(OH)_8]$	$P\bar{1}$	47d,e
Planerite	$[Al_6(PO_4)_2(PO_3\{OH\})_2(OH)_8]$	$P\bar{1}$	47d,e
Turquoise *	$[Al_6(PO_4)_4(OH)_8]$	$P\bar{1}$	47d,e
Leucophosphite*	$[Fe^{3+}{}_2(PO_4)_2(OH)(H_2O)]$	$P2_1/n$	48a,b,c
Tinsleyite	$[Al_2(PO_4)_2(OH)(H_2O)]$	$P2_1/n$	48a,b,c
Cacoxenite	$[Fe^{3+}{}_{25}(PO_4)_{17}O_6(OH)_{12}]$	$P6_3/m$	49a,b,c,d
Althausite	$[Mg_4\,(PO_4)_2(OH)F]$	*Pnma*	50a,b
Hureaulite	$[Mn^{2+}{}_5(PO_3\{OH\})_2(PO_4)_2(H_2O)_4]$	*C*2/*c*	50c,d
Thadeuite	$[CaMg_3(PO_4)_2(OH)_2]$	$C222_1$	50e,f
Bakhchisaraitsevite	$[Mg_5(PO_4)_4(H_2O)_5]$	$P2_1/c$	51a,b
Kryzhanovskite	$[Mn^{2+}Fe^{3+}{}_2(PO_4)_2(OH)_2(H_2O)]$	*Pbna*	51c,d
Phosphoferrite*	$[Fe^{2+}{}_3(PO_4)_2(H_2O)_3]$	*Pbna*	51c,d
Griphite	$[A_{24}Fe^{2+}{}_4Al_8(PO_4)_{24}]$	$Pa\bar{3}$	52a,b,c,d
Cornetite	$[Cu^{2+}{}_3(PO_4)(OH)_3]$	*Pbca*	52e,f
Chladniite	$[Mg_7(PO_4)_6]$	$R\bar{3}$	–
Fillowite*	$[Mn^{2+}{}_7(PO_4)_6]$	$R\bar{3}$	–
Galileiite	$[Fe^{2+}{}_7(PO_4)_6]$	$R\bar{3}$	–
Johnsomervilleite	$[Mg_7(PO_4)_6]$	$R\bar{3}$	–
Gladiusite	$[Fe^{2+}{}_4Fe^{3+}{}_2(PO_4)(OH)_{11}(H_2O)$	$P2_1/n$	53a,b,c
Lipscombite	$[Fe^{2+}Fe^{3+}{}_2(PO_4)_2(OH)_2]$	$P4_32_12$	53d,e
Burangaite	$[Fe^{2+}Al_5(PO_4)_4(OH)_6(H_2O)_2]$	*C*2/*c*	54a
Dufrénite	$[Fe^{2+}Fe^{3+}{}_5(PO_4)_4(OH)_6(H_2O)_2]$	*C*2/*c*	54a
Natrodufrénite	$[Fe^{2+}Fe^{3+}{}_5(PO_4)_4(OH)_6(H_2O)_2]$	*C*2/*c*	54a
Frondellite	$[Fe^{2+}Fe^{3+}{}_4(PO_4)_3(OH)_5]$	*Bbmm*	54b,c
Rockbridgeite*	$[Fe^{2+}Fe^{3+}{}_4(PO_4)_3(OH)_5]$	*Bbmm*	54b,c
Barbosalite	$[Fe^{3+}(PO_4)(OH)]_2$	$P2_1/c$	54d,e
Hentschelite	$[Fe^{3+}(PO_4)(OH)]_2$	$P2_1/c$	54d,e
Lazulite*	$[Al(PO_4)(OH)]_2$	$P2_1/c$	54d,e
Scorzalite	$[Al(PO_4)(OH)]_2$	$P2_1/c$	54d,e
Trolleite	$[Al_4(PO_4)_3(OH)_3]$	*I*2/*c*	55a,b
Seamanite	$[Mn^{2+}{}_3(PO_4)(B\{OH\}_4)(OH)_2]$	*Pbnm*	55c,d
Holtedahlite	$[Mg_{12}(PO_3\{OH\})(PO_4)_5(OH)_6]$	*P*31*m*	55e,f
Satterlyite	$[Fe^{2+}{}_4(PO_4)_2(OH)_2]$	$P\bar{3}\,1m$	55e,f
Triphylite*	$[Fe^{2+}(PO_4)]$	*Pbnm*	56a,b
Lithiophylite	$[Mn^{2+}(PO_4)]$	*Pbnm*	56a,b
Natrophilite	$[Mn^{2+}(PO_4)]$	*Pbnm*	56a,b
Ferrisicklerite	$[Mn^{2+},Fe^{3+}(PO_4)]$	*Pbnm*	56c,d
Sicklerite*	$[Fe^{2+},Mn^{3+}(PO_4)]$	*Pbnm*	56c,d
Heterosite*	$[Fe^{3+}(PO_4)]$	*Pmnb*	56e,f
Purpurite	$[Mn^{3+}(PO_4)]$	*Pmnb*	56e,f

Senegalite	$[Al_2(PO_4)(OH)_3(H_2O)]$	$P2_1nb$	57a,b,c
Sarcopside	$[Fe^{2+}{}_3(PO_4)_2]$	$P2_1/a$	58a,b
Bjarebyite*	$[Al_2(PO_4)_3(OH)_3]$	$P2_1/m$	58c,d
Kulanite	$[Al_2(PO_4)_3(OH)_3]$	$P2_1/m$	58c,d
Penikisite	$[Al_2(PO_4)_3(OH)_3]$	$P2_1/m$	58c,d
Perloffite	$[Fe^{3+}{}_2(PO_4)_3(OH)_3]$	$P2_1/m$	58c,d

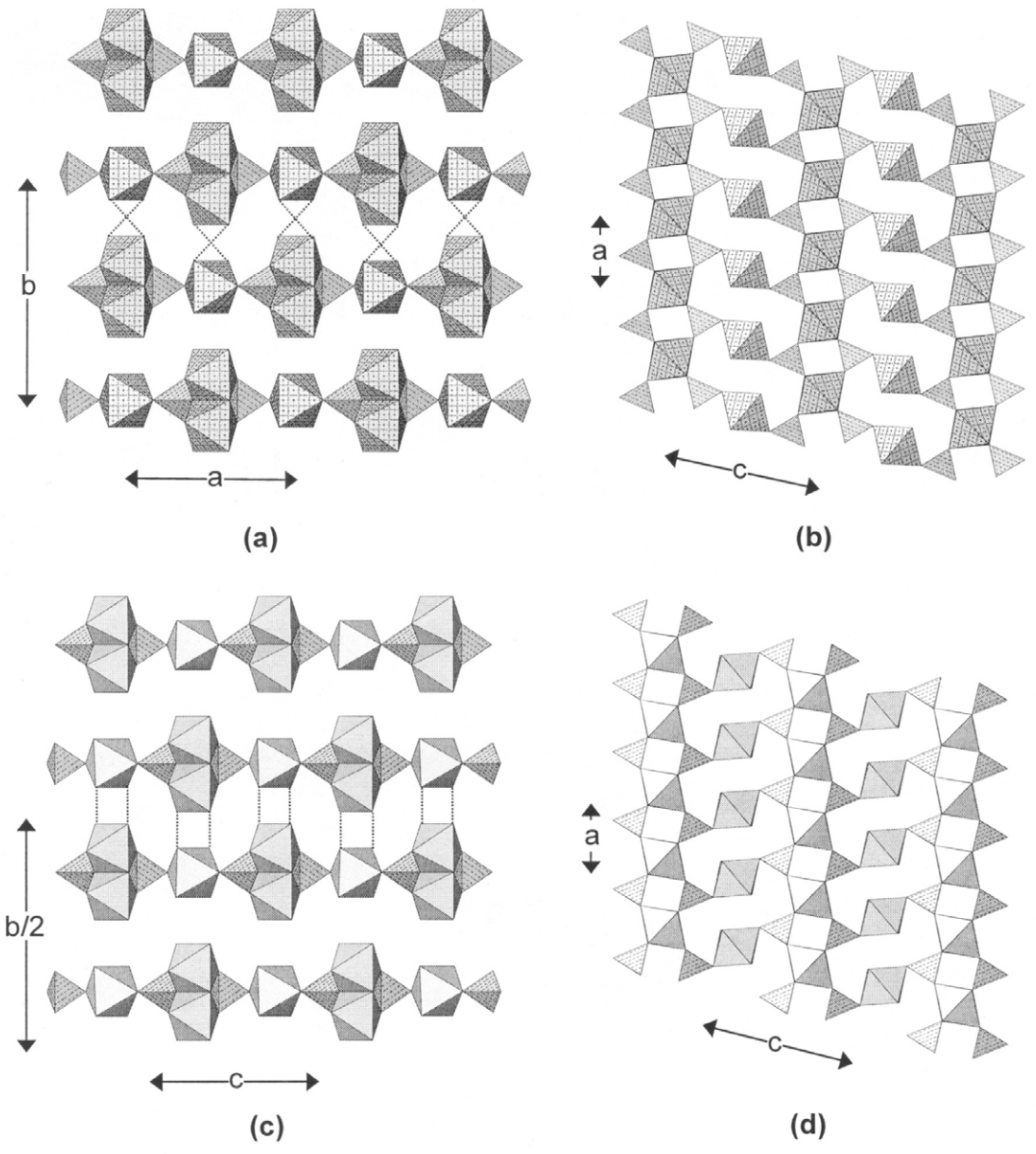

Figure 34. The crystal structures of vivianite and bobierrite: (a) vivianite projected onto (001); (b) vivianite projected onto (010); (c) bobierrite projected onto (100); (d) bobierrite projected onto (010). ($Fe^{2+}\phi_6$) octahedra are square-pattern-shaded, ($Mg\phi_6$) octahedra are shadow-shaded, donor-acceptor pairs for hydrogen bonds are shown by dotted lines.

M-T linkage. The minerals of the **metavariscite**, $[Al(PO_4)(H_2O)_2]$, and **variscite**, $[Al(PO_4)(H_2O)_2]$, groups consist of simple frameworks of alternating (PO_4) tetrahedra and ($Al\phi_6$) octahedra. As there are equal numbers of tetrahedra and octahedra, both

polyhedra are four-connected, and hence two vertices of the ($Al\phi_6$) octahedron must be one-connected. The local bond-valence requirements of the anions at these one-connected vertices require that the anions be (H_2O) groups. When viewed down the *c*-direction, octahedra and tetrahedra occupy the vertices of a 6^3 net, and Figures 35a,c show two layers of such nets. When metavariscite is viewed in the *a*-direction (Fig. 35b), the

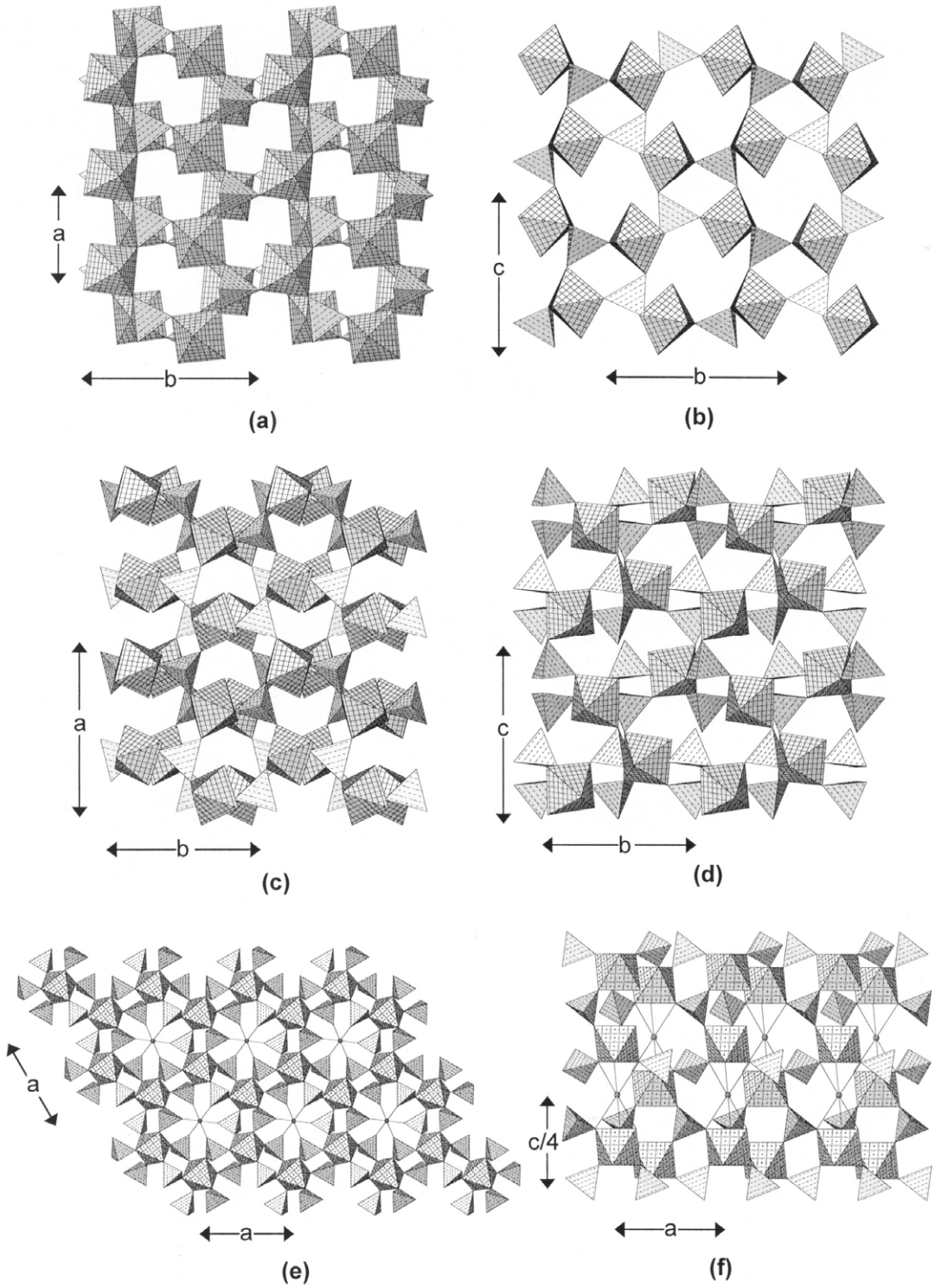

tetrahedra and octahedra occupy the vertices of a 4.8^2 plane net. Note how the one-connected vertices of the octahedra project into the large eight-membered ring, giving room for the H atoms of the (H_2O) groups at these vertices. When viewed down [100] (Fig. 35d), variscite shows alternating tetrahedra and octahedra occupying the vertices of a very puckered 8^3 net. As with metavariscite, the one-connected vertices of the octahedra project into the large cavities.

Kosnarite, X[$Zr_2(PO_4)_3$], contains octahedrally coordinated Zr. In projection down [001] (Fig. 35e), (ZrO_6) octahedra occupy the vertices of a 6^3 net, and all octahedron vertices link to (PO_4) tetrahedra, forming a slab with prominent interstices. These slabs stack in the *c*-direction and link by sharing of octahedron-tetrahedron vertices (Fig. 35f), with [6]-coordinated X cations in the interstices of the framework.

M-M, M-T linkage. The minerals of the **amblygonite**, Li[Al(PO_4)F], group and the phosphate members of the titanite group, such as **lacroixite**, Na[Al(PO_4)F], have topologically identical structural units. However, lacroixite is monoclinic, whereas the amblygonite-group minerals are triclinic; because of their topological identity, we use the unconventional space group $C\bar{1}$ to emphasize the congruity of these two structures (Table 8). A key feature of both structures is the 7-Å [$M\phi_5$] chain of corner-sharing octahedra that extends in the *c*-direction (Figs. 36a,c). This chain is decorated by staggered flanking (PO_4) groups that link the chains in both the *a*- and *b*-directions, a feature that is very apparent in an end-on view of the chains (Figs. 36b,d). The frameworks are strengthened by interstitial alkali cations Na and Li in the minerals of the amblygonite group and both Ca and Na in the minerals of the titanite group.

Cyrilovite, Na[$Fe^{3+}_3(PO_4)_2(OH)_4(H_2O)_2$] is a member of the wardite group (Table 8). The principal motif in cyrilovite is the [$Fe^{3+}\phi_5$] chain that is decorated by (PO_4) tetrahedra arranged in a staggered fashion at the periphery of the chain (the [$M(TO_4)\phi_3$] chain shown in Fig. 18c). These chains extend parallel to the *a*- and *b*-directions (note the tetragonal symmetry) to form a slab of corner-sharing octahedra and tetrahedra (Fig. 37a), tetrahedra on opposite sides of each chain pointing in opposing directions along *c*. The tetrahedral vertices that project out of the plane of the slab link to octahedra of adjacent slabs (Fig. 37a) to form a framework that consists of successive layers of octahedra and tetrahedra along the *c*-direction. [8]-coordinated Na occupies the large interstices in this framework (Fig. 37b), and hydrogen bonds strengthen the framework.

Fluellite, [$Al_2(PO_4)F_2(OH)(H_2O)_3$]($H_2O$)$_4$, is an open framework of corner-sharing (PO_4) tetrahedra and ($Al\phi_6$) octahedra. The principal motif of the framework is a 7-Å chain of the form [$M(TO_4)\phi_3$] (Fig. 18c) consisting of ($AlF_2\{OH\}(H_2O)_3$) octahedra linked through pairs of *trans* vertices (= F) and decorated by (PO_4) tetrahedra that link adjacent octahedra along the chain. These chains extend in both the *a*- and *b*-directions (Fig. 37c) by sharing (PO_4) groups between chains extending in orthogonal directions (Fig. 37d). There are large interstices within the framework that accommodate (H_2O) groups held in the structure solely by hydrogen bonds emanating from the (H_2O) groups bonded directly to the Al of the structural unit.

Wavellite, [$Al_3(PO_4)_2(OH)_3(H_2O)_4$]($H_2O$), is an open framework of corner-sharing octahedra and tetrahedra (Fig. 37e) with interstitial non-transformer (H_2O) groups held in the interstices by hydrogen bonds. ($Al\phi_6$) octahedra share one set of *trans* corners with each other to form [$M\phi_5$] chains that are decorated by (PO_4) tetrahedra bridging adjacent

~~~~~~~~~~~~~~~~~~~~~~~~~~~~~~~~~~~~~~~

Figure 35 (opposite page). The crystal structures of metavariscite, variscite and kosnarite: (a) metavariscite projected onto (001); (b) metavariscite projected onto (100); (c) variscite projected onto (001); (d) variscite projected onto (100); ($Al\phi_6$) octahedra are 4^4-net-shaded; (e) kosnarite projected onto (001); (f) kosnarite projected onto (010); ($Zr\phi_6$) octahedra are square-pattern-shaded.
~~~~~~~~~~~~~~~~~~~~~~~~~~~~~~~~~~~~~~~

octahedra (Fig. 37e) to give chains of the form $[M(TO_4)\phi]$ extending in the *c*-direction (Fig. 18c). These chains cross-link in the *a*-direction by sharing octahedron-tetrahedron corners (Fig. 37f) with undecorated $[Al\phi_5]$ chains (i.e., the tetrahedra linked to these chains do not bridge octahedra within the chain). The resulting framework (Figs. 37e,f) has large cavities that contain the interstitial (H_2O) groups held in the structure solely by hydrogen bonds.

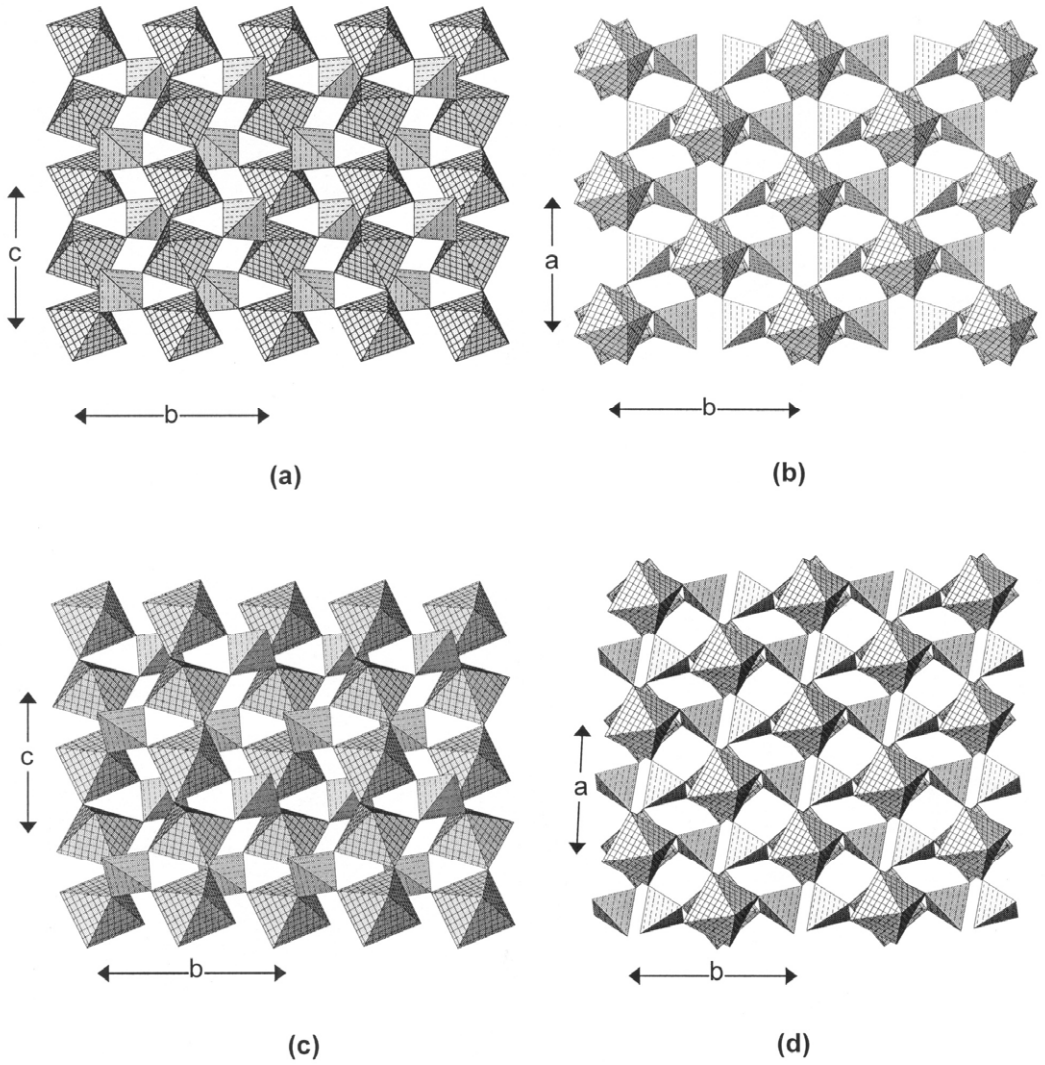

Figure 36. The crystal structures of lacroixite and amblygonite: (a) lacroixite projected onto (100); (b) lacroixite projected onto (001); (c) amblygonite projected onto (100); note the similarity with (a); (d) amblygonite projected onto (001); note the similarity with (b). ($Al\phi_6$) octahedra are 4^4-net-shaded.

M=M, M-T linkage. **Augelite**, $[Al_2(PO_4)(OH)_3]$, contains Al in both octahedral and trigonal-bipyramidal coordinations. Pairs of ($Al\phi_6$) octahedra share an edge to form $[Al_2\phi_{10}]$ dimers that are oriented with their long axis in the *b*-direction. The dimers are arranged at the vertices of a centered orthorhombic plane net (Fig. 38a), and dimers adjacent in the *b*-direction are linked through pairs of (PO_4) tetrahedra to form $[Al_2(PO_4)_2\phi_6]$ chains. The dimers are decorated by ($Al\phi_5$) trigonal bipyramids that bridge pairs of vertices from each octahedron. These ($Al\phi_5$) groups link to (PO_4) groups of adjacent chains to link them in the *a*-direction. Viewed in the *b*-direction (Fig. 38b), the structure appears as layers of dimers linked by chains of (PO_4) and ($Al\phi_5$) groups.

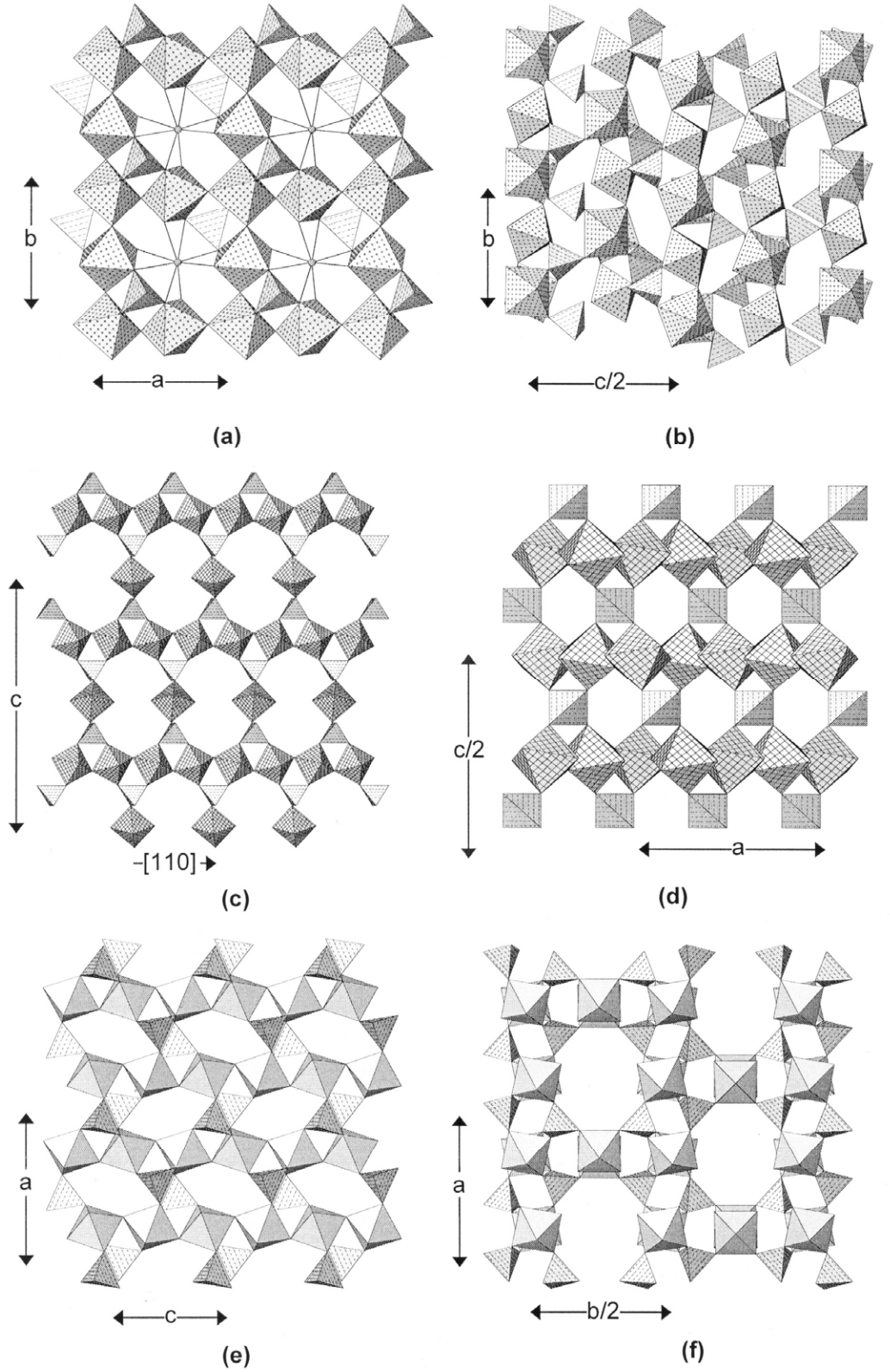

Figure 37. The crystal structures of cyrilovite, fluellite and wavellite: (a) cyrilovite projected a few degrees away from onto (001); (b) cyrilovite projected onto (100); (c) fluellite projected down [110]; (d) fluellite projected onto (010); (e) wavellite projected onto (010); (f) wavellite projected onto (001). ($Al\phi_6$) octahedra are 4^4-net-shaded and shadow-shaded, ($Fe^{3+}\phi_6$) octahedra are dot-shaded.

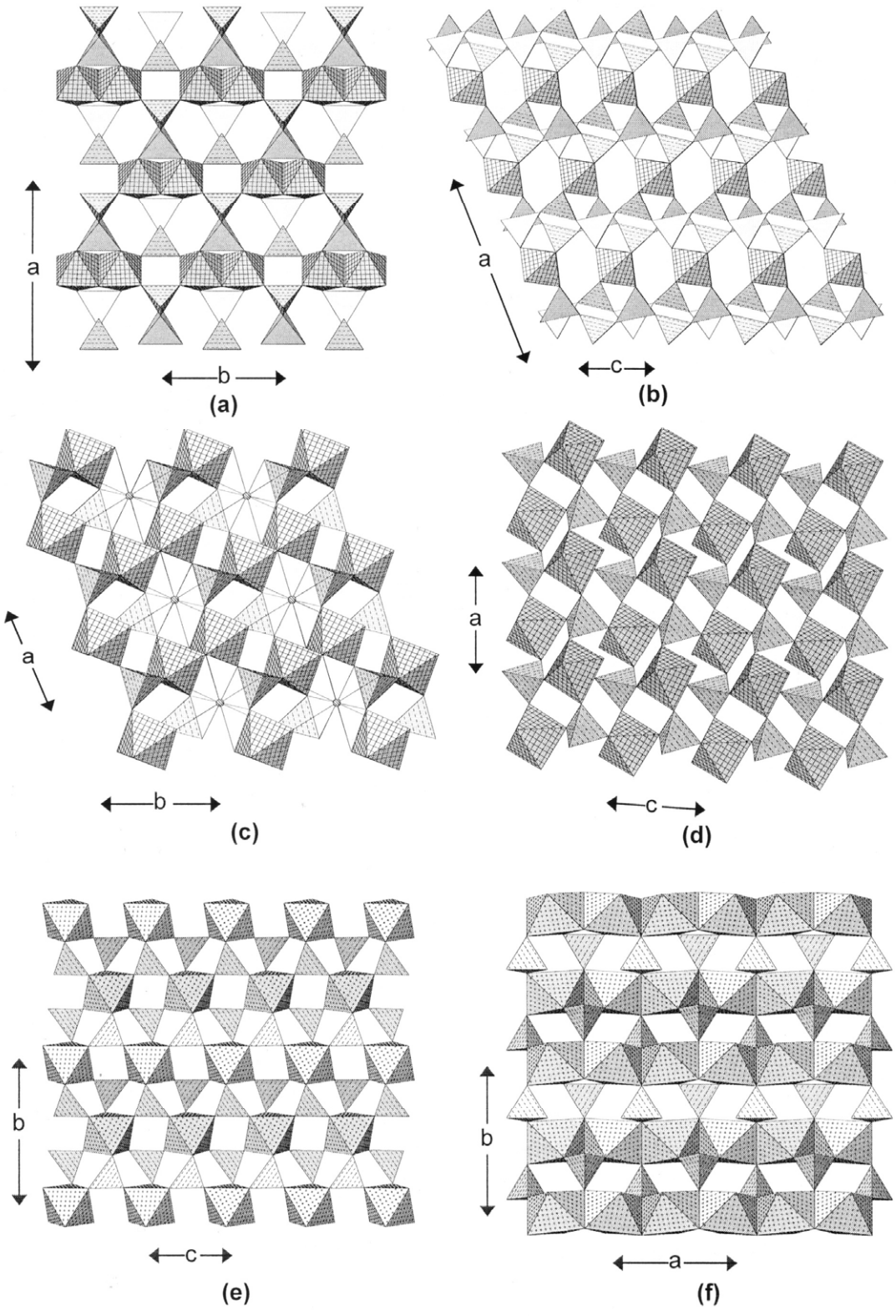

Figure 38. The crystal structures of augellite, jagowerite and maricite: (a) augelite projected onto (001); (b) augelite projected onto (010); (c) jagowerite projected onto (001); (d) jagowerite projected a few degrees away from onto (010); (e) maricite projected onto (100); (e) maricite projected a few degrees away from onto (001). Legend as in Figure 37.

Maricite, $Na[Fe^{2+}(PO_4)]$, is a dense-packed framework of $(Fe^{2+}O_6)$ octahedra and (PO_4) tetrahedra. Each $(Fe^{2+}O_6)$ octahedron links to six (PO_4) groups to form what Moore (1973b) calls a 'pinwheel'. The octahedra occupy the vertices of a 3^6 net, and the resulting sheet (Fig. 38e) is topologically identical to the $[Mg(PO_4)_2]$ sheet in brianite (Fig. 23c). These sheets stack along the *a*-direction with octahedra from adjacent sheets sharing edges to form $[MO_4]$-type chains extending in the *a*-direction when viewed down [001] (Fig. 38f). [10]-coordinated Na occupies interstices in the framework.

Kovdorskite, $[Mg_2(PO_4)(OH)(H_2O)_3]$, consists of two distinct $(Mg\phi_6)$ octahedra that condense to form tetramers via edge-sharing. These tetramers are decorated by pairs of (PO_4) tetrahedra to form $[Mg_4(PO_4)_2\phi_8]$ clusters. The clusters occur at the vertices of a 4^4 plane net and link together by sharing octahedron-tetrahedron vertices to form open sheets parallel to (001) (Fig. 39a). These sheets stack in the *c*-direction by sharing octahedron-tetrahedron vertices (Fig. 39b) to form a very open framework that is strengthened by extensive hydrogen bonding involving the (OH) and (H_2O) groups of the structural unit.

Libethenite, $[Cu^{2+}_2(PO_4)(OH)]$, is a member of the **adamite** group (Table 8) (Hawthorne 1976) in which Cu^{2+} is both [5]- and [6]-coordinated, triangular bipyramidal and octahedral, respectively. Chains of *trans* edge-sharing $(Cu^{2+}\phi_6)$ octahedra extend in the *c*-direction and are decorated by (PO_4) tetrahedra to give chains of the general form $[M_2(TO_4)_2\phi_4]$ (Fig. 39c). These chains link in the *a*- and *b*-directions by sharing octahedron-tetrahedron corners (Fig. 39d) to form an open framework with channels extending in the *c*-direction. These channels are clogged with dimers of edge-sharing $(Cu\phi_5)$ triangular bipyramids. Note that this is also the structure of andalusite, $[Al_2(SiO_4)O]$.

Tarbuttite, $[Zn_2(PO_4)(OH)]$, is a member of the paradamite group (Table 8) (Hawthorne 1979b). $(Zn\phi_5)$ bipyramids share edges to form a chain extending in the *b*-direction: $[Zn\phi_4]$. (PO_4) groups and $(Zn\phi_3)$ bipyramids alternate along a chain of corner-sharing polyhedra that also extends in the *b*-direction. These chains link in the *a*-direction by sharing polyhedron vertices (Fig. 39e) to form a rather thick slab parallel to (001). These slabs stack in the *c*-direction (Fig. 39f) by sharing polyhedron edges and corners. Apart from the presence of both [5]-coordinated divalent cations, there is no structural relation with the stoichiometrically similar libethnite, $Cu^{2+}_2(PO_4)(OH)$.

Petersite-(Y), $Y[Cu^{2+}_6(PO_4)_3(OH)_6](H_2O)_3$, is the only phosphate member of the mixite group (Table 8). Cu^{2+} is [5]-coordinated with a long sixth distance to (H_2O). Six-member rings of corner-sharing alternating (PO_4) tetrahedra and $(Cu^{2+}\phi_5)$ square-pyramids occur parallel to (001) and link by corner-sharing to form four-membered and twelve-membered rings of polyhedra (Fig. 40a). An alternative description is as six-member rings occupying the vertices of a 6^3 net. The layers of Figure 40a stack along the *c*-direction (Fig. 40b), and link by edge-sharing between the $(Cu^{2+}\phi_5)$ square pyramids. In the cross-linkage of the rings in the (001) plane, note how the (PO_4) groups bridge apical vertices of square pyramids adjacent along the *c*-direction (Fig. 40b). The interstitial (H_2O) groups occupy the channels of the twelve-membered rings, and interstitial Y occupies the channels generated by the six-membered rings (Fig. 40a).

Brazilianite, $Na[Al_3(PO_4)_2(OH)_4]$, contains chains of edge-sharing $(Al\phi_6)$ octahedra that extend in the [101] direction (Fig. 40c). These chains are fairly contorted as the shared edges are not in a *trans* configuration and hence a slight helical character results. The chains are decorated by (PO_4) tetrahedra which link next-nearest-neighbor octahedra, a rather unusual linkage that is promoted by the helical nature of the chains (Fig. 40c). Adjacent chains link by sharing octahedron vertices with the decorating tetrahedra (Fig. 40c,d). Interchain linkage is also promoted by [7]-coordinated interstitial Na.

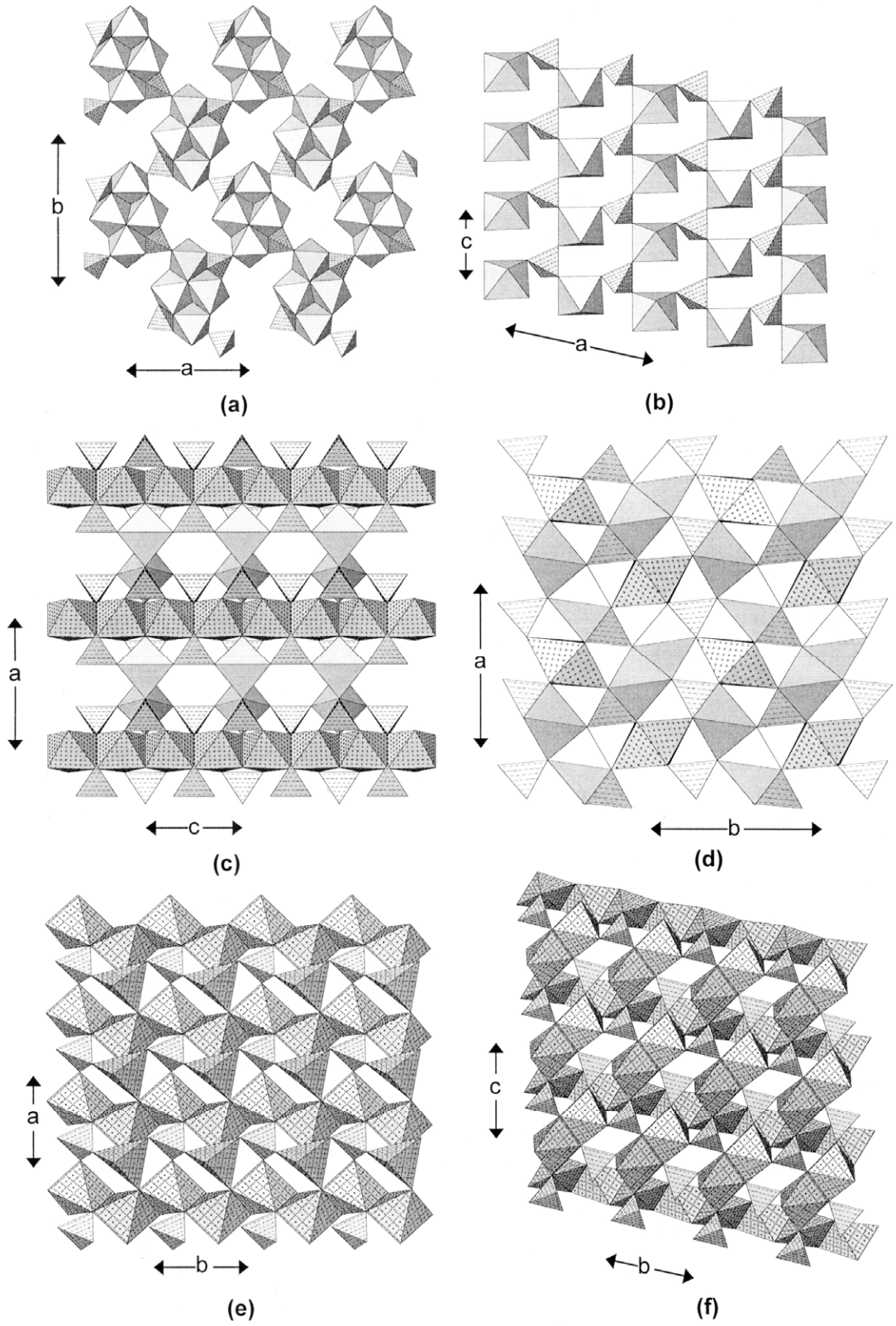

Figure 39. The crystal structures of kovdorskite, libethenite and tarbuttite: (a) kovdorskite projected onto (001); (b) kovdorskite projected onto (010); (Mgϕ_6) octahedra are shadow-shaded; (c) libethenite projected onto (010); (d) libethenite projected onto (001); ($Cu^{2+}\phi_6$) are dot-shaded, ($Cu^{2+}\phi_5$) are shadow-shaded; (e) tarbuttite projected onto (001); (f) tarbuttite projected onto (100); (Znϕ_6) octahedra and (Znϕ_5) polyhedra are square-pattern-shaded.

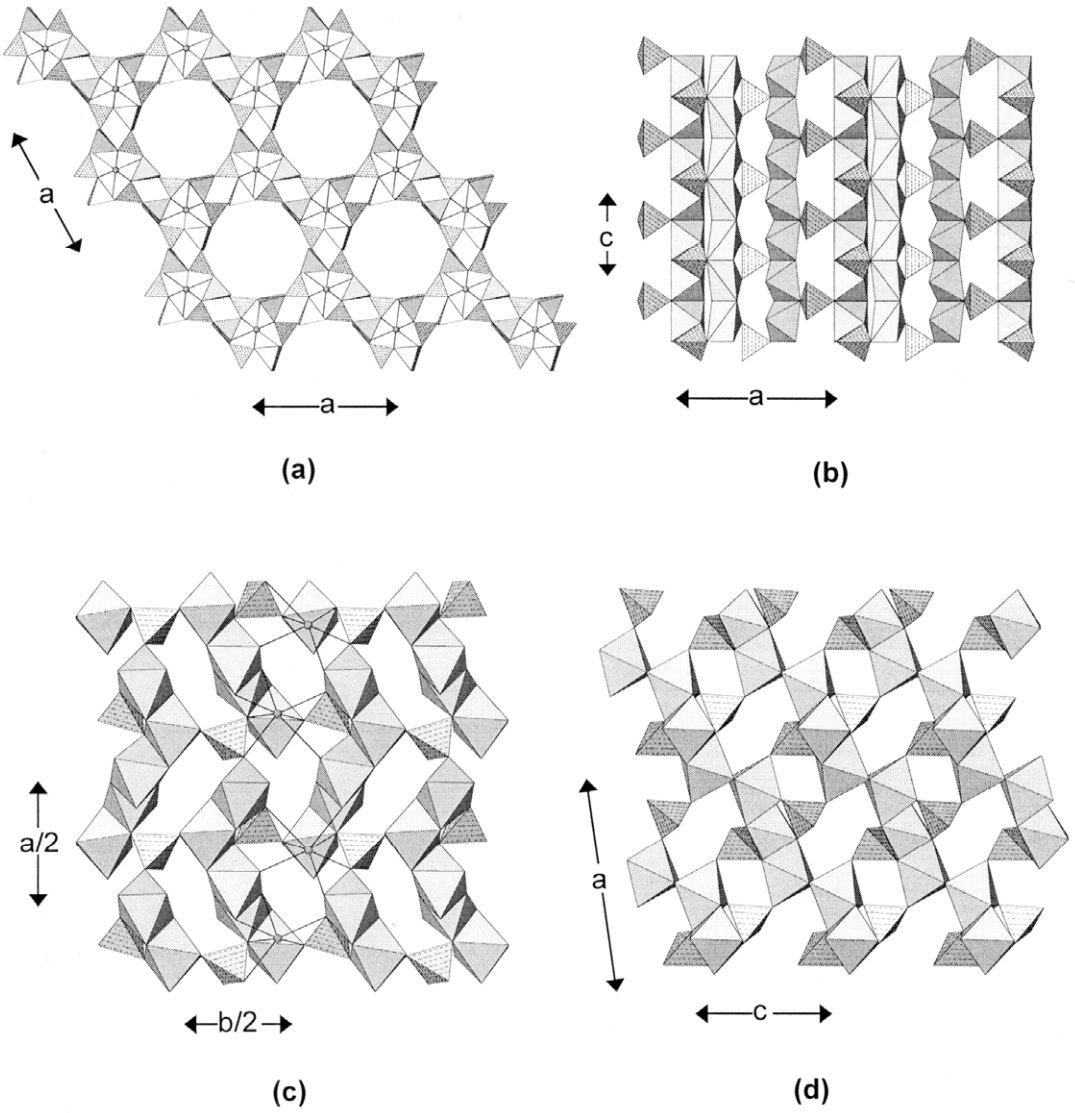

Figure 40. The crystal structures of petersite-(Y) and brazilianite: (a) petersite-(Y) projected onto (001); (b) petersite-(Y) projected onto (010); ($Cu^{2+}\phi_6$) octahedra are shadow-shaded, Y is shown as shaded circles; (c) brazilianite projected onto (001); (d) brazilianite projected onto (010); ($Al\phi_6$) octahedra are shadow-shaded, Na is shown as shaded circles.

M=M, M-M, M-T linkage. There are three polymorphs of $[Cu^{2+}{}_5(PO_4)_2(OH)_4(H_2O)]$, pseudomalachite, reichenbachite and ludjibaite, and their structures are all based on sheets of octahedra that are linked by (PO_4) tetrahedra. The sheets of octahedra are somewhat unusual in that they are not close-packed octahedra interspersed with vacancies (as is common in this type of structure). In pseudomalachite (Fig. 41a), linear [$M\phi_4$] chains of octahedra extend in the *b*-direction at $z \approx {}^1/_4$ and ${}^3/_4$, and are linked by trimers of edge-sharing octahedra packed such that there are square interstices in the sheet. The sheets stack in the *a*-direction and are linked by (PO_4) groups that share two vertices with each sheet (Fig. 41b). In reichenbachite (Fig. 41c), the arrangement of octahedra within the sheet is fairly irregular. It can be envisioned as edge-sharing trimers of octahedra at (0 1/2 *z*) and (1/2 0 *z*) linked by edge-sharing with dimers of edge-sharing octahedra at (0 1/8 *z*) and at (5/8 3/8 *z*) (Fig. 41c). These sheets stack in the *c*-direction (Fig. 41d) and are linked by (PO_4) groups that each share two vertices with adjacent sheets. In ludjibaite (Fig. 41e), linear [$M\phi_4$] chains extend in both the *b* and *c*-directions,

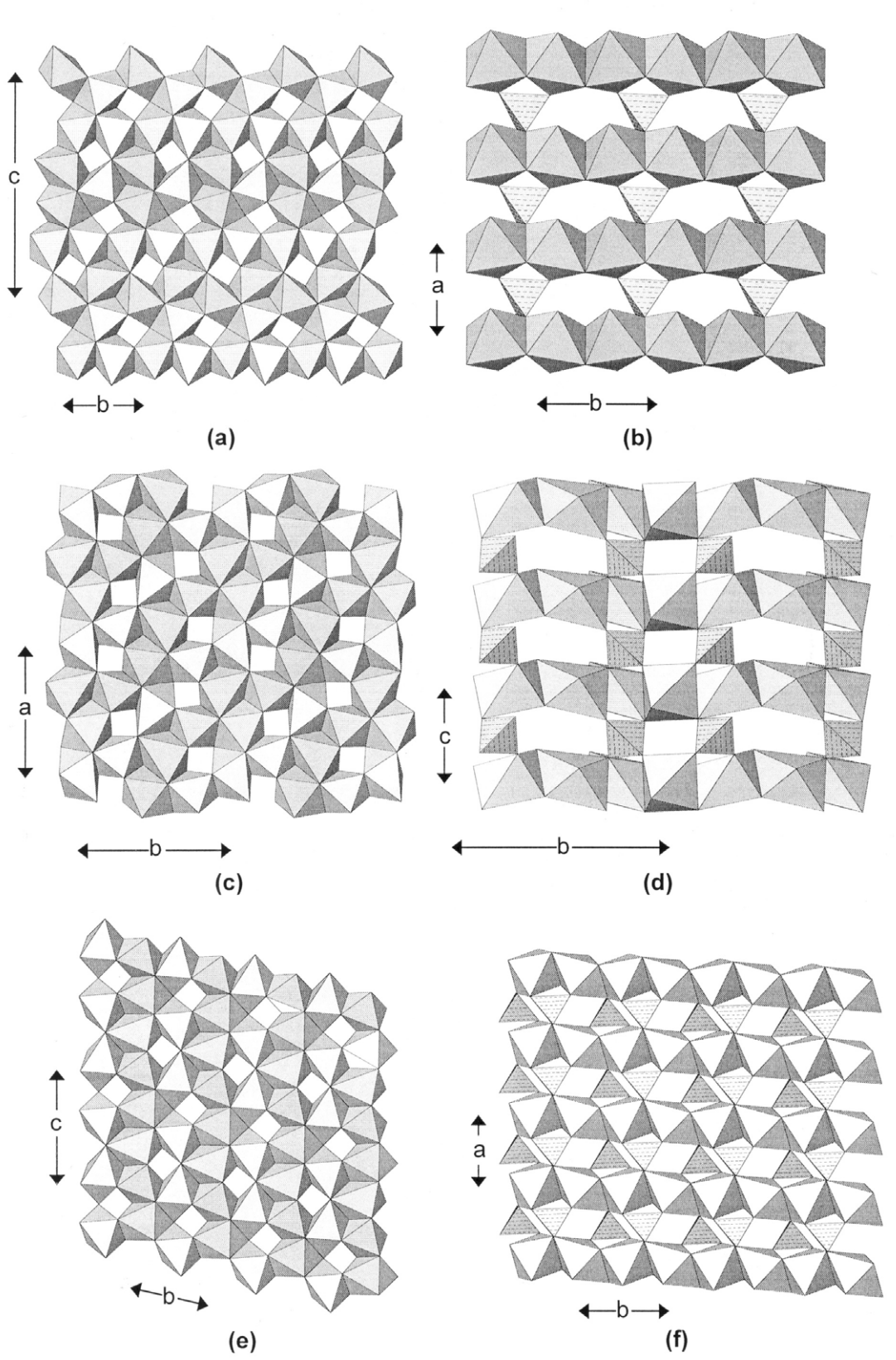

Figure 41. The crystal structures of pseudomalachite, reichenbachite and ludjibaite: (a) pseudomalachite projected onto (100); (b) pseudomalachite projected onto (001); (c) reichenbachite projected onto (001); (d) reichenbachite projected onto (100); (e) ludjibaite projected onto (100); (f) ludjibaite projected onto (001). ($Cu^{2+}\phi_6$) octahedra are shadow-shaded.

and link together by sharing edges with a [$M\phi_5$] chain of corner-sharing octahedra that extends in the *c*-direction. These sheets stack in the *a*-direction (Fig. 41f) and, as with the other two structures, are linked by (PO_4) groups that share pairs of vertices with adjacent sheets.

In the minerals of the **triplite**, [$Mn^{2+}_2(PO_4)F$], group (Table 8), ($M^{2+}\phi_6$) octahedra share edges to form [$M^{2+}_2\phi_{10}$] dimers (Fig. 42a) that share corners with (PO_4) tetrahedra to form slightly corrugated layers that are parallel to (010) (Fig. 42a). These layers link in the *b*-direction by sharing corners between tetrahedra and octahedra (Fig. 42b).

The minerals of the **triploidite**, [$Mn^{2+}_2(PO_4)(OH)$], group have divalent cations in both octahedral and triangular bipyramidal coordinations. Pairs of octahedra share an edge to form [$M^{2+}_2\phi_{10}$] dimers, and these dimers are linked by sharing corners with both

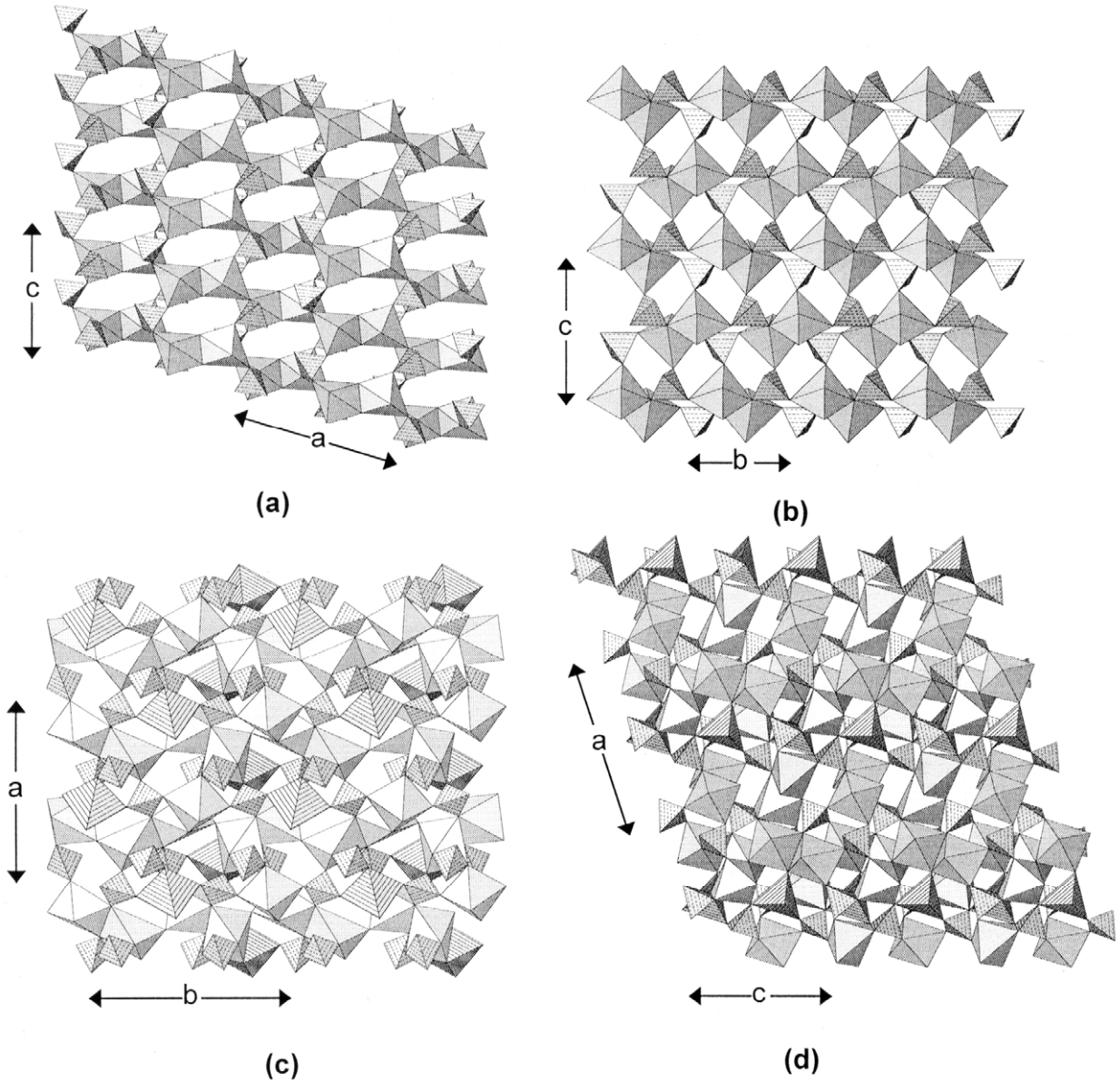

Figure 42. The crystal structures of triplite and triploidite: (a) triplite projected onto (010); (b) triplite projected onto (100); (c) triploidite projected onto (001); (d) triploidite projected onto (001). ($Mn\phi_6$) octahedra are shadow-shaded, ($Mn\phi_5$) polyhedra are line-shaded.

triangular bipyramids and (PO_4) groups, and by sharing one octahedron edge with a tetrahedron (Fig. 42c). Triangular bipyramids also form edge-sharing dimers, [$M^{2+}{}_2\phi_8$], and chains of corner-sharing octahedra, triangular bipyramids and tetrahedra extend in the *b*-direction (Fig. 42d). It should be noted that this is an extremely complicated structure, and is not easily related to any other structure, except at a trivial level.

Table 9. Cell dimensions for the different structures of the alluaudite-group (*sensu lato*) minerals.

	a (Å)	*b*(Å)	*c* (Å)	β (°)	Sp grp	*V* (Å^3)	Ref.
Alluaudite	12.004(2)	12.533(45)	6.404(1)	114.4(1)	*C*2/*c*	877.4	(1)
Wyllieite	11.868(15)	12.382(12)	6.354(9)	114.5(1)	$P2_1/n$	849.5	(2)
Bobfergusonite	12.776(2)	12.488(2)	11.035(2)	97.21(1)	$P2_1/n$	1746.7(4)	(3)

References: (1) Fisher (1965); (2) Moore and Molin-Case (1974); (3) Ercit et al. (1986a,b)

The minerals of the **alluaudite**, **wyllieite** and **bobfergusonite** groups are topologically identical but are distinguished by different cation-ordering schemes over the octahedrally coordinated cation sites in the basic structure. The cell dimensions of the principal mineral in each group are given in Table 9. The principal feature of each structure is a linear trimer of edge-sharing octahedra (Figs. 43a,c,e). These trimers link together by sharing edges to form chains of octahedra in (010) that are linked by sharing octahedron corners with (PO_4) groups to form thick sheets parallel to (010). These sheets link in the *b*-direction by sharing corners between tetrahedra and octahedra (Figs. 43b,d,f). The minerals of these three groups differ primarily in their Al content and the pattern of cation order over the trimer of edge-sharing octahedra. The minerals of the alluaudite group (sensu stricto) contain negligible Al (Al_2O_3 < 0.10 wt %), the minerals of the wyllieite group contain moderate Al (Al_2O_3 ≈ 3 wt %), and bobfergusonite contains far more Al than wyllieite (Al_2O_3 ≈ 7.5 wt %). In addition, there is a fourth (as yet undescribed) structure type with ~15 wt % Al_2O_3 (unpublished data). The differences in cation order in these three structure types are summarized in Figure 44. In alluaudite, there is no Al, and hence Al is not involved in the ordering scheme. There are only two distinct sites in the trimer in alluaudite, and the pattern of cation order can vary from complete M^{2+}-cation disorder to complete Fe^{3+}-M^{2+} order (Fig. 44a). In wyllieite, there are three distinct sites in the trimer; Al is completely ordered at one site, and the other two sites can vary from complete M^{2+}-cation disorder to complete Fe^{3+}-M^{2+} order (Fig. 44b). In bobfergusonite, there are two crystallographically distinct trimers (Fig. 44c); Al is ordered in one trimer, Fe^{3+} is ordered in the other trimer, and M^{2+} is disordered over the other sites. This picture is somewhat idealized, and each structure-type may show minor ordering characteristic of one or more of the other structure types. Moore and Ito (1979) discuss the nomenclature of the alluaudite and wyllieite groups in detail and propose a nomenclature based on suffixes, but this has not been used very extensively.

~~~~~~~~~~~~~~~~~~~~~~~~~~~~~~~~~~~~

Figure 43 (opposite page). The crystal structures of alluaudite, wyllieite and bobfergusonite: (a) alluaudite projected onto (001); (b) alluaudite projected onto (100); shadow-shaded octahedra are occupied predominantly by Mn^{2+}, 4^4-net-shaded octahedra are occupied predominantly by Fe^{3+}; (c) wyllieite projected onto (010); (d) wyllieite projected onto (100); dot-shaded octahedra are occupied predominantly by Fe, 4^4-net-shaded octahedra are occupied by Al; (e) bobfergusonite projected onto (010); (f) bobfergusonite projected onto (100); shadow-shaded octahedra are occupied by Mn^{2+}, Fe^{3+} and Al.
~~~~~~~~~~~~~~~~~~~~~~~~~~~~~~~~~~~~

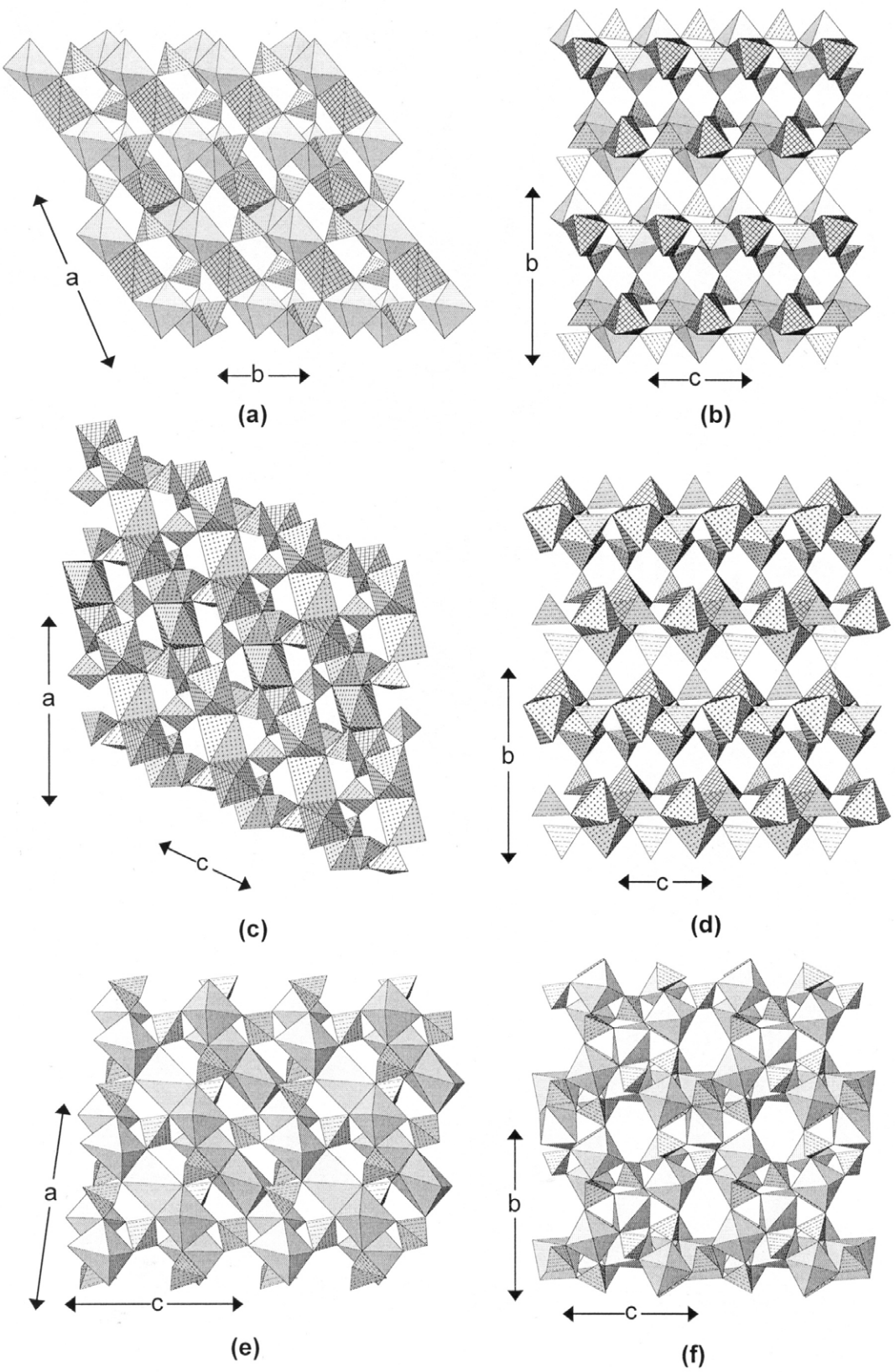
a
b
(a)
b
c
(b)
a
c
(c)
b
c
(d)
a
c
(e)
b
c
(f)

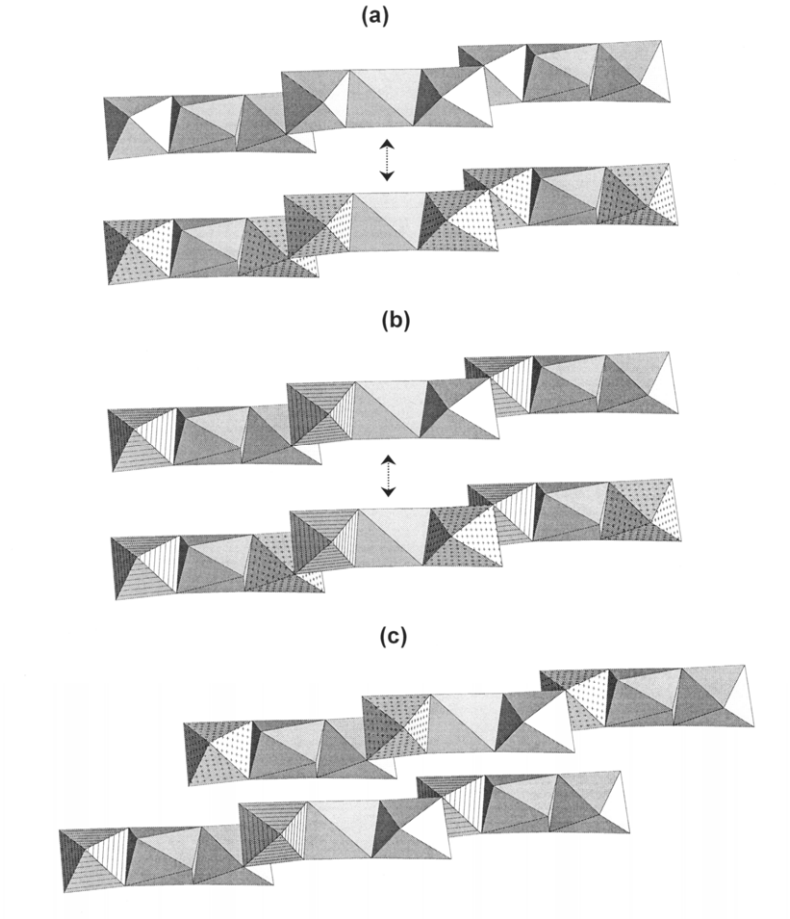

Figure 44. Octahedral-cation-ordering patterns in (a) alluaudite; (b) wyllieite; (c) bobfergusonite; shadow-shaded octahedra are occupied by any divalent M^{2+} cation, dot-shaded octahedra are occupied by Fe^{3+}, line-shaded octahedra are occupied by Al. In (a) and (b), the arrows indicate the range of possible ordering within a single chain; in (c), there are two distinct chains (shown here) in which the ordering is different (after Ercit et al. 1986a).

Ludlamite, $[Fe^{3+}{}_3(PO_4)_2(H_2O)_4]$ consists of $(Fe^{3+}\phi_6)$ octahedra that share edges to form $[Fe^{3+}{}_3\phi_{14}]$ linear trimers with (PO_4) tetrahedra bridging between adjacent octahedra in a staggered fashion on each site of the trimer: $[Fe^{3+}{}_3(PO_4)_2\phi_{10}]$. These trimers extend in the *c*-direction and link by sharing octahedron corners (Fig. 45a). The crankshaft chains link in the *b*-direction by sharing octahedron corners and by sharing corners between tetrahedra and octahedra (Fig. 45a) to form a sheet parallel to (100). These sheets link in the *a*-direction by sharing corners between (PO_4) tetrahedra and octahedra (Fig. 45b). Note that the chains of octahedra shown in this figure are not completely edge-sharing; for every third octahedra, the linkage is by corner-sharing, as is apparent by the change in direction of the top triangular faces of the octahedra (Fig. 45a).

In **melonjosephite**, $Ca[Fe^{2+}Fe^{3+}(PO_4)_2(OH)]$, there are two crystallographically distinct octahedra, both of which are occupied by equal amounts of Fe^{2+} and Fe^{3+}. One type of octahedron forms linear chains of edge-sharing octahedra ($[M\phi_4]$ of the rutile-type) extending in the *c*-direction. This chain is decorated by (PO_4) tetrahedra linking free vertices of adjacent octahedra in a staggered arrangement, producing an $[M(T\phi_4)\phi_2]$ chain (Fig. 18e). The other crystallographically distinct octahedron links to (PO_4) tetrahedra to form $[M(PO_4)\phi_4]$ chains. These $[M(PO_4)\phi_4]$ chains link in a pair-wise fashion by the octahedra sharing edges, and the resulting structure consists of the two types of chains,

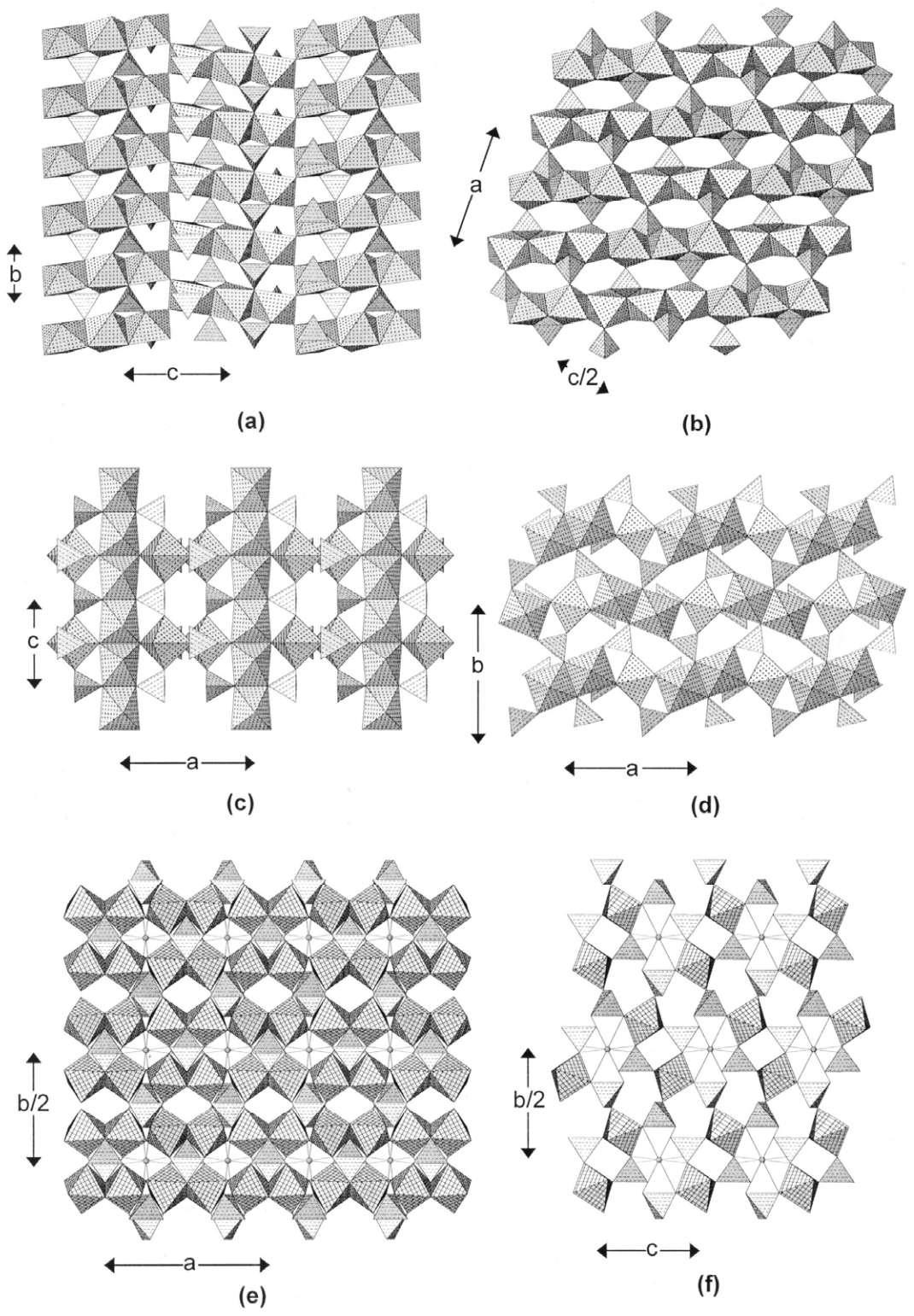

Figure 45. The crystal structures of ludlamite, melonjosephite and palermoite: (a) ludlamite projected onto (100); (b) ludlamite projected onto (010); (c) melonjosephite projected onto (010); (d) melonjosephite projected onto (001); ($\{Fe^{2+},Fe^{3+}\}\phi_6$) octahedra are dot-shaded; (e) palermoite projected onto (001); (f) palermoite projected onto (100); ($Al\phi_6$) octahedra are 4^4-net-shaded, Ca is shown as small shaded circles.

both extending in the *c*-direction and cross-linked by sharing octahedron-tetrahedron and octahedron-octahedron corners (Fig. 45c). Viewed down the length of the chains (Fig. 45d), the dimers that link the two $[M(PO_4)\phi_4]$ chains are very prominent, and the key role of the (PO_4) groups in cross-linking the chains is very apparent. The interstices of the framework are occupied by [7]-coordinated Ca.

In **palermoite**, $SrLi_2[Al(PO_4)(OH)]_4$, $(Al\phi_6)$ octahedra condense by sharing edges to form $[Al_2\phi_{10}]$ dimers, and these dimers share corners to form an $[Al_2\phi_8]$ chain that extends in the *a*-direction. One pair of octahedron vertices in each dimer is bridged by a (PO_4) tetrahedron to form an $[Al_2(PO_4)\phi_6]$ chain (Fig. 45e); these chains link in the *b*-direction by sharing octahedron-tetrahedron vertices. These chains are seen end-on when viewed in the *a*-direction (Fig. 45f), cross-linked by (PO_4) tetrahedra. The framework has large interstices that are occupied by [8]-coordinated Sr and [5]-coordinated Li.

Arrojadite, $KNa_4Ca[Fe^{2+}{}_{14}Al(PO_4)_{12}(OH)_2]$, and **dickinsonite**, the Mn^{2+} analogue, are infernally complex structures, each with several partly occupied cation sites, and the complete details of their structure exceeds our spatial parameters. Moore et al. (1981) describe the structure as six distinct rods (columns) of cation polyhedra decorated by (PO_4) tetrahedra and occurring at the vertices of a {6·3·6·3} and {6·6·3·3} net. Moore et al. (1981) also compare the structure of arrojadite with wyllieite, but the relation to the general alluaudite-type structures has not been explored.

Farringtonite, $[Mg_3(PO_4)_2]$, contains Mg in both octahedral and square-pyramidal coordinations. As is common with [5]-coordinated polyhedra, $[Mg\phi_5]$ square pyramids share an edge to form $[Mg_2\phi_8]$ dimers, and the terminal edges of this dimer are shared with (PO_4) tetrahedra to form a $[Mg_2(PO_4)_2\phi_4]$ cluster (Fig. 46a). These clusters are linked by sharing corners with $(Mg\phi_6)$ octahedra. When projected onto (010), prominent $[Mg(PO_4)_2\phi_2]$ chains are evident, extending in the *c*-direction (Fig. 18b). These chains are bridged in the a-direction by $[Mg_2(PO_4)_2\phi_4]$ clusters (Fig. 46b).

Beusite, $[Mn^{2+}{}_3(PO_4)_2]$, and **graftonite**, $[Fe^{2+}{}_3(PO_4)_2]$, show unusual coordination numbers for the divalent cations: $^{[7]}M(1)$, $^{[5]}M(2)$, $^{[6]}M(3)$. Perhaps as a result of this unusual coordination these minerals can accept considerable Ca at the *M*(1) site (Wise et al. 1990), and the latter authors report a composition for Ca-rich beusite close to $CaFe^{2+}Mn(PO_4)_2$. $^{[7]}M(1)$ polyhedra share an edge to form a dimer; these dimers occur at the vertices of a 4^4 net and share corners to form a sheet parallel to (100) that is strengthened by (PO_4) groups (Fig. 46c). Pyroxene-like edge-sharing chains of *M*(3) octahedra extend in the *c*-direction and are linked by chains of alternating (PO_4) groups and *M*(2) square pyramids (Fig. 46d), and these two types of sheet alternate in the [100] direction.

Wicksite, $NaCa_2[Fe^{2+}{}_2(Fe^{2+}Fe^{3+})Fe^{2+}{}_2(PO_4)_6(H_2O)_2]$, and the isostructural **bederite**, $\square Ca_2[Mn^{2+}{}_2Fe^{3+}{}_2Mn^{2+}{}_2(PO_4)_6(H_2O)_2]$, are complex heteropolyhedral framework structures that may be resolved into layers parallel to (001). In wicksite at $z \approx 1/4$, $(Fe^{2+}\phi_6)$ and $(Fe^{3+}\phi_6)$ octahedra share an edge to form $[M_2\phi_{10}]$ dimers that are canted to both the *a* and *b* axes, and are linked by (PO_4) tetrahedra to form the sheet shown in Figure 47a. At $z \approx 0$, two $(Fe^{2+}\phi_6)$ octahedra share edges with an $(Na\phi_6)$ octahedra to form an $[M_3\phi_{14}]$ trimer that is decorated by (PO_4) tetrahedra linking adjacent free octahedron vertices to form a cluster of the form $[M_3(PO_4)_2\phi_6]$. These clusters link by sharing of octahedron-tetrahedron vertices to form the layer shown in Figure 47b. There are two types of interstice within this layer. In the first type of interstice is the Ca site coordinated by nine anions, and in the second type of interstice are four H atoms that belong to the two peripheral (H_2O) groups (Fig. 47b). The layers of Figure 47a and 47b link by edge-sharing between the $(Fe^{2+}\phi_6)$ [= *M*(1)] octahedron of one sheet with the $(Fe^{2+}\phi_6)$ [= *M*(3) octahedron of the other sheet (Fig. 47c). The relation between wicksite

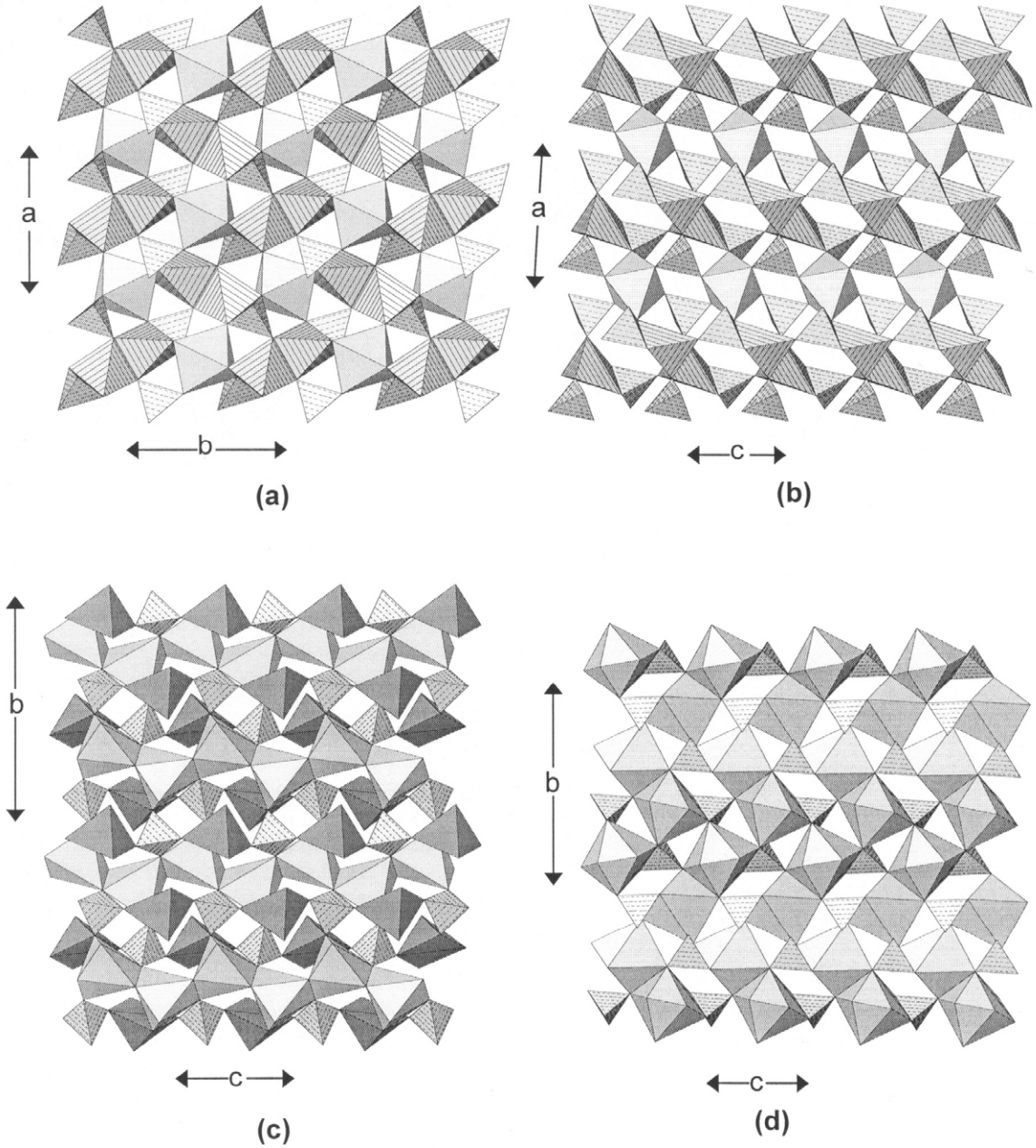

Figure 46. The crystal structures of farringtonite and beusite: (a) farringtonite projected onto (001); (b) farringtonite projected onto (010); (MgO_6) octahedra are shadow-shaded, (MgO_5) polyhedra are line-shaded; (c) a layer of the beusite structure projected onto (100); (d) another layer of the beusite structure projected onto (100); [7]- and [6]-coordinated polyhedra are shadow-shaded, [5]-coordinated polyhedra are dark-shadow-shaded.

and bederite is as follows: the Fe^{2+} = Na = Fe^{2+} triplet in wicksite (cf. Fig. 47b) is replaced by the [Mn^{2+} = □ = Mn^{2+}] triplet in bederite.

Chalcosiderite, $[Cu^{2+}Fe^{3+}{}_6(PO_4)_4(OH)_8(H_2O)_4]$, is a member of the turquoise group (Table 8). The structure contains trimers of edge-sharing octahedra, two ($Fe^{3+}\phi_6$) and one ($Cu^{2+}\phi_6$) octahedra that link by sharing corners with (PO_4) tetrahedra and other ($Fe^{3+}\phi_6$) octahedra parallel to (100) (Fig. 47d). This linkage is also seen in Figure 47e, with additional linkage between trimers through corner-sharing with additional ($Fe^{3+}\phi_6$) octahedra

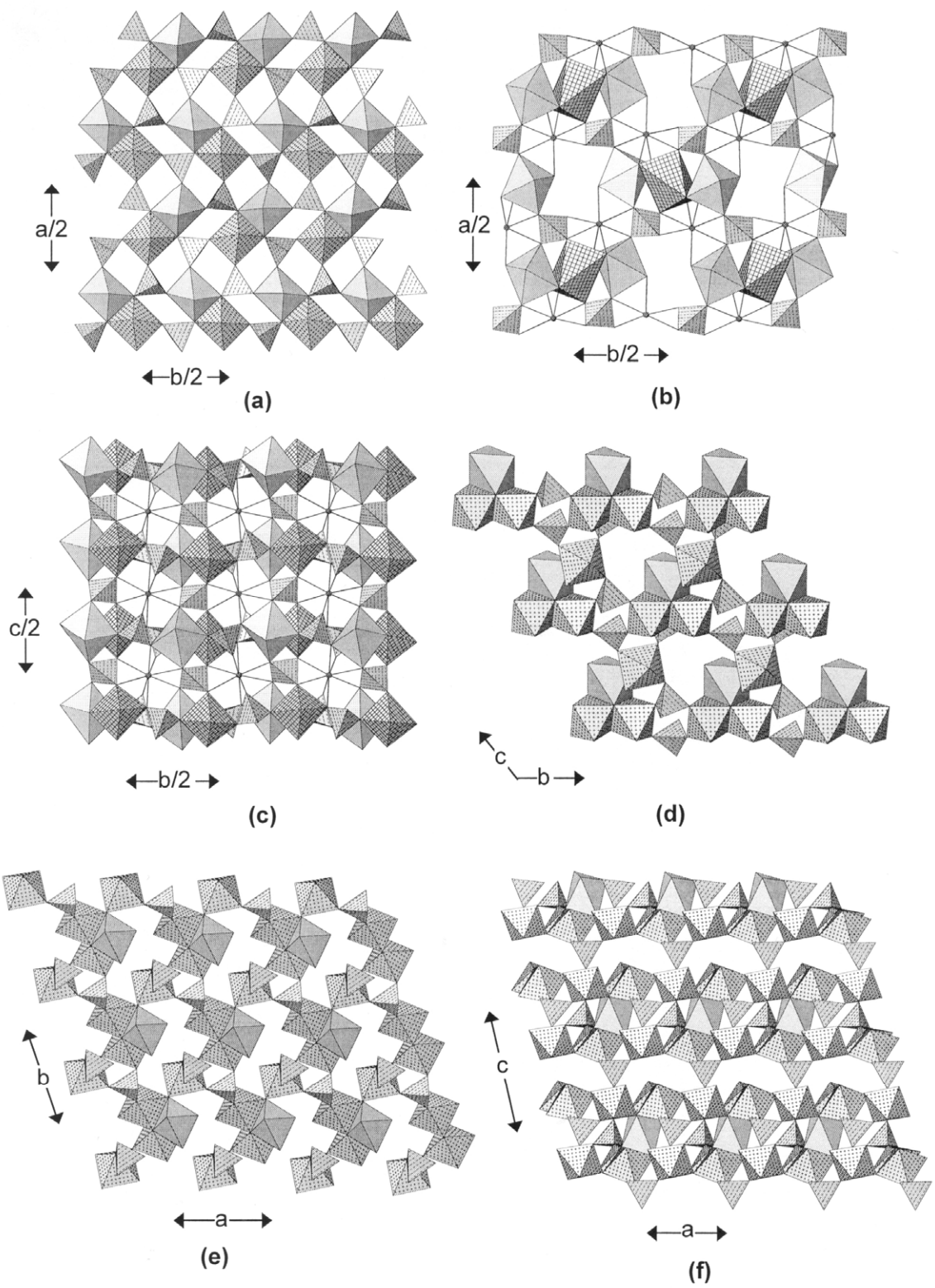

Figure 47. The crystal structures of bederite and chalcosiderite: (a) layer 1 of bederite projected onto (001); (b) layer 2 of bederite projected onto (001); (c) stacking of layers projected onto (100); ($Fe^{3+}\phi_6$) octahedra are 4^4-net-shaded, ($Fe^{2+}\phi_6$) octahedra are shadow-shaded, Ca atoms are shown as shaded circles; (d) chalcosiderite projected onto (100); (e) chalcosiderite projected onto (001); (f) chalcosiderite projected onto (010); ($Fe^{3+}\phi_6$) octahedra are dot-shaded and shadow-shaded.

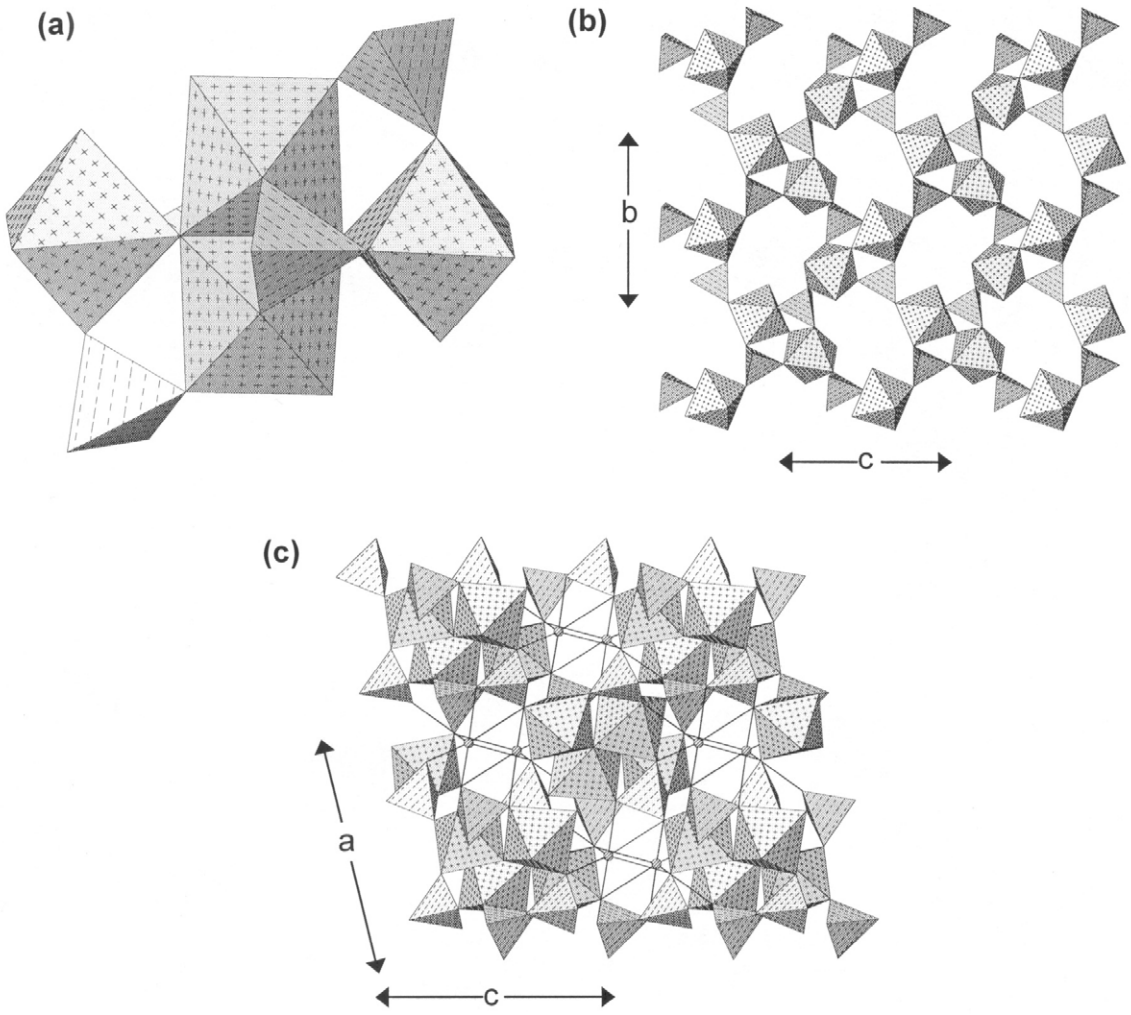

Figure 48. The crystal structure of leucophosphite: (a) the $[Fe^{3+}{}_4(PO_4)_4\phi_{12}]$ cluster; (b) projected onto (100); (c) projected onto (010). ($Fe^{3+}\phi_6$) octahedra are cross/dot-shaded, K is shown as shaded circles.

and (PO_4) groups to form a thick slab parallel to (001). These slabs stack along the *c*-direction (Fig. 47f) and are linked through bridging (PO_4) tetrahedra. The structure is fairly open to accommodate the extensive hydrogen-bonding associated with the (OH) and (H_2O) groups of the structural unit.

Leucophosphite, $K_2(H_2O)[Fe^{3+}{}_2(PO_4)_2(OH)(H_2O)]_2(H_2O)$, and **tinsleyite**, $K_2(H_2O)$-$[Al_2(PO_4)_2(OH)(H_2O)]_2(H_2O)$, are based on a prominent tetramer of octahedra in which two ($Fe^{3+}O_6$) octahedra share an edge and an additional ($Fe^{3+}O_6$) octahedron links to the anions at each end of the shared edge. Moore (1972b) notes that the topologically identical cluster occurs in the sulfate mineral amarantite. This cluster is decorated by four (PO_4) tetrahedra to form an $[Fe^{3+}{}_4(SO_4)_4\phi_{12}]$ cluster (Fig. 48a). These clusters link by sharing vertices between octahedra and tetrahedra to form a framework (Figs. 48b,c) with K in the interstices. Inspection of Figure 48a shows that the decorated tetramer can be regarded as a condensation of two $[M_2(TO_4)_2\phi_7]$ clusters (Fig. 17e), a group that Hawthorne (1979a) showed is common as a fragment in several complex phosphate structures. In fact, when the structure is viewed down [100], it can be considered as

sheets of corner-shared $[M_2(TO_4)_2\phi_3]$ clusters, similar to those in the structure of minyulite (Fig. 25a).

Cacoxenite, $[Fe^{3+}{}_{24}Al(PO_4)_{17}O_6(OH)_{12}(H_2O)_{24}](H_2O)_{51}$, surely has to qualify as one of the more complicated of Nature's masterpieces. Moore and Shen (1983a) identified two key *FBB*s in this structure. Pairs of $(Fe^{3+}\phi_6)$ octahedra share an edge to form dimers, and three dimers share octahedron corners to form a ring that has a (PO_4) group at its core, linking to one end of each of the shared edges in the cluster (Fig. 49a). The resulting *FBB* has the form $[Fe^{3+}{}_6(PO_4)\phi_{24}]$ and resembles the $[Fe^{3+}{}_6(PO_4)\phi_{24}]$ group in mitridatite (Fig. 33) and the central girdle of the Keggin molecule. The second *FBB* consists of one dimer of edge-sharing octahedra with two additional octahedra linked by sharing corners with each end of the shared edge of the dimer. Four (PO_4) groups each share two corners with octahedra at the periphery of the cluster, and a fifth (PO_4) group shares corners with three of the octahedra (Fig. 49b). The resulting *FBB* has the form $[Fe^{3+}{}_3Al(PO_4)_5\phi_9]$, and has some similarities with clusters in melonjosephite (Fig. 45c) and leucophosphate (Fig. 48a). These two *FBB*s polymerize by sharing polyhedron corners to form rings consisting of twelve *FBB*s, each type alternating around the ring. These rings are arranged at the vertices of a 3^6 net (Fig. 49c). The layer shown in Figure 49c repeats in the *c*-direction (Fig. 49d), linking by sharing polyhedron edges and corners, with the addition of some linking octahedra, to form a framework with extremely wide channels that are filled with (H_2O) groups.

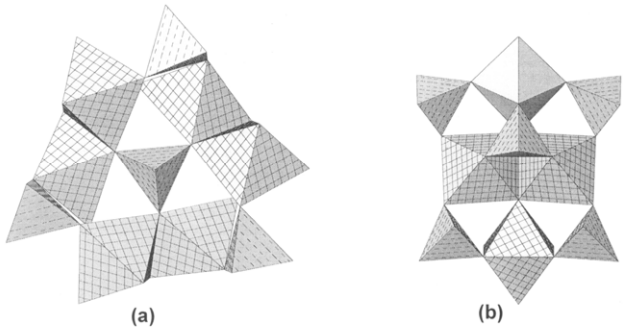

Figure 49. The structure of cacoxenite: (a) the $[Fe^{3+}{}_6(PO_4)\ \phi_{24}]$ cluster; (b) the $[Fe^{3+}{}_3Al(PO_4)_5\phi_9]$ cluster. $(Fe^{3+}\phi_6)$ octahedra are 4^4-net-shaded, $(Al\phi_6)$ octahedra are shadow-shaded.

Althausite, $[Mg_4(PO_4)_2(OH)F]$, and **satterlyite**, $[Fe^{2+}{}_4(PO_4)_2(OH)_2]$, have their divalent cations in both [5]- and [6]-coordination, triangular bipyramidal and octahedral. In althausite, $[M\phi_4]$ chains of *trans* edge-sharing $(Mg\phi_6)$ octahedra extend in the *b*-direction. These chains link in the *a*-direction by sharing corners between tetrahedra and octahedra (Fig. 50a) to form a sheet parallel to (001). These sheets are linked in the *c*-direction by sharing octahedron edges with $(Mg\phi_5)$ triangular bipyramids (Fig. 50b). In althausite, ~20% of the (OH) is replaced by O^{2-} and the excess charge is compensated by omission (i.e., incorporation of vacancies) of F.

In **hureaulite**, $[Mn^{2+}{}_5(PO_3\{OH\})_2(PO_4)_2(H_2O)_4]$, five $(Mn^{2+}\phi_6)$ octahedra share edges to form a kinked linear pentamer that extends in the *a*-direction (Fig. 50c). These pentamers occur at the vertices of a plane centered orthorhombic net and link by sharing corners (4 per pentamer) to form a sheet of octahedra parallel to (001). Adjacent pentamers are also linked through (PO_4) groups with which they share corners to form a thick slab parallel to (001). These slabs link in the *c*-direction through corner sharing between octahedra and tetrahedra (Fig. 50d). There are fairly large interstices within the resulting framework (Fig. 50c), but these are usually unoccupied. However, Moore and Araki (1973) suggest that alkalis or alkaline earths could occupy this cavity with loss of the acid character of the acid-phosphate groups.

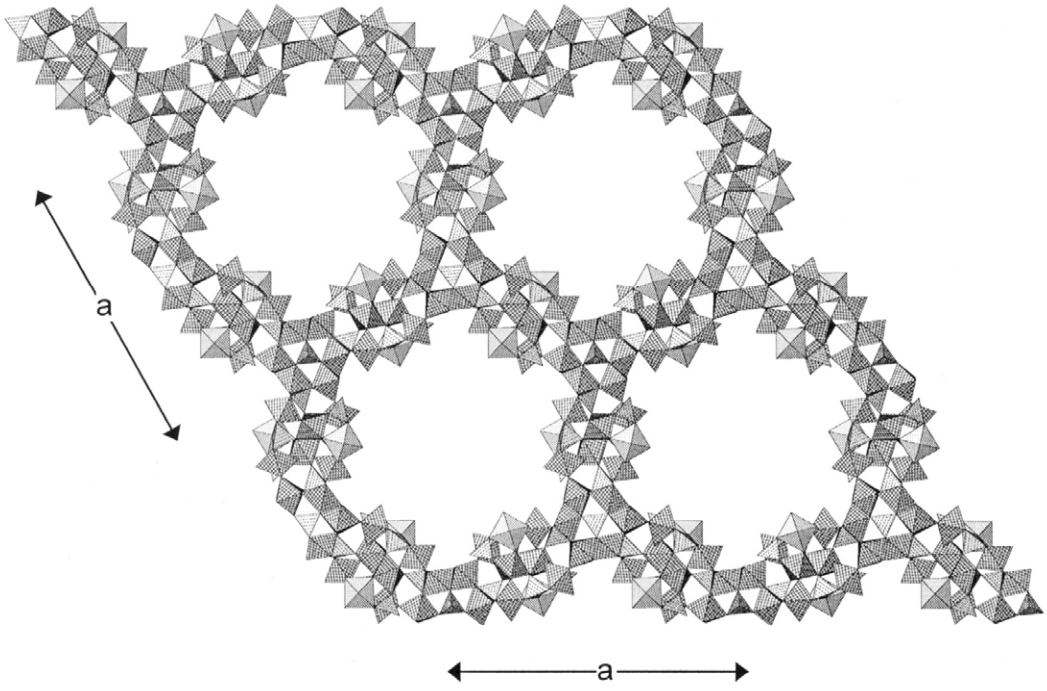

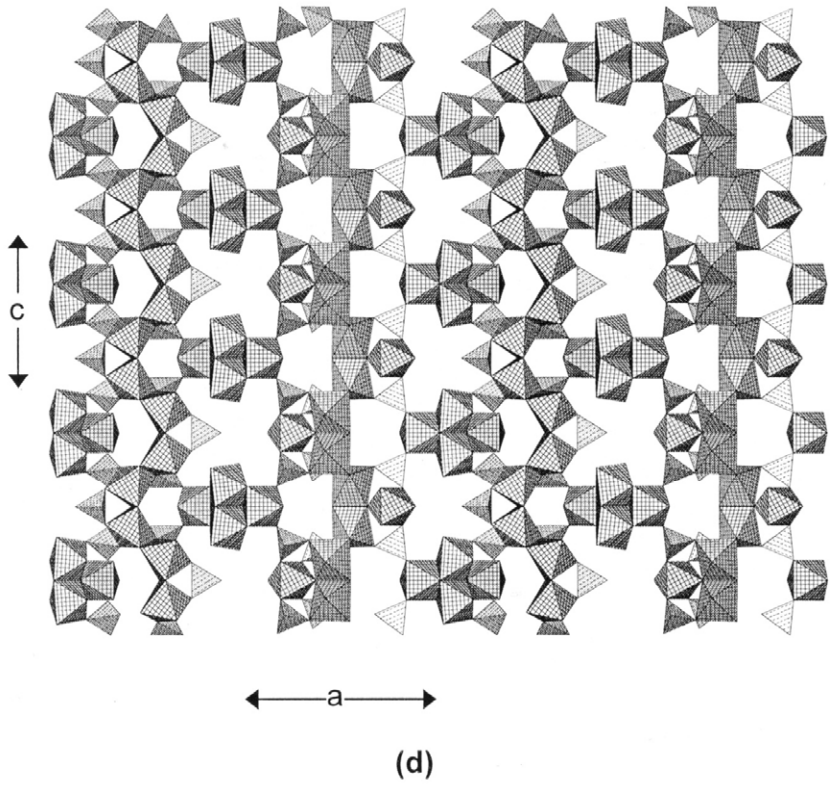

Figure 49 (continued). The structure of cacoxenite: (c) projected onto (001); (d) projected onto (010). ($Fe^{3+}\phi_6$) octahedra are 4^4-net-shaded, ($Al\phi_6$) octahedra are shadow-shaded.

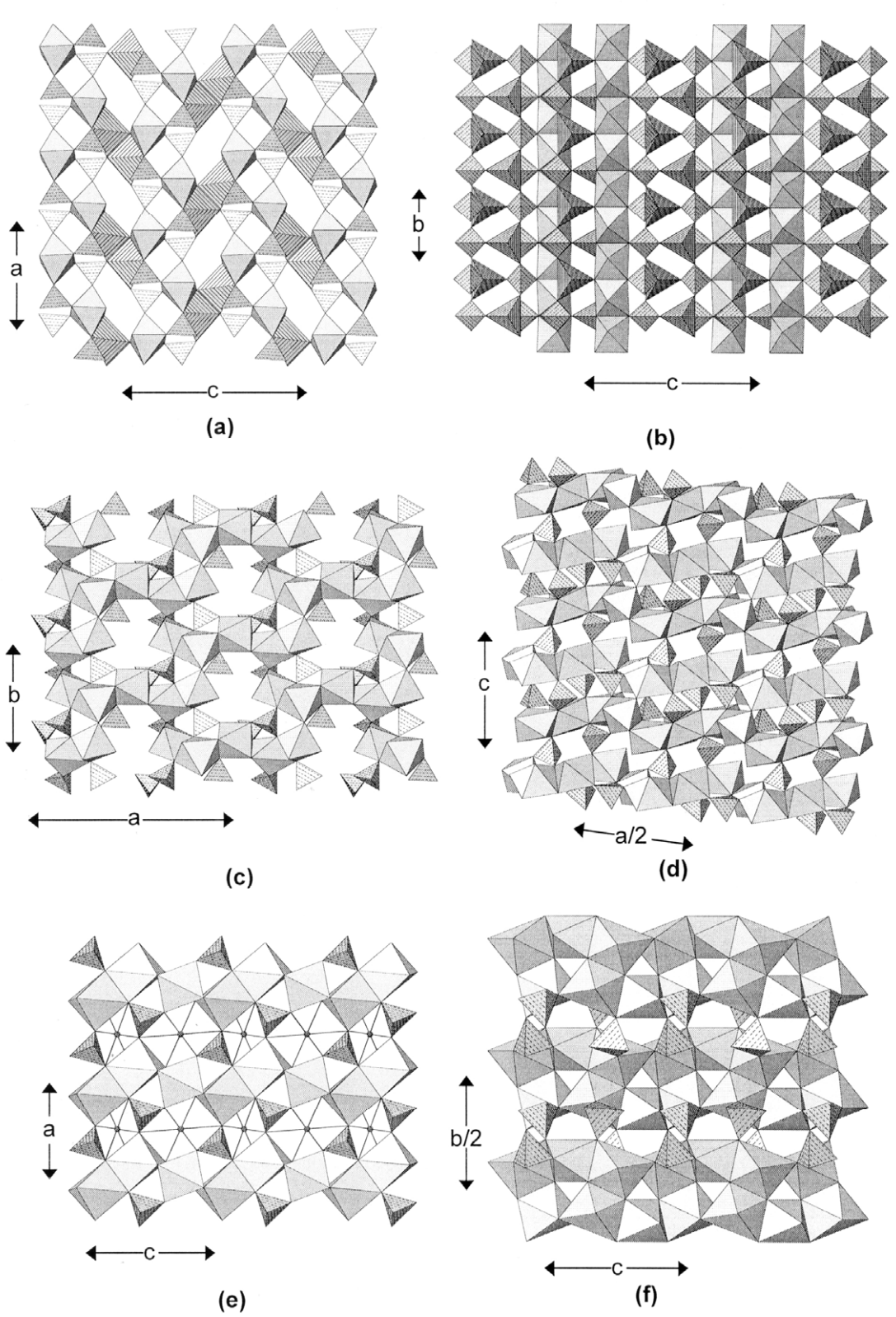

Figure 50. The crystal structures of althausite, hureaulite and thadeuite: (a) althausite projected onto (010); (b) althausite projected onto (100); ($Mg\phi_6$) octahedra are shadow-shaded, ($Mg\phi_5$) triangular bipyramids are line-shaded; (c) hureaulite projected onto (001); (d) hureaulite projected onto (010); ($Mn^{2+}\phi_6$) octahedra are shadow-shaded; (e) thadeuite projected onto (010); (f) thadeuite projected onto (100); ($Mg\phi_6$) octahedra are shadow-shaded.

Thadeuite, $[CaMg_3(PO_4)_2(OH)_2]$, is a densely packed framework of (PO_4) tetrahedra and both $(Ca\phi_6)$ and $(Mg\phi_6)$ octahedra. $(Mg\phi_6)$ octahedra share edges to form chains that extend in the *c*-direction (Fig. 50e). These chains are decorated by (PO_4) tetrahedra that link octahedra along the chain, and also link between chains in the *a*-direction. Interchain linkage also occurs by edge-sharing with $(Ca\phi_6)$ octahedra (shown as ball-and-stick in Fig. 50e). The resulting layers stack in the *b*-direction (Fig. 50f) and are linked by (PO_4) groups. In this view, the more complicated nature of the chains of octahedra is apparent: two single $[M\phi_4]$ chains are joined by edge-sharing between octahedra, and these two chains twist together in a helical fashion. Despite its common stoichiometry, $M_2(T\phi_4)\phi$, thadeuite shows no close structural relation with any other minerals of this stoichiometry.

Bakhchisaraitsevite, $Na_2(H_2O)[Mg_5(PO_4)_4(H_2O)_5](H_2O)$, has to be one of Nature's masterpieces of complexity. Pairs of $(Mg\phi_6)$ octahedra meld to form $[Mg_2\phi_{10}]$ dimers which then link by sharing edges to form zig-zag $[Mg\phi_4]$ chains that extend in the *a*-direction (Fig. 51a). The vertices of the shared edge of each dimer link to (PO_4) groups which also link to the corresponding vertices of the neighboring dimer in the chain, and chains adjacent in the *b*-direction link by octahedron-tetrahedron and octahedron-octahedron corner-linkages, forming a complex sheet parallel to (001). These sheets are cross-linked in the *c*-direction by $[Mg_2\phi_{10}]$ dimers, leaving large interstices between the sheets (Fig. 51b). Within these interstices are interstitial Na and (H_2O) groups: [5]- and [7]-coordinated Na each bond to one (H_2O) group and four and six O-atoms, respectively, of the structural unit, and there is one interstitial (H_2O) group not bonded to any cations, but held in the structure solely by hydrogen bonds.

The minerals of the **phosphoferrite** group have the general formula $M(1)M(2)_2(PO_4)_2X_3$, where the *M* cations may be divalent or trivalent and *X* = (OH), (H_2O); these minerals are isostructural, despite differences in both cation and anion charges (Moore and Araki 1976; Moore et al. 1980). The currently known species of this group are **phosphoferrite**, $[Fe^{2+}{}_3(PO_4)_2(H_2O)_3]$, **reddingite**, $[Mn^{2+}{}_3(PO_4)_2(H_2O)_3]$, **landesite**, $[Fe^{3+}Mn^{2+}{}_2(PO_4)_2(OH)(H_2O)_2]$, and **kryzhanovskite**, $[Fe^{3+}{}_3(PO_4)_2(OH)_3]$. A prominent feature of these structures is a trimer of edge-sharing octahedra that is canted at about 20^o to the *c*-axis (Fig. 51c). These trimers link by sharing octahedron edges to form chains of en-echelon trimers that extend in the *c*-direction. These chains link in the *b*-direction by sharing octahedron vertices to form a sheet of octahedra parallel to (100). The upper and lower surfaces of the sheet are decorated by (PO_4) tetrahedra, and a prominent feature of this decorated sheet is the $[M_2(TO_4)_2\phi_7]$ cluster (Fig. 17e) (Hawthorne 1979a). These sheets stack in the *a*-direction, and link by sharing octahedron and tetrahedron vertices (Fig. 51d). Moore and Araki (1976) showed that single crystals of phosphoferrite can be transformed by heating (oxidation-dehydroxylation) in air to single crystals of kryzhanovskite.

Griphite, $Ca_4F_8[A_{24}Fe^{2+}{}_4Al_8(PO_4)_{24}]$, where $A \approx Li_2Na_4Ca_2Fe^{2+}{}_2Mn^{2+}{}_{14}$ and has triangular bipyramidal coordination, is rather complicated from both a chemical and a structural perspective, and we could not write a satisfactory end-member chemical formula; even the simplification of the above formula produces a substantial charge imbalance ($\sim 2^+$). (AlO_6) octahedra share all vertices with (PO_4) tetrahedra, forming -(AlO_6)-(PO_4)-(AlO_6)-(PO_4)- chains that extend in the *a*-, *b*- and *c*-directions to form a very open framework of the form $[Al_8(PO_4)_{24}]$ (Fig. 52a). The $(Fe^{2+}O_6)$ octahedron links to six (PO_4) groups by sharing corners, and the resultant clusters link to a framework of corner-sharing (PO_4) groups and (CaO_8) cubes (Fig. 52b). The triangular bipyramids of the *A* cations share corners to form a very irregular sheet centered on $z \approx 0.62$ (Fig. 52c). The three sheets of Figures 52a,b,c meld to form a very complicated hetero-polyhedral framework (Fig. 52d, in which the *A* cations are shown as circles for simplicity).

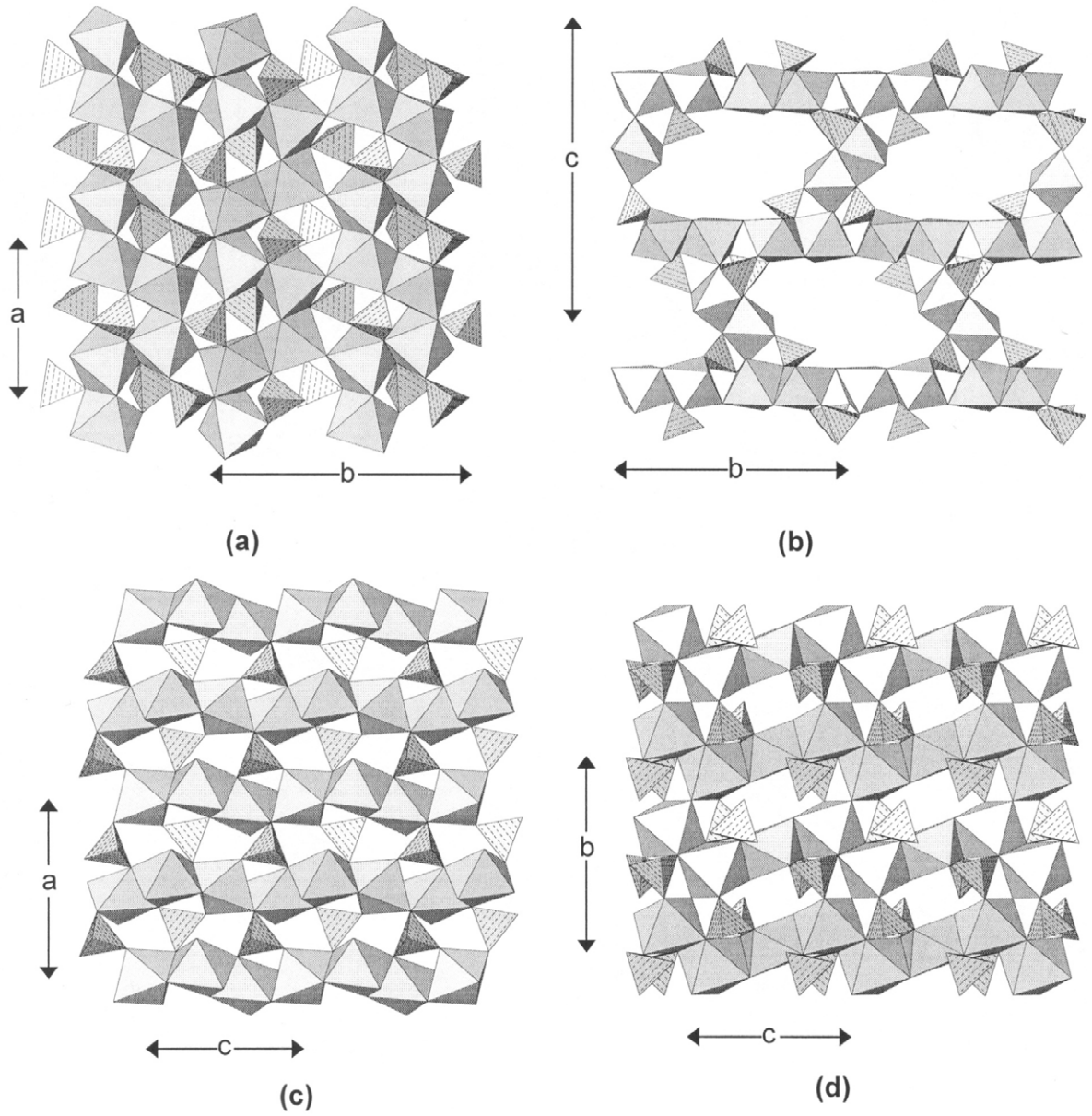

Figure 51. The crystal structures of bakhchisaraitsevite and kryzhanovskite/phosphoferrite: (a) bakhchisaraitsevite projected onto (001); (b) bakhchisaraitsevite projected onto (100); (c) kryzhanovskite/phosphoferrite projected onto (010); (d) kryzhanovskite/phosphoferrite projected onto (100). (Feϕ_6) octahedra are shadow-shaded.

Cornetite, $[Cu^{2+}{}_3(PO_4)(OH)_3]$, contains Cu^{2+} in both octahedral and triangular bipyramidal coordinations. Pairs of ($Cu^{2+}\phi_6$) octahedra share an edge to form $[Cu^{2+}{}_2\phi_{10}]$ dimers that are inclined at ~30° to the *b*-direction (Fig. 52e). Dimers adjacent in the *c*-direction show opposite cants and link by an octahedron from one dimer bridging the apical vertices of the adjacent dimer to form serrated ribbons that extend in the *c*-direction. These ribbons are linked by sharing corners with (PO_4) tetrahedra, and edges and corners with($Cu^{2+}\phi_5$) triangular bipyramids (Fig. 52f).

Gladiusite, $Fe^{2+}{}_4Fe^{3+}{}_2(PO_4)(OH)_{11}(H_2O)$, is an open framework structure with extensive hydrogen bonding. In the structure, ($Fe^{2+}\phi_6$) and ($Fe^{3+}\phi_6$) octahedra form [$M\phi_4$]

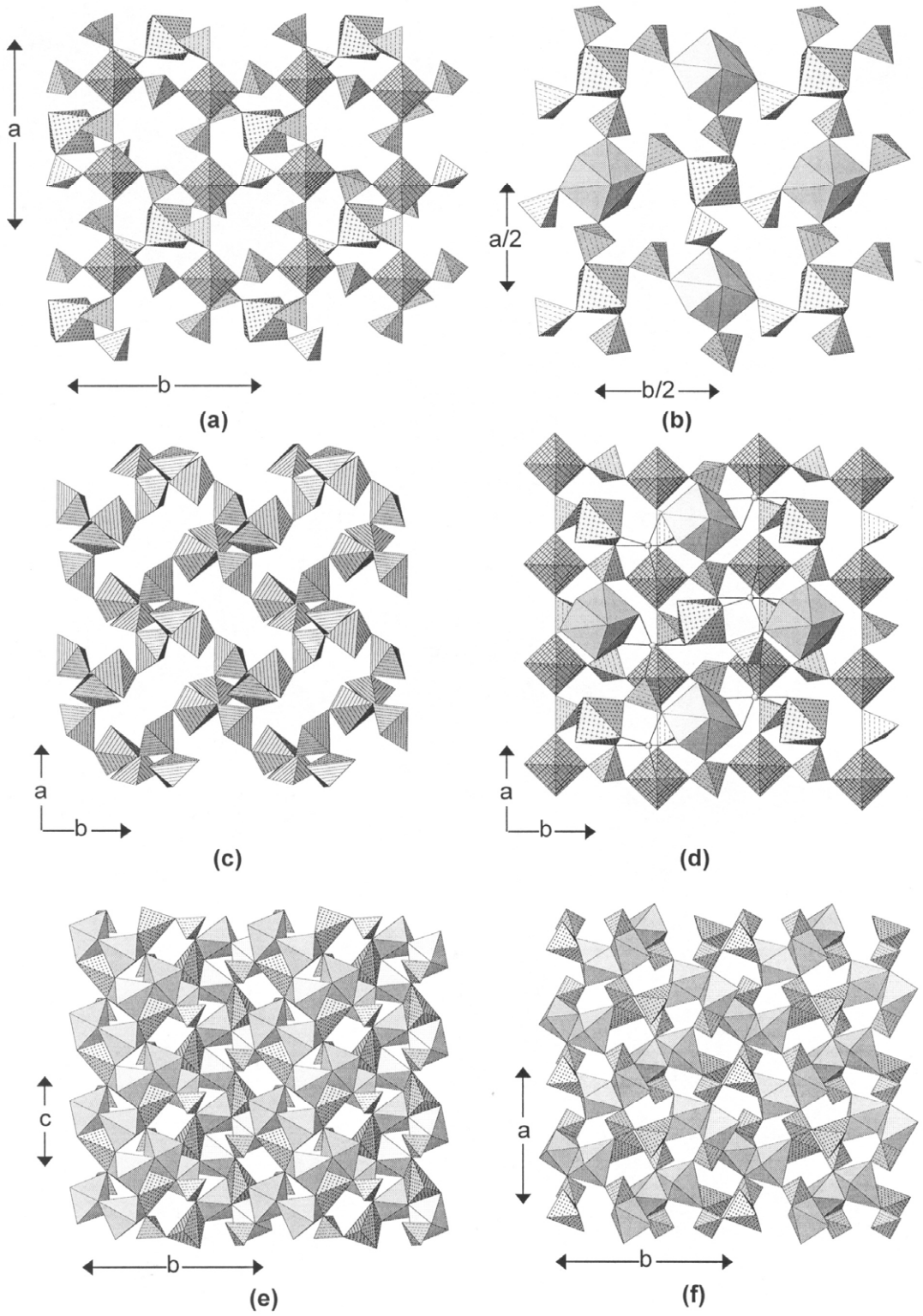

Figure 52. The crystal structures of griphite and cornetite: (a) griphite layer at $z \sim 0.25¼$ projected onto (001); (b) griphite layer at $z \sim 0.50½$ projected onto (001); (c) griphite layer at $z \sim 0.62$ projected onto (001); (d) griphite structure projected onto (001); ($Al\phi_6$) octahedra are 4^4-net-shaded, ($Ca\phi_8$) cubes are shadow-shaded, ($Fe^{3+}\phi_6$) octahedra are dot-shaded, triangular bipyramids are line-shaded; in (d), the triangular-bipyramidally coordinated cation is shown as a circle; (e) cornetite projected onto (100); (f) cornetite projected onto (001); ($Cu^{2+}\phi_6$) octahedra are shadow-shaded, ($Cu^{2+}\phi_5$) polyhedra are dot-shaded.

chains of edge-sharing octahedra that extend in the *c*-direction (Fig. 53a). Pairs of these chains meld by sharing edges to form ribbons, and these ribbons link in triplets by sharing corners between octahedra such that the plane of each succeeding ribbon is offset from the first (Fig. 53b). The ribbons are further linked through ($P\phi_4$) groups that share one vertex with each ribbon (Figs. 53a,b). Figure 53c illustrates the linkage between these ribbons in three dimensions. The ribbons are inclined at ~45° to the *c*-axis and are repeated by the *b*-translation to form a row of parallel ribbons centered on $z \approx 0$. Adjacent rows centered on $z \approx {}^1/_2$ have the ribbons arranged with the opposite inclination to the *a*-axis, and adjacent ribbons link by sharing octahedron vertices (Fig. 53c). The resultant framework is very open, and the interstitial space is criss-crossed by a network of hydrogen bonds.

M≡M, M-M, M-T linkage. **Lipscombite**, $[Fe^{2+}Fe^{3+}{}_2(PO_4)_2(OH)_2]$, is an enigma. Katz and Lipscomb (1951) applied this name to synthetic $Fe_7(PO_4)_4(OH)_4$ with symmetry $I4_122$ and a = 5.37, c = 12.81 Å. Gheith (1953) used the name for tetragonal synthetic compounds varying between $Fe^{2+}{}_8(PO_4)_4(OH)_4$ and $Fe^{3+}{}_{3.5}(PO_4)_4(OH)_4$. More recently, Vochten and DeGrave (1981) and Vochten et al. (1983) gave the cell parameters of synthetic lipscombite as $a = b$ = 5.3020(5), c = 12.8800(5) Å. However, Lindberg (1962) reported natural manganoan lipscombite with symmetry $P4_12_12$ and a = 7.40, c = 12.81 Å. Vencato et al. (1989) presented the structure of synthetic lipscombite with symmetry $P4_32_12$ and a = 7.310(3), c = 13.212(7) Å, in accord with the results of Lindberg (1962), who seems to be the only person who has actually characterized the mineral.

The structure reported by Vencato et al. (1989) consists of face-sharing chains of ($Fe^{2+}\phi_6$) and ($Fe^{3+}\phi_6$) octahedra that extend in the [110] and [1$\bar{1}$0] directions (Fig. 53d,e). These chains link by corner-sharing between octahedra of adjacent chains and also by sharing corners with (PO_4) tetrahedra. Because of the 4_3 symmetry, the structure consists of layers in which the face-sharing chains extend only in a single direction, and adjacent layers that are related by 4_3 symmetry have the chains extending in orthogonal directions. A single layer is shown in Figure 50e, in which all the chains extend along [110] and are linked within the layer by rows of bridging (PO_4) groups. Note that in the face-sharing chain, two of the three symmetrically distinct octahedra are partly occupied.

The minerals of the **burangaite**, $Na[Fe^{2+}Al_5(PO_4)_4(OH)_6(H_2O)_2]$, group contain a trimer of face-sharing octahedra that is a feature of several basic iron-phosphate minerals (Moore 1970). An ($Fe^{2+}\phi_6$) octahedron shares two *trans* faces with ($Al\phi_6$) octahedron to form a trimer of the form $[M_3\phi_{12}]$ (the *h* cluster of Moore 1970). This trimer is corner linked to two ($Al\phi_6$) octahedra and two (PO_4) tetrahedra to produce a cluster of the general form $[M_5(TO_4)_2\phi_{18}]$. This cluster polymerizes in the *c*-direction to form a dense slab by corner-sharing between ($Al\phi_6$) octahedra and by corner-sharing between octahedra and tetrahedra. This slab is oriented parallel to (100) (Fig. 54a) and adjacent slabs are weakly linked in the [100] direction by additional ($Al\phi_6$) octahedra that share corners with both tetrahedra and octahedra. The resulting framework has large interstices that are occupied by [8]-coordinated Na that is bonded to two (H_2O) groups. Note that Moore (1970) gave the formula of the isostructural dufrénite as $Ca_{0.5}Fe^{2+}Fe^{3+}{}_5(PO_4)_4(OH)_6\ (H_2O)_2$, which is in accord with the requirements for an end-member composition (Hawthorne 2002). However, both Moore (1984) and Nriagu (1984) incorrectly list the formula of dufrénite as $CaFe^{3+}{}_6(PO_4)_4(OH)_6(H_2O)_2$; this formula has a net charge of 2^+. Van der Westhuizen et al. (1990) reported electron-microprobe analyses for dufrénite, but many of the resultant formulae are incompatible with the dufrénite structure.

The minerals of the **rockbridgeite**, $[Fe^{2+}Fe^{3+}{}_4(PO_4)_3(OH)_5]$, group are also based on the *h* cluster, but the mode of linkage of these clusters is very different from that in the

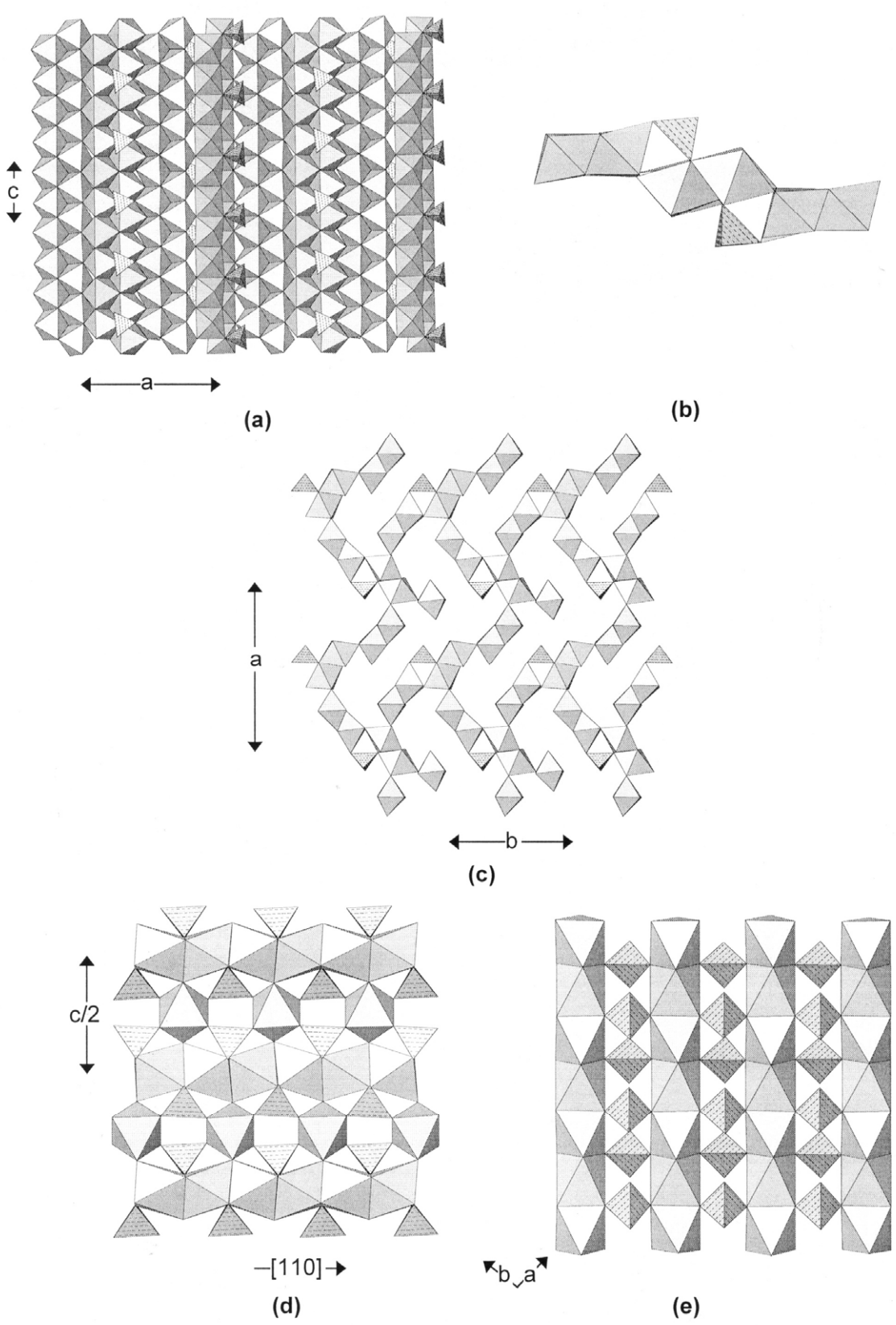

Figure 53. The crystal structures of gladiusite and lipscombite: (a) gladiusite projected onto (010); (b) in gladiusite, the linking of adjacent pairs of chains to form a triplet of offset chains with linking (PO_4) tetrahedra; (c) gladiusite projected onto (001); (d) lipscombite projected onto 100); (e) lipscombite projected onto (001). ($\{Fe^{2+},Fe^{3+}\}\phi_6$) octahedra are shadow-shaded.

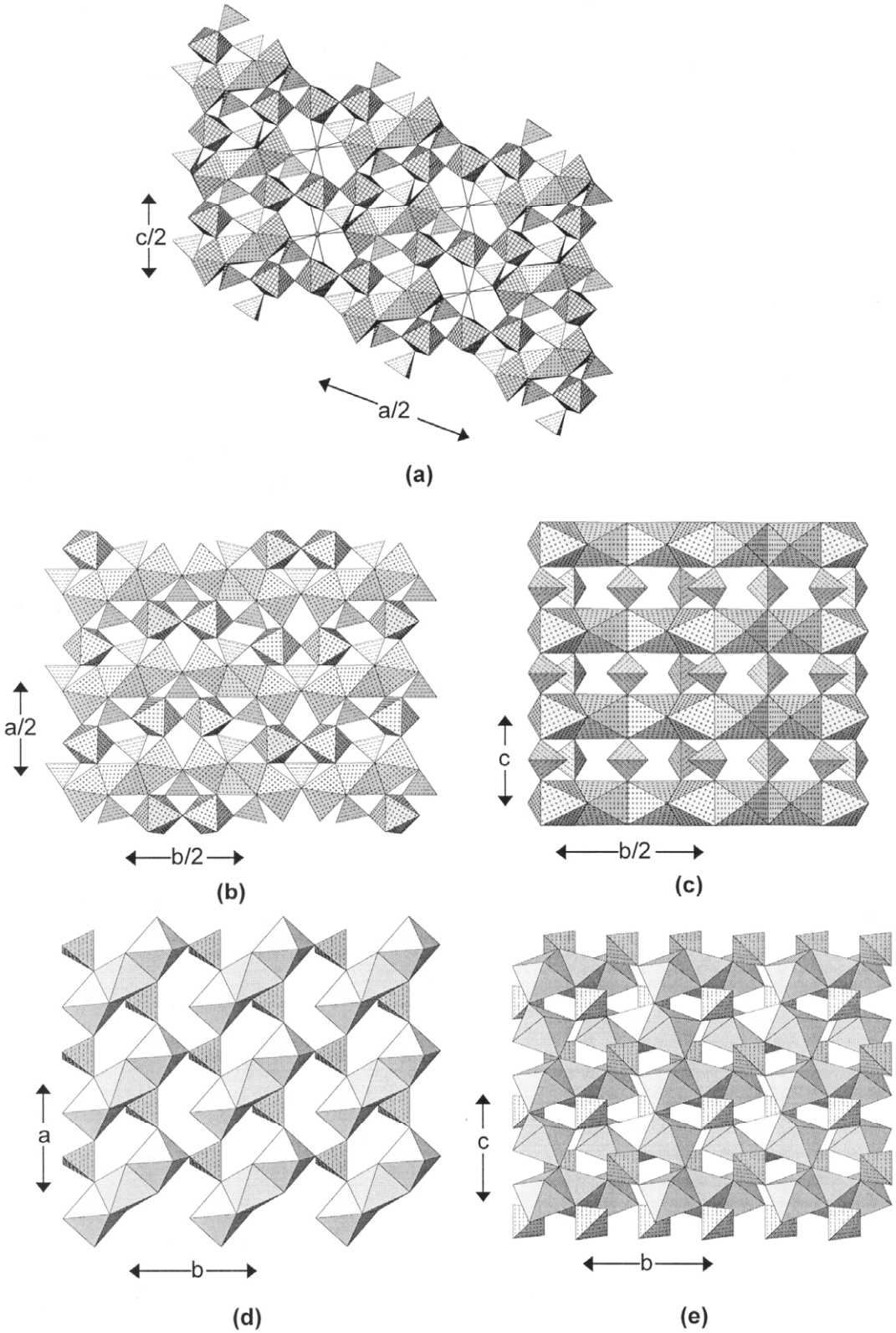

Figure 54. The crystal structures of burangaite, rockbridgeite and lazulite: (a) burangaite projected onto (010); (Alϕ_6) octahedra are 4^4-net-shaded, ($Fe^{2+}\phi_6$) octahedra are dot-shaded, Na is shown as shaded circles; (b) rockbridgeite projected onto (001), (c) rockbridgeite projected onto (100); ({Fe^{3+},Fe^{2+}})ϕ_6) octahedra are dot-shaded; (d) lazulite projected onto (001); (e) lazulite projected onto (100); ({Mg,Al}ϕ_6) octahedra are shadow-shaded.

minerals of the burangaite group The face-sharing trimers link by sharing octahedron corners to form chains of octahedra that extend in the *b*-direction (Fig. 54b). Chains adjacent in the *a*-direction are linked by $[M_2(TO_4)\phi_8]$ clusters and (PO_4) groups that link to two adjacent trimers and two $[M_2(TO_4)\phi_8]$ clusters, forming complex sheets parallel to (001). When viewed in the *a*-direction (Fig. 54c), the very layered aspect of the structure is apparent, layers of octahedra alternating with layers of tetrahedra.

The minerals of the **lazulite**, $[MgAl_2(PO_4)_2(OH)_2]$, group contain the *h* cluster, a trimer of face-sharing octahedra, that is characteristic of several basic phosphate minerals. An $(Mg\phi_6)$ octahedron is sandwiched between two $(Al\phi_6)$ octahedra, and the resulting trimers are arranged at the vertices of a 4^4 net and extending in the [110] direction (Fig. 54d). Adjacent trimers are linked by sharing corners with (PO_4) groups, and when viewed down [001], the structure consists of layers of octahedra and tetrahedra. When viewed down [100] (Fig. 54e), it can be seen that the trimers of adjacent layers are canted in opposing direction, thereby promoting linkage of each (PO_4) tetrahedron to four different trimers. The resulting arrangement is quite densely packed.

Trolleite, $[Al_4(PO_4)_3(OH)_3]$, is a very dense structure with some similarities to the structural arrangement of the minerals of the lazulite group (Table 8). There are two prominent chain motifs that constitute the building blocks of this structure. There is an $[Al(PO_4)\phi_3]$ 7-Å chain (Fig. 18c) that extends in the *c*-direction (Fig. 55a), giving the 7.1 Å repeat along the *c*-axis. There is also an $[Al(PO_4)\phi_4]$ chain that assumes a very contorted geometry (Fig. 55a) so that it has the same repeat distance along its length as the $[Al(PO_4)\phi_3]$ chain to which it is attached by sharing octahedron faces. These rather complex double-chains link in the *b*-direction by sharing vertices of the tetrahedra of the $[Al(PO_4)\phi_3]$ chain with the octahedra of the $[Al(PO_4)\phi_4]$ chain (Fig. 55a). These slabs repeat in the *a*-direction in a very complex manner. As shown in Figure 55b, these slabs meld by sharing octahedron-tetrahedron vertices between adjacent $[Al(PO_4)\phi_3]$ chains to form a thick slab: $[Al(PO_4)\phi_4]$-$[Al(PO_4)\phi_3]$-$[Al(PO_4)\phi_3]$-$[Al(PO_4)\phi_4]$ that constitute one-half the cell in the *a*-direction. The thick slabs link by sharing octahedron vertices between $[Al(PO_4)\phi_4]$ chains to form a very dense framework.

Seamanite, $[Mn^{2+}_3(B\{OH\}_4)(PO_4)]$, is a mixed phosphate-borate mineral based on chains of $(Mn\phi_6)$ octahedra that consist of free-sharing $[M_3\phi_{12}]$ trimers that link by sharing octahedron edges to form an $[M_3\phi_{10}]$ chain that extends in the *c*-direction (Fig. 55c). The rather unusual $[M_3\phi_{12}]$ trimer is apparently stabilized by the $(B\phi_4)$ group that spans the apical vertices of the edge-sharing octahedra (Moore and Ghose 1971). Additional linkage along the length of the chain is provided by (PO_4) tetrahedra that link apical vertices on neighboring $(M\phi_6)$ octahedra such that the (PO_4) and $(B\phi_4)$ tetrahedra adopt a staggered configuration on either side of the $[M(B\phi_4)(PO_4)\phi_6]$ chain. These chains condense in pairs by sharing both octahedron-octahedron and octahedron-tetrahedron vertices to form columns, seen end-on in Figure 55d. These columns link together in the *a*- and *b*-directions by sharing vertices between tetrahedra and octahedra, with additional linkage involving hydrogen bonds.

M=M, M=T, M-T linkage. **Holtedahlite**, $[Mg_{12}(PO_3\{OH\})(PO_4)_5(OH)_6]$, contains dimers of face-sharing $(Mg\phi_6)$ (Fig. 55e). These dimers link by sharing edges to form ribbons that extend in the *c*-direction and contain $(PO_3\{OH\})$ tetrahedra that link to all three ribbons (Fig. 55e). These channels link in the *a*- and *b*-directions by sharing octahedron corners and by sharing octahedron corners with bridging (PO_4) tetrahedra (Figs. 55e,f).

The crystallographic and chemical details of the minerals of the **triphylite-lithiophyllite**, **sicklerite-ferrisicklerite** and **heterosite-purpurite** groups are summarized in Table 10 (for consistency, some of the axial orientations have been changed from

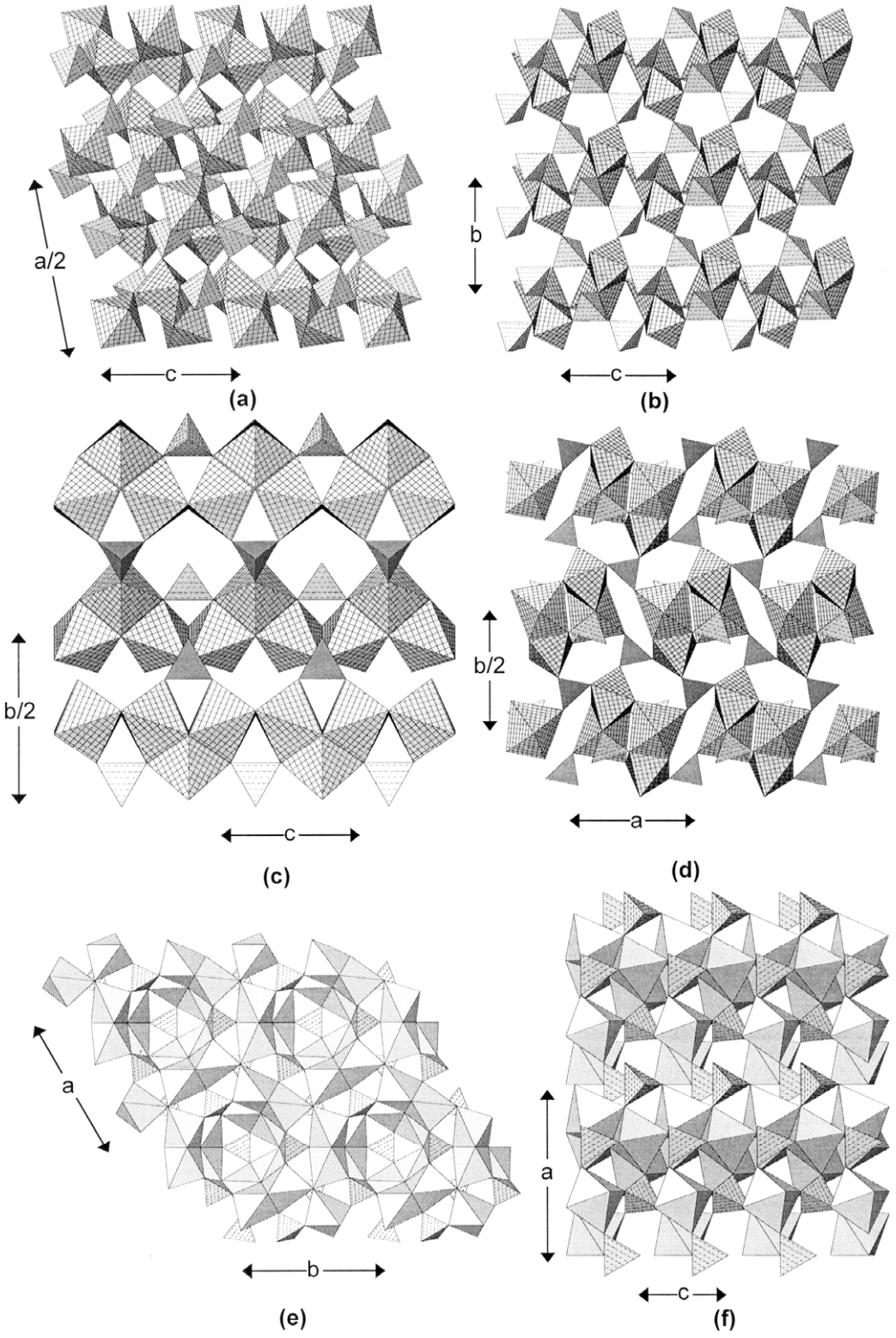

Figure 55. The crystal structures of trolleite, seamanite and holtedahlite: (a) trolleite projected onto (010); (b) trolleite projected onto (100); (Alϕ_6) octahedra are 4^4-net-shaded; (c) seamanite projected onto (100); (d) seamanite projected onto (001); ($Mn^{2+}\phi_6$) octahedra are 4^4-net-shaded; (e) holtedahlite projected onto (001); (f) holtedahlite projected onto (010); (Mgϕ_6) octahedra are shadow-shaded.

Table 10. Details of the minerals of the triphylite-lithiophyllite, sicklerite-ferrisicklerite and heterosite-purpurite groups.

	a (Å)	*b*(Å)	*c* (Å)	Sp grp	Ref.
Triphylite	4.704	10.347	6.0189	*Pbnm*	(1)
Lithiophyllite	4.744(10)	10.460(30)	6.100(20)	*Pbnm*	(2)
Sicklerite	4.794	10.063	5.947	*Pbnm*	(3)
Ferrisicklerite	4.978	10.037	5.918	*Pbnm*	(4)
Heterosite	4.769(5)	9.760(10)	5.830(10)	*Pbnm*	(5)
Purpurite	4.76	9.68	5.819	*Pbnm*	(6)

References: (1) Yakubovich et al. (1977), (2) Geller and Durand (1960), (3) Blanchard (1981), (4) Alberti (1976), (5) Eventoff et al. (1972), (6) Bjoerling and Westgren (1938).

those reported in the original papers). All of these structures have the olivine arrangement. [MO_4] chains of edge-sharing (LiO_6) or (NaO_6) octahedra extend parallel to the *a*-direction (Fig. 56a,c,e**)** and are decorated by (Fe^{2+},$Mn^{2+}O_6$) or ($\square O_6$) octahedra ($\square$ = vacancy). These decorated chains are linked in the *b*-direction by sharing octahedron corners with (PO_4) groups, although such 'linkage' is not effective when the decorating octahedra are vacant (Fig. 56e); in this case, the chains link to other chains above and below the plane (Fig. 56f).

Consider the Fe end-members of each group:

triphylite	Li	Fe^{2+}	(PO_4)
ferrisicklerite	(Li,$\square$)	(Fe^{2+},Fe^{3+})	(PO_4)
heterosite	$\square$	Fe^{3+}	(PO_4)

As all three minerals have the same structure, the ranges in chemical composition for triphylite and heterosite are $LiFe^{2+}(PO_4)B(Li_{0.5}\square_{0.5})(Fe^{2+}{}_{0.5}Fe^{3+}{}_{0.5})(PO_4)$ and $\square_{0.5}Li_{0.5}(Fe^{3+}{}_{0.5}Fe^{2+}{}_{0.5})(PO_4)$- $\square Fe^{3+}(PO_4)$, respectively. Ferrisicklerite is an unnecessary name for intermediate-composition triphylite and heterosite. Similarly, sicklerite is an unnecessary name for intermediate lithiophyllite and purpurite.

Senegalite, [$Al_2(PO_4)(OH)_3(H_2O)$], contains Al in both triangular bipyramidal and octahedral coordinations. ($Al\phi_5$) and ($Al\phi_6$) polyhedra share an edge to form a dimer, and these dimers link by sharing corners to form a [$^{[5]}Al^{[6]}Al\phi_8$] chain that extends in the [101] (and [$1\bar{0}1$]) direction (Fig. 57a). These chains are decorated by (PO_4) groups that link them to form a slab parallel to (010). These slabs stack in the *b*-direction, and link by sharing tetrahedron-octahedron and tetrahedron-bipyramid corners (Fig. 57b). This framework is fairly open, and the interstices are criss-crossed by a network of hydrogen bonds.

M=M, M-M, M=T, M-T linkage. **Sarcopside**, [$Fe^{2+}{}_3(PO_4)_2$], is chemically similar to the minerals of the graftonite group but is structurally more similar to the structures of triphylite-lithiophyllite and its derivatives (Table 8). When viewed down [100] (Fig. 58a), the structure consists of a sheet of corner-linked octahedra at the vertices of a 4^4 net, and further linked by edges and corners with (PO_4) tetrahedra. When viewed down [010], the structure consists of trimers of edge-sharing octahedra linked into a sheet by sharing corners with (PO_4) groups (Fig. 58b). Sarcopside usually contains significant Mn^{2+}, but assuming complete solid-solution between graftonite and beusite, it seems that sarcopside is a polymorph of graftonite.

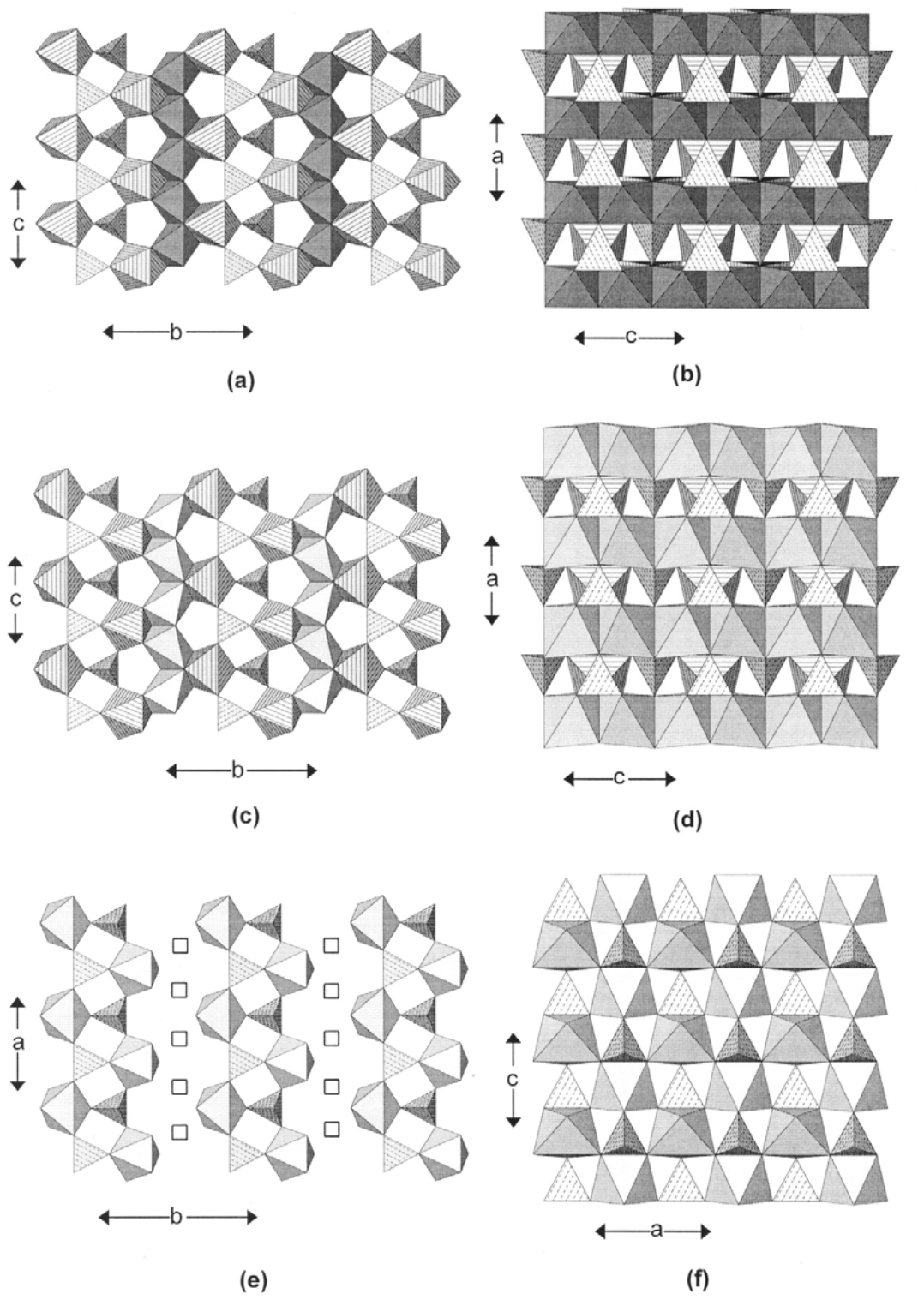

Figure 56. The crystal structures of lithiophylite, ferrisicklerite and heterosite: (a) lithiophylite projected onto (100); (b) lithiophylite projected onto (010); (c) ferrisicklerite projected onto (100); (d) ferrisicklerite projected onto (010); (e) heterosite projected onto (001); (f) heterosite projected onto (010). ($Fe^{2+}O_6$) octahedra are dark-shadow-shaded, (Fe^{2+},Fe^{3+}) octahedra are shadow-shaded, ({Li,□}O_6) octahedra are line-shaded, vacancies are shown as squares.

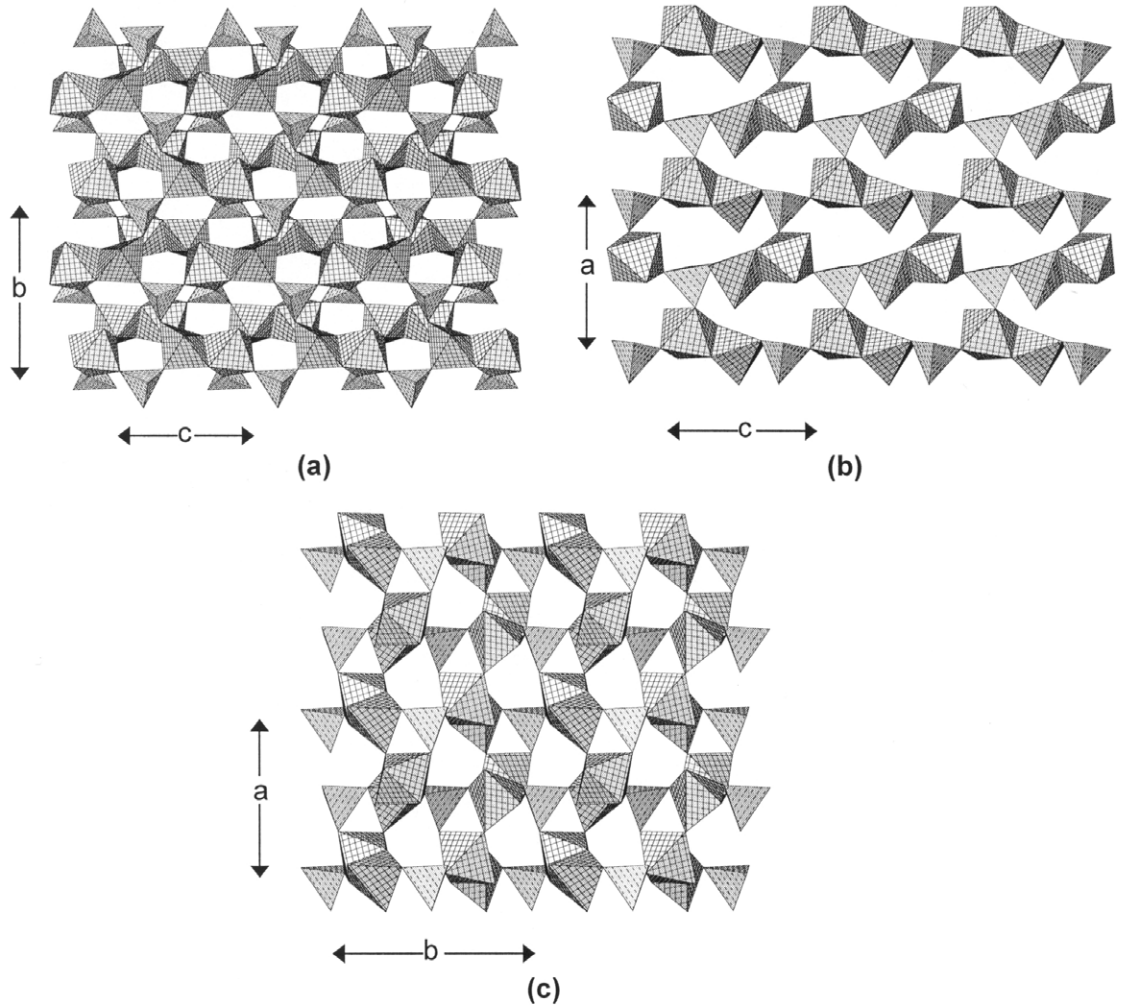

Figure 57. The crystal structure of senegalite: (a) projected onto (100); (b) projected onto (010); (c) projected onto (001). ($A\ell\phi_n$) polyhedra are 4^4-net-shaded.

In **bjarebyite**, $BaMn^{2+}{}_2[Al_2(PO_4)_3(OH)_3]$, and the minerals of the bjarebyite group (Table 8), pairs of ($A\ell\phi_6$) octahedra link by sharing edges to form dimers, and these dimers link together by sharing corners to form a chain of the form $[Al_2\phi_9]$, intermediate between the corner-sharing $[A\ell\phi_5]$ chain and the edge-sharing $[A\ell\phi_4]$ chain (i.e., $[Al_2\phi_9] \equiv 2\ [A\ell\phi_{4.5}]$). Octahedra that share corners are also linked by a flanking (PO_4) tetrahedron, similar to the linkage in the chain of Figure 18c. The *cis* vertex of each octahedron also links to a (PO_4) tetrahedron to give a chain of the form $[Al_2(PO_4)_3(OH)_3]$. These chains extend in the *b*-direction (Fig. 58c) and are linked in the *a*-direction by [6]-coordinated Mn^{2+} and by [11]-coordinated Ba (Fig. 58d). Kulanite and penikisite were originally reported as triclinic (Mandarino and Sturman 1976; Mandarino et al. 1977). However, Cooper and Hawthorne (1994a) showed that kulanite is monoclinic (and is isostructural with bjarebyite). It is probable that penikisite is also monoclinic.

STRUCTURES WITH ($T\phi_4$) GROUPS AND LARGE CATIONS

Xenotime-(REE), (REE)(PO_4), and **pretulite**, Sc(PO_4) (Table 11), belong to the zircon, Zr(SiO_4), group. The larger trivalent cation is coordinated by eight O-atoms in an arrangement that is known as a Siamese dodecahedron (Hawthorne and Ferguson 1975).

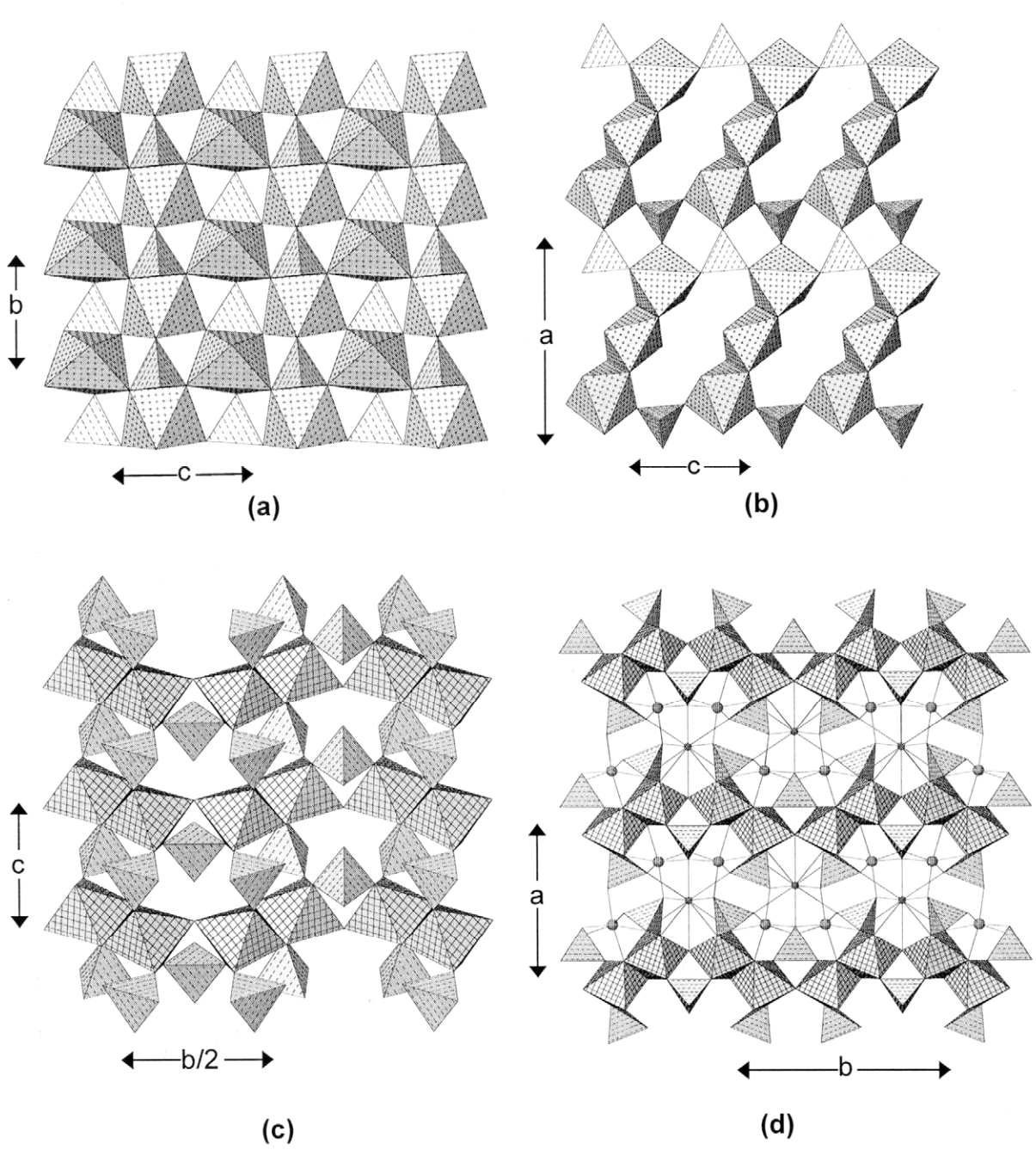

Figure 58. The crystal structures of sarcopside and bjarebyite: (a) sarcopside projected onto (100); (b) sarcopside projected onto (010); ($Fe^{2+}\phi_6$) octahedra are dot-shaded; (c) bjarebyite projected onto (100); (d) bjarebyite projected onto (001). ($Al\phi_6$) octahedra are 4^4-net-shaded, Mn^{2+} are shown as large shaded circles, Ba are shown as small shaded circles.

These dodecahedra link by sharing edges to form chains that extend in the *b*-direction (Fig. 59a). These chains are linked in the *c*-direction by (PO_4) tetrahedra that share an edge with a dodecahedron of one chain and a vertex with a dodecahedron of the adjacent chain, forming a layer in the (100) plane (Fig. 59a). These layers stack in the *a*-direction by edge-sharing between dodecahedra of adjacent layers to form dodecahedral chains orthogonal to the layers. Hence the zircon structure is tetragonal (Fig. 59b).

Monazite-(REE), (REE)(PO_4), is a dimorph of xenotime-(REE). In this structure, the larger trivalent cation is coordinated by nine O-atoms in a rather irregular arrange-

Table 11. Large-cation phosphate minerals.

Mineral	*Formula*	*Space group*	*Figure*
	Xenotime group		
Pretulite	$Sc(PO_4)$	$I4_1/amd$	59a,b
Xenotime-(Y)	$Y(PO_4)$	$I4_1/amd$	59a,b
Xenotime-(Yb)	$Yb(PO_4)$	$I4_1/amd$	59a,b
	Monazite group		
Brabantite	$CaTh(PO_4)_2$	$P2_1$	59c,d
Cheralite-(Ce)	$Ce(PO_4)$	$P2_1/n$	59c,d
Monazite-(Ce)	$Ce(PO_4)$	$P2_1/n$	59c,d
	Rhabdophane group		
Brockite		Aa	60a,b
Grayite	$Th(PO_4)(H_2O)$	$P6_222$	60a,b
Ningyoite	$U_2(PO_4)_2(H_2O)_{1–2}$	$P222$	60a,b
Rhabdophane	$Ce(PO_4)$	$P6_222$	60a,b
	General		
Archerite	$K(PO_3\{OH\}_2)$	$I\bar{4}2d$	60c,d
Biphosphammite	$(NH_4)(PO_2\{OH\}_2)$	$I\bar{4}2d$	60c,d
Brushite	$Ca(PO_3\{OH\})(H_2O)_2$	Ia	61a,b
Churchite-(Y)	$Y(PO_4)(H_2O)_2$	$I2/a$	61a,b
Ardealite	$Ca_2(PO_3\{OH\})(SO_4)(H_2O)_4$	Cc	61c,d,e
Dorfmanite	$Na_2(PO_3\{OH\})(H_2O)_2$	$Pbca$	62a,b,c
Monetite	$Ca(PO_3\{OH\})$	$Pmna$	62d
Nacaphite	$Na_2Ca(PO_4)F$	$P\bar{1}$	63a,b
Arctite	$(Na_5Ca)Ca_6Ba(PO_4)_6F_3$	$P\bar{1}$	63c,d
Nabaphite	$NaBa(PO_4)(H_2O)_9$	$P2_13$	–
Nastrophite	$NaSr(PO_4)(H_2O)_9$	$P2_13$	–
Lithiophosphate	$[Li_3(PO_4)]$	$Pcmn$	64a,b
Nalipoite	$NaLi_2(PO_4)$	$Pmnb$	64c,d
Nefedovite	$Na_5Ca_4(PO_4)_4F$	$I\bar{4}$	65a,b
Olgite	$NaSr(PO_4)$	$P3$	65c,d,e
Phosphammite	$(NH_4)_2(PO_3\{OH\})$	$P2_1/c$	66a,b
Vitusite-(Ce)	$Na_3Ce(PO_4)_2$	$Pca2_1$	66c
Stercorite	$Na(NH_4)(PO_3\{OH\})(H_2O)_4$	$P\bar{1}$	67a,b
Natrophosphate	$Na_7(PO_4)_2F(H_2O)_{19}$	$Fd\bar{3}c$	67c
Buchwaldite	$NaCa(PO_4)$	$Pn2_1a$	68a,b
Olympite	$LiNa_5(PO_4)_2$	$Pcmn$	–

ment. These polyhedra link by sharing edges to form chains that extend in the *b*-direction (Fig. 59c). The chains are linked in the *c*-direction by (PO_4) tetrahedra that share edges with polyhedra of adjacent chain to form a layer parallel to (100) (Fig. 59c). These layers stack in the *a*-direction by sharing edges between the ({REE}O_9) polyhedra to form rather staggered chains that extend in the [101] direction (Fig. 59d). The monazite structure preferentially incorporates the larger light REEs whereas the xenotime structure preferentially incorporates the smaller heavy REEs (Ni et al. 1995); this is in accord with the difference in trivalent-cation coordination numbers in these two structure-types, and is also in accord with Sc(PO_4) crystallizing in the xenotime (zircon) structure (as pretulite) rather than in the monazite-type structure.

Rhabdophane, Ca(PO_4), contains Ce coordinated by eight O-atoms in a dodeca-

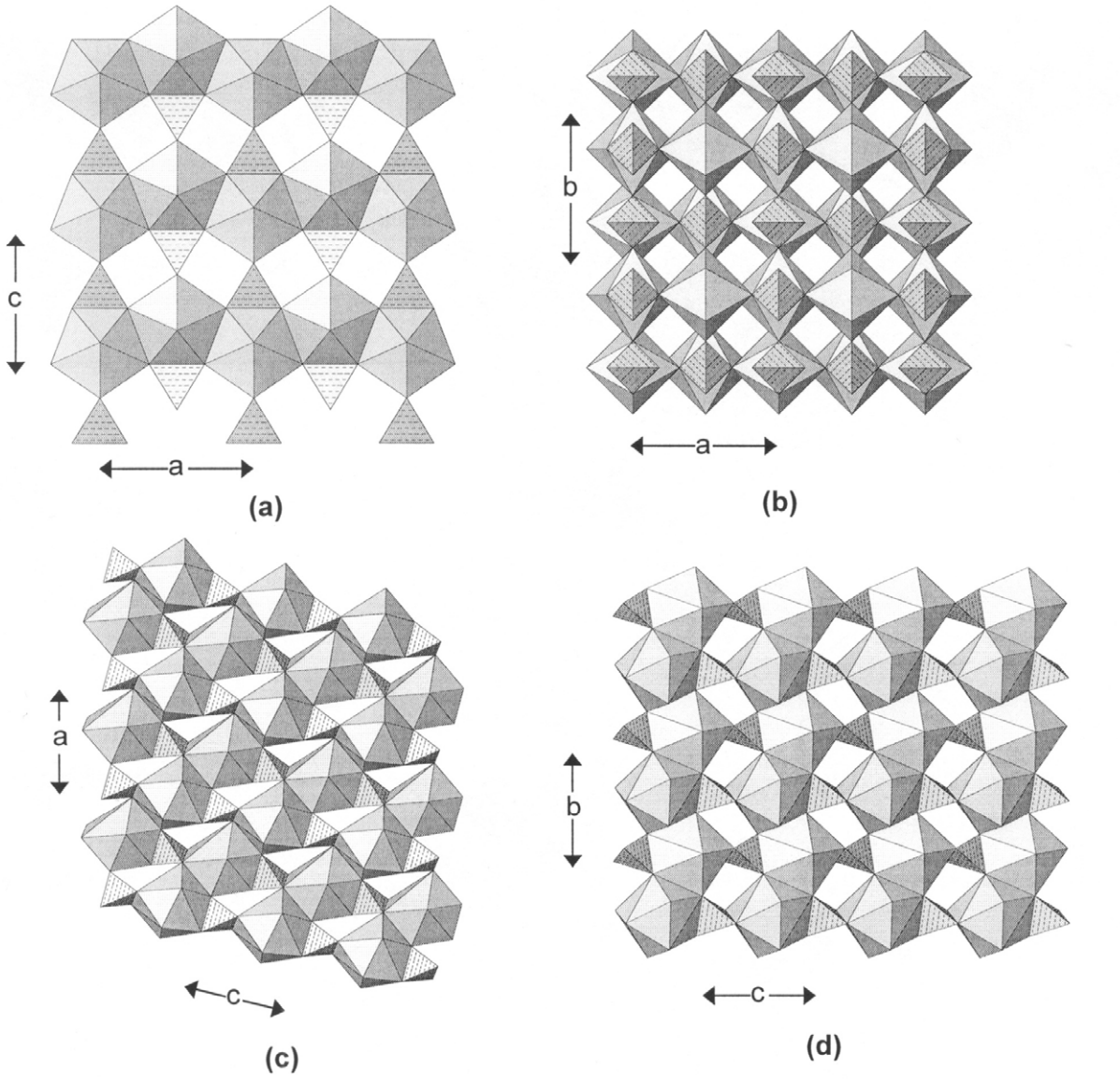

Figure 59. The crystal structures of xenotime and monazite: (a) xenotime-(Y) projected onto (010); (b) xenotime-(Y) projected onto (001); (c) monazite-(Ce) projected onto (010); (d) monazite-(Ce) projected onto (100). (REEϕ_7) polyhedra are shadow-shaded.

hedral arrangement. These dodecahedra polymerize by sharing edges to form chains that extend in the *a*- and *b*-directions (Fig. 60a). These chains link in the *c*-direction by sharing edges with (PO_4) tetrahedra to form sheets parallel to (100) and (010) (Fig. 60a). These sheets interpenetrate in the *a*- and *b*-directions (Fig. 60b) to form a framework with large hexagonal channels extending parallel to the *c*-axis.

Archerite, $K(PO_2\{OH\}_2)$, and **biphosphammite**, $(NH_4)(PO_2\{OH\}_2)$, are isostructural. In archerite, K is [8]-coordinated by O-atoms that are arranged at the vertices of a Siamese dodecahedron. These dodecahedra share edges to form a chain in the *b*- (and *a*-) directions, and adjacent chains link by sharing edges with (PO_4) tetrahedra (Fig. 60c) to form layers parallel to (011) and (101). These layers meld by sharing edges (i.e., mutually intersecting) to form a framework (Fig. 60d) that is topologically identical to the

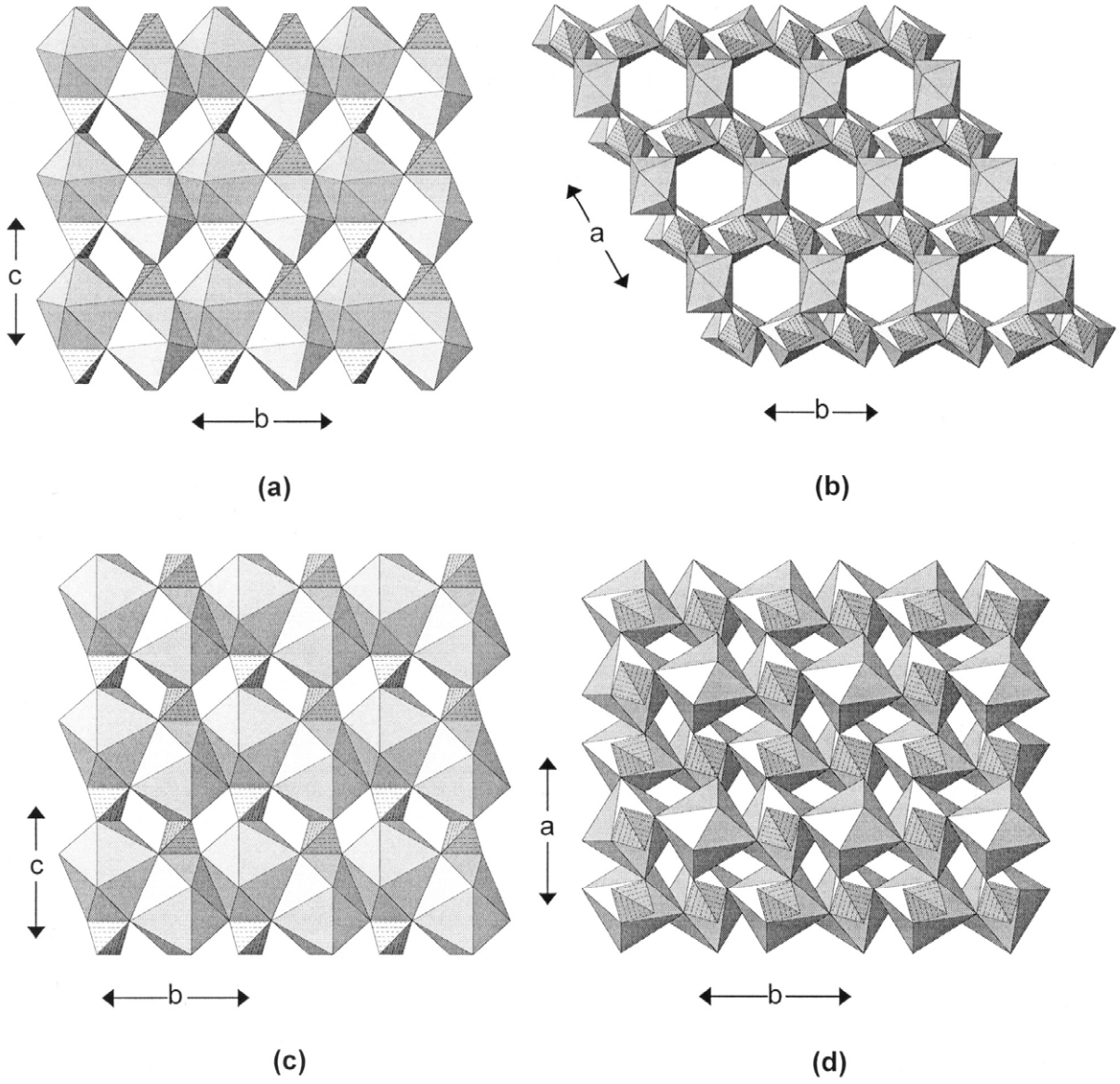

Figure 60. The crystal structure of rhabdophane and archerite: (a) rhabdophane projected onto (010); (b) rhabdophane projected onto (001); (REEϕ_7) polyhedra are shadow-shaded; (c) archerite projected onto (100); (d) archerite projected onto (001); (Kϕ_8) polyhedra are shadow-shaded.

framework in xenotime (Figs. 59a,b), although geometrical distortions result in a lower symmetry arrangement in archerite ($I\bar{4}2d$) as compared with xenotime ($I4_1/amd$).

Brushite, $Ca(H_2O)_2(PO_3\{OH\})$, and **churchite**, $Y(H_2O)_2(PO_4)$, are essentially isostructural, although Curry and Jones (1971) report the space group *Ia* for brushite and Kohlmann et al. (1994) report *I*2/*a* for churchite. The large cation is [8]-coordinated with the bonded anions in a dodecahedral arrangement. The dodecahedra share edges with the ($P\phi_4$) tetrahedra to form chains that extend in the [101] direction (Fig. 61a); these chains are a common feature of large-cation structures, and occur in gypsum and other Ca-sulfate minerals. These chains link in the [101] direction by sharing edges between ($Ca\phi_8$) polyhedra of adjacent chains, and by sharing of vertices between ($P\phi_4$) tetrahedra and ($Ca\phi_8$) dodecahedra, forming a dense sheet parallel to (101) (Fig. 61a). These sheets stack in the *b*-direction (Fig. 61b) and are linked solely by hydrogen bonds (not shown in Fig. 61b).

Ardealite, $Ca_2(H_2O)_4(PO_3\{OH\})(SO_4)$, is an intriguing structure in that P and S seem to be disordered over the two symmetrically distinct tetrahedrally coordinated sites (Sakae et al. 1978); presumably, the acid H atom is locally associated with the ($P\phi_4$) tetrahedra and hence shows analogous disorder. In the synthetic analogue, each of the two Ca atoms is coordinated by six O-atoms and two (H_2O) groups in a dodecahedral arrangement (as is the case in brushite). Chains of ($Ca\phi_8$) and ($\{P,S\}\phi_4$) polyhedra are formed by edge-sharing between the two types of polyhedra, chains that are topologically identical to the corresponding chains in brushite (Fig. 61a). These chains extend along [110] (Fig. 61c) and [001] (Fig. 61d), forming thick slabs that resemble the slabs in brushite (cf. Figs. 61b,e). Intercalated between these slabs are sheets of [8]-coordinated Ca and tetrahedra (Fig. 61e), and the structure is held together by a network of hydrogen bonds, the details of which are not known.

Dorfmanite, $Na_2(PO_3\{OH\})(H_2O)_2$, contains Na in both [5]- and [6]-coordination. ($Na\phi_5$) polyhedra occur at the vertices of a 6^3 plane net and link by sharing corners (Fig. 62a) to form a sheet that is decorated by ($P\phi_4$) tetrahedra. ($Na\phi_6$) octahedra share edges to form chains that extend in the *c*-direction and are linked in the *b*-direction by the ($P\phi_4$) groups (Fig. 62b) that decorate the underlying sheet of Figure 62a. These two sheets stack in the *a*-direction (Fig. 62c) and link through the ($P\phi_4$) groups.

Monetite, $CaH(PO_4)$, contains Ca in both [7]- and [8]-coordination, and the polyhedra share edges to form chains that extend in the *a*-direction. These chains are linked in the *b*-direction by sharing edges and vertices of the (CaO_n) polyhedra with ($P\phi_4$) groups (Fig. 62d). These sheets link in the *c*-direction via corner-sharing between (CaO_n) polyhedra and ($P\phi_4$) groups. Catti et al. (1977a) have carefully examined the evidence for a symmetrical hydrogen-bond in monetite. In space group $P\bar{1}$, one of the three symmetrically distinct H-atom sites lies on, or disordered off, a centre of symmetry, and another H-atom is statistically distributed between two centrosymmetric positions. In space group *P*1, the first H-atom is displaced slightly off the pseudo-centre of symmetry, and another H-atom is either ordered or disordered. Catti et al. (1977a) propose that the crystal they examined is a mixture of domains of both $P\bar{1}$ and *P*1 structure.

Nacaphite, $Na_2Ca(PO_4)F$, contains six octahedrally coordinated sites, four of which are each half-occupied by Ca and Na, and two of which are occupied solely by Na. Two $\{(Ca_2Na_2)O_6]$ and one (NaO_6) octahedra link to form an $[M_3\phi_{11}]$ trimer, and there are two such symmetrically distinct trimers in this structure. The trimers link in the (100) plane by sharing corners (Fig. 63a), and the resultant sheet is braced by (PO_4) tetrahedra that link three adjacent trimers. The sheets stack in the *a*-direction (Fig. 63b), and are linked by edge-and face-sharing between trimers and by corner-sharing between (PO_4) groups and trimers of adjacent layers. This nacaphite structure is related to the structures of

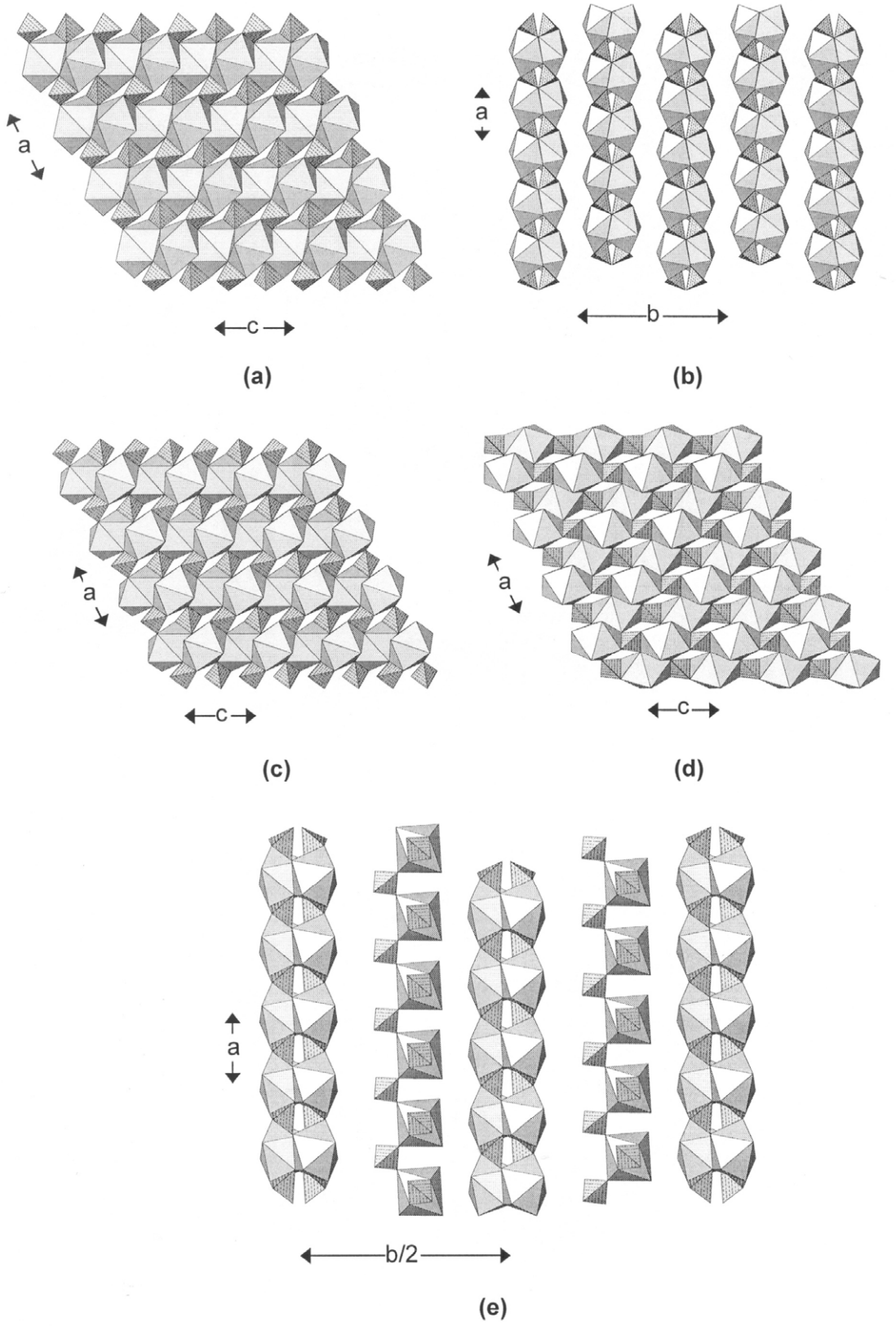

Figure 61. The crystal structures of brushite and ardealite: (a) brushite projected onto (010); (b) brushite projected onto (001); (c) ardealite: one layer projected onto (010); (d) ardealite: the next layer projected onto (010); (e) ardealite projected onto (001). ($Ca\phi_8$) polyhedra are shadow-shaded.

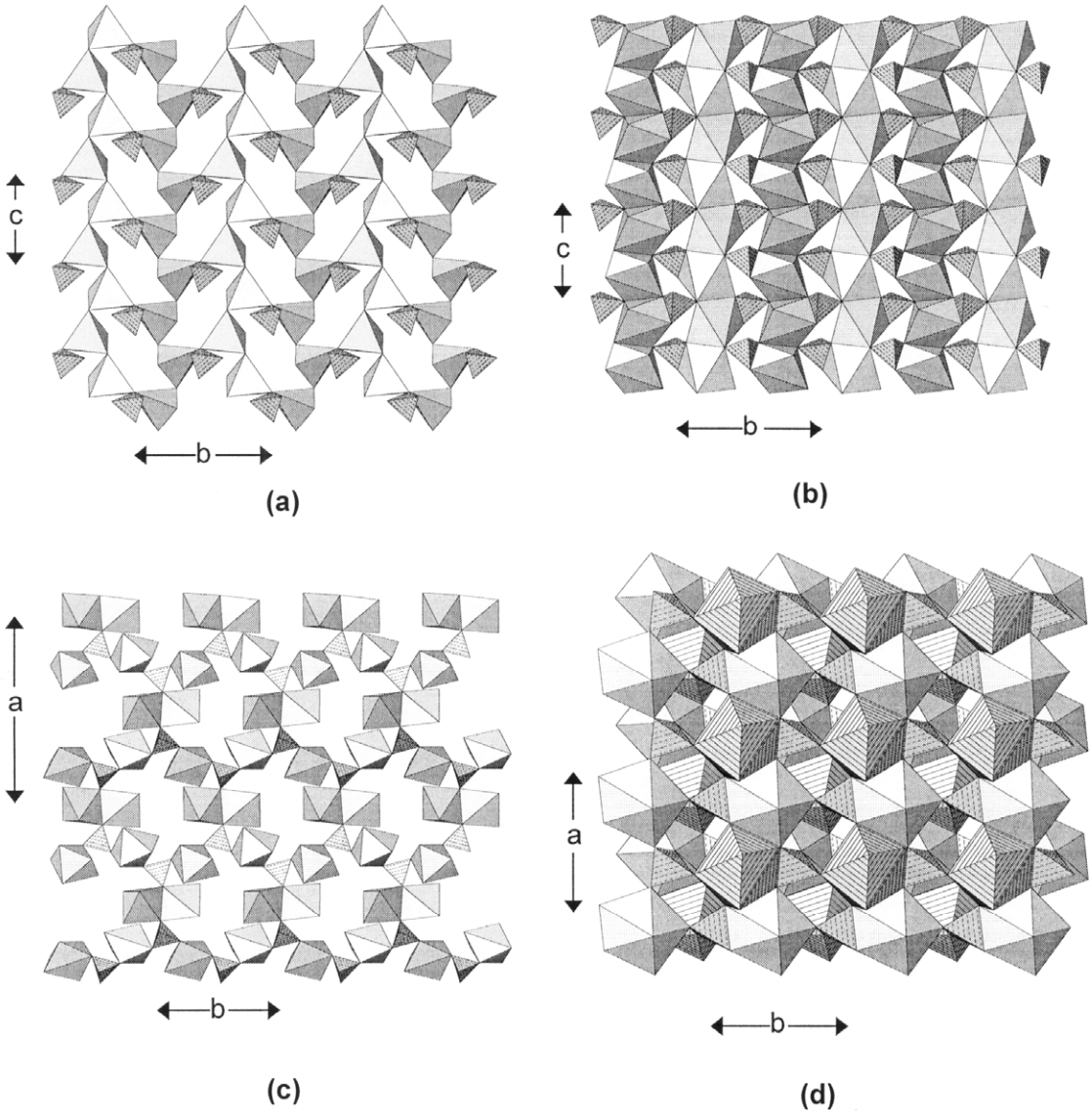

Figure 62. The crystal structures of dorfmanite and monetite: (a), (b) dorfmanite sheets projected onto (100); (c) dorfmanite projected onto (001); ($Na\phi_5$) and ($Na\phi_6$) polyhedra are shadow-shaded; (d) monetite projected onto (001); ($Ca\phi_7$) polyhedra are shadow-shaded, ($Ca\phi_8$) polyhedra are line-shaded.

arctite, quadruphite (Table 13, below) and several alkali-sulfate minerals (Sokolova and Hawthorne 2001).

Arctite, $(Na_5Ca)Ca_6Ba(PO_4)_6F$, contains one [12]-coordinated Ba, one [7]-coordinated Ca, and one [7]-coordinated site occupied by both Na and Ca. The (CaO_7) and ($\{Na,Ca\}O_7$) polyhedra link to form trimers (Fig. 63c), and these trimers link in the (001) plane to form a sheet. These sheets stack in the *c*-direction, the trimers linking to form truncated columns parallel to the *c*-direction; the result is a thick slab parallel to (001). The (BaO_{12}) icosahedra form a hexagonal array parallel to (001) and are linked by corner-sharing with (PO_4) groups in an arrangement that is also found in the glaserite (and related) structures. This layer is intercalated with the thick slabs to form the rather densely packed arctite arrangement (Fig. 63d).

Nabaphite, $NaBa(PO_4)(H_2O)_9$, and **nastrophite**, $NaSr(PO_4)(H_2O)_9$, are isostructural. Their cation positions have been located but the (PO_4) groups show extensive orientational disorder. There is one Na site and one Ba(Sr) site; the former is octahedrally coordinated and the latter is [9]-coordinated with the anions in a triaugmented triangular-prismatic arrangement. Baturin et al. (1981) note that nastrophite dehydrates easily 'in air,' and the (PO_4)-group disorder may be associated with incipient dehydration.

Lithiophosphate, Li_3PO_4, consists of a framework of (LiO_4) and (PO_4) tetrahedra.

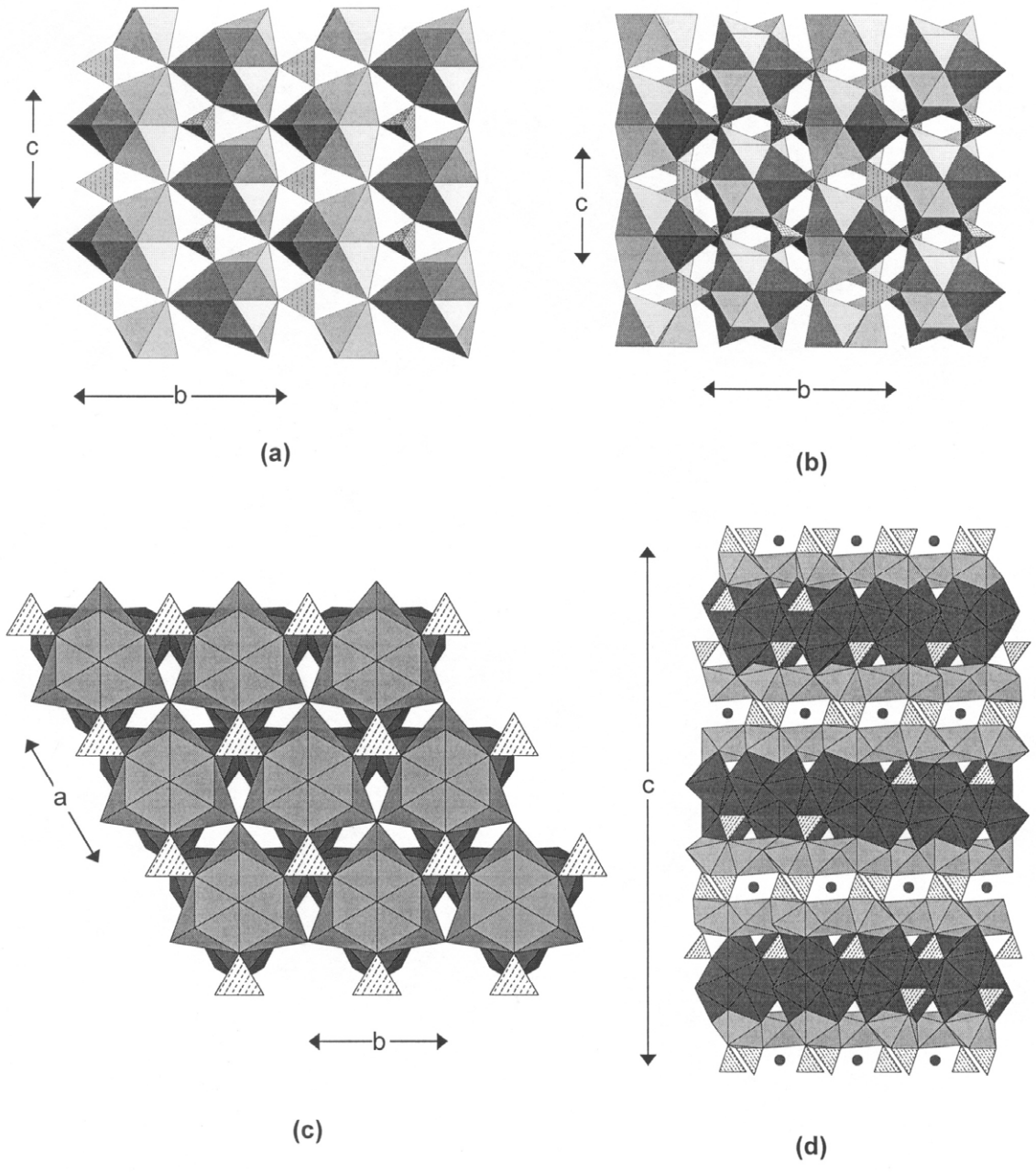

Figure 63. The crystal structures of nacaphite and arctite: (a) one layer of nacaphite projected onto (100); (b) two layers of nacaphite projected onto (100); (c) two layers of arctite projected onto (001); (d) the stacking of layers along [001] in arctite. ($\{Na,Ca\}\phi_n$) polyhedra are shadow-shaded, Ba are shown as dark circles.

From a geometrical perspective, it could also be classified as a member of the class of structures with polymerized (TO_4) groups (i.e., a framework structure of the types listed in Table 4). However, because of the low bond-valence (~0.25 vu) of the (LiO_4) groups, we have chosen to classify it as a 'large-cation' phosphate. (LiO_4) and (PO_4) tetrahedra are arranged at the vertices of a 3^6 plane net (Fig. 64a) and link by sharing corners; each (PO_4) group is surrounded by six (LiO_4) groups, and each (LiO_4) group is surrounded by two (PO_4) groups and four (LiO_4) groups. Both types of tetrahedra point both up and down the *c*-axis and link between adjacent sheets that stack in the *c*-direction (Fig. 64b).

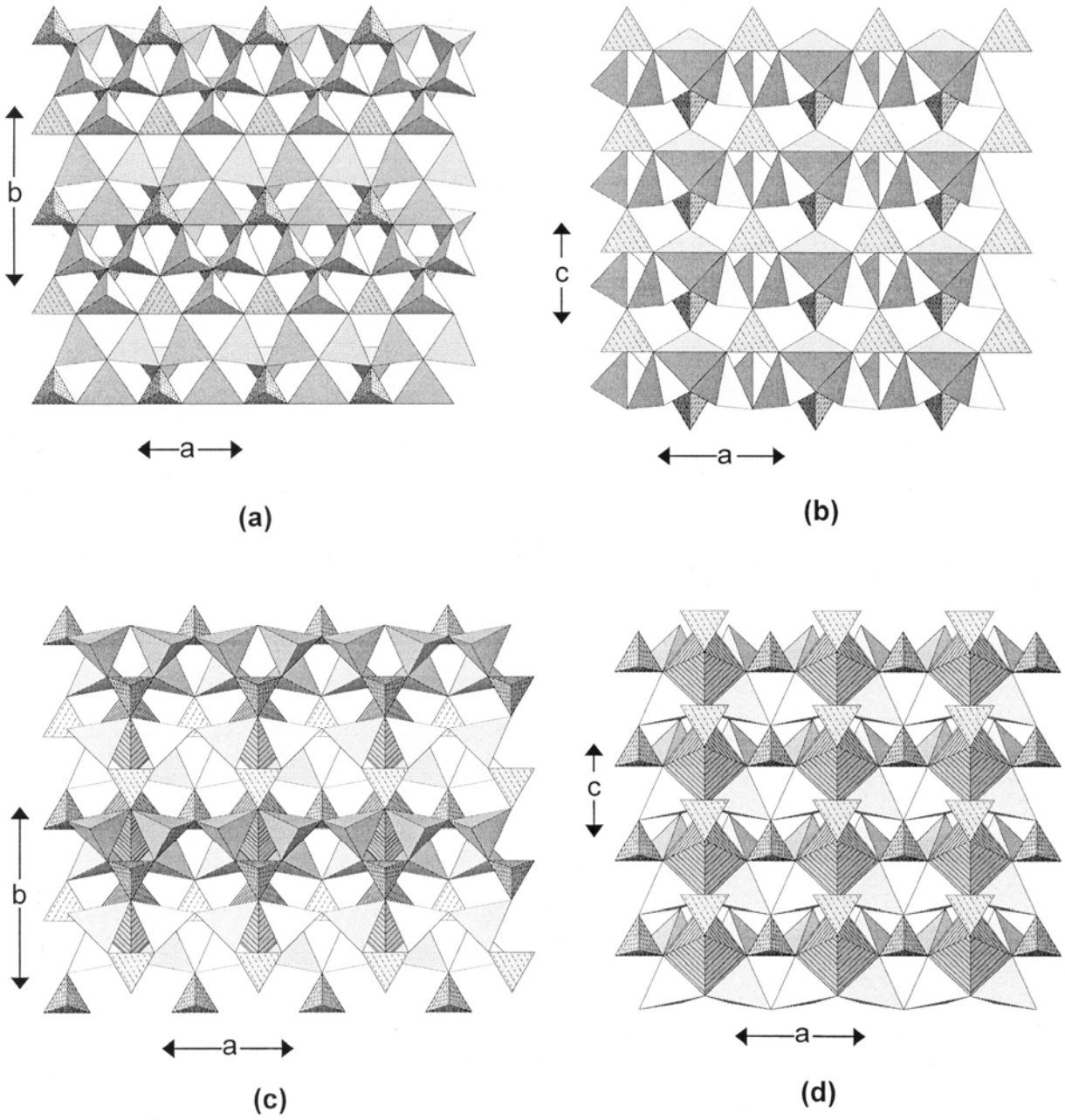

Figure 64. The crystal structures of lithiophosphate and nalipoite: (a) lithiophosphate projected onto (001); (b) lithiophosphate projected onto (010); (c) nalipoite projected onto (001); (d) nalipoite projected onto (010). (LiO_4) are shadow-shaded, (NaO_6) are line-shaded.

Nalipoite, $NaLi_2(PO_4)$, contains octahedrally coordinated Na and tetrahedrally coordinated Li. From a geometrical perspective, nalipoite could be classified as a structure involving polymerization of tetrahedra. Conversely, it can be classified as a large-cation structure from a bond-valence perspective, as the bond valence of $^{[4]}$Li-O is only 0.25 vu. We adopt the latter approach here. The (PO_4) and (LiO_4) tetrahedra occur at the vertices of a (6·3·6·3)(3·6·6·3) net; all 3-rings consist of two (LiO_4) tetrahedra and one (PO_4) tetrahedron, and the 6-rings show the sequence (Li-Li-P-Li-Li-P). The result is a layer of tetrahedra parallel to (100) (Fig. 64c,d) in which chains of corner-sharing (LiO_8) tetrahedra extend in the *a*-direction, and are linked in the *b*-direction by (PO_4) tetrahedra. Tetrahedra point along ±*c*, and layers of tetrahedra meld in this direction to form a framework. Octahedrally coordinated Na occupies the interstices within this framework.

Nefedovite, $Na_5Ca_4(PO_4)_4F$, consists of [8]-coordinated Ca and both [7]- and [10]-coordinated Na. The ($Na\phi_{10}$) polyhedra share apical corners to form chains that extend in the *c*-direction (Fig. 65a) with (PO_4) tetrahedra linked to half of the meridional vertices. The (NaO_7) polyhedra share apical corners to form chains extending in the *c*-direction, and the individual polyhedra share corners with the ($Na\phi_{10}$) polyhedra, each bridging adjacent polyhedra along each chain (Fig. 65a). These chains are linked in the (001) plane by ($Ca\phi_8$) polyhedra. The decorated ($Na\phi_{10}$)-polyhedron chains have a square pinwheel appearance when viewed down [001] (Fig. 65b), and they are surrounded by a dense edge-sharing array of (NaO_7) and ($Ca\phi_8$) polyhedra.

Olgite, $NaSr(PO_4)$, contains one [12]-coordinated site occupied by Sr (+ Ba), one [6]-coordinated site occupied by Na, and two [10]-coordinated sites occupied by both Sr and Na. The Sr site is situated at the vertices of a 3^6 plane net and is icosahedrally coordinated; adjacent icosahedra share edges to form a continuous sheet parallel to (001) (Fig. 65c) that is decorated by (PO_4) tetrahedra that share edges with the icosahedra. The [10]-coordinated Sr, Na sites share corners to form a sheet parallel to (001) (Fig. 65d). The [10]-coordinated polyhedra each have six peripheral anions, one apical anion along +*c* and three apical anions along -*c* (obscured in Fig. 65d). (NaO_6) octahedra are embedded on the underside of this sheet, sharing faces with the (Sr,NaO_{10}) polyhedra, and only one octahedron face is visible in Figure 65d (except at the edges of the sheet). This sheet is also decorated with (PO_4) tetrahedra. These two types of sheets stack alternately in the *c*-direction (Fig. 65e).

Phosphammite, $(NH_4)_2(PO_3\{OH\})$, consists of isolated ($P\phi_4$) groups linked by hydrogen bonds involving (NH_4) groups. Khan et al. (1972) show that there are five oxygen atoms closer than 3.4 Å, but give a persuasive argument (based on stereochemistry) that there are only four hydrogen bonds from the (NH_4) group to the coordinating oxygen atoms. Consequently, we have drawn the 'large-cation' polyhedron as an $\{(NH_4)O_4\}$ tetrahedron (Figs. 66a,b). The $\{(NH_4)O_4\}$ tetrahedra occur at the vertices of a 6^3 net, linking to adjacent $\{(NH_4)O_4\}$ tetrahedra by sharing corners. The ($PO_3\{OH\}$) tetrahedra link to the $\{(NH_4)O_4\}$ tetrahedra, bridging across the six-membered rings of $\{(NH_4)O_4\}$ tetrahedra (Fig. 66a). The resultant layers link in the *c*-direction by corner-sharing between both $\{(NH_4)O_4\}$ tetrahedra, and between $\{(NH_4)O_4\}$ and ($PO_3\{OH\}$) tetrahedra (Fig. 66b).

Vitusite-(Ce), $Na_3Ce(PO_4)_2$, is a modulated structure, the substructure of which is related to the glaserite structure-type. The substructure contains two [8]-coordinated REE sites and six Na sites, two of which are [6]-coordinated and four of which are [7]-coordinated, together with four distinct (PO_4) groups. The typical unit of the glaserite arrangement is a large-cation polyhedron surrounded by a 'pinwheel' of six tetrahedra. In

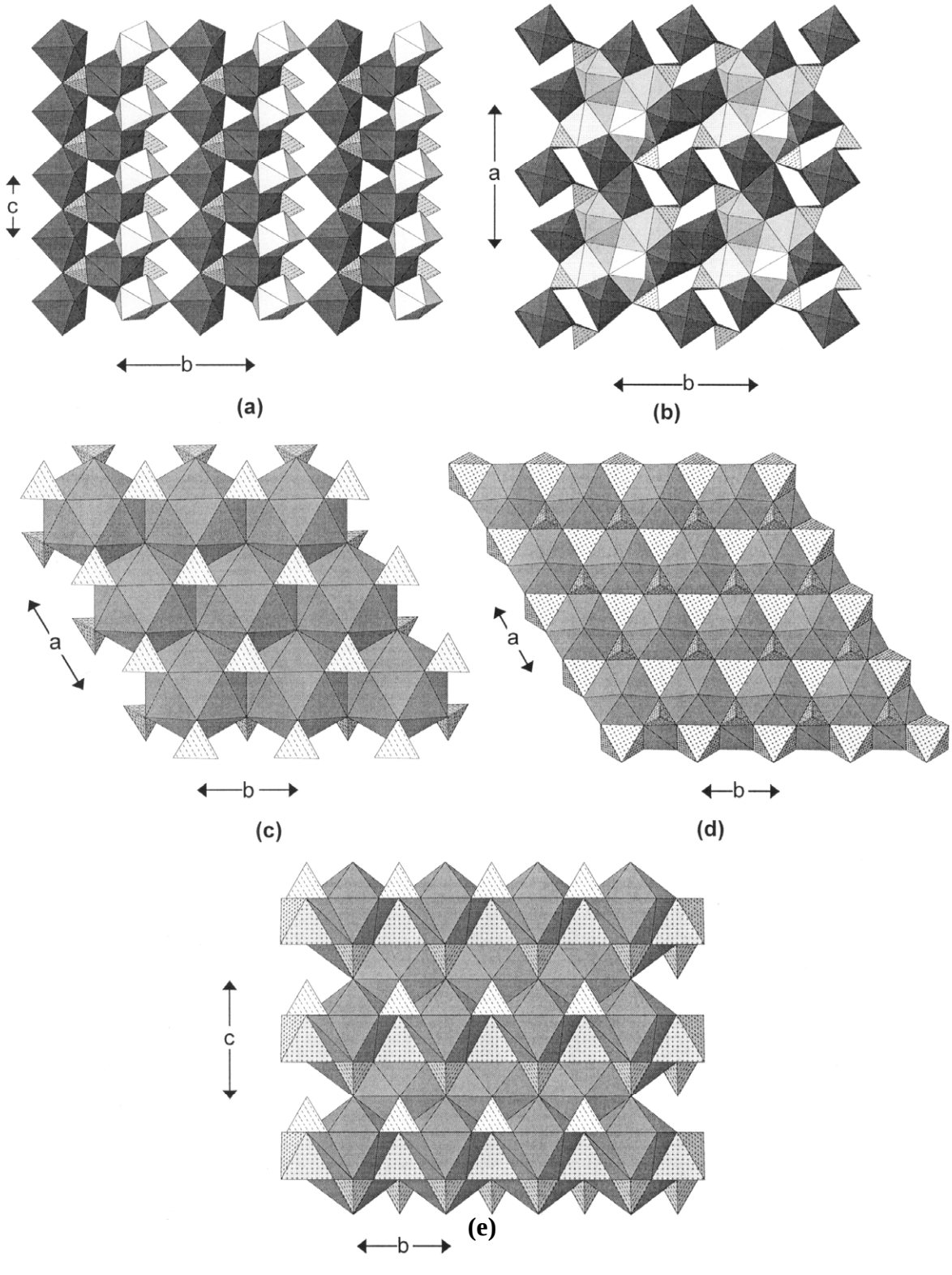

Figure 65. The crystal structures of nefedovite and olgite: (a) nefedovite projected onto (100); (b) nefedovite projected onto (001); ($Na\phi_n$) polyhedra are dark-shadow-shaded, ($Ca\phi_8$) polyhedra are light-shadow-shaded; (c) (SrO_{12})-icosahedron layer in olgite projected onto (001); (d) the (Sr,NaO_{10})-(NaO_7)-polyhedron layer in olgite projected onto (001); (e) the stacking of layers along [001] in olgite; (SrO_{12}) icosahedra are dark-shadow-shaded, (NaO_{10}) polyhedra are dark-shaded, (NaO_6) octahedra are dot-shaded.

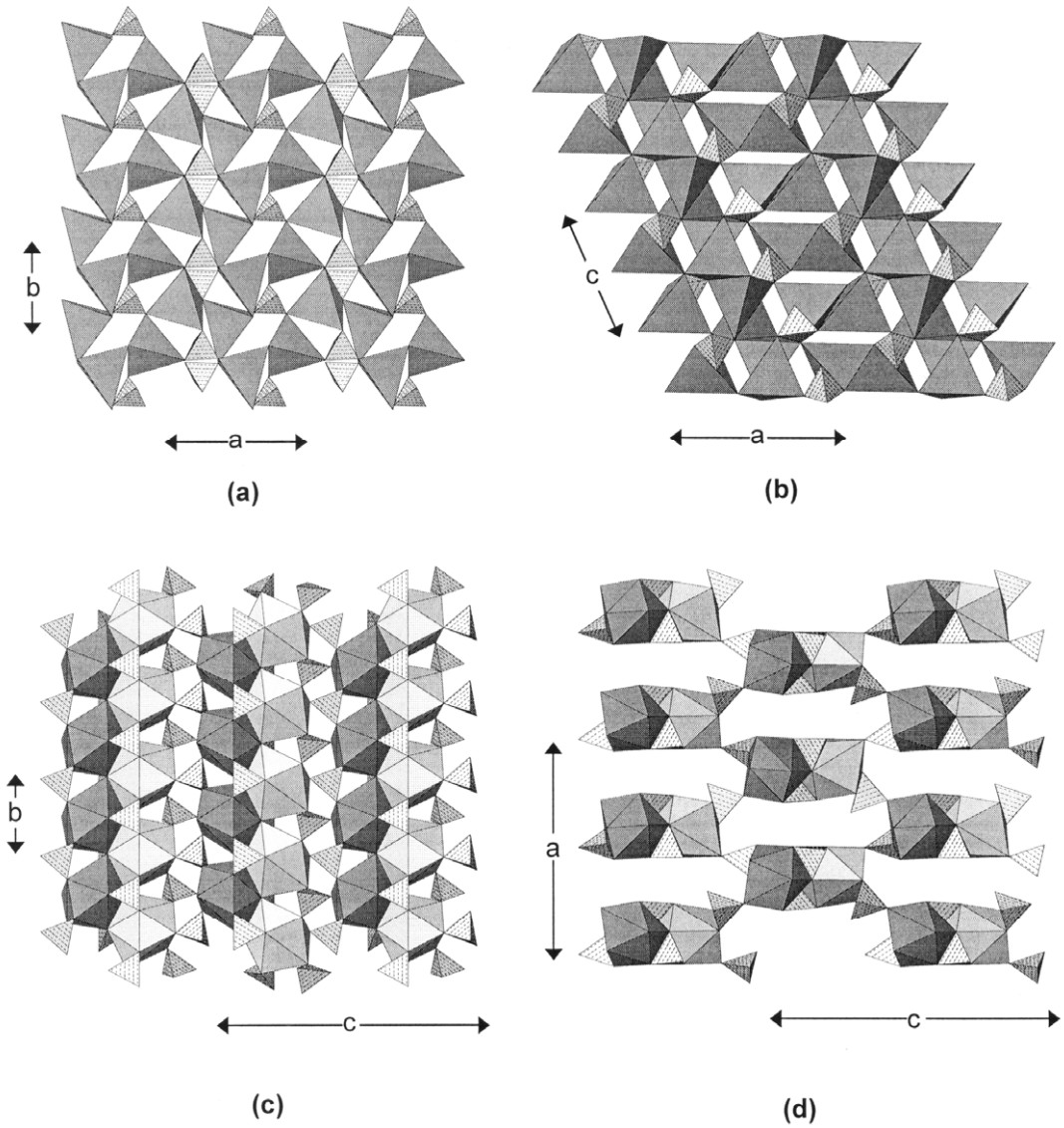

Figure 66. The crystal structures of phosphammite and vitusite: (a) phosphammite projected onto (001); (b) phosphammite projected onto (010); ($\{NH_4\}O_4$) tetrahedra are shadow-shaded; (c) vitusite-(Ce) projected onto (100); (d) vitusite-(Ce) projected onto (010). ($REEO_8$) polyhedra are shadow-shaded.

vitusite-(Ce), this unit is present (Fig. 66c), but is perturbed by edge-sharing between the large-cation polyhedra. The layers of Figure 65e stack in the *a*-direction by linkage between (PO_4) groups and the large-cation polyhedra. The structure is modulated in the *a*-direction, producing 5*a*, 8*a* and 11*a* modulations; the 8*a*-modulated structure seems to be the most common, and it was characterized by Mazzi and Ungaretti (1994). The modulations involve displacements of some O-atoms of the structure such that there are changes in the large-cation coordinations from those observed in the substructure.

Stercorite, $(NH_4)Na(H_2O)_3(PO_3\{OH\})(H_2O)$, consists of octahedrally coordinated Na that polymerizes by sharing *trans* edges to form an [$Na\phi_4$] chain that extends in the *b*-direction and is decorated by acid ($P\phi_4$) groups that share vertices with the octahedra and are arranged in a staggered fashion on each side of the chain (Figs. 67a,b). All ligands not involving ($P\phi_4$) groups are (H_2O) groups, i.e., ($NaO\{H_2O\}_5$). Chains are linked in the *a*- and *c*-directions by a complicated network of hydrogen bonds (Ferraris and Franchini-

Angela 1974) involving the interstitial (NH_4) group and an interstitial (H_2O) group that is held in the structure solely by hydrogen bonds.

Natrophosphate, $Na_7(PO_4)_2F(H_2O)_{19}$, contains octahedrally and tetrahedrally

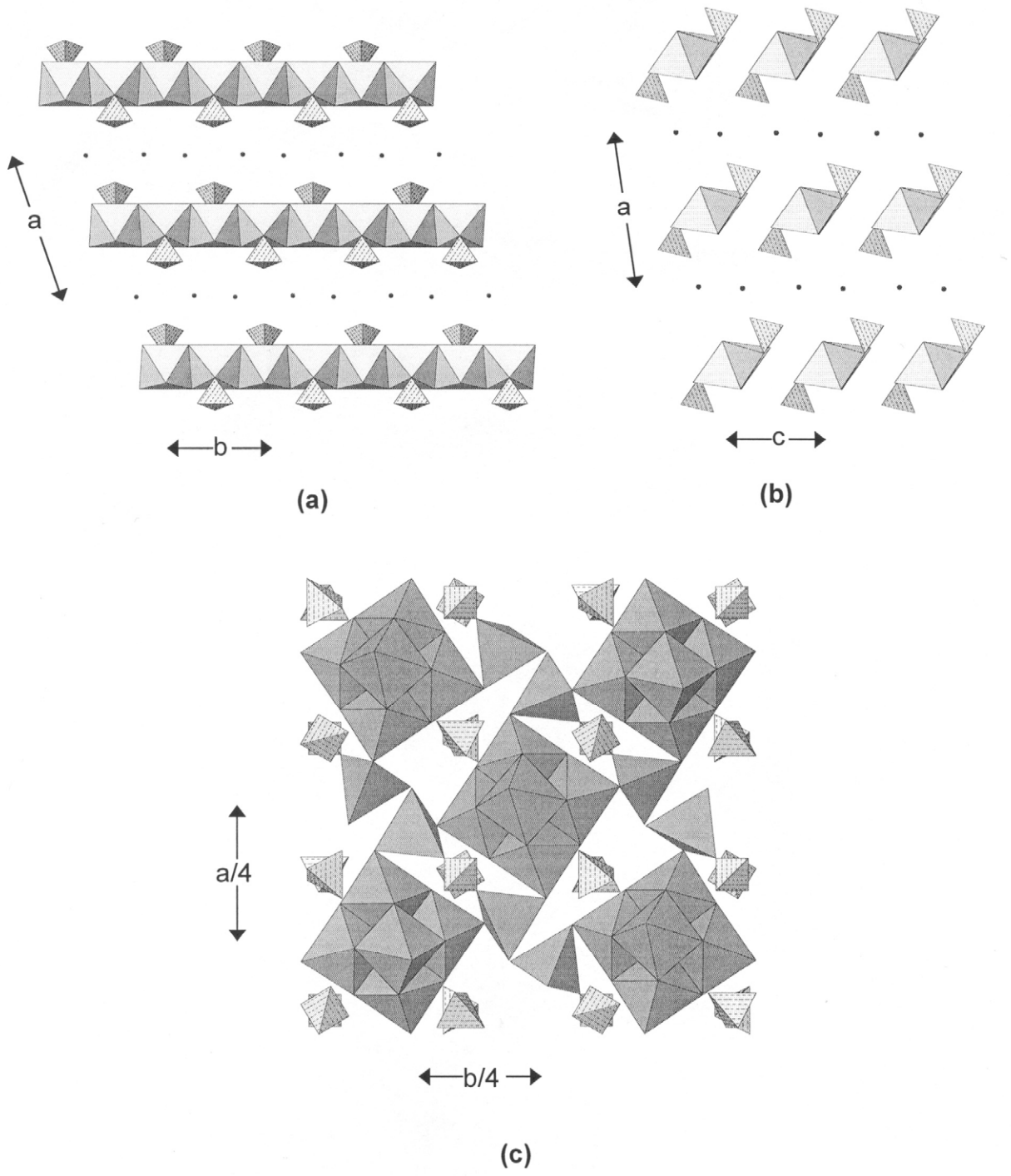

Figure 67. The crystal structures of stercorite and natrophosphate: (a) stercorite projected onto (001); (b) stercorite projected onto (010); (c) natrophosphate projected onto (001). ($Na\phi_6$) octahedra are shadow-shaded, ($Na\phi_5$) polyhedron is shadow-shaded, (NH_4) are shown as small black circles.

coordinated Na. Six ($Na\phi_6$) octahedra share edges to form a compact cluster of the form [$Na_6\phi_{18}$] (Fig. 67c). At the centre of this cluster is one F atom that is coordinated by six Na atoms; the remaining anions of the cluster are either [2]- or [1]-coordinated and hence are (H_2O) groups. The (PO_4) groups do not link directly to these clusters, but link to ($Na\phi_4$) tetrahedra that also bridge adjacent clusters (Fig. 67c). The [4]-coordinated site is only half-occupied (as required for electroneutrality) by Na, and is also half-occupied by (H_2O), giving rise to the rather unusual stoichiometry (for such a high-symmetry mineral).

Buchwaldite, $NaCa(PO_4)$, contains three unique Ca atoms, each with a coordination number of [8], and three distinct Na atoms with coordination numbers of [7], [6] and [9], respectively. The (CaO_8) polyhedra share edges to form two distinct chains that extend in the *a*-direction (Fig. 68a). These chains link in the *c*-direction through (NaO_n) polyhedra and (PO_4) groups. The (CaO_8) polyhedra share both edges and vertices with (PO_4) groups to link in the *b*-direction (Fig. 68b), further linkage being provided by (NaO_n) polyhedra to produce a densely packed structure.

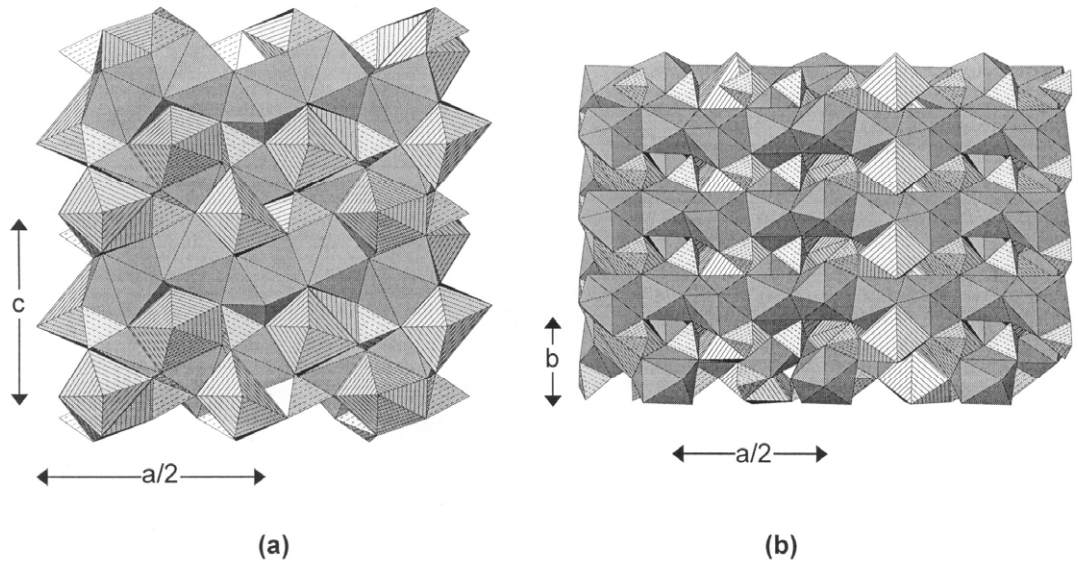

Figure 68. The crystal structure of buchwaldite: (a) projected onto (010); (b) projected onto (001). (CaO_8) polyhedra are shadow-shaded, (NaO_n) polyhedra are line-shaded.

APATITE-RELATED MINERALS

The minerals with apatite-like structures are dealt with in detail elsewhere in this volume and will not be considered here, except to list the relevant minerals (for completeness) in Table 12.

SILICOPHOSPHATE MINERALS

The silicophosphate (and related phosphate) minerals are a small group of extremely complicated structures that we will not describe here, because their complexity requires extensive illustration. For completeness, these minerals are listed in Table 13.

HEXAVALENT-URANIUM PHOSPHATE MINERALS

The hexavalent-uranium phosphate minerals (Table 14) are important and widespread uranyl-oxysalt minerals. Their structures and behavior are dominated by the crystal chemistry of the $(U^{6+}O_2)^{2+}$ uranyl group; they have been described in detail by Burns (1999) and will not be considered any further here.

Table 12. Minerals with apatite-like structures.

Mineral	*Formula*
Alforsite	$Ba_5(PO_4)_3Cl$
Belovite-(Ce)	$Sr_3NaCe(PO_4)_3(OH)$
Belovite-(La)	$Sr_3NaLa(PO_4)_3F$
Carbonate-fluorapatite	$Ca_5(PO_4,CO_3)_3F$
Carbonate-hydroxylapatite	$Ca_5(PO_4,CO_3)_3(OH)$
Chlorapatite	$Ca_5(PO_4)_3(Cl,F)$
Fluorapatite	$Ca_5(PO_4)_3F$
Hydroxylapatite	$Ca_5(PO_4)_3(OH)$
Pyromorphite	$Pb_5(PO_4)_3Cl$
Strontiumapatite	$Sr_6Ca_4(PO_4)_6F_2$

Table 13. Silicophosphate (and related phosphate) minerals.

Name	*Formula*	*Space group*
Attakolite	$CaMn^{2+}Al_4(SiO_3\{OH\})(PO_4)_3(OH)_4$	*C*2/*m*
Clinophosinaite	$Na_3Ca(SiO_3)(PO_4)$	*P*2/*c*
Harrisonite	$CaFe^{2+}(SiO_4)_2(PO_4)_2$	$R\,\bar{3}\,m$
Lomonosovite	$Na_5Ti^{4+}{}_2(Si_2O_7)(PO_4)O_2$	$P\bar{1}$
Polyphite	$Na_{17}Ca_3MgTi_4(Si_2O_7)_2(PO_4)_6O_3F_5$	$P\bar{1}$
Quadruphite	$Na_{14}CaMgTi^{4+}{}_4(Si_2O_7)_2(PO_4)_4O_4F_2$	$P\bar{1}$
Sobolevite	$Na_{11}(Na,Ca)_4(Mg,Mn^{2+})Ti^{4+}{}_4(Si_2O_7)_2(PO_4)_4O_3F_3$	$P\bar{1}$
Steenstrupine	$Na_{14}Ce_6Mn^{2+}Mn^{3+}Fe^{2+}{}_2Zr(Si_6O_{18})_2(PO_4)_7(H_2O)_3$	$R\,\bar{3}\,m$
Vuonnemite	$Na_{11}Ti^{4+}Nb_2(Si_2O_7)_2(PO_4)_2O_3(OH)$	$P\bar{1}$
Yoshimuraite	$Ba_2Mn_2TiO(Si_2O_7)(PO_4)(OH)$	$P\bar{1}$
Benyacarite	$(H_2O,K)_2TiMn^{2+}{}_2(Fe^{3+},Ti)_2(PO_4)_4(OH)_2(H_2O)_{14}$	*Pbca*

AN ADDENDUM ON CRYSTAL-CHEMICAL RELATIONS AMONG PHOSPHATE MINERALS

In providing a (fairly) complete hierarchical ordering of phosphate structures in this chapter, of necessity we have adopted a fairly broad-brush approach. There is a wealth of structural relations that we have not considered, and much of this is to be found in the original literature. Some papers have considered broader issues of structure and variations in bond topology in phosphates (and related minerals): Moore (1965b, 1970, 1973a,b; 1975b, 1976, 1984), Moore and Araki (1977c), Fanfani et al. (1978), Hawthorne (1979a, 1983a, 1985a,b; 1990, 1994, 1997, 1998). However, much work remains to be done in this area.

Table 14. Hexavalent-uranium phosphate minerals.

Meta-autunite group		***Phosphuranylite group***	
Meta-autunite*	$^{[6]}Ca(H_2O)_5[(UO_2)(PO_4)]_2(H_2O)$	Phuralumite	$^{[6]}Al_2(H_2O)_4(OH)_4[(UO_2)_3(PO_4)_2(OH)_2](H_2O)_6$
Meta-	$^{[9]}Ba(H_2O)_4[(UO_2)(PO_4)]_2(H_2O)_2$		
Meta-ankoleite	$^{[8]}K(D_2O)_2[(UO_2)(PO_4)](LT)$	Upalite	$^{[6]}Al(H_2O)_6[(UO_2)_3(PO_4)_2(OH)O](H_2O)_1$
Meta-torbernite	$^{[6]}Cu^{2+}(H_2O)_4[(UO_2)(PO_4)]_2(H_2O)_4$	Mundite	$Al[(UO_2)_3(PO_4)_2(OH)O](H_2O)_{6.5}$
Saléeite	$^{[6]}Cu^{2+}(H_2O)_4[(UO_2)(PO_4)]_2(H_2O)_4$	Dewindite	$^{[8]}Pb^{2+}{}_2{}^{[11]}Pb^{2+}(H_2O)_{11}[(UO_2)_3(PO_4)_2(OH)O]_2(H_2O)_1$
Uramphite	$(NH_4)_2[(UO_2)(PO_4)]_2(H_2O)_6$	Francoisite(-Nd)	$^{[9]}Nd(H_2O)_5[(UO_2)_3(PO_4)_2(OH)O](H_2O)_1$
Na-meta-	$Na_2[(UO_2)(PO_4)]_2(H_2O)_5$		
Bassetite	$Fe^{2+}[(UO_2)(PO_4)]_2(H_2O)_8$	Dumonite	$^{[8]}Pb^{2+}(H_2O)_4[(UO_2)_3(PO_4)_2O_2](H_2O)_1$
Lehnerite	$Mn^{2+}[(UO_2)(PO_4)]_2(H_2O)_8$	Phurcalite	$^{[8]}Ca^{[7]}Ca(H_2O)_7[(UO_2)_3(PO_4)_2O_2]$
Meta-autunite	$Ca[(UO_2)(PO_4)]_2(H_2O)_2$	Bergenite	$(Ba,Ca)_2[(UO_2)_3O_2(PO_4)_2](H_2O)_{6.5}$
Przhevaskite	$Pb^{2+}[(UO_2)(PO_4)]_2(H_2O)_4$	Huegelite	$Pb^{2+}{}_2[(UO_2)_3(PO_4)_2O_2](H_2O)_5$
Chernikovite	$(H_3O)_2[(UO_2)(PO_4)]_2(H_2O)_6$		
Vochtenite	$(Fe^{2+},Mg)Fe^{3+}[(UO_2)(PO_4)]_4(OH)(H_2O)_1$	Althupite	$^{[6]}Al^{[9]}Th(H_2O)_8(OH)_3[(UO_2)\{(UO_2)_3(PO_4)_2(OH)O\}_2](H_2O)_7$
Ranunculite	$Al(OH)_3H[(UO_2)(PO_4)](H_2O)_4$	Yingjiangite	$K_2Ca[(UO_2)\{(UO_2)_3(PO_4)_2(OH)O_2\}_2](H_2O)_8$
		Renardite	$Pb^{2+}[(UO_2)\{(UO_2)_3(PO_4)_2O_2\}](H_2O)_9$
Walpurgite group		Phosphuranylite*	$^{[9]}K^{[8]}Ca(^{[3]}H_3O)_3(H_2O)_8[(UO_2)\{(UO_2)_3(PO_4)_2O_2\}_2]$
Walpurgite*	$^{[6]}Bi^{3+}{}_2{}^{[7]}Bi_2(H_2O)_2O_4[(UO_2)(AsO_4)_2]$	Meta-	$[U^{6+}(UO_2)_3(PO_4)(OH)_6](H_2O)_2$
Parsonite	$^{[9]}Pb^{2+}{}^{[6]}Pb[(UO_2)(PO_4)_2]$	Vanmeersscheite	$[U^{6+}(UO_2)_3(PO_4)(OH)_6](H_2O)_4$
Ulrichite	$CaCu^{2+}[(UO_2)(PO_4)_2](H_2O)_4$		
Pseudo-autunite	$Ca_2[(UO_2)_2(PO_4)_4](H_2O)_9$	**Miscellaneous**	
		Hallimondite	$Pb^{2+}[(UO_2)(AsO_4)_2]$

ACKNOWLEDGMENTS

We thank John Hughes for persuading us to write this chapter, for reviewing it, and for his indulgence regarding its length. We also thank Donna Danyluk for her assistance with compiling the references and the appendix. This work was supported by a Canada Research Chair in Crystallography and Mineralogy and by a Research Grant from the Natural Sciences and Engineering Research Council of Canada to FCH.

REFERENCES

Abbona F, Calleri M, Ivaldi G (1984) Synthetic struvite, $MgNH_4PO_4 \cdot 6H_2O$: correct polarity and surface features of some complementary forms. Acta Crystallogr B40:223-227

Abrahams SC (1966) Ferromagnetic and crystal structure of ludlamite, $Fe_3(PO_4)_2(H_2O)_4$ at 4.2 K. J Chem Phys 44:2230-2237

Adiwidjaja G, Friese K, Klaska K-H, Schlueter J (1999) The crystal structure of kastningite $(Fe_{0.5}Mn_{0.5})(H_2O)_4(Al_2(OH)_2(H_2O)_2(PO_4)_2)(H_2O)_2$, a new hydroxyl aquated orthophosphate hydrate mineral. Z Kristallogr 214:465-468

Alberti A (1976) Crystal structure of ferrisicklerite, $Li_{<1}(Fe^{(3+)},Mn^{(2+)})PO_4$. Acta Crystallogr B32: 2761-2764

Alkemper J, Fuess H (1998) The crystal structures of $NaMgPO_4$, $Na_2CaMg(PO_4)_2$ and $Na_{18}Ca_{13}Mg_5(PO_4)_{18}$: new examples for glaserite related structures. Z Kristallogr 213:282-287

Anderson JB, Shoemaker GL, Kostiner E, Ruszala FA (1977) The crystal structure of synthetic $Cu_5(PO_4)_2(OH)_4$, a polymorph of pseudomalachite. Am Mineral 62:115-121

Ankinovich EA, Bekanova GK, Shabanova TA, Zazubina IS, Sandomirsakaya SM (1997) Mitryaevaite, $Al_{10}[(PO_4)_{8.7}(SO_3OH)_{1.3}]_{10}AlF_3 \cdot 30H_2O$, a new mineral species from a Cambrian carbonaceous chert formation, Karatau Range and Zhabagly Mountains, southern Kazakhstan. Can Mineral 35:1415-1419

Antenucci D, Fontan F, Fransolet A-M (1989) X-ray powder diffraction data for wolfeite: $(Fe_{0.59}Mn_{0.40}Mg_{0.01})_2PO_4(OH)$. Powder Diffraction 4:34-35

Araki T, Moore PB (1981) Fillowite, $Na_2Ca(Mn, Fe)_7(PO_4)_6$: its crystal structure. Am Mineral 66:827-842

Araki T, Zoltai T (1968) The crystal structure of wavellite. Z Kristallogr 127:21-33

Araki T, Finney JJ, Zoltai T (1968) The crystal structure of augelite. Am Mineral 53:1096-1103

Arnold H (1986) Crystal structure of $FePO_4$ at 294 and 20 K. Z Kristallogr 177:139-142

Atencio D (1988) Chernikovite, a new mineral name for $(H_3O)_2(UO_2)_2(PO_4)_2 \cdot 6H_2O$ superseding "hydorgen autunite." Mineral Rec 19:249-252

Atencio D, Neumann R, Silva AJGC, Mascarenhas YP (1991) Phurcalite from Perus, Sao Paulo, Brazil, and redetermination of its crystal structure. Can Mineral 29:95-105

Bakakin VV, Rylov GM, Alekseev VI (1974) Refinement of the crystal structure of hurlbutite $CaBe_2P_2O_8$. Kristallografiya 19:1283-1285 (in Russian)

Bartl H (1989) Water of crystallization and its hydrogen-bonded cross linking in vivianite $Fe_3(PO_4)_2 \cdot 8(H_2O)$; a neutron diffraction investigation. Z Anal Chem 333:401-403

Baturin SV, Malinovskii YA, Belov NV (1981) The crystal structure of nastrophite $Na(Sr,Ba)(PO_4)(H_2O)_9$. Dokl Akad Nauk SSSR 261:619-623

Baturin SV, Malinovskii YA, Belov NV (1982) The crystal structure of nabaphite $NaBa(PO_4)(H_2O)_9$. Dokl Akad Nauk SSSR 266:624-627

Baur WH (1969a) The crystal structure of paravauxite, $FeAl_2(PO_4)_2(OH)_2(OH_2)_6(H_2O)_2$. N Jahrb Mineral Monatsh 430-433

Baur WH (1969b) A comparison of the crystal structures of pseudolaueite and laueite. Am Mineral 54: 1312-1322

Baur WH (1970) Bond length variation and distorted coordination polyhedra in inorganic crystals. Trans Am Crystallogr Assoc. 6:129-155

Baur WH (1974) The geometry of polyhedral distortions. Predictive relationships for the phosphate group. Acta Crystallogr B30:1195-1215

Baur WH (1977) Computer simulation of crystal structures. Phys Chem Minerals 2:3-20

Baur WH, Rama Rao B (1967) The crystal structure of metavauxite. Naturwiss 54:561

Baur WH, Rama Rao B (1968) The crystal structure and the chemical composition of vauxite. Am Mineral 53:1025-1028

Ben Amara M, Vlasse M, le Flem G, Hagenmueller P (1983) Structure of the low-temperature variety of calcium sodium orthophosphate, $NaCaPO_4$. Acta Crystallogr C39:1483-1485

Bernhard F, Walter F, Ettinger K, Taucher J, Mereiter K (1998) Pretulite, $ScPO_4$, a new scandium mineral from the Styrian and lower Austrian lazulite occurrences, Austria. Am Mineral 83:625-630

Birch WD, Mumme WG, Segnit ER (1988) Ulrichite: A new copper calcium uranium phosphate from Lake Boga, Victoria, Australia. Aust Mineral 3:125-131

Birch WD, Pring A, Bevan DJM, Kharisun (1994) Wycheproofite: a new hydrated sodium aluminum zirconium phosphate frmom Wycheproof, Victoria, Australia, and a new occurrence of kosnarite. Mineral Mag 58:635-639

Birch WD, Pring A, Foord EE (1995) Selwynite, $NaK(Be,Al)Zr_2(PO_4)_4 \cdot 2H_2O$, a new gainesite-like mineral from Wycheproof, Victoria, Australia. Can Mineral 33:55-58

Birch WD, Pring A, Self PG, Gibbs RB, Keck E, Jensen MC, Foord EE (1996) Meurigite, a new fibrous iron phosphate resembling kidwellite. Mineral Mag 60:787-793

Birch WD, Pring A, Kolitsch U (1999) Bleasdaleite $(Ca,Fe^{3+})_2\ Cu_5\ (Bi,Cu)\ (PO_4)_4\ (H_2O,OH,Cl)_{13}$, a new mineral from Lake Boga, Victoria, Australia. Aust J Mineral 5:69-75

Bjoerling CO, Westgren A (1938) Minerals of the Varutraesk pegmatite. IX. X-ray studies on triphylite, varulite and their oxidation products. Geolog Foereningen Stockholm Foerhandlingar 412

Blanchard F (1981) ICDD Card # 33-0802 (sicklerite)

Blount AM (1974) The crystal structure of crandallite. Am Mineral 59:41-47

Borodin LS, Kazakova ME (1954) Belovite-(Ce): a new mineral from an alkaline pegmatite. Dokl Akad Nauk SSSR 96:613-616

Bowen NL (1928) The Evolution of Igneous Rocks. Princeton University Press, Princeton, New Jersey

Bragg WL (1930) The structure of silicates. Z Kristallogr 74:237-305

Bridge PJ, Clark RM (1983) Mundrabillaite, a new cave mineral from Western Australia. Mineral Mag 47: 80-81

Bridge PJ, Robinson BW (1983) Niahite—a new mineral from Malaysia. Mineral Mag 47:79-80

Britvin SN, Pakhomovskii YA, Bogdanova AN, Skiba VI (1991) Strontiowhitlockite, $Sr_9Mg(PO_3OH)(PO_4)_6$, a new mineral species from the Kovdor deposit, Kola Peninsula, U.S.S.R. Can Mineral 29: 87-93

Britvin SN, Pakhomovskii YaA, Bogdanova AN, Khomyakov AP, Krasnova NI (1995) Rimkorolgite $(Mg,Mn)_5(Ba,Sr,Ca)(PO_4)_4 \cdot 8H_2O$—a new mineral from Kovdor iron deposit, Kola Peninsula. Zap Vser Mineral Obshch 124:90-95 (in Russian)

Britvin SN, Pakhomovskii YaA, Bogdanova AN (1996) Krasnovite $Ba(Al,Mg)(PO_4,CO_3)(OH)_2 \cdot H_2O$—a new mineral. Zap Vser Mineral Obshch 125:110-112

Brotherton PD, Maslen EN, Pryce MW, White AH (1974) Crystal structure of collinsite. Aust J Chem 27: 653-656

Brown ID (1981) The bond-valence method: an empirical approach to chemical structure and bonding. *In* Structure and Bonding in Crystals II. O'Keeffe M, Navrotsky A (eds) Academic Press, New York, p 1-30

Brown ID, Shannon RD (1973) Empirical bond strength-bond length curves for oxides. Acta Crystallogr A29:266-282

Brownfield ME, Foord EE, Sutley SJ, Bottinelly T (1993) Kosnarite, $KZr_2(PO_4)_3$, a new mineral from Mount Mica and Black Mountain, Oxford County, Maine. Am Mineral 78:653-656

Buchwald VF (1990) A new mineral, arupite, $Ni_3(PO_4)_2 \cdot 8H_2O$, the nickel analogue of vivianite. N Jahrb Mineral Monatsh 76-80

Buck HM, Cooper MA, ČCernyý P, Grice JD, Hawthorne FC (1999) Xenotime-(Yb), $YbPO_4$, a new mineral species from the Shatford Lake pegmatite group, southeastern Manitoba. Can Mineral 37:1303-1306

Burdett JK, Hawthorne FC (1993) An orbital approach to the theory of bond valence. Am Mineral 78: 884-892

Burns PC (1999) The crystal chemistry of uranium. Rev. Mineral 38: 23-91

Burns PC (2000) A new uranyl phosphate chain in the structure of parsonite. Am Mineral 85:801-805

Burns PC, Hawthorne FC (1995) The crystal structure of sinkankasite, a complex heteropolyhedral sheet mineral. Am Mineral 80:620-627

Byrappa K (1983) The possible reasons for absence of condensed phosphates in Nature. Phys Chem Minerals 10:94-95

Cahill CL, Krivovichev SV, Burns PC, Bekenova GK, Shabanova TA (2001) The crystal structure of mitryaevaite, $Al_5(PO_4)_2[(P,S)O_3(OH,O)]_2F_2(OH)_2(H_2O)_8 \cdot 6.48H_2O$, determined from a microcrystal using synchrotron radiation. Can Mineral 39:179-186

Calvo C (1968) The crystal structure of graftonite. Am Mineral 53:742-750

Carling SG, Day P, Visser D (1995) Crystal and magnetic structures of layer transition metal phosphate hydrates. Inorg Chem 34:3917-3927

Catti M, Franchini-Angela M (1976) Hydrogen bonding in the crystalline state. Structure of $Mg_3(NH_4)_2(HPO_4)_4(H_2O)_8$ (hannayite), and crystal-chemical relationships with schertelite and struvite. Acta Crystallogr B32:2842-2848

Catti M, Ferraris G, Filhol A (1977a) Hydrogen bonding in the crystalline state. $CaHPO_4$ (monetite), $P\bar{1}$ or $P1$? A novel neutron diffraction study. Acta Crystallogr B33:1223-1229

Catti M, Ferraris G, Franchini-Angela M (1977b) The crystal structure of $Na_2HPO_4(H_2O)_2$. Competition between coordination and hydrogen bonds. Acta Crystallogr B33:3449-3452

Catti M, Ferraris G, Ivaldi G (1977c) Hydrogen bondng in the crystalline state. Structure of talmessite, $Ca_2(Mg,Co)(AsO_4)_2{\cdot}2H_2O$, and crystal chemistry of related minerals. Bull Minéral 100:230-236

Catti M, Ferraris G, Ivaldi G (1979) Refinement of the crystal structure of anapaite, $Ca_2Fe(PO_4)_2(H_2O)_4$. Hydrogen bonding and relationships with the bihydrated phase. Bull Minéral 102:314-318

Cavellec M, Riou D, Ferey G (1994) Synthetic spheniscidite. Acta Crystallogr C50:1379-1381

Cech F, Povondra P (1979) A re-examination of borickyite. Tschermaks Mineral Petrogr Mitt 26:79-86

Chao GY (1969) Refinement of the crystal structure of parahopeite. Z Kristallogr 130:261-266

Chen Z, Huang Y, Gu X (1990) A new uranium mineral-yingjiangite. Acta Mineral Sinica 10:102-105

Chernorukov N, Karyakin N, Suleimanov E, Belova Yu, Russ J (1997) ICDD Card #50-1561 (uranocircite)

Chopin C, Brunet F, Gebert W, Medenbach O, Tillmanns E (1993) Bearthite, $Ca_2Al(PO_4)_2(OH)$, a new mineral from high-pressure terranes of the western Alps. Schweiz Mineral Petrogr Mitt 73:1-9

Chopin C, Ferraris G, Prencipe M, Brunet F, Medenbach O (2001) Raadeite, $Mg_7(PO_4)_2(OH)_8$: A new dense-packed phosphate from Modum (Norway). Eur J Mineral 13:319-327

Cid-Dresdner H (1965) Determination and refinement of the crystal structure of turquois, $CuAl_6(PO_4)(OH)_8(H_2O)_4$. Z Kristallogr 121:87-113

Cipriani C, Mellini M, Pratesi G, Viti C (1997) Rodolicoite and grattarolaite, two new phosphate minerals from Santa Barbara mine, Italy. Eur J Mineral 9:1101-1106

Clark AM, Couper AG, Embrey PG, Fejer EE (1986) Waylandite: New data, from an occurrence in Cornwall, with a note on "agnesite." Mineral Mag 50:731-733

Cocco G, Fanfani L, Zanzzi PF (1966) The crystal structure of tarbuttite, $Zn_2(OH)PO_4$. Z Kristallogr 123: 321-329

Coda A, Guiseppetti G, Tadini C, Carobbi SG (1967) The crystal structure of wagnerite. Atti Accad Naz Lincei 43:212-224

Coleman LC, Robertson BT (1981) Nahpoite, Na_2HPO_4, a new mineral from the Big Fish River area, Yukon Territory. Can Mineral 19:373-376

Cooper M, Hawthorne FC (1994a) Refinement of the crystal structure of kulanite. Can Mineral 32:15-19

Cooper M, Hawthorne FC (1994b) The crystal structure of curetonite, a complex heteropolyhedral sheet mineral. Am Mineral 79:545-549

Cooper MA, Hawthorne FC (1999) The crystal structure of wooldridgeite, $Na_2CaCu^{(2+)}{}_2(P_2O_7)_2(H_2O)_{10}$, a novel copper pyrophosphate mineral. Can Mineral 37:73-81

Cooper MA, Hawthorne FC, Cerny P (2000) Refinement of the crystal structure of cyrilovite from Cyrilov, Western Moravia, Czech Republic. J Czech Geol Soc 45:95-100

Corbin DR, Abrams L, Jones GA, Harlow RL, Dunn PJ (1991) Flexibility of the zeolite RHO framework: effect of dehydration on the crystal structure of the beryllophosphate mineral, pahasapaite. Zeolites 11: 364-367

Corbridge DEC (1985) Phosphorous. An outline of its chemistry, biochemistry and technology (3rd edn). Elsevier, Amsterdam

Cozzupoli D, Grubessi O, Mottan A, Zanazzi PF (1987) Cyrilovite from Italy: Structure and crystal chemistry. Mineral Petrol 37:1-14

Curry NA, Jones DW (1971) Crystal structure of brushite, calcium hydrogen orthophosphate dihydrate: A neutron-diffraction investigation. J Chem Soc 3725-3729

Dai Y, Hughes JM (1989) Crystal-structure refinements of vanadinite and pyromorphite. Can Mineral 27: 189-192

de Bruiyn H, Beukes GJ, van der Westhuizen WA, Tordiffe EAW (1989) Unit cell dimensions of the hydrated aluminium phosphate-sulphate minerals sanjuanite, kribergite and hotsonite. Mineral Mag 53:385-386

Deliens M, Piret P (1981) Les phosphates d'uranyle et d'aluminum de Kobokobo. V. La mundite, nouveau mineral. Bull Minéral 104:669-671

Deliens M, Piret P (1982) Les phosphates d'uranyle et d'aluminum de Kobokobo. VI. La triangulite, $Al_3(OH)_5[(UO_2)(PO_4)]_4(H_2O)_5$, nouveau mineral. Bull Minéral 105:611-614

Deliens M, Piret P (1985) Les phosphates d'uranyle et d'aluminum de Kobokobo. V. La moreauite, $Al_3UO_2(PO_4)_3(OH)_2{\cdot}13H_2O$, nouveau mineral. Bull Minéral 108:9-13

Demartin F, Diella V, Donzelli S, Gramaccioli CM, Pilati T (1991) The importance of accurate crystal structure determination of uranium minerals. I. Phosphuranylite $KCa(H_3O)_3(UO_2)_7(PO_4)_4O_{4.8}H_2O$. Acta Crystallogr B47:439-446

Demartin F, Pilati T, Gay DD, Gramaccioli CM (1993) The crystal structure of a mineral related to paulkerrite. Z Kristallogr 208:57-71

Demartin F, Gramaccioli CM, Pilati T, Sciesa E (1996) Sigismundite, (Ba,K,Pb)Na_3(Ca,Sr)(Fe,Mg,Mn)$_{14}$Al$(OH)_2(PO_4)_{12}$, a new Ba-rich member of the arrojadite group from Spluga Valley, Italy. Can Mineral 34:827-834

Demartin F, Gay HD, Gramaccioli CM, Pilati T (1997) Benyacarite, a new titanium-bearing phosphate mineral species from Cerro Blanco, Argentina. Can Mineral 35:707-712

Dempsey MJ, Strens RGJ (1976) Modelling crystal structures. *In* Physics and Chemistry of Rocks and Minerals. Strens RGJ (ed) Wiley, New York, p 443-458

Di Cossato YMF, Orlandi P, Pasero M (1989a) Manganese-bearing beraunite from Mangualde, Portugal: Mineral data and structure refinement. Can Mineral 27:441-446

Di Cossato YMF, Orlandi P, Vezzalini G (1989b) Rittmanite, a new mineral species of the whiteite group from the Mangualde granitic pegmatite, Portugal. Can Mineral 27:447-449

Dick S (1999) Ueber die Struktur von synthetischem Tinsleyit $K(Al_2(PO_4)_2(OH)(H_2O))\cdot(H_2O)$. Z Naturforsch Anorg Chem Org Chem 54:1358-1390

Dick S, Zeiske T (1997) Leucophosphite $K(Fe_2(PO_4)_2(OH)(H_2O))\cdot(H_2O)$; hydrogen bonding and structural relationships. J Solid State Chem 133:508-515

Dick S, Zeiske T (1998) Francoanellit $K_3Al_5(HPO_4)_6(PO_4)_2\cdot 12H_2O$: Struktur und Synthese durch topochemische Entwaesserung von Taranakit. Z Naturforsch Anorg Chem Org Chem 53:711-719

Dick S, Gossner U, Weis A, Robl C, Grossmann G, Ohms G, Zeiske T (1998) Taranakite—the mineral with the longest crystallographic axis. Inorg Chim Acta 269:47-57

Dickens B, Brown WE (1971) The crystal structure of Ca_7Mg_9(Ca, Mg)$_2(PO_4)_{12}$. Tschermaks Mineral Petrogr Mitt 16:79-104

Dooley JR Jr, Hathaway JC (1961) Two occurrences of thorium-bearing minerals with rhabdophane-like structure. U S Geol Surv Prof Paper 424C:339

Dormann J, Gasperin M, Poullen JF (1982) Etude structurale de la sequence d'oxydation de la vivianite $Fe_3(PO_4)_2(H_2O)_8$. Bull Minéral 105:147-160

Dunn PJ, Rouse RC, Campbell TJ, Roberts WL (1984a) Tinsleyite, the aluminous analogue of leucophosphite, from the Tip Top pegmatite in South Dakota. Am Mineral 69:374-376

Dunn PJ, Rouse RC, Nelen JA (1984b) Englishite: New chemical data and a second occurrence, from the Tip Top pegmatite, Custer, South Dakota. Can Mineral 22:469-470

Dunn PJ, Peacor DR, Sturman DB, Ramik RA, Roberts WL, Nelen JA (1986) Johnwalkite, the Mn-analogue of olmsteadite, from South Dakota. N. Jahrb Mineral Monatsh 115-120

Eby RK, Hawthorne FC (1989) Cornetite: Modulated densely-packed Cu^{2+} oxysalt. Mineral Petrol 40: 127-136

Effenberger H, Mereiter K, Pimminger M, Zemann J (1982) Machatschkiite: Crystal structure and revision of the chemical formula. Tschermaks Mineral Petrogr Mitt 30:145-155

Effenberger H, Krause W, Belendorff K, Bernhardt HBJ, Medenbach O, Hybler J, Petricek V (1994) Revision of the crystal structure of mrazekite, $Bi_2Cu_3(OH)_2O_2(PO_4)_{2.2}(H_2O)$. Can Mineral 32:365-372

Egorov BL, Dara AD, Senderova VM (1969) Melkovite, a new phosphate-molybdate from the zone of oxidation. Zap Vses Mineral Obshch 98:207-212 (in Russian)

Ercit TS (1991) The crystal structure of nalipoite. Can Mineral 29:569-573

Ercit TS, Hawthorne FC, Cerny P (1986a) The crystal structure of bobfergusonite. Can Mineral 24:605-614

Ercit TS, Anderson AJ, Cerny P, Hawthorne FC (1986b) Bobfergusonite, a new primary phosphate mineral from Cross Lake, Manitoba. Can Mineral 24:599-604

Ercit TS, Cooper MA, Hawthorne FC (1998) The crystal structure of vuonnemite, $Na_{11}Ti^{(4+)}Nb_2(Si_2O_7)_2(PO_4)_2O_3$(F, OH), a phosphate-bearing sorosilicate of the lomonosovite group. Can Mineral 36:1311-1320

Eventoff W, Martin R, Peacor DR (1972) The crystal structure of heterosite. Am Mineral 57:45-51

Eversheim VP, Kleber W (1953) Morphologie und Struktur des Reddingits, $P_2O_5\cdot 3FeO\cdot 3H_2O$. Acta Crystallogr 6:215-216

Fanfani L, Zanazzi PF (1966) La struttura cristallina della metastrengite. Atti Accad Naz Lincei Serie 8 40:889

Fanfani L, Zanazzi PF (1967a) The crystal structure of beraunite. Acta Crystallogr 22:173-181

Fanfani L, Zanazzi PF (1967b) Structural similarities of some secondary lead minerals. Mineral Mag 36: 522-529

Fanfani L, Zanazzi PF (1968) The crystal structure of vauquelinite and the relationships to fornacite. Z Kristallogr 126:433-443

Fanfani L, Zanazzi PF (1979) Switzerite: its chemical formula and crystal structure. Tschermaks Mineral Petrogr Mitt 26:255-269

Fanfani L, Nunzi A, Zanazzi PF (1970a) The crystal structure of wardite. Mineral Mag 37:598-605

Fanfani L, Nunzi A, Zanazzi PF (1970b) The crystal structure of fairfieldite. Acta Crystallogr B26:640-645

Fanfani L, Nunzi A, Zanazzi PF (1972) Structure and twinning in spencerite. Mineral Mag 38:687-692

Fanfani L, Nunzi A, Zanazzi PF, Zanzari AR (1975) The crystal structure of roscherite. Tschermaks Mineral Petrogr Mitt 22:266-277

Fanfani L, Nunzi A, Zanazzi PF, Zanzari AR (1976) Additional data on the crystal structure of montgomeryite. Am Mineral 61:12-14

Fanfani L, Zanazzi PF, Zanzari AR (1977) The crystal structure of a triclinic roscherite. Tschermaks Mineral Petrogr Mitt 24:169-178

Fanfani L, Tomassini M, Zanazzi PF, Zanzari AR (1978) The crystal structure of strunzite, a contribution to the crystal chemistry of basic ferric-manganous hydrated phosphates. Tschermaks Mineral Petrogr Mitt 25:77-87

Ferraris G, Franchini-Angela M (1973) Hydrogen bonding in the crystalline state. Crystal structure of $MgHAsO_4 \cdot 7H_2O$, rosslerite. Acta Crystallogr B29:286-292

Ferraris G, Franchini-Angela M (1974) Hydrogen bonding in the crystalline state. Crystal structure and twinning of $NaNH_4HPO_4(H_2O)_4$ (stercorite). Acta Crystallogr B30:504-510

Ferraris G, Fuess H, Joswig W (1986) Neutron diffraction study of $MgNH_4PO_4(H_2O)_6$ (struvite) and survey of water molecules donating short hydrogen bonds. Acta Crystallogr B42:253-258

Fisher DJ (1956) Hagendorfite unit cell. Geol Soc Am Bull 67:1694-1695

Fisher DJ (1965) Dickinsonites, fillowite and alluaudites. Am Mineral 50:1647-1669

Fisher FG, Meyrowitz R (1962) Brockite, a new calcium thorium phosphate from the Wet Mountains, Colorado. Am Mineral 47:1346-1355

Fitch AN, Cole M (1991) The structure of $KUO_2PO_{4.3}D_2O$ refined from neutron and synchrotron-radiation powder diffraction data. Material Res Bull 26:407-414

Fitch AN, Fender BEF (1983) The structure of deuterated ammonium uranyl phosphate trihydrate, $ND_4UO_2PO_4(D_2O)_3$ by powder neutron diffraction. Acta Crystallogr C39:162-166

Flachsbart I (1963) Zur Kristallstruktur von Phosphoferrit (Fe, $Mn)_3(PO_4)_2(H_2O)_3$. Z Kristallogr 118: 327-331

Fontan F, Pillard F, Permingeat F (1982) Natrodufrenite, $(Na,Fe^{3+},Fe^{2+})(Fe^{3+},Al)_5(PO_4)_4(OH)_6 \cdot 2(H_2O)$, a new mineral species of the dufrenite group. Bull Mineral 105:321 -326

Foord EE, Taggart JE Jr (1998) A reexamination of the turquoise group, the mineral aheylite, planerite (redefined), turquoise and coeruleolactite. Mineral Mag 62:93-111

Foord EE, Brownfield ME, Lichte FE, Davis AM, Sutley SJ (1994) McCrillisite, $NaCs(Be,Li)Zr_2(PO_4)_4 \cdot 1\text{-}2H_2O$, a new mineral species from Mount Mica, Oxford County, Maine, and new data for gainesite. Can Mineral 32:839-842

Fransolet A-M (1989) The problem of Na-Li substitution in primary Li-Al phosphates: New data on lacroixite, a relatively widespread mineral. Can Mineral 27:211-217

Fransolet A-M (1995) Wyllieite et rosemaryite dans la pegmatite de Buranga, Rwanda. Eur J Mineral 7: 567-575

Fransolet A-M, Cooper MA, Cernyý P, Hawthorne FC, Chapman R, Grice JD (2000) The Tanco pegmatite at Bernic Lake, southeastern Manitoba. XV. Ercitite, $NaMn^{3+}PO_4(OH)(H_2O)_2$, a new phosphate mineral species. Can Mineral 38:893-898

Freeman K, Bayliss P (1991) ICDD card # 44-1429 (natromontebrasite)

Frondel C, Riska DD, Frondel JW (1956) X-ray powder data for uranium and thorium minerals. U S Geol Surv Bull B 1036-G:91-153

Galliski MA, Cooper MA, Hawthorne FC, Cerny P (1999) Bederite, a new pegmatite phosphate mineral from Nevados de Palermo, Argentina: description and crystal structure. Am Mineral 84:1674-1679

Galliski MA, Hawthorne FC, Cooper MA (2001) Refinement of the crystal structure of ushkovite from Nevados de Palermo, Republica Argentina. Can Mineral (accepted)

García-Guinea J, Chagoyen AM, Nickel EH (1995) A re-investigation of bolivarite and evansite. Can Mineral 33:59-65

Gatehouse BM, Miskin BK (1974) The crystal structure of brazilianite, $NaAl_3(PO_4)_2(OH)_4$. Acta Crystallogr B30:1311-1317

Geller S, Durand JL (1960) Refinement of the structure of $LiMnPO_4$. Acta Crystallogr 13:325-331

Genkina EA, Khomyakov AP (1992) Refinement of the structure of natural sodiumphosphate. Kristallografiya 37:1559-1560

Genkina EA, Kabalov YuK, Maksimov BA, Mel'nikov OK (1984) The crystal structure of synthetic tavorite $LiFe(PO_4)(OH,F)$. Kristallografiya 29:50-55

Genkina EA, Maksimov BA, Melnikov OK (1985) Crystal structure of synthetic tarbuttite $Zn_2(PO_4)(OH)$. Dokl Akad Nauk SSSR 282:314-317

Gheith MA (1953) Lipscombite: a new synthetic iron lazulite. Am Mineral 38:612-628

Ghose S, Leo SR, Wan C (1974) Structural chemistry of copper and zinc minerals. Part I. Veszelyite, $(Cu_{0.5}Zn_{0.5})_2ZnPO_4NOH)_3(H_2O)_3$: a novel type of sheet structure and crystal chemistry of copper-zinc substitution. Am Mineral 59:573-581

Giuseppetti G, Tadini C (1973) Refinement of the crystal structure of beryllonite, $NaBePO_4$. Tschermaks Mineral Petrogr Mitt 20:1-12

Giuseppetti G, Tadini C (1983) Lazulite, (Mg,Fe) $Al_2(OH)_2(PO_4)_2$: structure refinement and hydrogen bonding. N Jahrb Mineral Monatsh 410-416

Giuseppetti G, Tadini C (1984) The crystal structure of childrenite from Tavistock (SW England), $Ch_{89}Eo_{11}$ term of childrenite-eosphorite series. N Jahrb Mineral Monatsh 263-271

Giusepetti G, Tadini C (1987) Corkite, $PbFe_3(SO_4)(PO_4)(OH)_6$, its crystal structure and ordered arrangement of the tetrahedral cations. N Jahrb Mineral Monatsh 71-81

Giuseppetti G, Mazzi F, Tadini C (1989) The crystal structure of chalcosiderite $CuFe_6(PO_4)_4(OH)_8(H_2O)_4$. N Jahrb Mineral Monatsh 227-239

Gopal R, Calvo C, Ito J, Sabine WK (1974) Crystal structure of synthetic Mg-whitlockite, $Ca_{18}Mg_2H_2(PO_4)_{14}$. Can J Chem 52:1152-1164

Grice JD, Dunn PJ (1992) Attakolite: new data and crystal-structure determination. Am Mineral 77: 1285-1291

Grice JD, Groat LA (1988) Crystal structure of paulkellerite. Am Mineral 73:873-875

Grice JD, Roberts AC (1993) Harrisonite, a well-ordered silico-phosphate with a layered crystal structure. Can Mineral 31:781-785

Grice JD, Peacor DR, Robinson GW, van Velthuizen J, Roberts WL, Campbell TJ, Dunn PJ (1985) Tiptopite, $(Li,K,Na,Ca,G)_8Be_6(PO_4)_6(OH)_4$, a new mineral species from the Black Hills, South Dakota. Can Mineral 23:43-46

Grice JD, Dunn PJ, Ramik RA (1989) Whiteite-(CaMnMg), a new mineral species from the Tip Top pegmatite, Custer, South Dakota. Can Mineral 27:699-702

Grice JD, Dunn PJ, Ramik RA (1990) Jahnsite-(CaMnMn), a new member of the whiteite group from Mangualde, Beira, Portugal. Am Mineral 75:401-404

Griffen DT, Ribbe PH (1979) Distortions in the tetrahedral oxyanions of crystalline substances. N Jahrb Mineral Abh 137:54-73

Groat LA, Hawthorne FC (1990) The crystal structure of nissonite. Am Mineral 75:1170-1175

Groat LA, Raudsepp M, Hawthorne FC, Ercit TS, Sherriff BL, Hartman JS (1990) The amblygonite-montebrasite series: characterization by single-crystal structure refinement, infrared spectroscopy and multinuclear MAS-NMR spectroscopy. Am Mineral 75:992-1008

Guy BB, Jeffrey GA (1966) The crystal structure of fluellite, $Al_2PO_4F_2(OH)(H_2O)_7$. Am Mineral 51: 1579-1592

Hanson AW (1960) The crystal structure of eosphorite. Acta Crystallogr 13:384-387

Harrowfield IR, Segnit ER, Watts JA (1981) Aldermanite, a new magnesium aluminum phosphate. Mineral Mag 44:59-62

Hata M, Marumo F, Iwai SI (1979) Structure of barium chlorapatite. Acta Crystallogr B35:2382-2384

Hawthorne FC (1976) Refinement of the crystal structure of adamite. Can Mineral 14:143-148

Hawthorne FC (1979a) The crystal structure of morinite. Can Mineral 17:93-102

Hawthorne FC (1979b) Paradamite. Acta Crystallogr B35:720-722

Hawthorne FC (1982) The crystal structure of bøggildite. Can Mineral 20:263-270

Hawthorne FC (1983a) Enumeration of polyhedral clusters. Acta Crystallogr A39:724-736

Hawthorne FC (1983b) The crystal structure of tancoite. Tschermaks Mineral Petrogr Mitt 31:121-135

Hawthorne FC (1984) The crystal structure of stenonite and the classification of the aluminofluoride minerals. Can Mineral 22:245-251

Hawthorne FC (1985a) Towards a structural classification of minerals: the $^{vi}M^{iv}T_2O_n$ minerals. Am Mineral 70:455-473

Hawthorne FC (1985b) Refinement of the crystal structure of bloedite: structural similarities in the $[^{VI}M(^{IV}T\phi_4)_2\phi_n]$ finite-cluster minerals. Can Mineral 23:669-674

Hawthorne FC (1988) Sigloite: The oxidation mechanism in $[(M_2^{3+}(PO_4)_2(OH)_2(H_2O)_2)]^{2-}$ structures. Mineral Petrol 38:201-211

Hawthorne FC (1990) Structural hierarchy in $^{[6]}M^{[4]}TO_4$ minerals. Z Kristallogr 192:1-52

Hawthorne FC (1992) The role of OH and H_2O in oxide and oxysalt minerals. Z Kristallogr 201:183-206

Hawthorne FC (1994) Structural aspects of oxide and oxysalt crystals. Acta Crystallogr B50:481-510

Hawthorne FC (1997) Structural aspects of oxide and oxysalt minerals. *In* European Mineralogical Union Notes in Mineralogy, Vol.1, "Modular Aspects of Minerals". Merlino S (ed) Eötvös University Press, Budapest, p 373-429

Hawthorne FC (1998) Structure and chemistry of phosphate minerals. Mineral Mag 62:141-164

Hawthorne FC (2002) The use of end-member charge-arrangements in defining new minerals and heterovalent substitutions in complex minerals. Can Mineral (accepted)

Hawthorne FC, Ferguson RB (1975) Anhydrous sulphates. II Refinement of the crystal structure of anhydrite. Can Mineral 13:289-292

Hawthorne FC, Grice JD (1987) The crystal structure of ehrleite, a tetrahedral sheet structure. Can Mineral 25:767-774

Hawthorne FC, Schindler MS (2000) Topological enumeration of decorated $[Cu^{2+}\phi_2]_N$ sheets in hydroxy-hydrated copper-oxysalt minerals. Can Mineral 38:751-761

Hawthorne FC, Sokolova EV (2002) Simonkolleite, $Zn_5(OH)_8Cl_2(H_2O)$, a decorated interrupted-sheet structure of the form $[M\phi_2]_4$. Can Mineral (submitted)

Hawthorne FC, Groat LA, Raudsepp M, Ercit TS (1987) Kieserite, a titanite-group mineral. N Jahrb Mineral Abh 157:121-132

Hawthorne FC, Cooper MA, Green DI, Starkey RE, Roberts AC, Grice JD (1999) Wooldridgeite, $Na_2CaCu^{2+}{}_2(P_2O_7)_2(H_2O)_{10}$: a new mineral from Judkins quarry, Warwickshire, England. Mineral Mag 63:13-16

Hawthorne FC, Krivovichev SV, Burns PC (2000) The crystal chemistry of sulfate minerals. Rev Mineral 40:1-112

Hey MH, Milton C, Dwornik WJ (1982) Eggonite (kolbeckite, sterrettite), $ScPO_4{\cdot}2H_2O$. Mineral Mag 46: 493-497

Hill RG (1977) The crystal structure of phosphophyllite. Am Mineral 63:812-817

Hill RG, Jones JB (1976) The crystal structure of hopeite. Am Mineral 61:987-995

Hoyos MA, Calderon T, Vergara I, Garcia-Sole J (1993) New structural and spectroscopic data for eosphorite. Mineral Mag 57:329-336

Hughes JM, Drexler JW (1991) Cation substitution in the apatite tetrahedral site: crystal structures of type hydroxylellestadtite and type fermorite. N Jahrb Mineral Monatsh 327-336

Hughes JM, Cameron M, Crowley KD (1990) Crystal structures of natural ternary apatites: solid solution in the $Ca_5(PO_4)_3X$ (X= F, OH, Cl) system. Am Mineral 75:295-304

Hughes JM, Foord EE, Hubbard MA, Ni YX (1995) The crystal structure of cheralite-(Ce), (LREE, Ca, Th, U)(P, Si)O_4, a monazite-group mineral. N Jahrb Mineral Monatsh 344-350

Huminicki DMC, Hawthorne FC (2000) Refinement of the crystal structure of väyrynenite. Can Mineral 38:1425-1432

Huminicki DMC, Hawthorne FC (2002) Hydrogen bonding in the crystal structure of seamanite. Can Mineral (accepted)

Hurlbut CS (1942) Sampleite, a new mineral from Chuquicamata, Chile. Am Mineral 27:586-589

Ilyukhin AB, Katser SB, Levin AA (1995) Structure refinement of two crystals from the KDP family $(ND_4)D_2PO_4$ and KH_2AsO_4 in the paraphase. Z Neorg Khim 40:1599-1600

Isaaks AM, Peacor DR (1981) Panasqueiratite, a new mineral: The OH-equivalent of isokite. Can Mineral 19:389-392

Isaaks AM, Peacor DR (1982) The crystal structure of thadeuite, $Mg(Ca,Mn)(Mg, Fe, Mn)_2(PO_4)_2(OH,F)_2$. Am Mineral 67:120-125

Johan Z, Slansky E, Povondra P (1983) Vashegyite, a sheet aluminum phosphate: new data. Can Mineral 21:489-498

Kabalov YuK, Sokolova EV, Pekov IV (1997) Crystal structure of belovite-(La). Phys Dokl 42:344-348

Kampf AR (1977a) Schoonerite: its atomic arrangement. Am Mineral 62:250-255

Kampf AR (1977b) Minyulite: its atomic arrangement. Am Mineral 62:256-262

Kampf AR (1977c) A new mineral: perloffite, the Fe^{3+} analogue of bjarebyite. Mineral Rec 8:112-114

Kampf AR (1992) Beryllophosphate chains in the structures of fransoletite, parafransoletite, and ehrleite and some general comments on beryllophosphate linkages. Am Mineral 77:848-856

Kampf AR, Moore PB (1976) The crystal structure of bermanite, a hydrated manganese phosphate. Am Mineral 61:1241-1248

Kampf AR, Moore PB (1977) Melonjosephite, calcium iron hydroxy phosphate: its crystal structure. Am Mineral 62:60-66

Kampf AR, Dunn PJ, Foord EE (1992) Parafransoletite, a new dimorph of fransoletite from the Tip Top Pegmatite, Custer, South Dakota. Am Mineral 77:843-847

Kato T (1970) Cell dimensions of the hydrated phosphate, kingite. Am Mineral 55:515-517

Kato T (1971) The crystal structures of goyazite and woodhouseite. N Jahrb Mineral Monatsh 241-247

Kato T (1987) Further refinement of the goyazite structure. Mineral J 13:390-396

Kato T (1990) The crystal structure of florencite. N Jahrb Mineral Monatsh 227-231

Kato T, Miura Y (1977) The crystal structures of jarosite and svanbergite. Mineral J 8:418-430

Katz L, Lipscomb WN (1951) The crystal structure of iron lazulite, a synthetic mineral related to lazulite. Acta Crystallogr 4:345-348

Keegan TD, Araki T, Moore PB (1979) Senegalite, $Al_2(OH)_3(H_2O)(PO_4)$, a novel structure type. Am Mineral 64:1243-1247

Keller P, Fontan F, Velasco Roldan F, Melgarejo I, Draper JC (1997) Stanékite, $Fe^{3+}(Mn,Fe^{2+},Mg)(PO_4)O$: A new phosphate mineral in pegmatites at Karibib (Namibia) and French Pyrénées (France). Eur J Mineral 9:475-482

Khan AA, Baur WH (1972) Salt hydrates. VIII. The crystal structures of sodium ammonium orthochromate dihydrate and magnesium diammonium bis(hydrogen ortho phosphate) tetrahydrate and a discussion of the ammonium ion. Acta Crystallogr B28:683-693

Khan AA, Roux JP, James WJ (1972) The crystal structure of diammonium hydrogen phosphate, $(NH_4)_2HPO_4$. Acta Crystallogr B28:2065-2069

Kharisun, Taylor MR, Bevan DJM, Pring A (1997) The crystal structure of kintoreite, $PbFe_3(PO_4)_2(OH,H_2O)_6$. Mineral Mag 61:123-129

Khomyakov AP, Aleksandrov VV, Krasnova NI, Ermilov VV, Smolyaninova (1982) Bonshtedtite, $Na_3Fe(PO_4)(CO_3)$, a new mineral. Zap Vses Mineral Obshch 111:486-490 (in Russian)

Khomyakov AP, Nechelyustov GN, Sokolova EV, Dorokhova GI (1992) Quadruphite, $Na_{14}CaMgTi_4[Si_2O_7]_2[PO_4]_4O_4F_2$ and polyphite $Na_{17}Ca_3Mg\ (Ti,Mn)_4[Si_2O_7]_2\ [PO_4]_6\ O_2F_6$—new minerals of the lomonovosite family. Zap Vser Mineral Obshch 121:105-112 (in Russian)

Khomyakov AP, Polezhaeva LI, Sokolova EV (1994) Crawfordite, $Na_3Sr(PO_4)(CO_3)$—a new mineral from the bradleyite. Zap Vser Mineral Obshch 123:107-111 (in Russian)

Khomyakov AP, Lisitsin DV, Kulikova IM, Rastsvetsaeva RK (1996) Deloneite-(Ce) $NaCa_2SrCe(PO_4)_3F$—a new mineral with a belovite-like structure. Zap Vser Mineral Obshch 125:83-94 (in Russian)

Khomyakov AP, Kulikova IM, Rastsvetaeva RK (1997) Fluorcaphite, $Ca(Sr,Na,Ca)(Ca,Sr,Ce)_3(PO_4)_3F$—a new mineral with the apatite structural motif. Zap Vser Mineral Obshch 126:87-97 (in Russian)

Khosrawan-Sazedj F (1982a) The crystal structure of meta-uranocircite II, $Ba(UO_2)_2(PO_4)_2(H_2O)_6$. Tschermaks Mineral Petrogr Mitt 29:193-204

Khosrawan-Sazedj F (1982b) On the space group of threadgoldite. Tschermaks Mineral Petrogr Mitt 30: 111-115

Kim Y, Kirkpatrick RJ (1996) Application of MAS NMR spectroscopy to poorly crystalline materials: Viséite. Mineral Mag 60:957-962

King GSD, Sengier Roberts L (1988) Drugmanite, $Pb_2(Fe_{0.78}Al_{0.22})H(PO_4)_2(OH)_2$: Its crystal structure and place in the datolite group. Bull Minéral 111:431-437

Klevtsova RF (1964) About the crystal structure of strontiumapatite. Z Strukt Khim 5:318-320

Kniep R, Mootz D (1973) Metavariscite—a redetermination of its crystal structure. Acta Crystallogr B29: 2292-2294

Kniep R, Mootz D, Vegas A (1977) Variscite. Acta Crystallogr B33:263-265

Kohlmann M, Sowa H, Reithmayer K, Schulz H, Krueger RBR, Abriel W (1994) Structure of a $[Y_{(1-x)}(Gd,Dy,Er)_x]PO_4{\cdot}2H_2O$ microcrystal using synchrotron radiation. Acta Crystallogr C50: 1651-1652

Kolitsch U, Giester G (2000) The crystal structure of faustite and its copper analogue turquoise. Mineral Mag 64:905-913

Kolitsch U, Taylor MR, Fallon GD, Pring A (1999a) Springcreekite, $BaV^{3+}{}_3(PO_4)_2(OH,H_2O)_6$, a new member of the crandalite group, from the Spring Creek mine, South Australia: the first natural V^{3+}-member of the alunite family and its crystal structure. N Jahrb Mineral Monatsh 529-544

Kolitsch U, Tiekink ERT, Slade PG, Taylor MR, Pring A (1999b) Hinsdalite and plumbogummite, their atomic arrangements and disordered lead sites. Eur J Mineral 11:513-520

Kolitsch U, Pring A, Tiekink ERT (2000) Johntomaite, a new member of the bjarebyite group of barium phosphates: description and structure refinement. Mineral Petrol 70:1-14

Kolkovski B (1971) ICDD card # 29-0756 (orpheite)

Krause W, Belendorff K, Bernhardt H-J (1993) Petitjeanite, $Bi_3O(OH)(PO_4)_2$, a new mineral, and additional data for the corresponding arsenate and vanadate, preisingerite and schumacherite. Neues Jahrb Mineral Monatsh 487-503

Krause W, Belendorff K, Bernhardt H-J, Petitjean K (1998a) Phosphogartrellite, $PbCuFe^{3+}(PO_4)_2(OH){\cdot}H_2O$, a new member of the tsumcorite group. N Jahrb Mineral Monatsh 111-118

Krause W, Belendorff K, Bernhardt H-J, McCammon C, Effenberger H, Mikenda W (1998b) Crystal chemistry of the tsumcorite-group minerals. New data on ferrilotharmeyerite, tsumcorite, thometzekite, mounanaite, helmutwinklerite, and a redefinition of gartrellite. Eur J Mineral 10:179-206

Krause W, Bernhardt H-J, McCammon C, Effenberger H (1998c) Brendelite, $(Bi,Pb)_2Fe^{(3+,2+)}O_2(OH)(PO_4)$, a new mineral from Schneeberg, Germany: description and crystal structure. Mineral Petrol 63:263-277

Krutik VM, Pushcharovskii DYu, Khomyakov AP, Pobedimskaya EA, Belov NV (1980) Anion radical of mixed type (four (S_4O_{12}) rings and P orthotetrahedral) in the structure of monoclinic phosinaite. Kristallografiya 25:240-247

Kumbasar I, Finney JJ (1968) The crystal structure of parahopeite. Mineral Mag 36:621-624
Kurova TA, Shumyatskaya NG, Voronkov AA, Pyatenko YA (1980) Crystal structure of sidorenkite $Na_3Mn(PO_4)(CO_3)$. Dokl Akad Nauk SSSR 251:605-607
Lager GA, Gibbs GV (1974) A refinement of the crystal structure of herderite, $CaBePO_4OH$. Am Mineral 59:919-925
Lahti SI (1981) The granite pegmatites of the Eräjärevi area in Orivesi, southern Finland. Geol Surv Finland Bull 314:1-82
Lahti SI, Pajunen A (1985) New data on lacroixite, $NaAlFPO_4$. I. Occurrence, physical properties and chemical composition. Am Mineral 70:849-855
Leavens PB, Rheingold AL (1988) Crystal structures of gordonite, $MgAl_2(PO_4)_2(OH)_2(H_2O)_6$ $(H_2O)_2$, and its Mn analog. N Jahrb Mineral Monatsh 265-270
Leavens PB, White JS, Nelen JA (1990) Zanazziite, a new mineral from Minas Gerais, Brazil. Mineral Rec 21:413-417
Lefebvre J-J, Gasparrini C (1980) Florencite, an occurrence in the Zairian copperbelt. Can Mineral 18: 301-311
Le Page Y, Donnay G (1977) The crystal structure of the new mineral maricite $NaFePO_4$. Can Mineral 15: 518-521
Liebau F (1985) Structural Chemistry of Silicates. Springer-Verlag, Berlin
Liferovich RP, Yakovenchuk VN, Pakhomovsky YaA, Bogdanova AN, Britvin SN (1997) Juonniite, a new mineral of scandium from dolomitic carbonatites of the Kovdor massif. Zap Vser Mineral Obshch 126: 80-88
Liferovich RP, Sokolova EV, Hawthorne FC, Laajoki K, Gehör S, Pakhomovsky YuA, Sorokhtina NV (2000a) Gladiusite, $Fe^{3+}{}_2(Fe^{2+},Mg_4)(PO_4)(OH)_{11}(H_2O)$, a new hydrothermal mineral from the phoscorite-carbonatite unit, Kovdor Complex, Kola Peninsula, Russia. Can Mineral 38:1477-1485
Liferovich RP, Pakhomovsky YaA, Yakubovich OV, Massa W, Laajoki K, Gehör S, Bogdanova AN, Sorokhtina NV (2000b) Bakhchisaraitsevite, $Na_2Mg_5[PO_4]_4{\cdot}7H_2O$, a new mineral from hydrothermal assemblages related to phoscorite-carbonatite complex of the Kovdor massif, Russia. N Jahrb Mineral Monatsh 402-418
Lightfoot P, Cheetham AK, Sleight AW (1987) Structure of $MnPO_4{\cdot}H_2O$ by synchrotron X-ray powder diffraction. Inorg Chem 26:3544-3547
Lindberg ML (1949) Frondelite and the frondelite-rockbridgeite series. Am Mineral 34:541-549
Lindberg ML (1958) The beryllium content of roscherite from the Sapucaia pegmatite mine, Minas Gerais, Brazil and from other localities. Am Mineral 43:824-838
Lindberg (1962) Manganoan lipscombite from the Sapucaia pegmatite mine, Minas Gerais, Brazil. First occurrence of lipscombite in nature. Am Mineral 47:353-359
Lindberg ML, Christ CL (1959) Crystal structures of the isostructural minerals lazulite, scorzalite and barbosalite. Acta Crystallogr 12:695-697
Livingstone A (1980) Johnsomervilleite, a new transition-metal phosphate mineral from the Loch Quoich area, Scotland. Mineral Mag 43:833-836
Makarov YS, Ivanov VI (1960) The crystal structure of meta-autunite, $Ca(UO_2)_2(PO_4)_2{\cdot}6H_2O$. Dokl Akad Nauk SSSR 132:601-603
Makarov YS, Tobelko KI (1960) The crystal structure of metatorbernite. Dokl Akad Nauk SSSR 131:87-89
Malinovskii YuA, Genkina EA (1992) Crystal structure of olympite $LiNa_5[PO_4]_2$. Sov Phys Crystallogr 37: 772-782
Mandarino JA, Sturman BD (1976) Kulanite, a new barium iron aluminum phosphate from the Yukon territory, Canada. Can Mineral 14:127-131
Mandarino JA, Sturman BD, Corlett MI (1977) Penikisite, the magnesium analogue of kulanite, from Yukon Territory. Can Mineral 15:393-395
Mandarino JA, Sturman BD, Corlett MI (1978) Satterlyite, a new hydroxyl-bearing ferrous phosphate from the Big Fish area, Yukon Territory. Can Mineral 16:411-413
Martini JEJ (1978) Sasaite, a new phosphate mineral from West Driefontein Cave, Transvaal, South Africa. Mineral Mag 42:401-404
Martini JEJ (1991) Swaknoite [$Ca(NH_4)_2(HPO_4)_2{\cdot}H_2O$, orthorhombic]: a new mineral from Arnheim Cave, Namibia. Bull S African Speleol Assoc 32:72-74
Martini JEJ (1993) ICDD Card # 45-1411 (swaknoite)
Matsubara S (2000) Vivianite nodules and secondary phosphates in Pliocene-Pleistocene clay deposits from Hime-Shima, Oita Prefecture and Kobe, Hyogo Prefecture, eastern Japan. Mem National Sci Mus, Tokyo 33:15-27
Mazzi F, Ungaretti L (1994) The crystal structure of vitusite from Illimaussaq (South Greenland): $Na_3REE(PO_4)_2$. N Jahrb Mineral Monatsh 49-66

McConnell D (1952) Viséite, a zeolite with the analcime structure and containing linked SiO_4, PO_4 and H_xO_4 groups. Am Mineral 37:609-617
McConnell D (1963) Thermocrystallization of richellite to produce a lazulite structure (calcium lipscombite). Am Mineral 48:300-307
McConnell (1990) Kehoeite and viséite reviewed: comments on dahllite and francolite. Mineral Mag 54: 657-658
McCoy TJ, Steele IM, Keil K, Leonard BF, Endres M (1994) Chladniite, $Na_2CaMg_7(PO_4)_6$: a new mineral from the Carlton (IIICD) iron meteorite. Am Mineral 79:375-380
McDonald AM, Chao GY, Grice JD (1994) Abenakiite-(Ce), a new silicophosphate carbonate mineral from Mont Saint-Hilaire, Quebec: Description and structure determination. Can Mineral 32:843-854
McDonald AM, Chao GY, Grice JD (1996) Phosinaite-(Ce) from Mont Saint-Hilaire, Quebec: New data and structure refinement. Can Mineral 34:107-114
McDonald AM, Grice JD, Chao GY (2000) The crystal structure of yoshimuraite, a layered Ba-Mn-Ti silicophosphate, with comments on five-coordinated Ti^{4+}. Can Mineral 38:649-656
Meagher EP, Gibbons CS, Trotter J (1974) The crystal structure of jagowerite. $BaAl_2P_2O_8(OH)_2$. Am Mineral 59:291-295
Medrano MD, Evans HTJr, Wenk H-R, Piper DZ (1998) Phosphovanadylite: a new vanadium phosphate mineral with a zeolite-type structure. Am Mineral 83:889-895
Mereiter K, Niedermayr G, Walter F (1994) Uralolite, $Ca_2Be_4(PO_4)_3(OH)\cdot 3.5(H_2O)$: new data and crystal structure. Eur J Mineral 6:887-896
Merlino S, Pasero M (1992) Crystal chemistry of beryllophosphates: The crystal structure of moraesite, $Be_2(PO_4)(OH)\cdot 4H_2O$. Z Kristallogr 201:253-262
Merlino S, Mellini M, Zanazzi PF (1981) Structure of arrojadite, $KNa_4CaMn_4Fe_{10}Al(PO_4)_{12}(OH)_2$. Acta Crystallogr B37:1733-1736
Miller SA, Taylor JC (1986) The crystal structure of saleeite, $Mg(UO_2PO_4)_2\cdot 10H_2O$. Z Kristallogr 177: 247-253
Milton DJ, Bastron H (1971) Churchite and florencite (Nd) from Sausalito, California. Mineral Rec 2: 166-168
Milton C, McGee JJ, Evans HT Jr (1993) Mahlmoodite, $FeZr(PO_4)_2\cdot 4H_2O$, a new iron zirconium phosphate mineral from Wilson Springs, Arkansas. Am Mineral 78:437-440
Moëlo Y, Lasnier B, Palvadeau P, Léone P, Fontan F (2000) Lulzacite, $Sr_2Fe^{2+}(Fe^{2+},Mg)_2Al_4(PO_4)_4(OH)_{10}$, a new strontium phosphate (Saint Aubin-des-Châteaux, Loire-Atlantique, France). CR Acad Sci Paris, Earth Planet Sci 330:317-324
Mooney RCL (1948) Crystal structure of a series of rare earth phosphates. J Chem Phys 16:1003
Mooney RCL (1950) X-ray diffraction study of cerous phosphate and related crystals. I. Hexagonal modification. Acta Crystallogr 3:337-340
Moore PB (1965a) The crystal structure of laueite, $MnFe_2(OH)_2(PO_4)_2(H_2O)_6(H_2O)_2$. Am Mineral 50: 1884-1892
Moore PB (1965b) A structural classification of Fe-Mn orthophosphate hydrates. Am Mineral 50: 2052-2062
Moore PB (1966) The crystal structure of metastrengite and its relationship to strengite and phosphophyllite. Am Mineral 51:168-176
Moore PB (1970) Crystal chemistry of the basic iron phosphates. Am Mineral 55:135-169
Moore PB (1971a) The $Fe_3^{2+}(H_2O)_n(PO_4)_2$ homologous series: Crystal-chemical relationships and oxidized equivalents. Am Mineral 56:1-16
Moore PB (1971b) Crystal chemistry of the alluaudite structure type: Contribution to the paragenesis of pegmatite phosphate giant crystals. Am Mineral 56:1955-1975
Moore PB (1972a) Natrophilite, $NaMn(PO_4)$, has ordered cations. Am Mineral 57:1333-1344
Moore PB (1972b) Octahedral tetramer in the crystal structure of leucophosphite, $K_2[Fe^{3+}_4(OH)_2(H_2O)_2(PO_4)_4]\cdot 2H_2O$. Am Mineral 57:397-410
Moore PB (1973a) Pegmatite phosphates. Descriptive mineralogy and crystal chemistry. Mineral Rec 4: 103-130
Moore PB (1973b) Bracelets and pinwheels: A topological-geometrical approach to the calcium orthosilicate and alkali sulfate structures. Am Mineral 58:32-42
Moore PB (1974) I. Jahnsite, segelerite, and robertsite, three new transition metal phosphate species. II. Redefinition of overite, an isotype of segelerite. III. Isotypy of robertsite, mitridatite, and arseniosiderite. Am Mineral 59:48-59, 640
Moore PB (1975a) Brianite, $Na_2CaMg[PO_4]_2$: a phosphate analog of merwinite, $Ca_2CaMg[SiO_4]_2$. Am Mineral 60:717-718
Moore PB (1975b) Laueite, pseudolaueite, stewartite and metavauxite: a study in combinatorial polymorphism. N Jahrb Mineral Abh 123:148-59

Moore PB (1976) Derivative structures based on the alunite octahedral sheet: mitridatite and englishite. Mineral Mag 40:863-866

Moore PB (1984) Crystallochemical aspects of the phosphate minerals. *In* Phosphate Minerals. Nriagu JO, Moore PB (eds) Springer-Verlag, Berlin, p 155-170

Moore PB, Araki T (1973) Hureaulite, $(Mn^{2+})_5(H_2O)_4(PO_3(OH))_2(PO_4)_2$: Its atomic arrangement. Am Mineral 58:302-307

Moore PB, Araki T (1974a) Jahnsite, $CaMnMg_2(H_2O)_8Fe_2(OH)_2(PO_4)_4$. A novel stereoisomerism of ligands about octahedral corner-chains. Am Mineral 59:964-973

Moore PB, Araki T (1974b) Trolleite, $Al_4(OH)_3(PO_4)_3$. A very dense structure with octahedral face-sharing dimers. Am Mineral 59:974-984

Moore PB, Araki T (1974c) Bjarebyite, $Ba(Mn,Fe)_2Al_3(OH)_3(PO_4)_3$. Its atomic arrangement. Am Mineral 59:567-572

Moore PB, Araki T (1974d) Stewartite, $Mn^{2+}Fe_2^{3+}(OH)_2(H_2O)_6(PO_4)_2(H_2O)_2$. Its atomic arrangement. Am Mineral 59:1272-1276

Moore PB, Araki T (1974e) Montgomeryite, $Ca_4Mg(H_2O)_{12}[Al_4(OH)_4(PO_4)_6]$: Its crystal structure and relaton to vauxite, $Fe^{2+}{}_2(H_2O)_4[Al_4(OH)_4(H_2O)_4(PO_4)_4]\cdot 4H_2O$. Am Mineral 59:843-850

Moore PB, Araki T (1975) Palermoite, $SrLi_2(Al_4(OH)_4(PO_4)$. Its atomic arrangement and relationship to carminite, $Pb_2(Fe_4(OH)_4(AsO_4)_4)$. Am Mineral 60:460-465

Moore PB, Araki T (1976) A mixed-valence solid solution series: Crystal structures of phosphoferrite and kryzhanovskite. Inorg Chem 15:316-321

Moore PB, Araki T (1977a) Samuelsonite: its crystal structure and relation to apatite and octacalcium phosphate. Am Mineral 62:229-245

Moore PB, Araki T (1977b) Mitridatite, $Ca_6(H_2O)_6(Fe_9O_6(PO_4)_9)(H_2O)_3$. A noteworthy octahedral sheet structure. Mineral Mag 41:527-528

Moore PB, Araki T (1977c) Overite, segelerite, and jahnsite: a study in combinatorial polymorphism. Am Mineral 62:692-702

Moore PB, Ghose S (1971) A novel face-sharing octahedral trimer in the crystal structure of seamanite. Am Mineral 56:1527-1538

Moore PB, Ito J (1978) I. Whiteite, a new species, and a proposed nomenclature for the jahnsite-whiteite complex series. II. New data on xanthoxenite. Mineral Mag 42:309-316

Moore PB, Ito J (1979) Alluaudites, wyllieites, arrojadites: crystal chemistry and nomenclature. Mineral Mag 43:227-35

Moore PB, Kampf AR (1977) Schoonerite, a new zinc-manganese-iron-phosphate mineral. Am Mineral 62:246-249

Moore PB, Molin-Case J (1974) Contribution to pegmatite phosphate giant crystal paragenesis. II. The crystal chemistry of wyllieite, $Na_2Fe(II)_2Al(PO_4)_3$, a primary phase. Am Mineral 59:280-290

Moore PB, Shen J (1983a) An X-ray structural study of cacoxenite, a mineral phosphate. Nature 306: 356-358

Moore Pb, Shen J (1983b) Crystal structure of steenstrupine: a rod structure of unusual complexity. Tschermaks Mineral Petrogr Mitt 31:47-67

Moore PB, Kampf AR, Irving AJ (1974) Whitmoreite, $Fe(II)Fe(III)_2(OH)_2(H_2O)_4(PO_4)_2$, a new species. Its description and atomic arrangement. Am Mineral 59:900-905

Moore PB, Irving AJ, Kampf AR (1975a) Foggite, $CaAl(OH)_2(H_2O)[PO_4]$; goedkenite, $(Sr,Ca)_2Al(OH)[PO_4]_2$; and samuelsonite, $(Ca,Ba)Fe^{2+}{}_2Mn^{2+}{}_2Ca_8Al_2(OH)_2[PO_4]_{10}$: Three new species from the Palermo No. 1 Pegmatite, North Groton, New Hampshire. Am Mineral 60:957-964

Moore PB, Kampf AR, Araki T (1975b) Foggite, $(CaH_2O)_2(CaAl_2(OH)_4(PO_4)_2)$. Its atomic arrangement and relationship to calcium Tschermak's pyroxene. Am Mineral 60:965-971

Moore PB, Araki T, Kampf AR, Steele IM (1976) Olmsteadite, $K_2(Fe^{2+})_2((Fe^{2+})_2((Nb^{6+})(Ta^{6+}))_2O_4(H_2O)_4(PO_4)_4)$, a new species, its crystal structure and relation to vauxite and montgomeryite. Am Mineral 61:5-11

Moore PB, Araki T, Kampf AR (1980) Nomenclature of the phosphoferrite structure type: refinements of landesite and kryzhanovskite. Mineral Mag 43:789-795

Moore PB, Araki T, Merlino S, Mellini M, Zanazzi PF (1981) The arrojadite-dickinsonite series, $KNa_4Ca(Fe,Mn)^{2+}{}_{14}Al(OH)_2(PO_4)_{12}$: crystal structure and crystal chemistry. Am Mineral 66:1034-1049

Moore PB, Araki T, Steele IM, Swihart GH, Kampf AR (1983) Gainesite, sodium zirkonium beryllophosphate: a new mineral and its crystal structure. Am Mineral 68:1022-1028

Moring J, Kostiner E (1986) The crystal structure of $NaMnPO_4$. J Sol State Chem 61:379-383

Mrose ME (1971) Dittmarite. US Geol Surv Prof Pap 750-A:A115

Mücke A (1979) Keckit, $(Ca,Mg)(Mn,Zn)_2Fe^{3+}{}_3[(OH)_3(PO_4)_4]\cdot 2H_2O$, ein neues Mineral von Hagendorf/Opf, und seine genetische Stellung. N Jahrb Mineral Abh 134:183-192

Mücke A (1983) Wilhelmvierlingite, (Ca,Zn)$MnFe^{3+}[OH(PO_4)_2]\cdot 2H_2O$, a new mineral from Hagendorf/Oberpfalz. Aufschluss 34:267-274

Mücke A (1988) Lehnerit, $Mn[UO_2/PO_4]_2\cdot 8H_2O$, ein neues Mineral aus dem Pegmatit von Hagendorf/Oberpfalz. Aufschluss 39:209-217

Muto T, Meyrowitz R, Pommer AM, Murano T (1959) Ningyoite, a new uranous phosphate mineral from Japan. Am Mineral 44:633-650

Ng HN, Calvo C (1976) X-ray study of the alpha-beta transformation of berlinite, $AlPO_4$. Can J Phys 54:638-647

Ni YX, Hughes JM, Mariano AN (1995) Crystal chemistry of the monazite and xenotime structures. Am Mineral 80:21-26

Nord AG, Kierkegaard P (1968) The crystal structure of $Mg_3(PO_4)_2$. Acta Chem Scand 22:1466-1474

Nriagu JO (1984) Phosphate minerals: Their properties and general modes of occurrence. *In* Phosphate Minerals. Nriagu JO, Moore PB (eds) Springer-Verlag, Berlin, p 1-136

Olsen EJ, Steele IM (1997) Galileiite: a new meteoritic phosphate mineral. Meteor Planet Sci 32: A155-A156

Ono Y, Yamada N (1991) A structural study of the mixed crystal $K_{0.77}(NH_4)_{0.23}H_2PO_4$. J Phys Soc Japan 60:533-538

Ovchinnikov VE, Solov'eva LP, Pudovkina ZV, Kapustin YuL, Belov NV (1980) The crystal structure of kovdorskite $Mg_2(PO_4)(OH)(H_2O)_3$. Dokl Akad Nauk SSSR 255:351-354

Owens JP, Altschuler ZS, Berman R (1960) Millisite in phosphorite from Homeland, Florida. Am Mineral 45:547-561

Pajunen A, Lahti SI (1984) The crystal structure of viitaniemiite. Am Mineral 69:961-966

Pajunen A, Lahti SI (1985) New data on lacroixite, $NaAlFPO_4$. II. Crystal structure. Am Mineral 70: 849-855

Pauling LS (1929) The principles determining the structure of complex ionic crystals. J Am Chem Soc 51:1010-1026

Pauling L (1960) The nature of the chemical bond. 3rd ed. Cornell University Press, Ithaca, New York

Pavlov PV, Belov NV (1957) The crystal structures of herderite, datolite and gadolinite. Dokl Akad Nauk SSSR 114:884-887

Peacor DR, Dunn PJ (1982) Petersite, a REE and phospahte analogue of mixite. Am Mineral 67:1039-1042

Peacor DR, Dunn PJ, Simmons WB (1983) Ferrostrunzite, the ferrous iron analogue of strunzite from Mullica Hill, New Jersey N Jahrb Mineral Monatsh 524-528

Peacor DR, Dunn PJ, Simmons WB (1984) Earlshannonite, the Mn analogue of whitmoreite, from North Carolina. Can Mineral 22:471-474

Peacor DR, Rouse RC, Ahn T-H (1987) Crystal structure of tiptopite, a framework beryllophosphate isotypic with basic cancrinite. Am Mineral 72:816-820

Peacor DR, Rouse RC, Coskren TD, Essene EJ (1999) Destinezite ("diadochite"), $Fe_2(PO_4)(SO_4)$-$(OH)\cdot 6(H_2O)$: Its crystal structure and role as a soil mineral at Alum Cave Bluff, Tennessee. Clays Clay Mineral 47:1-11

Pekov IV, Kulikova IM, Kabalov YuK, Eletskaya OV, Chukanov NV, Menshikov YuP, Khomyakov AP (1996) Belovite-(La), $Sr_3Na(La,Ce)[PO_4]_3(F,OH)$—a new rare earth mineral in the apatite group. Zap Vser Mineral Obshch 125:101-109 (in Russian)

Piret P, Declercq J-P (1983) Structure cristalline de l'upalite $Al((UO_2)_3O(OH)(PO_4)_2\cdot 7(H_2O)$. Un exemple de macle mimetique. Bull Minéral 106:383-389

Piret P, Deliens M (1981) New data on holotype bergenite. Bull Mineral 104:16-18

Piret P, Deliens M (1982) La Vanmeersscheite, $U(UO_2)_3(PO_4)_2(OH)_6\cdot 4H_2O$ et la meta-vanmeersscheite, $U(UO_2)_3(PO_4)_2(OH)_6\cdot 2H_2O$, nouveaux mineraux. Bull Minéral 105:125-128

Piret P, Deliens M (1987) Les phosphates d'uranyle et d'aluminium de Kobokobo IX. L'althupite $AlTh(UO_2)((UO_2)_3O(OH)(PO_4)_2)_2(OH)_3(H_2O)_{15}$, nouveau mineral; proprietes et structure crystalline. Bull Minéral 110:65-72

Piret P, Deliens M (1988) Description of ludjibaite, a polymorph of pseudomalachite, $Cu_5(PO_4)_2(OH)_4$. Bull Minéral 111:167-171

Piret P, Piret-Meunier J (1988) Nouvelle determination de la structure cristalline de la dumontite $Pb_2((UO_2)_3O_2(PO_4)_3)(H_2O)5)$ Bull Minéral 111:439-442

Piret P, Piret-Meunier J, Declercq JP (1979) Structure of phuralumite. Acta Crystallogr B35:1880-1882

Piret P, Deliens M, Piret-Meunier J (1985) Occurrence and crystal structure of kipushite, a new copper-zinc phosphate from Kipushi, Zaire. Can Mineral 23:35-42

Piret P, Deliens M, Piret-Meunier J (1988) La francoisite-(Nd), nouveau phosphate d'uranyle et de terres rares; proprietes et structure crystalline. Bull Minéral 111:443-449

Piret P, Piret-Meunier J, Deliens M (1990) Composition chimique et structure cristalline de la dewindtite $Pb_3(H(UO_2)_3O_2(PO_4)_2)_2\cdot 12H_2O$. Eur J Mineral 2:399-405

Popova VI, Popov VA, Sokolova EV, Ferraris G, Chukanov NV (2001) Kanonerovite $MnNa_3P_3O_{10}\cdot 12H_2O$, first triphosphate mineral (Kazennitsa, Middle Urals, Russia). N Jahrb Mineral Monatsh 117-127

Potenza MF (1958) Autunite e metatorbernite nella Sienite di Biella. Rend Soc Mineral Ital 14:215-223

Pring A, Birch WD (1993) Gatehouseite, a new manganese hydroxy phosphate from Iron Monarch, South Australia. 57:309-313

Pring A, Birch WD, Dawe J, Taylor M, Deliens M, Walenta K (1995) Kintoreite, $PbFe_2(PO_4)_2(OH,H_2O)_6$, a new mineral of the jarosite-alunite family, and lusungite discredited. Mineral Mag 59:143-148

Pring A, Kolitsch U, Birch WD, Beyer BD, Elliott P, Ayyappan P, Ramanan A (1999) Bariosincosite, a new hydrated barium vanadium phosphate, from the Spring Creek mine, South Australia. Mineral Mag 63:735-741

Raade G, Roemming C, Medenbach O (1998) Carbonate-substituted phosphoellenbergerite from Modum, Norway: description and crystal structure. Mineral Petrol 62:89-101

Radoslovich EW, Slade PG (1980) Pseudo-trigonal symmetry and the structure of gorceixite. N Jahrb Mineral Monatsh 157-170

Rastsvetaeva RK (1971) Kristallicheskaya struktura lomonosovita $Na_5Ti_2(Si_2O_7)(PO_4)O_2$. Dokl Akad Nauk SSSR 197:81-84

Rastsvetsaeva RK, Khomyakov AP (1996) Crystal structure of deloneite-(Ce), the highly ordered Ca analogue of belovite. Dokl Ross Akad Nauk 349:354-357 (in Russian)

Richardson JM, Roberts AC, Grice JD, Ramik RA (1988) Mcauslanite, a supergene hydrated iron aluminum fluorophosphate from the East Kemptville tin mine, Yarmouth County, Nova Scotia. Can Mineral 26: 917-921

Rídkosil T, Sejkora J, Šrein VL (1996) Smrkovecite, monoclinic $Bi_2O(OH)(PO_4)$, a new mineral of the atelesite group. N Jahrb Mineral Monatsh 97-102

Rinaldi R (1978) The crystal structure of griphite, a complex phosphate, not a garnetoid. Bull Minéral 101: 543-547

Rius J, Louër D, Mouër M, Galí S, Melgarejo JC (2000) Structure solution from powder data of the phosphate hydrate tinticite. Eur J Mineral 12:581-588

Roberts AC, Dunn PJ, Grice JD, Newbury DE, Roberts WL (1988) The X-ray crystallography of tavorite from the Tip Top pegmatite, Custer, South Dakota. Powder Diffraction 3:93-95

Roberts AC, Sturman BD, Dunn PJ, Roberts WL (1989) Pararobertsite, $Ca_2Mn^{3+}{}_3(PO_4)_3O_2\cdot 3H_2O$, a new mineral species form the Tip Top pegmatite, Custer Country, South Dakota, and its relationship to robertsite. Can Mineral 27:451-455

Roca M, Marcos MD, Amorós P, Alamo J, Beltrán-Porter A, Beltrán-Porter D (1997) Synthesis and crystal structure of a novel lamellar barium derivative: $Ba(VOPO_4)_2\cdot 4H_2O$. Synthetic pathways for layered oxovanadium phosphate hydrates $M(VOPO_4)_2\cdot nH_2O$. Inorg Chem 36:3414-3421

Romming C, Raade G (1980) The crystal structure of althausite, $Mg_4(PO_4)_2(OH,O)F$. Am Mineral 65: 488-498

Romming C, Raade G (1986) The crystal structure of heneuite, $CaMg_5(CO_3)(PO_4)_3(OH)$. N Jahrb Mineral Monatsh 351-359

Romming C, Raade G (1989) The crystal structure of natural and synthetic holtedahlite. Mineral Petrol 40: 91-100

Rose D (1980) Brabantite, $CaTh[PO_4]_2$, a new mineral of the monazite group. N Jahrb Mineral Monatsh 247-257

Ross V (1956) Studies of uranium minerals XXII: Synthetic calcium and lead uranyl phosphate minerals. Am Mineral 41:915-926

Rouse RC, Peacor DR, Freed RL (1988) Pyrophosphate groups in the structure of canaphite, $CaNa_2P_2O_7.4(H_2O)$: The first occurrence of a condensed phosphate as a mineral. Am Mineral 73: 168-171

Rouse RC, Peacor DR, Merlino S (1989) Crystal structure of pahasapaite, a beryllophosphate mineral with a distorted zeolite rho framework. Am Mineral 74:1195-1202

Sakae T, Nagata H, Sudo T (1978) The crystal structure of synthetic calcium phosphate sulfate hydrate, $Ca_2(HPO_4)(SO_4)(H_2O)_4$, and its relation to brushite and gypsum. Am Mineral 63:520-527

Sales BC, Chakoumakos BC, Boatner LA, Ramey JO (1993) Structural properties of the amorphous phases produced by heating crystalline $MgHPO_4\cdot 3H_2O$. J Non-Crystalline Solids 159:121-139

Schindler M, Hawthorne FC (2001a) A bond-valence approach to the structure, chemistry and paragenesis of hydroxy-hydrated oxysalt minerals: I. Theory. Can Mineral 39:1225-1242

Schindler M, Hawthorne FC (2001b) A bond-valence approach to the structure, chemistry and paragenesis of hydroxy-hydrated oxysalt minerals: II. Crystal structure and chemical composition of borate minerals. Can Mineral 39:1243-1256

Schindler M, Hawthorne FC (2001c) A bond-valence approach to the structure, chemistry and paragenesis of hydroxy-hydrated oxysalt minerals: III. Paragenesis of borate minerals. Can Mineral 39:1257-1274

Schindler M, Huminicki DMC, Hawthorne FC (2002) A bond-valence approach to the chemical composition and occurrence of sulfate minerals. Chem Geol (submitted)

Schlüter J, Klaska K-H, Friese K, Adiwidjaja G (1999) Kastningite, $(Mn,Fe,Mg)Al_2(PO_4)_2(OH)_2 \cdot 8H_2O$, a new phosphate mineral from Waidhaus, Bavaria, Germany. N Jahrb Mineral Monatsh 40-48

Sebais M, Dorokhova GI, Pobedimskaya EA, Khomyakov AP (1984) The crystal structure of nefedovite and its typomorphism. Dokl Akad Nauk SSSR 278:353-357

Selway JB, Cooper MA, Hawthorne FC (1997) Refinement of the crystal structure of burangaite. Can Mineral 35:1515-1522

Sen Gupta PK, Swihart GH, Dimitrijevic R, Hossain MB (1991) The crystal structure of lueneburgite, $Mg_3(H_2O)_6(B_2(OH)_6(PO_4)_2)$. Am Mineral 76:1400-1407

Sergeev AS (1964) Pseudo-autunite, a new hydrous calcium phosphate. Mineral Geokhim 1:31-39 (in Russian)

Shannon RD (1976) Revised effective ionic radii and systematic studies of interatomic distances in halides and chalcogenides. Acta Crystallogr A32:751-767

Shen J, Peng Z (1981) The crystal structure of furongite. Acta Crystallogr A37, supp C-186

Shoemaker GL, Anderson JB, Kostiner E (1977) Refinement of the crystal structure of pseudomalachite. Am Mineral 62:1042-1048

Shoemaker GL, Anderson JB, Kostiner E (1981) The crystal structure of a third polymorph of $Cu_5(PO_4)_3(OH)_4$. Am Mineral 66:169-181

Sieber NHW, Tillmanns E, Medenbach O (1987) Hentschelite, $CuFe_2(PO_4)_2(OH)_2$, a new member of the lazulite group, and reichenbachite, $Cu_5(PO_4)_2(OH)_4$, a polymorph of pseudomalachite, two new copper phosphate minerals from Reichenbach, Germany. Am Mineral 72:404-408

Simonov MA, Egorov-Tismenko YK, Belov NV (1980) Use of modern X-ray equipment to solve fine problems of structural mineralogy by the example of the crystal RE of structure of babefphite $BaBe(PO_4)F$. Kristallografiya 25:55-59 (in Russian)

Slavik F (1914) Neue Phosphate vom Greifenstein bei Ehrenfriedersdorf. Ak Ceská, Bull intern ac sci Bohême 19:108-123

Sljukic M, Matkovic B, Prodic B, Anderson D (1969) The crystal structure of $KZr_2(PO_4)_3$. Z Kristallogr 130:148-161

Soboleva MV, Pudovkina IA (1957) Mineralogy of Uranium Handbook. Moscow: Dept Tech Lit USSR

Sokolova EV, Egorov-Tismenko YuK (1990) Crystal structure of girvasite. Dokl Akad Nauk SSSR 311: 1372-1376

Sokolova EV, Hawthorne FC (2001) The crystal chemistry of the $[M_3\phi_{11\text{-}14}]$ trimeric structures: from hyperagpaitic complexes to saline lakes. Can Mineral 39:1275-1294

Sokolova EV, Khomyakov AP (1992) Crystal structure of a new mineral, $Na_3Sr(PO_4)(CO_3)$, from the bredliit group. Dokl Akad Nauk SSSR 322:531-535

Sokolova EV, Yamnova NA, Egorov-Tismenko YK, Khomyakov AP (1984a) The crystal structure of a new phosphate of Na, Ca and $Ba(Na_5Ca)Ca_6Ba(PO_4)_6F_3$. Dokl Akad Nauk SSSR 274:78-83

Sokolova EV, Egorov-Tismenko YK, Yamnova NA, Simonov MA (1984b) The crystal structure of olgite $Na(Sr_{0.52}Ba_{0.48})(Sr_{0.58}Na_{0.42})(Na_{0.81}Sr_{0.19})(PO_{3.40})(P_{0.76}O_{3.88})$. Kristallografiya 29:1079-1083

Sokolova EV, Egorov-Tismenko YuK, Khomyakov AP (1987a) Crystal structure of lomonosovite and sulfohalite as a homolog of the structures of $Na_{14}CaMgTi_4(Si_2O_7)_2(PO_4)_4O_4F_2$. Mineral Z 9:28-35

Sokolova EV, Egorov-Tismenko YK, Khomyakov AP (1987b) Crystal structure of $Na_{17}Ca_3Mg(Ti,Mn)_4(Si_2O_7)_2(PO_4)_3O_2F_6$, a new representative of the family of layered titanium silicates. Dokl Akad Nauk SSSR 294:357-362

Sokolova EV, Egorov-Tismenko YuK, Khomyakov AP (1988) Crystal structure of sobolevite, Sov Phys Dokl 33:711-714

Sokolova EV, Hawthorne FC, McCammon C, Liferovich RP (2001) The crystal structure of gladiusite, $(Fe^{2+},Mg)_4Fe^{3+}{}_2(PO_4)(OH)_{11}(H_2O)$. Can Mineral 39:1121-1130

Steele IM, Olsen E, Pluth J, Davis AM (1991) Occurrence and crystal structure of Ca-free beusite in the El Sampal IIIA iron meteorite. Am Mineral 76:1985-1989

Stergiou AC, Rentzeperis PJ, Sklavounos S (1993) Refinement of the crystal structure of metatorbernite. Z Kristallogr 205:1-7

Street RLT, Whitaker A (1973) The isostructurality of rosslerite and phosphorosslerite. Z Kristallgr 137: 246-255

Sturman BD, Mandarino JA, Mrose ME, Dunn PJ (1981a) Gormanite, $Fe^{2+}{}_3Al_4(PO_4)_4(OH)_6 \cdot 2H_2O$, the ferrous analogue of souzalite, and new data for souzalite. Can Mineral 19:381-387

Sturman BD, Peacor DR, Dunn PJ (1981b) Wicksite, a new mineral from northeastern Yukon Territory. Can Mineral 19:377-380

Sutor DJ (1967) The crystal and molecular structure of newberyite, $MgHPO_4(H_2O)_3$. Acta Crystallogr 23: 418-422

Szymanski JT, Roberts AC (1990) The crystal structure of voggite, a new hydrated Na-Zr hydroxide-phosphate-carbonate mineral. Mineral Mag 54:495-500

Tadini C (1981) Magniotriplite: its crystal structure and relation to the triplite-triploidite group. Bull Minéral 104:677-680

Takagi S, Mathew M, Brown WE (1986) Crystal structures of bobierrite and synthetic $Mg_3(PO_4)_2(H_2O)_8$. Am Mineral 71:1229-1233

Taxer KJ (1975) Structural investigations on scholzite. Am Mineral 60:1019-1022

Taxer KJ, Bartl H (1997) Die "geordnete gemittelte" Kristallstruktur von Parascholzit. Zur Dimorphie von $CaZn_2(PO_4)_2{\cdot}2(H_2O)$, Parascholzit-Scholzit. Z Kristallogr 212:197-202

van der Westhuizen WA, deBruiyn H, Beukes GJ, Strydom D (1990) Dufrenite in iron-formation on the Kangnas farm, Aggeneys district, Bushmanland, South Africa. Mineral Mag 54:419-424

van Tassel R (1968) Données cristallographiques sur la koninckite. Bull Minéral 91:487-489

van Wambeke L (1972) Eylettersite, un nouveau phosphate de thorium appartenant à la série de la crandallite. Bull Mineral 95:98-105

van Wambeke L (1975) La zairite, un nouveau minéral appartenant à la serie de la crandallite. Bull Minéral 98:351-353

Vencato I, Mattievich E, Mascarenhas YP (1989) Crystal structure of synthetic lipscombite: A redetermination. Am Mineral 74:456-460

Vochten RD, De Grave E (1981) Crystallographic, Mössbauer, and electrokinetic study of synthetic lipscombite. Phys Chem Minerals 7:197-203

Vochten R, Pelsmaekers J (1983) Synthesis, solubility, electrokinetic properties and refined crystallographic data of sabugalite. Phys Chem Mineral 9:23-29

Vochten RF, van Acker P, De Grave E (1983) Mössbauer, electrokinetic and refine parameters study of synthetic manganoan lipscombite. Phys Chem Minerals 9:263-268

Vochten R, de Grave E, Pelsmaekers J (1984) Mineralogical study of bassetite in relation to its oxidation. Am Mineral 69:967-978

Voloshin AV, Pakhomovskiy YuA, Tyusheva FN (1983) Lun'okite; a new phosphate, the manganese analog of overite from granitic pegmatites of the Kola Peninsula. Int Geol Rev 25:1131-1136

Voloshin AV, Pakhomovskii YaA, Tyusheva EN (1992) Manganosegelerite (Mn,Ca)(Mn,Fe,Mg)-$Fe^{3+}(PO_4)_2(OH)\circ 4H_2O$-a new phosphate of the overite group from granitic pegmatites of the Kola Peninsula. Zap Vser Mineral Obshch 121:95-103

von Knorring O, Fransolet A-M (1977) Gatumbaite, $CaAl_2(PO_4)_2(OH)_2{\cdot}H_2O$: a new species from Buranga pegmatite, Rwanda. N Jahrb Mineral Monatsh 561-568

von Knorring O, Mrose ME (1966) Bertossaite, $(Li,Na)_2(Ca,Fe,Mn)Al_4(PO_4)_4(OH,F)_4$, a new mineral from Rwanda (Africa). Can Mineral 8:668

Waldrop L (1968a) Crystal structure of triplite. Naturwiss 55:178

Waldrop L (1968b) Crystal structure of triploidite. Naturwiss 55:296-297

Waldrop L (1970) The crystal structure of triploidite and its relations to the structures of other minerals of the triplite-triploidite group. Z Kristallogr 131:1-20

Walenta K (1978) Uranospathite and arsenuranospathite. Mineral Mag 42:117-28

Walenta K, Dunn PJ (1984) Phosphofibrite, ein neues Eisenphosphat aus der Grube Clara im mittleren Schwarzwald (BRD) Chem Erde 43:11-16

Walenta K, Theye T (1999) Haigerachit, ein neues Phosphatmineral von der Grube Silberbrünnle bei Gengenbach im mittleren Schwarzwald. Aufschluss 50:1-7

Walenta K, Birch WD, Dunn PJ (1996) Benauite, a new mineral of the crandallite group from the Clara mine in the central Black Forest, Germany. Chem Erde 56:171-176

Walter F (1992) Weinebeneite, $CaBe_3(PO_4)_2(OH)_2{\cdot}4(H_2O)$, a new mineral species: mineral data and crystal structure. Eur J Mineral 4:1275-1283

Warner JK, Cheetham AK, Nord AG, von Dreele RB, Yethiraj M (1992) Magnetic structure of iron(II) phosphate, sarcopside, $Fe_3(PO_4)_2$. J Mater Chem 2:191-196

White JS Jr, Henderson EP, Mason B (1967) Secondary minerals produced by weathering of the Wolf Creek meteorite. Am Mineral 52:1190-1197

White JS Jr, Leavens PB, Zanazzi PF (1986) Switzerite redefined as $Mn_3(PO_4)_2{\cdot}7H_2O$, and metaswitzerite, $Mn_3(PO_4)_2{\cdot}4H_2O$. Am Mineral 71:1221-1223

Wiench DM, Jansen M (1983) Kristallstruktur von wasserfreiem Na_2HPO_4. Z Anorg Allg Chem 501: 95-101

Wise MA, Hawthorne FC, ČCernyý P (1990) Crystal structure of a Ca-rich beusite from the Yellowknife pegmatite field, Northwest Territories. Can Mineral 28:141-146

Witzke T, Wegner R, Doering T, Pöllmann H, Schuckmann W (2000) Serrabrancaite, $MnPO_4{\cdot}H_2O$, a new mineral from the Alto Serra Branca pegmatite, Pedra Lavrada, Paraiba, Brazil. Am Mineral 85: 847-849

Yakubovich OV, Mel'nikov OK (1993) Libethenite $Cu_2(PO_4)(OH)$: Synthesis, crystal structure refinement, comparative crystal chemistry. Kristallografiya 38:63-70

Yakubovich OV, Urusov VS (1997) Electron density distribution in lithiophosphatite Li_3PO_4: Crystallochemical features of orthophosphates with hexagonal close packing. Kristallografiya 42: 301-308

Yakubovich OV, Simonov MA, Belov NV (1977) The crystal structure of a synthetic triphylite $LiFe(PO_4)$. Dokl Akad Nauk SSSR 235:93-95

Yakubovich OV, Simonov MA, Matvienko EN, Belov NV (1978) The crystal structure of the synthetic finite Fe-term of the series triplite B zwieselite $Fe_2(PO_4)$ F. Dokl Akad Nauk SSSR 238:576-579

Yakubovich OV, Massa W, Liferovich RP, Pakhomovsky YA (2000) The crystal structure of bakhchisaraitsevite, $[Na_2(H_2O)_2]$ $\{(Mg_{4.5}Fe_{0.5})(PO_4)_4(H_2O)_5\}$, a new mineral species of hydrothermal origin from the Kovdor phoscorite-carbonatite complex, Russia. Can Mineral 38:831-838

Yakubovich OV, Massa W, Liferovich RP, McCammon CA (2001) The crystal structure of barićite, $(Mg_{1.70}Fe_{1.30})(PO_4)_2{\cdot}8H_2O$, the magnesium-dominant member of the vivianite group. Can Mineral 39: 1317-1324

Young EJ, Weeks AD, Meyrowitz R (1966) Coconinoite, a new uranium mineral from Utah and Arizona. Am Mineral 51:651-663

Zanazzi PF, Leavens PB, White JS (1986) Crystal structure of switzerite, $Mn_3(PO_4)_2(H_2O)_7$ and its relationship to metaswitzerite, $Mn_3(PO_4)_2(H_2O)_4$. Am Mineral 71:1224-1228

Zhang J, Wan A, Gong W (1992) New data on yingjiangite. Acta Petrol Mineral 11:178-184

Zhesheng M, Nicheng S, Zhizhong P (1983) Crystal structure of a new phosphatic mineral—qingheiite. Scientia Sinica (Series B) 25:876-884

Zolensky ME (1985) New data on sincosite. Am Mineral 70:409-410

Zoltai T (1960) Classification of silicates and other minerals with tetrahedral structures. Am Mineral 45: 960-973

Zwaan PC, Arps CES, de Grave E (1989) Vochtenite, $(Fe^{2+},Mg)(Fe^{3+}[UO_2/PO_4]_4(OH){\cdot}12\text{-}13H_2O$, a new uranyl phosphate mineral from Wheal Basset, Redruth, Cornwall, England. Mineral Mag 53:473-478

APPENDIX

A tabulation of data and references for selected phosphate minerals

(on the following 17 pages)

APPENDIX. Data and references for selected phosphate minerals.

Mineral Name	Formula	*a* (Å)	*b* (Å)	*c* (Å)	α (°)	β (°)	γ (°)	Space Group	Ref.
Abenakiite-(Ce)	$Na_{26}(Ce_3Nd_2La)(SO_2)(SiO_3)_6(PO_4)_6(CO_3)_6$	16.018(2)	*a*	19.761(4)	90	90	120	$R\bar{3}$	(1)
Aheylite	$Fe^{2+}Al_6(PO_4)_4(OH)_8(H_2O)_4$	7.400(1)	9.896(1)	7.627(1)	110.87	115.00	69.96	$P\bar{1}$	(2)
Aldermanite	$Mg_5Al_{12}(PO_4)_8(OH)_{22}(H_2O)_{32}$	15.000(7)	8.330(6)	2.660(1)	90	90	90	*P* - - -	(3)
Alforsite	$Ba_5(PO_4)_3Cl$	10.284(2)	*a*	7.651(3)	90	90	120	$P6_3/m$	(4)
Alluaudite	$(Na,Ca)[Fe^{2+}(Mn^{2+},Fe^{2+},Fe^{3+},Mg)_2(PO_4)_3]$	12.004(2)	12.533(4)	6.404(1)	90	114.4(1)	90	*C*2/*c*	(5)
Althausite	$Mg_4(PO_4)_2(OH)F$	8.258(2)	6.054(2)	14.383(5)	90	90	90	*Pnma*	(6)
Althupite	$AlTh(UO_2)[(UO_2)_3(PO_4)_2O(OH)]_2(OH)_3(H_2O)_{15}$	10.953(3)	18.567(4)	13.504(3)	72.6(0)	68.2(0)	84.2(0)	$P\bar{1}$	(7)
Amblygonite	$Li[Al(PO_4)F]$	5.060	5.160	7.080	109.9	107.5	97.9	$P\bar{1}$	(8)
Anapaite	$Ca_2[Fe^{2+}(PO_4)_2(H_2O)_4]$	6.477(1)	6.816(1)	5.898(1)	101.64(3)	104.24(3)	70.76(4)	$P\bar{1}$	(9)
Archerite	$K[H_2(PO_4)]$	7.427(2)	*a*	7.046(2)	90	90	90	$I\bar{4}2d$	(10)
Arctite	$(Na_5Ca)Ca_6Ba(PO_4)_6F_3$	14.366(9)	*a*	14.366(9)	28.6(0)	28.6(0)	28.6(0)	$R\bar{3}m$	(11)
Ardealite	$Ca_2(PO_3\{OH\})(SO_4)(H_2O)_4$	5.721(5)	30.992(5)	6.250(4)	90	117.3(1)	90	*Cc*	(12)
Arrojadite	$KNa_4CaMn^{2+}{}_4Fe^{2+}{}_{10}Al(PO_4)_{12}(OH)_2$	16.526(4)	10.057(3)	24.730(5)	90	105.8	90	*C*2/*c*	(13)
Arupite	$Ni_3(PO_4)_2(H_2O)_8$	9.889	13.225	4.645	90	102.41	90	*I*2/*m*	(14)
Attakolite	$CaMn^{2+}Al_4(SiO_3\{OH\})(PO_4)_3(OH)_4$	17.188(4)	11.477(8)	7.322(5)	90	113.8(0)	90	*C*2/*m*	(15)
Augelite	$[Al_2PO_4(OH)_3]$	13.124(6)	7.988(5)	5.066(3)	90	112.3(0)	90	*C*2/*m*	(16)
Autunite	$Ca[(UO_2)(PO_4)]_2(H_2O)_{10\text{-}12}$	7.027	*a*	20.790	90	90	90	*I*4/*mmm*	(17)
Babefphite	$Ba[BePO_4F]$	6.889(3)	16.814(7)	6.902(3)	90.0(0)	90.0(0)	90.3(0)	*F*1	(18)
Bakhchisaraitsevite	$Na_2Mg_5(PO_4)_4(H_2O)_7$	8.3086(8)	12.906(1)	17.486(2)	90	102.01(1)	90	$P2_1/c$	(19)
Barbosalite	$Fe^{2+}[Fe^{3+}(PO_4)(OH)]_2$	7.250(20)	7.460(20)	7.490(20)	90	120.2(85)	90	$P2_1/c$	(20)
Baričite	$Mg_3(PO_4)_2(H_2O)_8$	10.085(2)	13.390(3)	4.6713(9)	90	104.96(3)	90	*C*2/*m*	(21)
Bariosincosite	$Ba(V^{4+}OPO_4)_2(H_2O)_4$	9.031(6)	*a*	12.755(8)	90	90	90	*P*4/*nmm*	(22)
Bassetite	$Fe^{2+}[(UO_2)(PO_4)]_2(H_2O)_8$	6.98(4)	17.07(4)	7.01(7)	90	90.53(1)	90	$P2_1/m$	(23)
Bearthite	$Ca_2Al(PO_4)_2(OH)$	7.231(3)	5.734(2)	8.263(4)	90	112.6(1)	90	$P2_1/m$	(24)
Bederite	$Ca_2(Mn^{2+}{}_2Fe^{3+}{}_2Mn^{3+}{}_2)(PO_4)_6(H_2O)_2$	12.559(2)	12.834(1)	11.714(2)	90	90	90	*Pcab*	(25)
Belovite-(Ce)	$Sr_3NaCe(PO_4)_3(OH)$	9.664(0)	*a*	7.182(0)	90	90	120	$P\bar{3}$	(26)
Belovite-(La)	$Sr_3NaLa(PO_4)_3F$	9.647	*a*	7.170	90	90	120	$P\bar{3}$	(27)

APPENDIX continued

Mineral Name	Formula	*a* (Å)	*b* (Å)	*c* (Å)	α (°)	β (°)	γ (°)	Space Group	Ref.
Benauite	$HSrFe^{3+}_3(PO_4)_2(OH)_6$	7.28	*a*	16.85	90	90	120	$R\bar{3}m$	(28)
Benyacarite	$(H_2O,K)_2TiMn^{2+}_2(Fe^{3+},Ti)_2(PO_4)_4(OH)_2(H_2O)_{14}$	10.561(5)	20.585(8)	12.516(2)	90	90	90	*Pbca*	(29)
Beraunite	$Fe^{2+}Fe^{3+}_5(PO_4)_4(OH)_5(H_2O)_6$	20.646(5)	5.129(7)	19.213(5)	90	93.62(7)	90	*C*2/*c*	(30)
Bergenite	$Ba[(UO_2)_3O_2(PO_4)_2](H_2O)_{6.5}$	22.32	17.19	20.63	90	93.0	90	$P2_1/c$	(31)
Berlinite	$[Al(PO_4)]$	4.943(0)	*a*	10.948(0)	90	90	120	$P3_12$	(32)
Bermanite	$Mn^{2+}[Mn^{3+}(PO_4)(OH)]_2(H_2O)_4$	5.446(3)	19.250(10)	5.428(3)	90	110.3(0)	90	$P2_1$	(33)
Bertossaite	$CaLi_2[Al(PO_4)(OH)]_4$	11.48(1)	15.73(2)	7.23(1)	90	90	90	*I*aa*	(34)
Beryllonite	$Na[BePO_4]$	8.178(3)	7.818(2)	14.114(6)	90	90	90	$P2_1/n$	(35)
Beusite	$(Mn^{2+},Fe^{2+})_3(PO_4)_2$	8.757(3)	11.381(4)	6.136(1)	90	99.1(0)	90	$P2_1/c$	(36)
Biphosphammite	$(NH_4)H_2PO_4$	7.514(0)	*a*	7.539(1)	90	90	90	$I\bar{4}2d$	(37)
Bjarebyite	$BaMn_2Al_2(OH)_3(PO_4)_3$	8.930(14)	12.073(24)	4.917(9)	90	100.2(1)	90	$P2_1/m$	(38)
Bleasdaleite	$(Ca,Fe^{3+})_2Cu^{2+}_5(Bi,Cu^{2+})(PO_4)_4(H_2O,OH,Cl)_{13}$	14.200(7)	13.832(7)	14.971(10)	90	102.08(8)	90	*C*2/*m*	(39)
Bobfergusonite	$Na_2Mn^{2+}_5Fe^{3+}Al(PO_4)_6$	12.776(2)	12.488(2)	11.035(2)	90	97.2(0)	90	$P2_1/n$	(40)
Bobierrite	$Mg_3(PO_4)_2(H_2O)_8$	4.667(1)	27.926(8)	10.067(3)	90	105.0(0)	90	*C*2/*c*	(41)
Böggildite	$Sr_2Na_2Al_2(PO_4)F_9$	5.251(3)	10.464(5)	18.577(9)	90	107.5(0)	90	$P2_1/c$	(42)
Bolivarite	$Al_2(PO_4)(OH)_3(H_2O)_4$	Amorphous	-	-	-	-	-	-	(43)
Bonshtedtite	$Na_3Fe^{2+}(PO_4)(CO_3)$	8.921	6.631	5.151	90	90.42	90	$P2_1/m$	(44)
Brabantite	$CaTh(PO_4)_2$	6.726(6)	6.933(5)	6.447(12)	90	103.89(3)	90	$P2_1$	(45)
Bradleyite	$Na_3Sr(PO_4)(CO_3)$	9.187(3)	5.279(1)	6.707(2)	90	90	90	$P2_1$	(46)
Brazilianite	$NaAl_3(PO_4)_2(OH)_4$	11.233(6)	10.142(5)	7.097(4)	90	97.4(0)	90	$P2_1/n$	(47)
Brendelite	$Bi^{3+}Fe^{3+}O_2(OH)(PO_4)$	12.278(2)	3.185(1)	6.899(1)	90	111.0(0)	90	*C*2/*m*	(48)
Brianite	$Na_2Ca[Mg(PO_4)_2]$	9.120(3)	5.198(2)	13.370(4)	90	90.8(0)	90	$P2_1/c$	(49)
Brockite	$(Ca,Th,REE)(PO_4)(H_2O)$	6.98(3)	6.98(3)	6.40(3)	90	90	90	*Aa*	(50)
Brushite	$Ca(PO_3\{OH\})(H_2O)_2$	5.812(2)	15.180(3)	6.239(2)	90	116.4(0)	90	*Ia*	(51)
Buchwaldite	$NaCa(PO_4)$	20.397(10)	5.412(4)	9.161(5)	90	90	90	$Pn2_1a$	(52)
Burangaite	$Na_2Fe^{2+}_2Al_{10}(PO_4)_8(OH)_{12}(H_2O)_4$	25.099(2)	5.049(1)	13.438(1)	90	110.9(0)	90	*C*2/*c*	(53)
Cacoxenite	$Fe^{3+}_{25}(PO_4)_{17}O_6(OH)_{12}(H_2O)_{75}$	27.559(1)	*a*	10.550(1)	90	90	120	$P6_3/m$	(54)

APPENDIX continued

Mineral Name	Formula	*a* (Å)	*b* (Å)	*c* (Å)	α (°)	β (°)	γ (°)	Space Group	Ref.
Canaphite	$CaNa_2P_2O_7(H_2O)_4$	5.673(4)	8.480(10)	10.529(5)	90	106.13(6)	90	*Pc*	(55)
Cassidyite	$Ca_2[Ni(PO_4)_2(H_2O)_2]$	5.71	6.73	5.41	96.83	107.36	104.58	$P\bar{1}$	(56)
Chalcosiderite	$Cu^{2+}Fe^{3+}_6(PO_4)_4(OH)_8(H_2O)_4$	7.653(4)	7.873(4)	10.190(4)	67.6(0)	69.2(0)	64.9(0)	$P\bar{1}$	(57)
Cheralite-(Ce)	$Ce(PO_4)$	6.747(2)	6.960(2)	6.453(1)	90	103.7(0)	90	$P2_1/n$	(58)
Chernikovite	$(H_3O)[(UO_2)(PO_4)]_2(H_2O)_8$	7.030(6)	*a*	9.034(8)	90	90	90	*P*4/*nmm*	(59)
Childrenite	$Mn^{2+}[Al(PO_4)(OH)_2(H_2O)]$	10.395(1)	13.394(1)	6.918(1)	90	90	90	*Bba*2	(60)
Chladniite	$Na_2CaMg_7(PO_4)_6$	14.967(2)	*a*	42.595(4)	90	90	120	$R\bar{3}$	(61)
Chlorapatite	$Ca_5(PO_4)_3Cl$	9.620(1)	*a*	6.776(1)	90	90	120	$P6_3/m$	(62)
Churchite-(Y)	$Y(PO_4)(H_2O)_2$	5.578(1)	15.006(3)	6.275(2)	90	117.8(0)	90	*I*2/*a*	(63)
Clinophosinaite	$Na_3Ca(SiO_3)(PO_4)$	7.303(2)	12.201(5)	14.715(4)	90	91.9	90	*P*2/*c*	(64)
Coconinoite	$Fe^{3+}_2Al_2(UO_2)_6(PO_4)_4(SO_4)(OH)_2(H_2O)_{20}$	12.50	12.97	23.00	90	106.6	90	*C*2/*c*	(65)
Coeruleolactite	$CaAl_6(PO_4)_4(OH)_8(H_2O)_{4\text{-}5}$	Existence dubious		-	-	-	-	-	(2)
Collinsite	$Ca_2[Mg(PO_4)_2(H_2O)_2]$	5.734(1)	6.780(1)	5.441(1)	97.3(0)	108.6(0)	107.3(0)	$P\bar{1}$	(66)
Corkite	$PbFe^{3+}_3(SO_4)(PO_4)(OH)_6$	7.280(1)	*a*	16.821(1)	90	90	120	$R\bar{3}m$	(67)
Cornetite	$Cu^{2+}_3PO_4(OH)_3$	10.854(1)	14.053(3)	7.086(2)	90	90	90	*Pbca*	(68)
Crandallite	$CaAl_3(PO_4)_2(OH)_5(H_2O)$	7.006(15)	*a*	16.192(32)	90	90	120	$R\bar{3}m$	(69)
Crawfordite	$Na_3Sr(PO_4)(CO_3)$	9.187	6.707	5.279	90	90	90	$P2_1$	(70)
Curetonite	$BaAl(PO_4)(OH)F$	6.977(2)	12.564(4)	5.223(1)	90	102.2(0)	90	$P2_1/n$	(71)
Cyrilovite	$NaFe^{3+}_3(OH)_4(PO_4)_2(H_2O)_2$	7.3255(4)	*a*	19.328(2)	90	90	90	$P4_12_12$	(72)
Deloneite-(Ce)	$NaCr_2SrCe(PO_4)_3F$	9.51	*a*	7.01	90	90	120	*P*3	(73)
Delvauxite	$CaFe^{3+}_4(PO_4)_2(OH)_8(H_2O)_{4\text{-}6}$	Amorphous	-	-	-	-	-	-	(74)
Destinezite	$Fe^{3+}_2(PO_4)(SO_4)(OH)(H_2O)_6$	9.570(1)	9.716(1)	7.313(1)	98.7(0)	107.9(0)	63.9(0)	$P\bar{1}$	(75)
Dewindtite	$Pb^{2+}_3[H(UO_2)_3O_2(PO_4)_2]_2(H_2O)_{12}$	16.031(6)	17.264(6)	13.605(2)	90	90	90	*Bmmb*	(76)
Dickinsonite	$(Na,Ca)_5(Mn,Fe,Mg)_{14}Al(PO_4)_{12}(OH)_2$	24.940(6)	10.131(4)	16.722(2)	90	105.6(0)	90	*A*2/*a*	(77)
Dittmarite	$(NH_4)Mg(PO_4)(H_2O)$	5.606	8.758	4.788	90	90	90	$Pmn2_1$	(78)
Dorfmanite	$Na_2(PO_3\{OH\})(H_2O)_2$	16.872(9)	10.359(4)	6.599(3)	90	90	90	*Pbca*	(79)
Drugmanite	$Pb^{2+}_2Fe^{3+}H(PO_4)_2(OH)_2$	11.111(5)	7.986(5)	4.643(3)	90	90.4(0)	90	$P2_1/a$	(80)

APPENDIX continued

Mineral Name	Formula	*a* (Å)	*b* (Å)	*c* (Å)	α (°)	β (°)	γ (°)	Space Group	Ref.
Dufrénite	$Fe^{2+}Fe^{3+}_5(PO_4)_3(OH)_5(H_2O)_2$	25.840(20)	5.126(3)	13.780(10)	90	111.2(1)	90	*C*2/*c*	(81)
Dumontite	$Pb^{2+}_2[(UO_2)_3(PO_4)_2O_2](H_2O)_5$	8.118(6)	16.819(8)	6.983(3)	90	109.0(0)	90	$P2_1/m$	(82)
Earlshannonite	$Mn^{2+}[Fe^{3+}(PO_4)(OH)]_2(H_2O)_4$	9.910(13)	9.669(8)	5.455(9)	90	93.95(9)	90	$P2_1/c$	(83)
Ehrleite	$Ca_2ZnBe(PO_4)_2(PO_3OH)(H_2O)_4$	7.130(4)	7.430(4)	12.479(9)	94.31(5)	102.07(4)	82.65(4)	$P\bar{1}$	(84)
Englishite	$Na_2K_3Ca_{10}Al_{15}(PO_4)_{21}(OH)_7(H_2O)_{26}$	38.43(2)	11.86	20.67	90	111.27	90	*A*2/*a*	(85)
Eosphorite	$Fe^{2+}[Al(PO_4)(OH)_2(H_2O)]$	10.445(1)	13.501(2)	6.970(30)	90	90	90	*Bba*2	(86)
Ercitite	$Na[Mn^{3+}(PO_4)(OH)](H_2O)_2$	5.362(5)	19.89(1)	5.362(5)	90	108.97(8)	90	$P2_1/n$	(87)
Evansite	$Al_3(PO_4)(OH)_6(H_2O)_8$	Amorphous	-	-	-	-	-	-	(43)
Eylettersite	$(Th,Pb)_{1Bx}Al_3(PO_4,SiO_4)_2(OH)_6$	6.99	*a*	16.70	90	90	90	$R\bar{3}m$	(88)
Fairfieldite	$Ca_2[Mn^{2+}(PO_4)_2(H_2O)_2]$	5.790(10)	6.570(10)	5.510(10)	102.3(2)	108.7(2)	90.3(2)	$P\bar{1}$	(89)
Farringtonite	$Mg_3(PO_4)_2$	7.596(1)	8.231(1)	5.077(1)	90	94.1(0)	90	$P2_1/n$	(90)
Faustite	$ZnAl_6(PO_4)_4(OH)_8(H_2O)_4$	7.419(2)	7.629(3)	9.905(3)	69.17(2)	69.88(2)	64.98(2)	$P\bar{1}$	(91)
Fermorite	$Ca_4Sr(PO_4)_3(OH)$	9.594(2)	9.597(2)	6.975(2)	90	90	120(0)	$P2_1/m$	(92)
Ferrisicklerite	$Li(Fe^{3+},Mn^{2+})(PO_4)$	5.918	10.037	4.798	90	90	90	*Pmnb*	(93)
Ferrostrunzite	$Fe^{2+}[Fe^{3+}(PO_4)(OH)(H_2O)]_2(H_2O)_4$	10.23(2)	9.77(3)	7.37(1)	89.65(16)	98.28(12)	117.26(16)	$P\bar{1}$	(94)
Fillowite	$Na_2CaMn^{2+}_7(PO_4)_6$	15.282(2)	*a*	43.507(3)	90	90	120	$R\bar{3}$	(95)
Florencite-(Ce)	$CeAl_3(PO_4)_2(OH)_6$	6.972(2)	*a*	16.261(6)	90	90	120	$R\bar{3}m$	(96)
Florencite-(La)	$LaAl_3(PO_4)_2(OH)_6$	6.987(2)	*a*	16.248(6)	90	90	120	$R\bar{3}m$	(97)
Florencite-(Nd)	$NdAl_3(PO_4)_2(OH)_6$	-	-	-	-	-	-	-	(98)
Fluellite	$Al_2(PO_4)F_2(OH)(H_2O)_7$	8.546(8)	11.222(5)	21.158(5)	90	90	90	*Fddd*	(99)
Fluorapatite	$Ca_5(PO_4)_3F$	9.367	*a*	6.884	90	90	90	$P6_3/m$	(62)
Fluorcaphite	$CaSrCa_3(PO_4)_3F$	9.485	*a*	7.000	90	90	120	$P6_3$	(100)
Foggite	$Ca[Al(PO_4)(OH)_2](H_2O)$	9.270(2)	21.324(7)	5.190(2)	90	90	90	$A2_122$	(101)
Francoanellite	$K_3Al_5(PO_3\{OH\})_6(PO_4)_2(H_2O)_{12}$	8.690(2)	*a*	82.271(13)	90	90	120	$R\bar{3}c$	(102)
Françoisite-(Nd)	$Nd[(UO_2)_3(PO_4)_2O(OH)](H_2O)_6$	9.298(2)	15.605(4)	13.668(2)	90	112.8(0)	90	$P2_1/c$	(103)
Fransoletite	$Ca_3[Be_2(PO_4)_2(PO_3\{OH\})_2](H_2O)_4$	7.348(1)	15.052(3)	7.068(1)	90	96.5(0)	90	$P2_1/a$	(104)
Frondellite	$Mn^{2+}Fe^{3+}_4(PO_4)_3(OH)_5$	13.89	17.01	5.21	90	90	90	$B22_12$	(105)

APPENDIX continued

Mineral Name	Formula	*a* (Å)	*b* (Å)	*c* (Å)	α (°)	β (°)	γ (°)	Space Group	Ref.
Furongite	$Al_2(OH)_2[(UO_2)(PO_4)_2](H_2O)_8$	17.87	14.18	12.18	67.8	77.5	79.9	$P\bar{1}$	(106)
Gainesite	$NaKZr_2[Be(P_4O_{16})]$	6.567(3)	*a*	17.119(5)	90	90	90	$I4_1/amd$	(107)
Galileiite	$NaFe^{2+}{}_4(PO_4)_3$	14.98	*a*	41.66	90	90	120	$R\bar{3}$	(108)
Gatehouseite	$Mn^{2+}{}_5(OH)_4(PO_4)_2$	9.097(2)	5.693(2)	18.002(10)	90	90	90	$P2_12_12_1$	(109)
Gatumbaite	$CaAl_2(PO_4)_2(OH)_2$	6.907(2)	5.095(2)	10.764(3)	90.68(8)	99.17(8)	90.17(8)	$P2/m$	(110)
Girvasite	$NaCa_2Mg_3(PO_4)_2[PO_2(OH)_2](CO_3)(OH)_2(H_2O)_4$	6.522(3)	12.250(30)	21.560(20)	90	89.5(0)	90	$P2_1/c$	(111)
Gladiusite	$Fe^{2+}{}_4Fe^{3+}{}_2(PO_4)(OH)_{11}(H_2O)$	16.950(2)	11.650(1)	6.2660(6)		90.000(4)		$P2_1/m$	(112)
Goedkenite	$Sr_2[Al(PO_4)_2(OH)]$	8.45(2)	5.74(2)	7.26(2)	90	113.7(1)	90	$P2_1/m$	(113)
Gorceixite	$BaAl_3(PO_4)(PO_3OH)(OH)_6$	7.036(0)	*a*	17.282(0)	90	90	120	$R3m$	(114)
Gordonite	$Mg[Al_2(PO_4)_2(OH)_2(H_2O)_2](H_2O)_4(H_2O)_2$	5.246(2)	10.532(5)	6.975(3)	107.5(0)	111.0(0)	72.2(0)	$P\bar{1}$	(115)
Gormanite	$Fe^{2+}{}_3Al_4(PO_4)_4(OH)_6(H_2O)_2$	11.76(1)	5.10(1)	13.57(1)	90.68(8)	99.17(8)	90.17(8)	$P\bar{1}$	(116)
Goyazite	$SrAl_3(PO_4)_2(OH)_5(H_2O)$	7.021(3)	*a*	16.505(15)	90	90	120	$R\bar{3}m$	(117)
Graftonite	$(Fe^{2+},Mn^{2+},Ca)_3(PO_4)_2$	8.910(10)	11.580(10)	6.239(8)	90	98.9(1)	90	$P2_1/c$	(118)
Grattarolaite	$Fe^{3+}{}_3O_3(PO_4)$	7.994(4)	*a*	6.855(4)	90	90	120	$R3m$	(119)
Grayite	$ThCa(PO_4)_2(H_2O)_2$	6.957	*a*	6.396	90	90	120	$P6_222$	(120)
Griphite	$Na_4Ca_6(Mn,Fe^{2+},Mg)_{19}Li_2Al_8(PO_4)_{24}F_8$	12.205(8)	*a*	*a*	90	90	90	$Pa\bar{3}$	(121)
Hagendorfite	$(Na,Ca)[Mn^{2+}(Fe^{2+},Mg,Fe^{3+})_2(PO_4)_3]$	11.92	12.59	6.52	90	114.7	90	$C2/c$	(122)
Haigerachite	$KFe^{3+}{}_3(PO_2\{OH\}_2)_6(PO_3\{OH\})_2(H_2O)_4$	16.95	9.59	17.57	90	90.85	90	$C2/c$	(123)
Hannayite	$Mg_3(NH_4)_2(PO_3\{OH\})_4(H_2O)_8$	10.728	7.670	6.702	97.87	96.97	104.74	$P\bar{1}$	(124)
Harrisonite	$CaFe^{2+}{}_6(SiO_4)_2(PO_4)_2$	6.248(1)	*a*	26.802(7)	90	90	120	$R\bar{3}m$	(125)
Heneuite	$CaMg_5(CO_3)(PO_4)_3(OH)$	6.311(1)	10.843(1)	8.676(1)	95.0(0)	93.4(0)	101.0(0)	$P\bar{1}$	(126)
Hentschelite	$Cu^{2+}Fe^{3+}{}_2(OH)_2(PO_4)_2$	6.984(3)	7.786(3)	7.266(3)	90	117.68(2)	90	$P2_1/n$	(127)
Herderite	$Ca[BePO_4F]$	9.800	7.680	4.800	90	90	90	$P2_1/a$	(128)
Heterosite	$Fe^{3+}(PO_4)$	5.830(10)	9.760(10)	4.769(5)	90	90	90	$Pmnb$	(129)
Hinsdalite	$Pb^{2+}[Al_3(OH)_6(PO_4)(SO_4)]$	7.029	*a*	16.789	90	90	120	$R\bar{3}m$	(130)
Holtedahlite	$Mg_{12}(PO_3\{OH\})(PO_4)_5(OH)_6$	11.203(3)	*a*	4.977(1)	90	90	90	$P31m$	(131)
Hopeite	$Zn_3(PO_4)_2(H_2O)_4$	10.597(3)	18.318(8)	5.031(1)	90	90	90	$Pnma$	(132)

APPENDIX continued

Mineral Name	Formula	*a* (Å)	*b* (Å)	*c* (Å)	α (°)	β (°)	γ (°)	Space Group	Ref.
Hotsonite	$Al_5(PO_4)(SO_4)(OH)_{10}$	11.29(6)	11.66(6)	10.55(7)	112.54(5)	107.52(5)	64.45(5)	$P\bar{1}$	(133)
Hureaulite	$Mn^{2+}{}_5(PO_3\{OH\})_2(PO_4)_2(H_2O)_4$	17.594(10)	9.086(5)	9.404(5)	90	96.67(8)	90	*C*2/*c*	(134)
Hurlbutite	$Ca[Be_2P_2O_8]$	8.306(1)	8.790(1)	7.804(1)	90	89.5(0)	90	$P2_1/a$	(135)
Hydroxylapatite	$Ca_5(PO_4)_3(OH)$	9.418	*a*	6.875	90	90	120	$P6_3/m$	(62)
Hydroxylherderite	$Ca[BePO_4(OH)]$	9.789(2)	7.661(1)	4.804(1)	90	90.02(1)	90	$P2_1/a$	(136)
Isokite	$Ca[Mg(PO_4)F]$	6.909	8.746	6.518	90	112.2	90	*A*2/*a*	(137)
Jagowerite	$Ba[Al(PO_4)(OH)]_2$	6.049(2)	6.964(3)	4.971(2)	116.51(4)	86.06(4)	112.59(3)	$P\bar{1}$	(138)
Jahnsite	$CaMnMg_2[Fe^{3+}(PO_4)_2(OH)]_2(H_2O)_8$	14.940(20)	7.140(10)	9.930(10)	90	110.16(8)	90	*P*2/*a*	(139)
Jahnsite-(CaMnMn)	$CaMn^{2+}Mn^{2+}{}_2Fe^{3+}{}_2(PO_4)_4(OH)_2(H_2O)_8$	14.887(8)	7.152(7)	9.966(6)	90	109.77(5)	90	*P*2/*a*	(140)
Johnsomervilleite	$Na_{10}Ca_6Mg_{18}(Fe^{2+},Mn^{2+})_{25}(PO_4)_{36}$	15.00	*a*	42.75	90	90	120	Hex	(141)
Johntomaite	$BaFe^{2+}{}_2Fe^{3+}{}_2(PO_4)_3(OH)_3$	9.199(9)	12.359(8)	5.004(2)	90	100.19(6)	90	$P2_1/m$	(142)
Johnwalkite	$KMn^{2+}{}_2[Nb(PO_4)_2O_2](H_2O)_2$	7.516(4)	10.023(8)	6.502(4)	90	90	90	$Pb2_1m$	(143)
Juonniite	$CaMgSc(PO_4)_2(OH)(H_2O)_4$	15.03	18.95	7.59	90	90	90	*Pbca*	(144)
Kanonerovite	$MnNa_3P_3O_{10}(H_2O)_{12}$	14.71(1)	9.33(1)	15.13(2)	90	89.8(1)	90	$P2_1/n$	(145)
Kastningite	$Mn(H_2O)_4[Al_2(OH)_2(H_2O)_2(PO_4)_2](H_2O)_2$	10.205(1)	10.504(1)	7.010(1)	90.38(1)	110.10(1)	71.82(1)	$P\bar{1}$	(146)
Keckite	$CaMn^{2+}{}_2Fe^{3+}{}_3(PO_4)_4(OH)_3(H_2O)_2$	15.02	7.19	19.74	90	110.5	90	$P2_1/a$	(147)
Kingite	$Al_3(PO_4)_2(OH)_3(H_2O)_9$	9.15(1)	10.00(1)	7.24(2)	98.6	93.6	93.2	$P\bar{1}$	(148)
Kintoreite	$Pb^{2+}Fe^{3+}{}_3(PO_4)_2(OH)_5(H_2O)$	7.331(1)	*a*	16.885(2)	90	90	120	$R\bar{3}m$	(149)
Kipushite	$[Cu^{2+}{}_5Zn(PO_4)_2](OH)_6(H_2O)$	12.197(2)	9.156(2)	10.667(2)	90	96.8(0)	90	$P2_1/c$	(150)
Kolbeckite	$[Sc(PO_4)(H_2O)_2]$	5.418	10.25	8.893	90	90.7	90	$P2_1/n$	(151)
Koninckite	$Fe^{3+}(PO_4)(H_2O)_3$	11.95	*a*	14.52	90	90	90	Tetragonal	(152)
Kosnarite	$KZr_2(PO_4)_3$	8.687(2)	*a*	23.877(7)	90	90	120	$R\bar{3}c$	(153)
Kovdorskite	$Mg_2(PO_4)(OH)(H_2O)_3$	10.350(40)	12.900(40)	4.730(20)	90	102.0(5)	90	$P2_1/a$	(154)
Krasnovite	$BaAl(PO_4)(OH)_2(H_2O)$	8.939	5.669	11.073	90	90	90	*Pnna*/*Pnnn*	(155)
Kribergite	$Al_5(PO_4)_3(SO_4)(OH)_4(H_2O)_4$	18.13(3)	13.5(2)	7.50(1)	70.50	117.87	136.58	$P\bar{1}$	(133)
Kryzhanovskite	$Mn^{2+}Fe^{3+}{}_2(PO_4)_2(OH)_2(H_2O)$	9.450(2)	10.013(2)	8.179(2)	90	90	90	*Pbna*	(156)
Kulanite	$BaFe^{2+}{}_2Al_2(PO_4)_3(OH)_3$	9.014(1)	12.074(1)	4.926(1)	90	100.48(1)	90	$P2_1/m$	(157)

APPENDIX continued

Mineral Name	Formula	*a* (Å)	*b* (Å)	*c* (Å)	α (°)	β (°)	γ (°)	Space Group	Ref.
Lacroixite	$Na[Al(PO_4)F]$	6.414(2)	8.207(2)	6.885(2)	90	115.5	90	*C*2/*c*	(158)
Landesite	$Fe^{3+}Mn^{2+}{}_2(PO_4)_2(OH)(H_2O)_2$	9.458(3)	10.185(2)	8.543(2)	90	90	90	*Pbna*	(159)
Laueite	$Mn^{2+}[Fe^{3+}{}_2(PO_4)_2(OH)_2(H_2O)_2](H_2O)_4(H_2O)_2$	5.280	10.660	7.140	107.9	111.0	71.1	$P\bar{1}$	(160)
Lazulite	$Mg[Al(PO_4)(OH)]_2$	7.144(1)	7.278(1)	7.228(1)	90	120.5(0)	90	$P2_1/c$	(161)
Lehnerite	$Mn^{2+}[(UO_2)(PO_4)]_2(H_2O)_8$	7.04(2)	17.16(4)	6.95(2)	90	90.18	90	$P2_1/n$	(162)
Leucophosphite	$K[Fe^{3+}{}_2(PO_4)_2(OH)(H_2O)](H_2O)_2$	9.782	9.658	9.751	90	102.24	90	$P2_1/n$	(163)
Libethenite	$Cu^{2+}{}_2(PO_4)(OH)$	8.071(2)	8.403(4)	5.898(3)	90	90	90	*Pnnm*	(164)
Lipscombite	$Fe^{2+}Fe^{3+}{}_2(PO_4)_2(OH)_2$	7.310	*a*	13.212	90	90	90	$P4_32_12_1$	(165)
Lithiophosphate	$Li_3(PO_4)$	10.490(3)	6.120(2)	4.9266(7)	90	90	90	*Pnma*	(166)
Lithiophyllite	$LiMn^{2+}(PO_4)$	6.100(20)	10.460(30)	4.744(10)	90	90	90	*Pmnb*	(167)
Lomonosovite	$Na_5Ti^{4+}{}_2(Si_2O_7)(PO_4)O_2$	5.440	7.163	14.830	99.0	106.0	90	$P\bar{1}$	(168)
Ludjibaite	$Cu^{2+}{}_5(PO_4)_2(OH)_4$	4.445(1)	5.873(1)	8.668(3)	103.6(0)	90.3(0)	93.0(0)	$P\bar{1}$	(169)
Ludlamite	$Fe^{2+}{}_3(PO_4)_2(H_2O)_4$	10.541(10)	4.638(8)	9.285(10)	90	100.7(1)	90	$P2_1/a$	(170)
Lulzacite	$Sr_2Fe^{2+}Fe^{2+}{}_2Al_4(PO_4)_4(OH)_{10}$	5.457(1)	9.131(2)	9.769(2)	108.47(3)	91.72(3)	97.44(3)	$P\bar{1}$	(171)
Lüneburgite	$Mg_3B_2(OH)_6(PO_4)_2(H_2O)_6$	6.347(1)	9.803(1)	6.298(1)	84.5(0)	106.4(0)	96.4(0)	$P\bar{1}$	(172)
Lun'okite	$Mn^{2+}{}_2Mg_2[Al(PO_4)_2(OH)]_2(H_2O)_8$	14.95	18.71	6.96	90	90	90	*Pbca*	(173)
Machatschkiite	$Ca_6(AsO_4)(AsO_3\{OH\})_3(PO_4)(H_2O)_{15}$	15.127(2)	*a*	22.471(3)	90	90	120	*R*3*c*	(174)
Maghagendorfite	$Na[Mn^{2+}MgFe^{2+}{}_2(PO_4)_3]$	-	-	-	-	-	-	-	(175)
Magniotriplite	$Mg_2(PO_4)F$	12.035(5)	6.432(4)	9.799(2)	90	108.1(0)	90	*I*2/*a*	(176)
Mahlmoodite	$FeZr(PO_4)_2(H_2O)_4$	9.12(2)	5.42(1)	19.17(2)	90	94.8(1)	90	$P2_1/c$	(177)
Mangangordonite	$Mn^{2+}[Al_2(PO_4)_2(OH)_2(H_2O)_6](H_2O)_2$	5.257(3)	10.363(4)	7.040(3)	105.4(0)	113.1(0)	78.7(0)	$P\bar{1}$	(115)
Manganosegelerite	$Mn^{2+}Mn^{2+}Fe^{3+}(PO_4)_2(OH)(H_2O)_4$	14.89	18.79	7.408	90	90	90	*Pbca*	(178)
Marićite	$NaFe^{2+}(PO_4)$	6.861(1)	8.987(1)	5.045(1)	90	90	90	*Pmnb*	(179)
Mcauslanite	$Fe^{2+}{}_3Al_2H(PO_4)_4F(H_2O)_{18}$	10.055(5)	11.568(5)	6.888(5)	105.84(6)	93.66(6)	106.47(5)	$P\bar{1}$	(180)
Mccrillisite	$NaCs[BeZr_2(PO_4)_4](H_2O)_{1\text{-}2}$	6.573(2)	*a*	17.28(2)	90	90	90	$I4_1/amd$	(181)
Melkovite	$CaFe^{3+}H_6(MoO_4)_4(PO_4)(H_2O)_6$	17.46	18.48	10.93	90	94.5	90	Mono	(182)
Mélonjosephite	$Ca[Fe^{2+}\ Fe^{3+}(PO_4)_2(OH)]$	9.542(1)	10.834(1)	6.374(2)	90	90	90	*Pbam*	(183)

APPENDIX continued

Mineral Name	Formula	*a* (Å)	*b* (Å)	*c* (Å)	α (°)	β (°)	γ (°)	Space Group	Ref.
Messelite	$Ca_2[Fe^{2+}(PO_4)_2(H_2O)_2]$	5.95(2)	6.52(2)	5.45(2)	102.3(4)	107.5(4)	90.8(2)	$P\bar{1}$	(184)
Meta-ankoleite	$K(UO_2)(PO_4)(H_2O)_3$	6.994(0)	*a*	17.784(0)	90	90	90	*P4/ncc*	(185)
Meta-autunite	$Ca[(UO_2)(PO_4)]_2(H_2O)_6$	6.960(10)	*a*	8.400(20)	90	90	90	*P4/nmm*	(186)
Metaswitzerite	$Mn^{2+}{}_3(PO_4)_2(H_2O)_4$	8.496(3)	13.173(3)	17.214(4)	90	96.7(0)	90	$P2_1/c$	(187)
Metatorbernite	$Cu^{2+}[(UO_2)(PO_4)]_2(H_2O)_8$	6.972(1)	*a*	17.277	90	90	90	*P4/n*	(188)
Meta-uranocircite	$Ba[(UO_2)(PO_4)]_2(H_2O)_6$	9.789(3)	9.882(3)	16.868(3)	90	90	89.9(0)	$P2_1/a$	(189)
Metavanmeerscheite	$U(OH)_4[(UO_2)_3(PO_4)(OH)_2](H_2O)_2$	34.18	33.88	14.074	90	90	90	*Fddd*	(190)
Metavariscite	$[Al(PO_4)(H_2O)_2]$	5.178(2)	9.514(2)	8.454(2)	90	90.35(2)	90	$P2_1/n$	(191)
Metavauxite	$Fe^{2+}(H_2O)_6[Al(PO_4)(OH)(H_2O)]_2(H_2O)_6$	10.220	9.560	6.940	90	97.9	90	$P2_1/c$	(192)
Metavivianite	$Fe^{2+}{}_3(PO_4)_2(H_2O)_8$	7.840(10)	9.110(10)	4.670(10)	95.0(0)	96.9(0)	107.7(0)	$P\bar{1}$	(193)
Meurigite	$KFe^{3+}{}_7(PO_4)_5(OH)_7(H_2O)_8$	29.52(4)	5.249(6)	18.26(1)	90	109.27(7)	90	*C2/m*	(194)
Millisite	$NaCaAl_6(PO_4)_4(OH)_9(H_2O)_3$	7.00	*a*	19.07	90	90	90	$P4_12_12$	(195)
Minyulite	$K[Al_2(PO_4)_2F(H_2O)_4]$	9.337(5)	9.740(5)	5.522(3)	90	90	90	*Pba2*	(196)
Mitridatite	$Ca_2[Fe^{3+}{}_3(PO_4)_3O_2](H_2O)_3$	17.553(2)	19.354(3)	11.248(2)	90	95.84(1)	90	*Aa*	(197)
Mitryaevaite	$Al_5(PO_4)_2(PO_3\{OH\})_2F_2(OH)_2(H_2O)_8(H_2O)_{6.5}$	6.918(1)	10.127(2)	10.296(2)	77.036(3)	73.989(4)	76.272(4)	$P\bar{1}$	(198)
Monazite-(Ce)	$Ce(PO_4)$	6.7902(10)	7.0203(6)	6.4674(7)	90	103.38(1)	90	$P2_1/n$	(199)
Monetite	$CaH[PO_4]$	6.910(1)	6.627(2)	6.998(2)	96.34(2)	103.82(2)	88.33(2)	$P\bar{1}$	(200)
Montebrasite	$Li[Al(PO_4)(OH)]$	6.713(1)	7.708(1)	7.019(1)	91.31(1)	117.93(1)	91.77(1)	$C\bar{1}$	(8)
Montgomeryite	$Ca_4MgAl_4(PO_4)_6(OH)_4(H_2O)_{12}$	10.023(1)	24.121(3)	6.243(1)	90	91.55(1)	90	*C2/c*	(201)
Moraesite	$[Be_2(PO_4)(OH)](H_2O)_4$	8.553(6)	12.319(6)	7.155(8)	90	97.9(1)	90	*C2/c*	(202)
Moreauite	$Al_3(UO_2)(PO_4)_3(OH)_2(H_2O)_{13}$	23.41	21.44	18.34	90	92.0	90	$P2_1/c$	(203)
Morinite	$Ca_2Na[Al_2(PO_4)_2F_4(OH)(H_2O)_2]$	9.454(3)	10.692(4)	5.444(2)	90	105.46(2)	90	$P2_1/m$	(204)
Mrázekite	$Bi^{3+}{}_2Cu^{2+}{}_3(OH)_2O_2(PO_4)_2(H_2O)_2$	9.065(1)	6.340(1)	21.239(3)	90	101.6(0)	90	$P2_1/n$	(205)
Mundite	$Al(OH)[(UO_2)_3(OH)_2(PO_4)_2](H_2O)_{5.5}$	17.08	30.98	13.76	90	90	90	*Pmcn*	(206)
Mundrabillaite	$(NH_4)_2Ca(PO_3\{OH\})_2(H_2O)$	8.643	8.184	6.411	90	98.0	90	*P2/m*	(207)
Nabaphite	$NaBa(PO_4)(H_2O)_9$	10.712(1)	*a*	*a*	90	90	90	$P2_13$	(208)
Nacaphite	$Na(Na\ Ca)(PO_4)F$	5.3232(2)	12.2103(4)	7.0961(2)	90.002(1)	89.998(1)	89.965(1)	$P\bar{1}$	(209)

APPENDIX continued

Mineral Name	Formula	*a* (Å)	*b* (Å)	*c* (Å)	α (°)	β (°)	γ (°)	Space Group	Ref.
Nahpoite	$Na_2H[PO_4]$	5.451(1)	6.847(2)	5.473(1)	90	116.33(8)	90	$P2_1/m$	(210)
Nalipoite	$NaLi_2(PO_4)$	6.884(2)	9.976(4)	4.927(2)	90	90	90	*Pmnb*	(211)
Nastrophite	$NaSr(PO_4)(H_2O)_9$	10.559(1)	*a*	*a*	90	90	90	$P2_13$	(212)
Natrodufrénite	$NaFe^{2+}Fe^{3+}_5(PO_4)_4(OH)_6(H_2O)_2$	25.83	5.150	13.772	90	111.53	90	*C*2/*c*	(213)
Natromontebrasite	$Na[Al(PO_4)(OH)]$	5.266	7.174	5.042	112.3	97.70	67.13	$P\bar{1}$	(214)
Natrophilite	$NaMn^{2+}(PO_4)$	10.523(5)	4.987(2)	6.312(3)	90	90	90	*Pnam*	(215)
Natrophosphate	$Na_7(PO_4)_2F(H_2O)_{19}$	27.712(2)	*a*	*a*	90	90	90	$Fd\bar{3}c$	(216)
Nefedovite	$Na_5Ca_4(PO_4)_4F$	11.644(2)	*a*	5.396(1)	90	90	90	$I\bar{4}$	(217)
Newberyite	$[Mg(PO_3\{OH\})(H_2O)_3]$	10.215(2)	10.681(2)	10.014(2)	90	90	90	*Pbca*	(218)
Niahite	$(NH_4)Mn^{2+}(PO_4)(H_2O)$	5.68	8.78	4.88	90	90	90	$Pmn2_1$	(219)
Ningyoite	$(U,Ca,Ce,Fe)_2(PO_4)_2(H_2O)_{1\text{-}2}$	6.78	12.10	6.38	90	90	90	*P*222	(220)
Nissonite	$Cu^{2+}_2Mg_2(PO_4)_2(OH)_2(H_2O)_5$	22.523(5)	5.015(2)	10.506(3)	90	99.62(2)	90	*C*2/*c*	(221)
Olgite	$NaSr(PO_4)$	5.565(2)	*a*	7.050(3)	90	90	120	*P*3	(222)
Olmsteadite	$KFe^{2+}_2(H_2O)_2[Nb(PO_4)_2O_2]$	7.512(1)	10.000(3)	6.492(2)	90	90	90	$Pb2_1m$	(223)
Olympite	$LiNa_5(PO_4)_2$	10.143(1)	14.819(3)	10.154(5)	90	90	90	*Pcmn*	(224)
Orpheite	$H_6Pb^{2+}_{10}Al_{20}(PO_4)_{12}(SO_4)_5(OH)_{40}(H_2O)_{11}$	7.016	*a*	16.730	90	90	120	$R\bar{3}m$	(225)
Overite	$Ca_2Mg_2[Al(PO_4)_2(OH)]_2(H_2O)_8$	14.723(14)	18.746(16)	7.107(4)	90	90	90	*Pbca*	(226)
Pahasapaite	$Ca_8Li_8[Be_{24}P_{24}O_{96}](H_2O)_{38}$	13.781(4)	*a*	13.783(1)	90	90	90	*I*23	(227)
Palermoite	$SrLi_2[Al(PO_4)(OH)]_4$	11.556(5)	15.847(7)	7.315(4)	90	90	90	*Imcb*	(228)
Panasqueiraite	$Ca[Mg(PO_4)(OH)]$	6.535(3)	8.753(4)	6.919(4)	90	112.33(4)	90	*C*2/*c*	(137)
Parafransoletite	$Ca_3[Be_2(PO_4)_2(PO_3\{OH\})_2](H_2O)_4$	7.327(1)	7.696(1)	7.061(1)	94.9(0)	96.8(0)	101.9(0)	$P\bar{1}$	(104)
Parahopeite	$Zn_3(PO_4)_2(H_2O)_4$	5.768(5)	7.550(5)	5.276(5)	93.42	91.18	91.37	$P\bar{1}$	(229)
Pararobertsite	$Ca_2Mn^{3+}_3(PO_4)_3O_2(H_2O)_3$	8.825(3)	13.258(4)	11.087(3)	90	101.19(4)	90	$P2_1/c$	(230)
Parascholzite	$CaZn_2(PO_4)_2(H_2O)_2$	17.186(6)	7.413(3)	6.663(2)	90	95.4(0)	90	*I*2/*c*	(231)
Paravauxite	$Fe^{2+}[Al_2(PO_4)_2(OH)_2(H_2O)_2](H_2O)_4(H_2O)_2$	5.233	10.541	6.962	106.9	110.8	72.1	$P\bar{1}$	(232)
Parsonsite	$Pb^{2+}_2[(UO_2)(PO_4)_2]$	6.842(4)	10.383(6)	6.670(4)	101.26(7)	98.17(7)	86.38(7)	$P\bar{1}$	(233)
Paulkellerite	$Bi^{3+}_2Fe^{3+}(PO_4)O_2(OH)_2$	11.380(3)	6.660(3)	9.653(3)	90	115.3(0)	90	*C*2/*c*	(234)

APPENDIX continued

Mineral Name	Formula	*a* (Å)	*b* (Å)	*c* (Å)	α (°)	β (°)	γ (°)	Space Group	Ref.
Penikisite	$BaMg_2Al_2(PO_4)_3(OH)_3$	8.999	12.069	4.921	90	100.52	90	$P2_1/m$	(235)
Perloffite	$BaMg_2Fe^{3+}{}_2(PO_4)_3(OH)_3$	9.223(5)	12.422(8)	4.995(7)	90	100.39(4)	90	$P2_1/m$	(236)
Petersite-(Y)	$YCu^{2+}{}_6(PO_4)_3(OH)_6(H_2O)_3$	13.288(5)	*a*	5.877(5)	90	90	120	$P6_3/m$	(237)
Petitjeanite	$Bi^{3+}{}_3(PO_4)_2O(OH)$	9.798	7.250	6.866	88.28	115.27	110.70	$P\bar{1}$	(238)
Phosinaite-(Ce)	$Na_{13}Ca_2Ce[Si_4O_{12}](PO_4)_4$	12.297(2)	14.660(3)	7.245(1)	90	90	90	$P22_12_1$	(239)
Phosphammite	$(NH_4)_2(PO_3\{OH\})$	11.043(6)	6.700(3)	8.031(4)	90	113.4(0)	90	$P2_1/c$	(240)
Phosphoellenbergite	$Mg_{14}(PO_4)_6(PO_3\{OH\})_2(OH)_6$	12.467(2)	*a*	5.044(0)	90	90	120	$P6_3mc$	(241)
Phosphoferrite	$Fe^{2+}{}_3(PO_4)_2(H_2O)_3$	8.660(30)	10.060(30)	9.410(30)	90	90	90	$Pcn2$	(242)
Phosphofibrite	$KCu^{2+}Fe^{3+}{}_{15}(PO_4)_{12}(OH)_{12}(H_2O)_{12}$	14.40	18.76	10.40	90	90	90	$Pbnm$	(243)
Phosphogartrellite	$Pb^{2+}Cu^{2+}Fe^{3+}(PO_4)_2(OH,H_2O)_2$	5.320	5.528	7.434	67.61	69.68	70.65	$P\bar{1}$	(244)
Phosphophyllite	$Zn_2Fe^{2+}(PO_4)_2(H_2O)_4$	10.378(3)	5.084(1)	10.553(3)	90	121.14(2)	90	$P2_1/c$	(245)
Phosphorrösslerite	$\{Mg(H_2O)_6\}(PO_3\{OH\})(H_2O)$	6.60	25.36	11.35	90	95	90	$C2/c$	(246)
Phosphosiderite	$[Fe^{3+}(PO_4)(H_2O)_2]$	5.330(3)	9.809(4)	8.714(5)	90	90.6(1)	90	$P2_1/n$	(247)
Phosphovanadylite	$V^{4+}{}_4P_2O_{10}(OH)_6(H_2O)_{12}$	15.470(4)	*a*	15.470(4)	90	90	90	$I\bar{4}3m$	(248)
Phosphuranylite	$KCa(H_3O)_3(UO_2)[(UO_2)_3(PO_4)_2O_2]_2(H_2O)_8$	15.899(2)	13.740(2)	17.300(3)	90	90	90	$Cmcm$	(249)
Phuralumite	$Al_2[(UO_2)_3(PO_4)_2(OH)_2](OH)_4(H_2O)_{10}$	13.836(6)	20.918(6)	9.428(3)	90	112.44	90	$P2_1/a$	(250)
Phurcalite	$Ca_2[(UO_2)_3O_2(PO_4)_2](H_2O)_7$	17.415(2)	16.035(3)	13.598(3)	90	90	90	$Pbca$	(251)
Planerite	$Al_6(PO_4)_2(PO_3\{OH\})_2(OH)_8(H_2O)_4$	7.505(2)	9.723(3)	7.814(2)	111.43	115.56	68.69	$P\bar{1}$	(2)
Plumbogummite	$Pb^{2+}Al_3(PO_4)_2(OH)_5(H_2O)$	7.039(5)	*a*	16.761(3)	90	90	120	$R\bar{3}m$	(130)
Polyphite	$Na_{17}Ca_3MgTi^{4+}{}_4(Si_2O_7)_2(PO_4)_6O_3F_5$	5.412(2)	7.079(3)	26.560(10)	95.2(0)	93.5(0)	90.1(0)	$P1$	(252)
Pretulite	$Sc(PO_4)$	6.589(1)	*a*	5.806(1)	90	90	90	$I4/amd$	(253)
Przhevalskite	$Pb[(UO_2)(PO_4)]_2(H_2O)_4$	7.24	*a*	18.22	90	90	90	Tetra	(254)
Pseudo-autunite	$Ca_2[(UO_2)_2(PO_4)_4](H_2O)_9$	6.964	*a*	12.85	90	90	120	Hexa	(255)
Pseudolaueite	$Mn^{2+}[Fe^{3+}(PO_4)(OH)(H_2O)]_2(H_2O)_4(H_2O)_2$	9.647	7.428	10.194	90	104.63	90	$P2_1/a$	(256)
Pseudomalachite	$Cu^{2+}{}_5(PO_4)_2(OH)_4$	4.4728(4)	5.7469(5)	17.032(3)	90	91.043(7)	90	$P2_1/c$	(257)
Purpurite	$Mn^{3+}(PO_4)$	4.760	9.680	5.819	90	90	90	$Pbnm$	(258)
Pyromorphite	$Pb_5(PO_4)_3Cl$	9.977(1)	9.976(1)	7.351(2)	90	90	120	$P6_3/m$	(259)

APPENDIX continued

Mineral Name	Formula	*a* (Å)	*b* (Å)	*c* (Å)	α (°)	β (°)	γ (°)	Space Group	Ref.
Qingheiite	$Na_2NaMn^{2+}{}_2Mg_2Al_2(PO_4)_6$	11.856(3)	12.411(3)	6.421(1)	90	114.45(2)	90	$P2_1/n$	(260)
Quadruphite	$Na_{14}CaMgTi^{4+}{}_4(Si_2O_7)_2(PO_4)_4O_4F_2$	5.4206(2)	7.0846(2)	20.364(1)	86.89(1)	94.42(1)	89.94(1)	$P1$	(209)
Raadeite	$Mg_7(PO_4)_2(OH)_8$	5.250(1)	11.647(2)	9.655(2)	90	95.94(1)	90	$P2_1/n$	(261)
Reddingite	$Mn^{2+}{}_3(PO_4)_2(H_2O)_3$	8.750(20)	10.173(8)	9.590(20)	90	90	90	$Pcmb$	(262)
Reichenbachite	$Cu^{2+}{}_5(PO_4)_2(OH)_4$	9.186(2)	10.684(2)	4.461(1)	90	92.31(1)	90	$P2_1/a$	(263)
Renardite	$Pb^{2+}(UO_2)[(UO_2)_3O_2(PO_4)_2](H_2O)_9$	15.9	17.6	13.8	90	90	90	$Bmmb$	(264)
Rhabdophane	$Ce(PO_4)(H_2O)$	7.055(3)	*a*	6.439(5)	90	90	120	$P6_222$	(265)
Richellite	$Ca_3Fe^{3+}{}_{10}(PO_4)_8(OH)_{12}(H_2O)_n$	Amorphous	-	-	-	-	-	-	(266)
Rimkorolgite	$Mg_5Ba(PO_4)_4(H_2O)_8$	12.829	8.335	18.312	90	90	90	$Pcmm$	(267)
Rittmanite	$Mn^{2+}Mn^{2+}Fe^{2+}{}_2[Al(PO_4)_2(OH)]_2(H_2O)_8$	15.01(4)	6.89(3)	10.16(3)	90	112.82(25)	90	$P2_1/a$	(268)
Robertsite	$Ca_2[Mn^{3+}{}_3(PO_4)_3O_2](H_2O)_3$	17.36(2)	19.53(5)	11.30(3)	90	96.0	90	Aa	(269)
Rockbridgeite	$Fe^{2+}Fe^{3+}{}_4(PO_4)_3(OH)_5$	13.873(12)	16.805(9)	5.172(4)	90	90	90	$Bbmm$	(81)
Rodolicoite	$Fe^{3+}(PO_4)$	5.048(3)	*a*	11.215(8)	90	90	120	$R3_121$	(270)
Roscherite	$Ca_2Mn^{2+}{}_5[Be_4P_6O_{24}(OH)_4](H_2O)_6$	15.874(4)	11.854(3)	6.605(1)	90	95.35(3)	90	$C2/c$	(271)
Rosemaryite	$NaMn^{2+}Fe^{3+}Al(PO_4)_3$	11.977(2)	12.388(2)	6.320(1)	90	114.45(2)	90	$P2_1/n$	(272)
Sabugalite	$Al[(UO_2)_4(PO_3\{OH\})(PO_4)_3](H_2O)_{16}$	19.426	9.843	9.850	90	96.16	90	$C2/m$	(273)
Saléeite	$Mg[(UO_2)(PO_4)]_2(H_2O)_{10}$	6.951(3)	19.947(8)	9.896(4)	90	135.17	90	$P2_1/c$	(274)
Sampleite	$NaCaCu^{2+}{}_5(PO_4)_4Cl(H_2O)_5$	9.70	38.40	9.65	90	90	90	Orth	(275)
Samuelsonite	$BaCa_8Fe^{2+}Al_2(OH)_2(PO_4)_{10}$	18.495(10)	6.804(4)	14.000(8)	90	112.8(1)	90	$C2/m$	(276)
Sanjuanite	$Al_2(PO_4)(SO_4)(OH)(H_2O)_9$	11.314(11)	9.018(9)	7.376(7)	93.07(1)	95.77(7)	105.66(7)	$P\bar{1}$	(133)
Sarcopside	$(Fe^{2+},Mn^{2+},Mg)_3(PO_4)_2$	6.019(0)	4.777(0)	10.419(1)	90	91.0(0)	90	$P2_1/c$	(277)
Sasaite	$Al_6(PO_4)_5(OH)_3(H_2O)_{35\text{-}36}$	10.75	15.02	46.03	90	90	90	P- - -	(278)
Satterlyite	$Fe^{2+}{}_2(PO_4)(OH)$	11.361	*a*	5.041	90	90	120	$P\bar{3}1m$	(279)
Schertelite	$(NH_4)_2[Mg(PO_3\{OH\})_2(H_2O)_4]$	11.49(2)	23.66(6)	8.62(1)	90	90	90	$Pbca$	(280)
Scholzite	$CaZn_2(PO_4)_2(H_2O)_2$	17.149(3)	22.236(2)	6.667(1)	90	90	90	$Pbc2_1$	(281)
Schoonerite	$Fe^{2+}{}_2ZnMn^{2+}(PO_4)_3(OH)_2(H_2O)_9$	11.119(4)	25.546(11)	6.437(3)	90	90	90	$Pmab$	(282)
Scorzalite	$Fe^{2+}[Al(PO_4)(OH)]_2$	7.15(2)	7.31(2)	7.25(2)	90	120.7(1)	90	$P2_1/c$	(20)

APPENDIX continued

Mineral Name	Formula	*a* (Å)	*b* (Å)	*c* (Å)	α (°)	β (°)	γ (°)	Space Group	Ref.
Seamanite	$[Mn^{2+}_3(B\{OH\}_4)(PO_4)(OH)_2]$	7.8231(9)	15.1405(14)	6.6999(7)	90	90	90	*Pbnm*	(283)
Segelerite	$Ca_2Mg_2[Fe^{3+}(PO_4)_2(OH)]_2(H_2O)_8$	14.826(5)	18.751(4)	7.307(1)	90	90	90	*Pbca*	(226)
Selwynite	$NaK[BeZr_2(PO_4)_4](H_2O)_2$	6.570(3)	*a*	17.142(6)	90	90	90	$I4_1/amd$	(284)
Senegalite	$Al_2(OH)_3(PO_4)(H_2O)$	7.675(4)	9.711(4)	7.635(4)	90	90	90	$P2_1nb$	(285)
Serrabrancaite	$Mn^{3+}(PO_4)(H_2O)$	6.914(2)	7.468(2)	7.364(2)	90	112.29(3)	90	*C*2/*c*	(286)
Sicklerite	$LiMn^{2+}(PO_4)$	4.794	10.063	5.947	90	90	90	*Pbnm*	(287)
Sidorenkite	$Na_3Mn^{2+}(PO_4)(CO_3)$	8.997(4)	6.741(2)	5.163(2)	90	90.16(4)	90	$P2_1/m$	(288)
Sigismundite	$BaNa_3CaFe^{2+}_{14}Al(PO_4)_{12}(OH)_2$	16.406(5)	9.945(3)	24.470(5)	90	105.73(2)	90	*C*2/*c*	(289)
Sigloite	$Fe^{3+}[Al_2(PO_4)_2(OH)_2(H_2O)_2](H_2O)_3(OH)(H_2O)_2$	5.190(2)	10.419(4)	7.033(3)	105.00(3)	111.31(3)	70.87(3)	$P\bar{1}$	(290)
Sincosite	$Ca(V^{4+}O)_2(PO_4)_2(OH)_4(H_2O)_3$	8.895(3)	*a*	12.747(2)	90	90	90	*P*4/*nmm*	(291)
Sinkankasite	$(Mn^{2+}(H_2O)_4)(Al(PO_3\{OH\})_2(OH))(H_2O)_2$	9.590(2)	9.818(2)	6.860(1)	108.0(0)	99.6(0)	98.9(0)	$P\bar{1}$	(292)
Smrkovecite	$Bi^{3+}_2O(PO_4)(OH)$	6.954	7.494	10.869	90	107.00	90	$P2_1/c$	(293)
Sobolevite	$Na_{11}Na_4MgTi^{4+}_4(Si_2O_7)_2(PO_4)_4O_3F_3$	7.078(1)	5.411(1)	40.618(10)	90	93.2(0)	90	*P*1	(294)
Souzalite	$Mg_3Al_4(PO_4)_4(OH)_6(H_2O)_2$	11.74(1)	5.11(1)	13.58(1)	90.83(8)	99.08(8)	90.33(8)	$P\bar{1}$	(116)
Spencerite	$Zn_4(PO_4)_2(OH)_2(H_2O)_3$	10.448(3)	5.282(1)	11.208(3)	90	116.73(3)	90	$P2_1/c$	(295)
Spheniscidite	$(NH_4)Fe^{3+}_2(OH)(PO_4)_2(H_2O)_2$	9.75	9.63	9.70	90	102.57	90	$P2_1/n$	(296)
Springcreekite	$BaV^{3+}_3(PO_4)_2(OH)_5(H_2O)$	7.258(1)	*a*	17.361(9)	90	90	120	$R\bar{3}m$	(297)
Stanekite	$Fe^{3+}Mn^{2+}(PO_4)O$	11.844(3)	12.662(3)	9.989(3)	90	105.93(2)	90	$P2_1/a$	(298)
Stanfieldite	$Mg_3Ca_3(PO_4)_4$	22.841(3)	9.994(1)	17.088(5)	90	99.6(0)	90	*C*2/*c*	(299)
Steenstrupine-(Ce)	$Na_{14}Ce_6Mn^{2+}Mn^{3+}Fe^{2+}_2Zr(Si_6O_{18})_2(PO_4)_7(H_2O)_3$	10.460(4)	*a*	45.479(15)	90	90	120	$R\bar{3}m$	(300)
Stercorite	$Na(NH_4)H[PO_4](H_2O)_4$	10.636(2)	6.919(1)	6.436(1)	90.46(3)	97.87(3)	109.20(3)	$P\bar{1}$	(301)
Stewartite	$Mn^{2+}[Fe^{3+}_2(PO_4)_2(OH)_2(H_2O)_2](H_2O)_4(H_2O)_2$	10.398(2)	10.672(3)	7.223(3)	90.10(3)	109.10(2)	71.83(2)	$P\bar{1}$	(302)
Strengite	$[Fe^{3+}(PO_4)(H_2O)_2]$	10.05	9.80	8.65	90	90	90	*Pcab*	(303)
Strontiowhitlockite	$Sr_9Mg(PO_4)_6(PO_3\{OH\})$	10.644(9)	*a*	39.54(6)	90	90	120	*R*3*c*	(304)
Strontium-apatite	$Sr_6Ca_4(PO_4)_6F_2$	9.630	*a*	7.220	90	90	120	$P6_3$	(305)
Strunzite	$Mn^{2+}[Fe^{3+}(PO_4)(OH)(H_2O)]_2(H_2O)_4$	10.228(5)	9.837(3)	7.284(5)	90.17(5)	98.44(5)	117.44(2)	$P\bar{1}$	(306)
Strüvite	$(NH_4)[Mg(H_2O)_6][PO_4]$	6.941(2)	6.941(2)	11.199(4)	90	90	90	$Pmn2_1$	(307)

APPENDIX continued

Mineral Name	Formula	*a* (Å)	*b* (Å)	*c* (Å)	α (°)	β (°)	γ (°)	Space Group	Ref.
Svanbergite	$Sr[Al_3(SO_4)(PO_4)(OH)_6]$	6.890	*a*	*a*	60.6	60.6	60.6	$R\bar{3}m$	(308)
Swaknoite	$Ca(NH_4)_2(PO_3\{OH\})_2(H_2O)$	20.959	7.403	6.478	90	90	90	*C*- - -	(309)
Switzerite	$Mn^{2+}_3(PO_4)_2(H_2O)_7$	8.528(4)	13.166(5)	11.812(4)	90	110.05(3)	90	$P2_1/a$	(310)
Tancoite	$Na_2Li[Al(PO_4)_2(OH)]H$	6.948(2)	14.089(4)	14.065(3)	90	90	90	*Pbcb*	(311)
Taranakite	$K_3Al_5(PO_3\{OH\})_6(PO_4)_2(H_2O)_{18}$	8.703(1)	*a*	95.050(10)	90	90	120	$R\bar{3}c$	(312)
Tarbuttite	$Zn_2(PO_4)(OH)$	5.499	5.654	6.465	102.85	102.77	86.83	$P\bar{1}$	(313)
Tavorite	$Li[Fe^{3+}(PO_4)(OH)]$	5.340(2)	7.283(2)	5.110(2)	109.29(2)	97.86(3)	106.32(3)	$P\bar{1}$	(314)
Thadeuite	$CaMg_3(PO_4)_2(OH)_2$	6.412(3)	13.563(8)	8.545(5)	90	90	90	$C222_1$	(315)
Threadgoldite	$Al[(UO_2)(PO_4)]_2(OH)(H_2O)_8$	20.168(8)	9.847(2)	19.719(4)	90	110.7(0)	90	*C*2/*c*	(316)
Tinsleyite	$K[Al_2(PO_4)_2(OH)(H_2O)](H_2O)$	9.499(2)	9.503(2)	9.535(2)	90	103.3(0)	90	$P2_1/n$	(317)
Tinticite	$Fe^{3+}_4(PO_4)_3(H_2O)_5$	7.965(2)	9.999(2)	7.644(2)	103.94(2)	115.91(2)	67.86(2)	$P\bar{1}$	(318)
Tiptopite	$K_2NaCaLi_3[Be_6P_6O_{24}(OH)_2](H_2O)_4$	11.655(5)	*a*	4.692(2)	90	90	120	$P6_3$	(319)
Torbernite	$Cu^{2+}[(UO_2)(PO_4)]_2(H_2O)_8$	7.06	*a*	20.5	90	90	90	*I*4/*mmm*	(320)
Triangulite	$Al_3(OH)_5[(UO_2(PO_4)]_4(H_2O)_5$	10.39	10.56	8.82	101.25	109.58	113.4	$P\bar{1}$	(321)
Triphylite	$LiFe^{2+}(PO_4)$	4.704	10.347	6.0189	90	90	90	*Pbnm*	(322)
Triplite	$Mn^{2+}_2(PO_4)F$	12.065	6.454	9.937	90	107.1	90	*I*2/*c*	(323)
Triploidite	$Mn^{2+}_2(PO_4)(OH)$	12.366(1)	13.276(2)	9.943(2)	90	108.2(0)	90	$P2_1/a$	(324)
Trolleite	$Al_4(OH)_3(PO_4)_3$	18.894(5)	7.161(1)	7.162(2)	90	99.99(2)	90	*I*2/*c*	(325)
Tsumebite	$Pb^{2+}_2[Cu^{2+}(PO_4)(SO_4)(OH)]$	7.85	5.80	8.70	90	111.5	90	$P2_1/m$	(326)
Turquoise	$Cu^{2+}Al_6(PO_4)_4(OH)_8(H_2O)_4$	7.410(1)	7.633(1)	9.904(1)	68.42(1)	69.65(1)	65.05(1)	$P\bar{1}$	(327)
Ulrichite	$Cu^{2+}[Ca(UO_2)(PO_4)_2](H_2O)_4$	12.790(30)	6.850(20)	13.020(30)	90	91.0(1)	90	*C*2/*m*	(328)
Upalite	$Al\,[(UO_2)_3O(OH)(PO_4)_2](H_2O)_7$	13.704	16.82	9.332	90	111.5	90	$P2_1/a$	(329)
Uralolite	$Ca_2[Be_4(PO_4)_3(OH)_3](H_2O)_5$	6.550(1)	16.005(3)	15.969(4)	90	101.64(2)	90	$P2_1/n$	(330)
Uramphite	$(NH_4)(UO_2)(PO_4)(H_2O)_3$	7.022(0)	*a*	18.091(0)	90	90	90	*P*4/*ncc*	(331)
Uranocircite	$Ba[(UO_2)(PO_4)]_2(H_2O)_{10}$	7.02	*a*	20.58	90	90	90	*P*4/*ncc*	(332)
Uranospathite	$AlH[(UO_2)(PO_4)]_4(H_2O)_{40}$	7.00	*a*	30.02	90	90	90	$P4_2/n$	(333)
Ushkovite	$Mg[Fe^{3+}_2(PO_4)_2(OH)_2(H_2O)_2](H_2O)_4(H_2O)_2$	5.3468(4)	10.592(1)	7.2251(7)	108.278(7)	111.739(7)	71.626(7)	$P\bar{1}$	(334)

APPENDIX continued

Mineral Name	Formula	*a* (Å)	*b* (Å)	*c* (Å)	α (°)	β (°)	γ (°)	Space Group	Ref.
Vanmeerscheite	$U(OH)_4[(UO_2)_3(PO_4)_2(OH)_2](H_2O)_4$	17.060(50)	16.760(30)	7.023(3)	90	90	90	$P2_1mn$	(190)
Variscite	$[Al(PO_4)(H_2O)_2]$	9.822(3)	8.561(3)	9.630(3)	90	90	90	*Pbca*	(335)
Varulite	$(Na,Ca)[Mn^{2+}(Mn,Fe^{2+},Fe^{3+})_2(PO_4)_3]$	11.99	12.64	6.51	90	114.64	90	*C*2/*c*	(336)
Vashegyite	$Pb^{2+}{}_2Cu^{2+}(CrO_4)(PO_4)(OH)$	10.773(3)	14.971(5)	20.626(6)	90	90	90	$Pna2_1$	(337)
Vauquelinite	$Pb^{2+}{}_2[Cu^{2+}(PO_4)(CrO_4)(OH)]$	13.754(5)	5.806(6)	9.563(3)	90	94.56(3)	90	$P2_1/n$	(338)
Vauxite	$Fe^{2+}Al_2(PO_4)_2(OH)_2(H_2O)_6$	9.13	11.59	6.14	98.3	92.0	108.4	$P\bar{1}$	(339)
Väyrynenite	$Mn^{2+}[Be(PO_4)(OH)]$	5.4044(6)	14.5145(12)	4.7052(6)	90	102.798(9)	90	$P2_1/a$	(340)
Veszelyite	$Cu^{2+}{}_3(PO_4)(OH)_3(H_2O)_2$	9.828(3)	10.224(3)	7.532(2)	90	103.18(2)	90	$P2_1/a$	(341)
Viitaniemiite	$NaCaAl(PO_4)(OH)F_2$	5.457(2)	7.151(2)	6.836(2)	90	109.36(3)	90	$P2_1/n$	(342)
Viséite	$Ca_{10}Al_{24}(SiO_4)_6(PO_4)_7O_{22}F_3(H_2O)_{72}$	6.89	*a*	18.065	90	90	120	$R\bar{3}m$	(343)
Vitusite-(Ce)	$Na_3Ce(PO_4)_2$	14.091(4)	5.357(1)	18.740(3)	90	90	90	$Pca2_1$	(344)
Vivianite	$Fe^{2+}{}_3(PO_4)_2(H_2O)_8$	10.021(5)	13.441(6)	4.721(3)	90	102.8(0)	90	*I*2/*m*	(345)
Vochtenite	$Fe^{2+}Fe^{3+}[(UO_2)(PO_4)]_4(OH)(H_2O)_{12\text{-}13}$	12.606	19.990	9.990	90	102.52	90	Mono	(346)
Voggite	$Na_2Zr(PO_4)(CO_3)(OH)(H_2O)_2$	12.261(2)	6.561(1)	11.757(2)	90	116.2(0)	90	*I*2/*m*	(347)
Vuonnemite	$Na_{11}Ti^{4+}Nb_2(Si_2O_7)_2(PO_4)_2O_3(OH)$	5.4984(6)	7.161(1)	14.450(2)	92.60(1)	95.30(1)	90.60(1)	$P\bar{1}$	(348)
Wagnerite	$Mg_2(PO_4)F$	11.957(8)	12.679(8)	9.644(7)	90	108.3(2)	90	$P2_1/a$	(349)
Wardite	$NaAl_3(OH)_4(PO_4)_2(H_2O)_2$	7.030(10)	*a*	19.040(10)	90	90	90	$P4_12_12$	(350)
Wavellite	$Al_3(OH)_3(PO_4)_2(H_2O)_5$	9.621(2)	17.363(4)	6.994(3)	90	90	90	*Pcmn*	(351)
Waylandite	$(Bi,Ca)Al_3(PO_4,SiO_4)_2(OH)_6$	6.983(3)	*a*	16.175(1)	90	90	120	$R\bar{3}m$	(352)
Weinbeneite	$Ca[Be_3(PO_4)_2(OH)_2](H_2O)_4$	11.897(2)	9.707(1)	9.633(1)	90	95.76(1)	90	*Cc*	(353)
Whiteite-(CaFeMg)	$CaFe^{2+}Mg_2[Fe^{3+}(PO_4)_2(OH)]_2(H_2O)_8$	14.90(4)	6.98(2)	10.13(2)	90	113.11(9)	90	*P*2/*a*	(354)
Whiteite-(CaMnMg)	$CaMn^{2+}Mg_2Al_2(PO_4)_4(OH)_2(H_2O)_8$	14.842(9)	6.976(1)	10.109(4)	90	112.59(5)	90	*P*2/*a*	(355)
Whitlockite	$Ca_9Mg(PO_4)_6(PO_3\{OH\})$	10.350(5)	*a*	37.085(12)	90	90	120	*R*3*c*	(356)
Whitmoreite	$Fe^{2+}[Fe^{3+}(PO_4)(OH)]_2(H_2O)_4$	10.00(2)	9.73(2)	5.471(8)	90	93.8(1)	90	$P2_1/c$	(357)
Wicksite	$NaCa_2Fe^{2+}{}_4MgFe^{3+}(PO_4)_6$	12.896(3)	12.511(3)	11.634(3)	90	90	90	*Pbca*	(358)
Wilhelmvierlingite	$Ca_2Mn_2[Fe^{3+}(PO_4)_2(OH)]_2(H_2O)_8$	14.80(5)	18.50(5)	7.31(2)	90	90	90	*Pbca*	(359)
Wolfeite	$Fe^{2+}{}_2(PO_4)(OH)$	12.319	13.230	9.840	90	108.40	90	$P2_1/a$	(360)

APPENDIX continued

Mineral Name	Formula	*a* (Å)	*b* (Å)	*c* (Å)	α (°)	β (°)	γ (°)	Space Group	Ref.
Woodhouseite	$CaAl_3(PO_4)(SO_4)(OH)_6$	6.976(2)	*a*	16.235(8)	90	90	120	$R\bar{3}m$	(361)
Wooldridgeite	$Na_2CaCu^{2+}{}_2(P_2O_7)_2(H_2O)_{10}$	11.938(1)	32.854(2)	11.017(1)	90	90	90	*Fdd*2	(362)
Wycheproofite	$NaAlZr(PO_4)_2(OH)_2(H_2O)$	10.926(5)	10.986(5)	12.479(9)	71.37(4)	77.39(4)	87.54(3)	*P*1 or $P\bar{1}$	(363)
Wyllieite	$Na(Mn^{2+},Fe^{2+})(Fe^{2+},Fe^{3+},Mg)Al(PO_4)_3$	11.868(15)	12.382(12)	6.354(9)	90	114.52(8)	90	$P2_1/n$	(364)
Xanthoxenite	$Ca_4Fe^{3+}{}_2(PO_4)_4(OH)_2(H_2O)_3$	6.70(4)	8.85(4)	6.54(3)	92.1(2)	110.2(2)	93.2(2)	$P\bar{1}$	(354)
Xenotime-(Y)	$Y(PO_4)$	6.895(1)	*a*	6.0276(6)	90	90	90	$I4_1/amd$	(199)
Xenotime-(Yb)	$YbPO_4$	6.866(2)	*a*	6.004(3)	90	90	90	$I4_1/amd$	(365)
Yingjiangite	$K_2Ca(UO_2)_7(PO_4)_4(OH)_6(H_2O)_6$	15.707	17.424	13.692	90	90	90	*Bmmb*	(366)
Yoshimuraite	$Ba_2Mn_2TiO(Si_2O_7)(PO_4)(OH)$	5.386(1)	6.999(1)	14.748(3)	89.98(1)	93.62(2)	95.50(2)	$P\bar{1}$	(367)
Zairite	$Bi(Fe^{3+},Al)_3(PO_4)_2(OH)_6$	7.015(5)	*a*	16.365(15)	90	90	120	$R\bar{3}m$	(368)
Zanazziite	$CaMg_5[Be_4P_6O_{24}(OH)_4](H_2O)_6$	15.874(4)	11.854(3)	6.605(1)	90	95.3(0)	90	*C*2/*c*	(369)
Zwieselite	$Fe_2(PO_4)F$	11.999(3)	9.890(3)	6.489(1)	90	90	107.7(0)	*I*2/*a*	(370)

References for mineral entries (1) through (370)

(1) McDonald et al. (1994), (2) Foord and Taggart (1998), (3) Harrowfield et al. (1981), (4) Hata et al. (1979), (5) Moore (1971b), (6) Romming and Raade (1980), (7) Piret and Deliens (1987), (8) Groat et al. (1990), (9) Catti et al. (1979), (10) Ono and Yamada (1991), (11) Sokolova et al. (1984a), (12) Sakae et al. (1978), (13) Moore et al. (1981), Merlino et al. (1981), (14) Buchwald (1990), (15) Grice and Dunn (1992), (16) Araki et al. (1968), (17) Potenza (1958), (18) Simonov et al. (1980), (19) Yakubovich et al. (2000), Liferovich et al. (2000b), (20) Lindberg and Christ (1959), (21) Yakubovich et al. (2001), (22) Roca et al. (1997), Pring et al. (1999), (23) Vochten et al. (1984), (24) Chopin et al. (1993), (25) Galliski et al. (1999), (26) Borodin and Kazakova (1954), (27) Pekov et al. (1996), Kabalov et al. (1997), (28) Walenta et al. (1996), (29) Demartin et al. (1993), Demartin et al. (1997), (30) di Cossato et al. (1989a), Fanfani and Zanazzi (1967a),

(31) Piret and Deliens (1981), (32) Ng and Calvo (1976), (33) Kampf and Moore (1976), (34) von Knorring and Mrose (1966), (35) Giuseppetti and Tadini (1973), (36) Steele et al. (1991), Wise et al. (1990), (37) Ilyukhin et al. (1995), (38) Moore and Araki (1974c), (39) Birch et al. (1999), (40) Ercit et al. (1986a), (41) Takagi et al. (1986), (42) Hawthorne (1982), (43) Garcia-Guinea et al. (1995), (44) Khomyakov et al. (1982), (45) Rose (1980), (46) Sokolova and Khomyakov (1992), (47) Gatehouse and Miskin (1974), (48) Krause et al. (1998c), (49) Moore (1975a), Alkemper and Fuess (1998), (50) Fisher and Meyrowitz (1962), (51) Curry and Jones (1971), (52) Ben Amara et al. (1983), (53) Selway et al. (1997), (54) Moore and Shen (1983a), (55) Rouse et al. (1988), (56) White et al. (1967), (57) Giuseppetti et al. (1989), (58) Hughes et al. (1995), (59) Atencio (1988), (60) Giuseppetti and Tadini (1984),

(61) McCoy et al. (1994), (62) Hughes et al. (1990), (63) Kohlmann et al. (1994), (64) Krutik et al. (1980), (65) Young et al. (1966), (66) Brotherton et al. (1974), (67) Giuseppetti and Tadini (1987), (68) Eby and Hawthorne (1989), (69) Blount (1974), (70) Khomyakov et al. (1994), (71) Cooper and Hawthorne (1994b), (72) Cozzupoli et al. (1987), Cooper et al. (2000), (73) Khomyakov et al. (1996), Rastsvetaeva and Khomyakov (1996), (74) Cech and Povondra (1979), (75) Peacor et al. (1999), (76) Piret et al. (1990), (77) Moore et al. (1981), (78) Mrose (1971), Carling et al. (1995), (79) Catti et al. (1977b), (80) King and Sengier Roberts (1988), (81) Moore (1970), (82) Piret and Piret-Meunier (1988), (83) Peacor et al. (1984), (84) Hawthorne and Grice (1987), (85) Dunn et al. (1984b), Moore (1976), (86) Hansen (1960), Hoyos et al. (1993), (87) Fransolet et al. (2000), (88) van Wambeke (1972), (89) Fanfani et al. (1970b), (90) Nord and Kierkegaard (1968),

(91) Kolitsch and Giester (2000), (92) Hughes and Drexler (1991), (93) Alberti (1976), (94) Peacor et al. (1983), (95) Araki and Moore (1981), (96) Kato (1990), (97) Lefebvre and Gasparrini (1980), (98) Milton and Bastron (1971), (99) Guy and Jeffrey (1966), (100) Khomyakov et al. (1997), (101) Moore et al. (1975b), (102) Dick and Zeiske (1998), (103) Piret et al. (1988), (104) Kampf (1992), Kampf et al. (1992), (105) Lindberg (1949), (106) Shen and Peng (1981), (107) Moore et al. (1983), (108) Olsen and Steele (1997), (109) Pring and Birch (1993), (110) von Knorring and Fransolet (1977), (111) Sokolova and Egorov-Tismenko (1990), (112) Liferovich et al. (2000a), Sokolova et al. (2001), (113) Moore et al. (1975a), (114) Radoslovich and Slade (1980), (115) Leavens and Rheingold (1988), (116) Sturman et al. (1981a), (117) Kato (1971), Kato (1987), (118) Calvo (1968), (119) Cipriani et al. (1997), (120) Dooley and Hathaway (1961),

(121) Rinaldi (1978), (122) Fisher (1956), (123) Walenta and Theye (1999), (124) Catti and Franchini-Angela (1976), (125) Grice and Roberts (1993), (126) Romming and Raade (1986), (127) Sieber et al. (1987), (128) Pavlov and Belov (1957), (129) Eventoff et al. (1972), (130) Kolitsch et al. (1999b), (131) Romming and Raade (1989), (132) Hill and Jones (1976), (133) de Bruiyn et al. (1989), (134) Moore and Araki (1973), (135) Bakakin et al. (1974), (136) Lager and Gibbs (1974), (137) Isaaks and Peacor (1981), (138) Meagher et al. (1974), (139) Moore (1974), Moore and Araki (1974a), (140) Grice et al. (1990), (141) Livingstone (1980), (142) Kolitsch et al. (2000), (143) Dunn et al. (1986), (144) Liferovich et al. (1997), (145) Popova et al. (2001), (146) Adiwidjaja et al. (1999), Schluter et al. (1999), (147) Mücke (1979), (148) Kato (1970), (149) Kharisun et al. (1997), Pring et al. (1995), (150) Piret et al. (1985),

(151) Hey et al. (1982), (152) van Tassel (1968), (153) Brownfield et al. (1993), Sljukic et al. (1969), (154) Ovchinnikov et al. (1980), (155) Britvin et al. (1996), (156) Moore (1971a), Moore and Araki (1976), Moore et al. (1980), (157) Cooper and Hawthorne (1994a), (158) Lahti and Pajunen (1985), Pajunen and Lahti (1985), Fransolet (1989), (159) Moore et al. (1980), (160) Moore (1965a), (161) Giuseppetti and Tadini (1983), (162) Mucke (1988), (163) Dick and Zeiske (1997), (164) Yakubovich and Mel=nikov (1993), (165) Vencato et al. (1989), (166) Yakubovich and Urusov (1997), (167) Geller and Durand (1960), (168) Rastvetaeva (1971), Sokolova et al. (1987a), (169) Piret and Deliens (1988), Shoemaker et al. (1981), (170) Abrahams (1966), (171) Moelo et al. (2000), (172) Sen Gupta et al. (1991), (173) Voloshin et al. (1983), (174) Effenberger et al. (1982), (175) Moore and Ito (1979), (176) Tadini (1981), (177) Milton et al. (1993), (178) Voloshin et al. (1992), (179) Le Page and Donnay (1977), (180) Richardson et al. (1988),

(181) Foord et al. (1994), (182) Egorov et al. (1969), (183) Kampf and Moore (1977), (184) Catti et al. (1977c), (185) Fitch and Cole (1991), (186) Makarov and Ivanov (1960), (187) Zanazzi et al. (1986), Fanfani and Zanazzi (1979), White et al. (1986), (188) Stergiou et al. (1993), Makarov and Tobelko (1960), (189) Khosrawan-Sazedj (1982a), (190) Piret and Deliens (1982), (191) Kniep and Mootz (1973), (192) Baur and Rama Rao (1967), (193) Dormann et al. (1982), (194) Birch et al. (1996), (195) Owens et al. (1960), (196) Kampf (1977b), (197) Moore and Araki (1977b), Moore (1976), (198) Cahill et al. (2001), Ankinovich et al. (1997), (199) Ni et al. (1995), (200) Catti et al. (1977a), (201) Fanfani et al. (1976), Moore and Araki (1974e), (202) Merlino and Pasero (1992), (203) Deliens and Piret (1985), (204) Hawthorne (1979a), (205) Effenberger et al. (1994), (206) Deliens and Piret (1981), (207) Bridge and Clark (1983), (208) Baturin et al. (1982), (209) Sokolova and Hawthorne (2001), (210) Coleman and Robertson (1981), Wiench and Jansen (1983),

(211) Ercit (1991), (212) Baturin et al. (1981), (213) Fontan et al. (1982), (214) Freeman and Bayliss (1991), (215) Moore (1972a), Moring and Kostiner (1986), (216) Genkina and Khomyakov (1992), (217) Sebais et al. (1984), (218) Sutor (1967), Sales et al. (1993), (219) Bridge and Robinson (1983), (220) Muto et al. (1959), (221) Groat and Hawthorne (1990), (222) Sokolova et al. (1984b), (223) Moore et al. (1976), (224) Malinovskii and Genkina (1992), (225) Kolkovski (1971), (226) Moore and Araki (1977c), (227) Corbin et al. (1991), Rouse et al. (1989), (228) Moore and Araki (1975), (229) Chao (1969), Kumbasar and Finney (1968), (230) Roberts et al. (1989), (231) Taxer and Bartl (1997), (232) Baur (1969a), (233) Burns (2000), (234) Grice and Groat (1988), (235) Mandarino et al. (1977 (see text)), (236) Kampf (1977c), (237) Peacor and Dunn (1982), (238) Krause et al. (1993), (239) McDonald et al. (1996), (240) Khan et al. (1972),

(241) Raade et al. (1998), (242) Flachsbart (1963), Moore and Araki (1976), (243) Walenta and Dunn (1984), (244) Krause et al. (1998a),

Krause et al. (1998b), (245) Hill (1977), (246) Ferraris and Franchini-Angela (1973), Street and Whitaker (1973), (247) Moore (1966), Fanfani and Zanazzi (1966), (248) Medrano et al. (1998), (249) Demartin et al. (1991), (250) Piret et al. (1979), (251) Atencio et al. (1991), (252) Sokolova et al. (1987b), Khomyakov et al. (1992), (253) Bernhard et al. (1998), (254) Soboleva and Pudovkina (1957), (255) Sergeev (1964), (256) Baur (1969b), (257) Shoemaker et al. (1977), (258) Bjoerling and Westgren (1938), (259) Dai and Hughes (1989), (260) Zhesheng et al. (1983), (261) Chopin et al. (2001), (262) Eversheim and Kleber (1953), (263) Anderson et al. (1977), Sieber et al. (1987), (264) Ross (1956), (265) Mooney (1948), (1950), (266) McConnell (1963), (267) Britvin et al. (1995), (268) di Cossato et al. (1989b), (269) Moore (1974), (270) Cipriani et al. (1997), Arnold (1986),

(271) Fanfani et al. (1975), (1977), (272) Fransolet (1995), (273) Vochten and Pelsmaekers (1983), (274) Miller and Taylor (1986), (275) Hurlbut (1942), (276) Moore and Araki (1977a), Moore et al. (1975a), (277) Warner et al. (1992), (278) Martini (1978), Johan et al. (1983), (279) Mandarino et al. (1978), (280) Khan and Baur (1972), (281) Taxer (1975), (282) Kampf (1977a), Moore and Kampf (1977), (283) Huminicki and Hawthorne (2002), (284) Birch et al. (1995), (285) Keegan et al. (1979), (286) Lightfoot et al. (1987), Witzke et al. (2000), (287) Blanchard (1981), (288) Kurova et al. (1980), (289) Demartin et al. (1996), (290) Hawthorne (1988), (291) Zolensky (1985), (292) Burns and Hawthorne (1995), (293) Rídkošil et al. (1996), (294) Sokolova et al. (1988), (295) Fanfani et al. (1972), (296) Cavellec et al. (1994), (297) Kolitsch et al. (1999a), (298) Keller et al. (1997), (299) Dickens and Brown (1971), (300) Moore and Shen (1983b),

(301) Ferraris and Franchini-Angela (1974), (302) Moore and Araki (1974d), (303) Moore (1966), (304) Britvin et al. (1991), (305) Klevtsova (1964), (306) Fanfani et al. (1978), (307) Abbona et al. (1984), Ferraris et al. (1986), (308) Kato and Miura (1977), (309) Martini (1991), (1993), (310) Fanfani and Zanazzi (1979), Zanazzi et al. (1986), White et al. (1986), (311) Hawthorne (1983b), (312) Dick et al. (1998), (313) Cocco et al. (1966), Genkina et al. (1985), (314) Roberts et al. (1988), Genkina et al. (1984), (315) Isaacs and Peacor (1982), (316) Khosrawan-Sazedj (1982b), (317) Dick (1999), Dunn et al. (1984a), (318) Rius et al. (2000), (319) Peacor et al. (1987), Grice et al. (1985), (320) Frondel et al. (1956), (321) Deliens and Piret (1982), (322) Yakubovich et al. (1977), (323) Waldrop (1968a), (324) Waldrop (1968b), Waldrop (1970), (325) Moore and Araki (1974b), (326) Fanfani and Zanazzi (1967b), (327) Cid-Dresner (1965), Kolitsch and Geister (2000), (328) Birch et al. (1988), (329) Piret and Declerq (1983), (330) Mereiter et al. (1994),

(331) Fitch and Fender (1983), (332) Chernorukov et al. (1997), (333) Walenta (1978), (334) Galliski et al. (2001), (335) Kniep et al. (1977), (336) Fisher (1965), (337) Johan et al. (1983), (338) Fanfani and Zanazzi (1968), (339) Baur and Rama Rao (1968), (340) Huminicki and Hawthorne (2000), (341) Ghose et al. (1974), (342) Pajunen and Lahti (1984), Lahti (1981), (343) McConnell (1952), Kim and Kirkpatrick (1996), (344) Mazzi and Ungaretti (1994), (345) Bartl (1989), (346) Zwaan et al. (1989), (347) Szymanski and Roberts (1990), (348) Ercit et al. (1998), (349) Coda et al. (1967), (350) Fanfani et al. (1970a), (351) Araki and Zoltai (1968), (352) Clark et al. (1986), (353) Walter (1992), (354) Moore and Ito (1978), (355) Grice et al. (1989), (356) Gopal et al. (1974), (357) Moore et al. (1974), (358) Sturman et al. (1981b), (359) Mücke (1983), (360) Antenucci et al. (1989), (361) Kato (1971), (362) Cooper and Hawthorne (1999), Hawthorne et al. (1999), (363) Birch et al. (1994), (364) Moore and Molin-Case (1974), Fransolet (1995), (365) Buck et al. (1999), (366) Zhang et al. (1992), (367) McDonald et al. (2000), (368) van Wambeke (1975), (369) Leavens et al. (1990), Fanfani et al. (1975), (370) Yakubovich et al. (1978).